

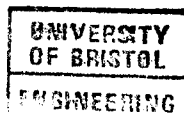
A STATISTICAL APPROACH
TO THE TREATMENT OF WIND LOADING
ON TALL MASTS AND SUSPENSION BRIDGES

by

A. G. Davenport

Department of Civil Engineering
University of Bristol

March 1961



This thesis is submitted in fulfillment of the requirements for the degree of Doctor of Philosophy at the University of Bristol.

It is supported by four shorter papers either published, or accepted for publication, as follows:

"The wind-induced vibration of guyed and self-supporting cylindrical columns"

Transactions of the Engineering Institute of Canada, Volume 3, pages 119-141, December 1959.

"Rationale for the determination of design wind velocities"
Journal of the Structural Division of the Proceedings of the American Society of Civil Engineers; Volume 86, pages 39-68, May 1960.

"The spectrum of horizontal gustiness near the ground in high winds"

Accepted for publication in the Quarterly Journal of the Royal Meteorological Society.

"The application of statistical concepts to the wind loading of structures"

Accepted for publication in the Proceedings of the Institution of Civil Engineers.

These are ^{available} ~~submitted~~ separately.

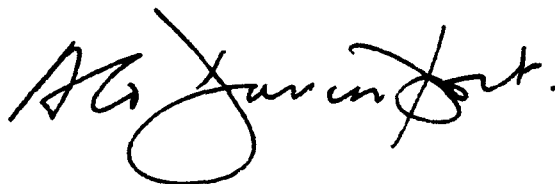
SUMMARY

This thesis describes the wind loading of two slender flexible structures, the tall mast and the suspension bridge. Aspects of the problem discussed are the long-term climatic and statistical properties of high winds, the properties of the mean wind and the turbulence near the ground and the resistance of structures to a gusty wind. Experimental results are given.

The response of the suspension bridge and mast to the mean wind and to random gust loads are analysed theoretically.

To illustrate the methods the wind loading of a 500 ft. high mast and a 3,300 ft. span suspension bridge are worked out and the peak stresses predicted. Vertical as well as lateral loads on suspension bridges are considered.

This is to certify that the contents of this thesis and of the four supporting papers listed in the explanation at the front of this thesis are the independent work of the undersigned except where acknowledgement to other persons is made in the text.

A handwritten signature in cursive script, appearing to read "A.G. Jurinfort.", written in black ink.

March 28th, 1961

TABLE OF CONTENTS

	page
1.0 INTRODUCTION.	1
1.1 HISTORICAL BACKGROUND TO THE STUDY OF WIND ACTION	1
1.1.1 Early Suspension Bridges.	1
1.1.2 The Growth of Understanding of Wind Action.	2
1.1.3 The Consequences of the Tay Bridge Disaster	5
1.1.4 The Eiffel Tower.	6
1.1.5 Early Wind Tunnel Experiments	8
1.2 THE QUASI-STATIC APPROACH TO WIND LOADING AND ITS SHORTCOMINGS.	9
1.3 THE LOADING IMPOSED BY STRONG WINDS	11
1.3.1 The Gust Problem.	11
1.3.2 The Relation of the Gust Problem to the General Strong Wind Problem	15
1.4 STATISTICAL CONCEPTS OF THE STATIONARY RANDOM PROCESS	17
1.5 THE CLIMATE AND STATISTICS OF EXTREME WINDS	21
2.0 WIND STRUCTURE NEAR THE GROUND.	22
2.1 GENERAL	22
2.2 VARIATION OF MEAN VELOCITY WITH HEIGHT.	25
2.3 THE CLIMATE AND STATISTICAL PROPERTIES OF EXTREME WINDS	29
3.0 THE RESPONSE OF BEAMS TO STATIC AND STOCHASTIC LOADING.	34
3.1 INTRODUCTION.	34
3.2 RESPONSE OF A BEAM TO A STATIC LOAD DISTRIBUTION.	34
3.3 THE RESPONSE OF BEAMS TO RANDOM LOADS	36

	page
4.0 PROPERTIES OF ATMOSPHERIC TURBULENCE.	41
4.1 GENERAL	41
4.2 STATISTICAL DISTRIBUTION OF VELOCITIES.	42
4.3 PROPERTIES OF THE SPECTRA	43
4.3.1 General	43
4.3.2 The Spectrum of Horizontal Gustiness.	45
4.3.3 Analysis of Severn Bridge Records	49
4.3.4 The Spectrum of Vertical Gustiness.	54
4.3.5 Cross-Correlation Coefficients.	55
4.3.6 The Vertical Correlation of the Horizontal Components of Turbulence.	60
4.4 REMARKS ON THE STRUCTURE OF TURBULENCE NEAR THE GROUND.	62
5.0 AERODYNAMIC RESPONSE TO FLUCTUATING FLOW.	68
5.1 GENERAL	68
5.2 RESISTANCE IN UNSTEADY FLOW	69
5.2.1 The Virtual Mass Effect	73
5.2.2 The General Problem	74
5.3 INVESTIGATION OF THE RESISTANCE OF BLUFF OBJECTS IN FLUCTUATING FLOW.	79
5.3.1 Outline of Experiments.	79
5.3.2 Test Procedure.	84
5.3.3 Theory of Experiments	87
5.3.4 Results	90
5.3.4.1 Introduction.	90
5.3.4.2 Calculations.	91
5.3.4.3 Determination of Effect of End Shields.	92
5.3.4.4 Determination of Steady Flow Drag	96
5.3.5 Discussion.	96
5.4 THE AERODYNAMIC FORCES IN A GUSTY WIND: RECAPITULATION AND CONCLUSIONS	111
5.4.1 Drag Forces	111
5.4.2 Lift Forces	113
6.0 DYNAMIC AND STATIC BEHAVIOUR OF THE SUSPENSION BRIDGE AND TALL MAST	115
6.1 INTRODUCTION.	115

	page
6.2 VIBRATION OF THE SUSPENSION BRIDGE.	115
6.2.1 Lateral Vibration	115
6.2.2 Vertical Vibrations	119
6.2.3 Torsional Oscillations.	121
6.3 THE VIBRATION OF THE GUYED MAST	122
6.3.1 General	122
6.3.2 The Influence of the Guys	123
6.3.3 Effect of Damping on the Guy Modulus.	130
6.3.4 Vibration of the Mast with Guys	132
6.4 DETERMINATION OF MOMENTS AND SHEARS	139
6.5 THE RESPONSE OF THE MAST AND SUSPENSION BRIDGE TO STEADY WIND LOADING.	141
6.5.1 General	141
6.5.2 The Suspension Bridge	142
6.5.3 The Tall Mast	142
7.0 MECHANICAL AND AERODYNAMIC DAMPING.	144
7.1 GENERAL	144
7.2 MECHANICAL DAMPING.	144
7.3 THE AERODYNAMIC DAMPING	145
8.0 TIME-HISTORY RELATIONSHIPS.	149
8.1 GENERAL	149
8.2	
8.2.1 The Number of Excesses per Unit Time.	150
8.2.2 The Distribution of the Peak Values Occurring Within a Given Period	150
8.2.3 The Distribution of Largest Average Values Occurring Within a Given Period	151
8.3 THE GUST FACTOR	151
9.0 APPLICATIONS.	156
9.1 THE WIND LOADING OF A SUSPENSION BRIDGE	156
9.1.1 Description of Bridge	156
9.1.2 Aerodynamic Properties.	156
9.1.3 Description of Site and Ground Roughness.	159
9.1.4 Estimation of Design Mean Wind Velocity	159

	page
9.1.5 The Response to Horizontal Winds.	160
9.1.5.1 The Lateral Modes and Natural Frequencies of Vibration	161
9.1.5.2 Determination of Lateral Response to Horizontal Gusts.	164
9.1.5.3 Response to Mean Wind	174
9.1.5.4 Discussion of the Effects of Horizontal Wind.	175
9.1.6 Response of Suspension Bridge to Vertical Gusts . .	179
9.1.6.1 The Vertical Modes and Natural Frequencies	179
9.1.6.2 Response to Vertical Gusts.	181
9.1.6.3 Discussion.	186
9.2 THE WIND LOADING OF A TALL MAST	190
9.2.1 Description of the Mast	190
9.2.2 Wind Loading Conditions	190
9.2.3 Behaviour of the Guys	190
9.2.4 Determination of the Natural Modes.	193
9.2.5 Response to Static Windload	197
9.2.6 Response to Horizontal Gusts.	201
9.2.7 Discussion.	
10.0 EVALUATION AND SUGGESTIONS FOR FUTURE RESEARCH.	212
10.1 GENERAL	212
10.2 SUGGESTIONS FOR FUTURE RESEARCH	214
Wind Structure and Climate	214
Aerodynamics	214
Structural	214
General	214
Suspension Bridges.	214
Mast.	215
APPENDIX I	216
USE OF THE PEAK GUST RATIO AS AN INDICATOR OF SURFACE ROUGHNESS.	216
APPENDIX II.	223
HORIZONTAL VELOCITY SPECTRA AT THREE HEIGHTS ON A TALL MAST . .	223
REFERENCES	230

ACKNOWLEDGMENTS

The writer is greatly indebted to a number of persons and parties who have helped, criticised, maintained, encouraged, loaned, drafted, computed and typed during the two and a half years of this research.

In particular the writer is grateful to the Department of Scientific and Industrial Research who awarded him a research fellowship for the latter year and a half. Other organizations whose assistance is acknowledged include the Bristol Aircraft Company's Mathematical Services department: Messrs. Freeman Fox and partners who loaned some of their wind records and supplied information on the Firth of Forth suspension bridge. Another record of high wind was kindly lent by Mr. G. Gimpel then of the Electrical Research Association. A special word of thanks is due to Mr. E.L. Deacon, director of the Division of Meteorological Physics of the Commonwealth of Australia Scientific and Industrial Research Organization who was extremely generous not only with his advice but also in providing a large number of valuable wind records for analysis: Without his assistance very little progress might have been made in discussing wind structure.

Within the Faculty of Engineering at the University of Bristol the writer wishes to warmly thank the laboratory staff for their help with experiments and with photography, Messrs. Boyd and Clarke who helped considerably with many of the drawings and Miss Watkins and Mrs. Tilley who calculated numerous numbers willingly and patiently. Any inaccuracies remaining in the numerical work, are unlikely to be theirs.

To Professor Sir Alfred Pugsley the writer owes very special thanks for his kindness, encouragement and interest throughout the

research. The many opportunities the writer was privileged to have had at Bristol were largely due to Sir Alfred's thoughtfulness. His book "The Theory of Suspension Bridges" sparked an interest which helped bring the writer to Bristol where interest became enthusiasm.

Finally the writer is indebted to Miss Shelagh Morrison of the University of Western Ontario who turned tangled notes into tidy typescript in a very short space of time.

1.0 INTRODUCTION

1.1 HISTORICAL BACKGROUND TO THE STUDY OF WIND ACTION

1.1.1 Early Suspension Bridges

The suspension bridge, in the form of twisted vines and creepers, supporting a simple deck of wooden slats, has been used by primitive people since antiquity. No appreciable development from this archetypal form occurred until the discovery of iron and the introduction of iron chains. Some fine bridges incorporating these innovations and built in the early seventeenth century, can still be seen in China. In Europe, however, suspension bridges using iron were not seen for another hundred years. An Act of Parliament of 1721 refers to a "chain bridge" across the Welland at Market Harborough, and this was probably the first.

In the first half of the nineteenth century a vigorous, upsurgent interest swept through Europe and North America in almost all aspects of engineering. During this period a number of notable suspension bridges arose - the forerunners of the modern structure. Unfortunately, few of them escaped without being either damaged or destroyed by the wind.

Perhaps the first pioneer suspension bridge builder of note was Captain (later Sir) Samuel Brown. One of his earliest and most ambitious structures was the Union Bridge across the river Tweed. Built in 1820, it had a span of 449 ft. and for the first time used eye-bars for chains. It was short lived, however, and was blown down six months after completion. Another of his better known structures was the Brighton Chain Pier, built three years later and consisting of four spans of 250 ft. each (Bishop - 1897). This was seriously damaged by wind on at least three occasions before being finally destroyed in 1896. His bridges at Broughton and Montrose shared a similar fate.

What is regarded as the finest suspension bridge of this period - Telford's 600 ft. span across the Menai Straits - was seriously damaged by wind in 1826 (six weeks after its opening), and also fifteen years later. After the latter occasion its deck was considerably stiffened, and it has suffered no further serious mishap since.

Bridges in the United States and in Europe fared no better. Ellett's Wheeling bridge of 1,010 ft. span (the first over 1,000ft.) over the Ohio river was built in 1848 and blown down six years later. Serrell's 1,043 ft. span at Lewiston near Niagara built in 1850 had the same fate. On the continent, the Nassau bridge across the Lahn river in Germany and the Tournon bridge over the Rhone were destroyed by storms during the same period.

One cause of destruction of these bridges was undoubtedly the form of aerodynamic instability which, more than a century later, in 1940, also destroyed the Tacoma Narrows bridge. This instability is now known to be due to certain unfavourable aerodynamic characteristics of the deck combined with extreme flexibility. The flexibility of these early bridges also made them vulnerable to gusts. The same is true today.

1.1.2. The Growth of Understanding of Wind Action

Perhaps the earliest practical information on wind pressures was that presented to the Royal Society by Smeaton in 1759, based on some results by Rouse. These values, which are given in Table 1.1, agree remarkably closely with the results of recent wind tunnel experiments on flat plates.

TABLE 1.1 (after Smeston - 1759)

Table containing the Velocity and Force of Wind, according to their Common Appellations.

Velocity of the wind		Perpendicular force on one foot area in pounds avoirdupois.	Common appellations of the force of winds
Miles in one hour	Feet in one second		
1	1.47	.005	Hardly perceptible
2	2.93	.020	
3	4.40	.044	Just perceptible
4	5.87	.079	
5	7.33	.123	Gentle pleasant wind
10	14.67	.492	
15	22.00	1.107	Pleasant brisk gale
20	29.34	1.968	
25	36.67	3.075	Very brisk
30	44.01	4.429	
35	51.34	6.027	High winds
40	58.68	7.873	
45	66.01	9.963	Very high
50	73.35	12.300	
60	88.02	17.715	A storm or tempest
80	117.36	31.490	A great storm
100	146.70	49.200	A hurricane
			A hurricane that tears up trees, carries buildings before it, etc.
1	2	3	

Although this information was undoubtedly available to these early engineers, it would have been hard for them to reconcile these steady pressures with the violent heaving movements of their bridges. Besides, the earliest mathematical technique for determining the effect of what is (somewhat misleadingly) termed the "static wind load" did not appear till 1913. Instead the problem had to be dealt with empirically.

Various schemes were put forward for overcoming the effects of the wind. Sir Marc Brunel, for example, in his design for the suspension bridge at the Island of Bourbon in 1821, incorporated a system of chain bracing (see Beamish, 1862). This consisted of two inverted catenaries situated below the bridge, and inclined to the vertical so as to provide some degree of lateral stability as well. Later, in 1830, he was consulted on the subject of wind action by a delegation of gentlemen from Bristol, who were engaged in judging a competition for the design of a bridge across the Avon gorge. On the strength of his experience, he was able to advise them on "how the lateral agitation may be prevented and how the effects of the wind might be counteracted". The winning design, submitted by his son, Isambard Kingdom Brunel, did in fact incorporate a system of wind bracing similar to that used earlier by his father. (I.K. Brunel - 1841).

At the same time, other systems of radiating cable stays were developed, but the most effective method of overcoming the wind effects was to stiffen the deck. This added weight to the structure which further increased the gravity stiffness. The first engineer to realise the significance of both these factors (of the importance of stiffening the deck and of weight in providing gravity stiffening) was Roebling. The structures he built -- which included the railway bridge (the first) at

Niagara Falls, (1855) the Cincinnati bridge across the Ohio river, (1867) his famous 1,596 ft. span at Brooklyn (1883) -- possessed greater rigidity than any previous suspension bridges. They exemplified the important principles he had learnt intuitively, and which were to stand succeeding suspension bridge designers in good stead until, in the present century, they were forgotten, with disastrous consequences.

1.1.3 The Consequences of the Tay Bridge Disaster

This trend towards increasingly rigid structures was greatly accelerated by an event which was to prove important in the later development of the theory of wind action on bridges. On the night of December 29th, 1879 the celebrated bridge across the Firth of Tay (then the world's longest), consisting of eighty-four truss spans, was blown down in a gale. A train plunged through the gap in the bridge and some seventy-five lives were lost.

In the inquiry that followed, it turned out that little or no allowance had been made for wind (none in fact had been called for in the specifications). The designer, Sir Thomas Bouch, was discredited and work begun on his design for a railway suspension bridge across the Firth of Forth, (two 1,600 ft. spans), was discontinued. With this inglorious swan-song the suspension bridge disappeared from the repertoire of British engineers for the next half century (until work was begun in 1958 on the 3,300 ft.-span, road suspension bridge near the same site). Its place was taken by more rigid forms - the arch and the cantilever structure.

The design for a new railway bridge across the Firth of Forth was placed in the hands of Sir John Fowler and Benjamin Baker. They advocated a cantilever design, and the monumental structure which

resulted epitomised this trend towards stiffer and stiffer structures. In the suspension bridge field this trend had already been started by Roebling, and reached a climax in 1903, in the very generous depth of stiffening truss used in the Williamsburg suspension bridge, with a depth to span ratio of 1/40.

One of the main consequences of the Tay Bridge disaster was to give impetus to a new field of scientific investigation, the study of the effect of wind on structures. Interest in this had also been aroused by the possibilities of aviation. In this Benjamin Baker figured prominently. From his study of the forces on large boards in the wind (see Baker 1895) was obtained the design wind pressure figure of 56 lb./ft.² used in the Forth Bridge. It was also the British Standard for several years. In the light of later investigations, this allowance for wind loads was perhaps over-generous (particularly since the main members of the Forth Bridge are round). Ignorance of the real effects of the wind were therefore to prove costly both in the Tay and the Forth bridges - but for different reasons.

1.1.4 The Eiffel Tower

In the same decade, the Eiffel tower was completed to mark the occasion of the Paris Exhibition of 1889. With a height of almost 1,000 ft., this became the world's tallest structure and almost double the height of the previous tallest, the 550 ft. Washington monument in Washington. There had been a number of previous proposals for tall towers, but none were built. Trevethick, for example, had suggested in 1832 that a 1,000 ft., cast iron tower should be built to celebrate the passing of the Reform Bill. Clarke, had proposed a tower of 1,000 ft. for the 1874

Exhibition at Philadelphia, and in 1881, Sébillot had suggested illuminating Paris with electric lights from the top of another 1,000 ft. high tower. It is possible that Eiffel's idea may have originated from the last of these.

It is interesting to compare the wind load assumptions Eiffel used, with the 56 lb./ft.² used in the Forth Bridge, built two years earlier. In his account presented to the Société des Ingénieurs Civils in 1885, Eiffel states:

"With regard the intensity (of the wind pressure) we have made two assumptions: one which supposes that the wind has a constant force of 300 kilogram/metre² (61.5 lb./ft.²); the other that this pressure increases from the base where it is 200 kg./m.², (41 lb./ft.²) to the top where it attains 400 kg./m.² (82 lb./ft.²)."

"With regard the exposed surfaces, we have not hesitated in assuming, in spite of the apparent severity of the assumption, that on the upper half of the tower, all the lattice work is replaced by solid surfaces; that in the intermediate section, where the openings become more important, the frontal area is taken as four times the actual area of iron; below this (the first stage gallery and the upper part of the arcs of the legs) we assume the frontal area is solid; finally at the base of the tower we count the legs as solid and struck twice by the wind (i.e. each leg separately exposed to the full force of the wind)."

These wind pressures were based on some results by Claudel, a French engineer of that period.

The deflexion of the tower in a 54 miles/hour (24 m./sec.), in which the wind pressure was taken as 78 kg./m.² (16 lb./sq.ft.), was calculated to be about 8 inches. At the same time it was assumed

that ~~the~~ vibration would be very slow, so that the effects of any movement on sight-seers would be imperceptible. He regarded the comfort of sight-seers in a 120 mile/hour wind (the full design wind) as only an academic consideration.

The deflexion of 8 inches indicates the comparative rigidity of the Eiffel tower compared to towers erected today. For example, the 700 ft., free-standing, concrete tower, built at Stuttgart, Germany in 1954 (which incorporates amongst other things a restaurant 500 ft. above the ground), deflects approximately 5 1/2 ft. under a similar wind-load, in spite of it being only two-thirds the length (see Leonhardt - 1956). A 1,200 ft. guyed tower at Thule, Greenland is calculated to deflect 9 ft. under similar conditions. (Sturgis - 1954).

1.1.5 Early Wind Tunnel Experiments

Contemporaneously with Baker's tests on boards, early wind tunnel tests were begun. It is in this field, probably, that the early pioneers made their greatest contributions. One of the earliest "wind-tunnels" was made by Irminger, the manager of a Copenhagen gas works. (see Baker - 1895). It consisted of a 4 1/2 in. x 9 in. conduit, connected to a vent in the base of one of the large chimneys, through which the air was sucked by the low-pressure, hot gases inside. In 1893, Stanton began his notable experiments at the National Physical Laboratories near London, and in Paris, Eiffel began his. A wide variety of objects were tested by these investigators, including basic shapes such as flat plates and cylinders, as well as building shapes, (see Stanton - 1903/4; Eiffel - 1913).

It was at this time that the foundations of what has now come to be the standard method for determining the wind forces on structures, were laid. So standard they are now traditional, they have been followed, often blindly, ever since. It is significant that they were evolved at a time when the trend to rigid structures had reached its climax; the structures were usually stiff enough to exclude the possibilities of dynamic excitation by the wind. Since then, however, this trend has reversed: with improvements in analysis, in strength of materials, and in construction, and with the aesthetic demand for light, graceful forms, structures have been made lighter and consequently more flexible. But although the structures have changed, the wind loads, by and large, have not. In 1940 one form of dynamic loading due to wind caused the catastrophic collapse of the Tacoma Narrows Bridge. Although the problems related to this have now largely been solved, another form of dynamic excitation still exists, due to the turbulent, gusty character of the wind.

1.2 THE QUASI-STATIC APPROACH TO WIND LOADING AND ITS SHORTCOMINGS

Traditionally, the wind pressures acting on a structure were calculated on the assumption that the fluctuations in the velocity and direction of the wind could be disregarded, and that the wind could be taken as horizontal and invariant with time and space. These simplifications were convenient in that pressures could then be determined from simple wind tunnel experiments on models, conducted in a steady airstream. From these, various coefficients -- such as the coefficients of pressure and drag -- were found which were assumed to apply to the model and its prototype alike. The only further information needed to

calculate the pressures was a suitable value for the 'design wind velocity'. Since the effects of sudden gusts could not be predicted with any certainty, it was common practice (and still is frequently) to use the highest instantaneous velocity recorded by some nearby anemometer. This, it was believed, would at least be a conservative estimate.

Although this traditional approach has been modified and improved with the passage of time, particularly with respect to the choice of "design wind velocity", the fundamentally quasi-static nature of the approach has been preserved. Although it may not be entirely unsatisfactory where rigid structures are concerned, it is incapable of dealing with two important dynamic problems affecting flexible structures, such as the tall mast and the long span suspension bridge. These are

1. forms of aeroelastic instability
- and 2. excitation due to gusts, both vertical and horizontal.

The forms of aeroelastic instability which affect bluff bodies are well known, mainly because of their catastrophic consequences. Usually they can be classified into "forced" and "self exciting" oscillations (although the dividing line is not always easy to draw in some cases where both types tend to manifest themselves). The forced oscillation is known to affect tall, cylindrical structures such as chimney stacks, (Scruton - 1955: Den.Hartog - 1954) pipeline suspension bridges (Baird - 1955), and some types of antennae mast (Davenport - 1959). The self-exciting oscillation is well known in connection with the ill-fated Tacoma Narrows bridge, which was shaken to pieces by the aeroelastic forces produced in a wind of no more than 42 mi./hr. (whereas, it was designed to withstand a "static" wind load corresponding to a wind of about 120 mi./hr.)

Although still only partially understood, these dangerous dynamic forces can usually be remedied, either by changing the shape of the structure to one that is aerodynamically stable, or by raising the natural frequency of the structure so that instability only occurs at improbably high wind speeds. (see papers by Scruton - 1959; Bleich - 1950; Farquarhson - 1952; and Frazer - 1952).

Although not unrelated to the present topic, these aeroelastic forces are not discussed in this thesis, which is concerned with the second of these problems, namely the forces produced by gusts of wind. These gusts may be either vertical or horizontal. Neglect of the vertical components of gustiness, and the assumption that the wind is purely horizontal, has led to the overlooking of the large lift forces that can develop on a bridge deck in a slightly inclined wind. This was at least partially responsible for the collapse of the Tay Bridge and, more recently, in 1944, of the Chester Bridge across the Mississippi.

1.3 THE LOADING IMPOSED BY STRONG WINDS

1.3.1 The Gust Problem

The transient and localized nature of gusts has been appreciated for some time and a number of attempts have been made to allow for it in estimating wind loads. In his experiments at the Forth Bridge, Baker (1895) found that the wind pressures on a 300 sq. ft. board were some 50 per cent less than those on a board 1 1/2 sq. ft. in area. This was later corroborated by Stanton's measurements (1925) of the average wind velocity at a number of points across a 420 ft. "front" and at a single point. These showed that the highest average velocity across the front was significantly less than that at a point.

The conclusion resulting from these experiments tended to suggest that some allowance might be made at least for the localized effect of gusts. This was later discounted, however, by the conclusions Stanton (1925) reached after his experiments at Tower Bridge, London. Here, pressure tubes were mounted both on the windward and leeward faces of the footway girders at intervals across the 225 ft. span. These were coupled to mechanically linked, aneroid pressure chambers in such a way as to yield the total average pressure acting on the footways. This average pressure and the simultaneous "point" pressure (measured across a single section of the span) were recorded continuously on a chart drum.

It is noteworthy that, these records appear to be the only continuous measurements ever made of the wind pressures exerted on a large structure. Unfortunately it was not possible to record simultaneously the velocity of the incident wind giving rise to these pressures, and the valuable opportunity to correlate the fluctuation of the pressures on a structure, with the corresponding fluctuations in the wind, was lost.

The records did indicate, however, that the pressures at a single station (measured on windward and leeward faces) corresponded closely with the average pressures acting on the span as a whole. From this Stanton concluded:

"...that in winds of moderate intensity, up to 50 miles per hour, the pressure on a large area during the passage of a gust is, in the majority of cases, appreciably less than that on a small area. There is, however, very definite evidence of the existence of gusts up to 50 miles per hour in which the variation in velocity over the front is so

small that, in the case of a structure in an exposed position and having a span of less than 250 ft., the pressure over the whole area is sensibly equal to that at a point in it. Obviously, if this condition were found to obtain for gusts of still higher intensity and for structures of much greater span, no reduction in the wind-pressure factor on account of lateral variation of wind-speed could be justified".

This conclusion introduced a strong note of caution into wind load specification which has survived since. In fact, the reasoning seems to be somewhat doubtful. While the conclusion refers to the "variations in velocity over the front" the measurements, in fact, referred to pressures at pairs of points, (on windward and leeward surfaces), separated by the full width of the bridge, and inside the wake and vortex regions created by the structure. The response characteristics of the instruments appeared also to be an unknown quantity.

Stanton's conclusion was reaffirmed by Bailey and Vincent (1939) in their "follow-up" experiments at the Severn Bridge, across a very much wider span. Their reasons for doing so are not altogether clear. In these experiments, velocities were measured, not pressures.

It seems fair to comment that these earlier investigators were seriously handicapped by the lack of a suitable statistical framework into which to fit their observations. In fact, the statistical theories of turbulence were then still in their infancy. This may account for their apparent tendency to try to distinguish between possible and impossible events rather than the probable and the improbable. From this point of view the results tended to be somewhat inconclusive.

A greater degree of success was achieved by Sherlock, who was also concerned with another problem. This was that the indicated 'maximum gust velocity' used in design depended largely on the response characteristics of the particular instrument. This could lead to the somewhat illegal situation in which design wind loads were higher where the nearby anemometer was less sluggish, or even better lubricated.

As an alternative to the practice then current, Sherlock (1947; 1953) advocated the use of an average instead of an instantaneous velocity, together with certain 'gust factors' which would allow for the additional effects of gusts. A five minute averaging period was suggested for the former, since climatological records for this period were available in the United States. In deciding suitable gust-factors, Sherlock inferred, from measurements of the build-up of lift forces on an aerofoil penetrating a "sharp-edged" gust that, analogously, a gust must traverse eight or ten diameters of an object before the full drag pressures would be felt. On this basis, for example, he concluded that smaller structures, such as houses, would not respond to gusts lasting less than about two seconds. For larger structures the period would be correspondingly longer.

From detailed measurements of wind velocity made on a tall tower during several winter storms, Sherlock was able to determine the ratio of the 'most probable' two second mean velocity to the simultaneous five minute mean velocity. This was the so-called 'two second gust-factor'. The gust factors for other intervals were also determined. In each case they were found to decrease with height above the ground, a feature also noted by Deacon (1955), who investigated a somewhat greater height range. From these investigations it was also concluded that tall

masts should be designed for 'moving load effects', as shown in Fig. 1.1.

Although this approach undoubtedly represented a notable advance in the understanding of wind-loading, and, in particular, of the effect of gusts, it still possessed serious limitations. First, the results could only be expected to apply to open-country sites similar to that used in the investigations; at much rougher sites, such as the centre of a large city, the gustiness would almost certainly be more intense. Second, the approach fails to take account of the history of the loading pattern. It is, for example, incapable of predicting either the consequences of a sequence of gusts striking the structure or the likelihood of such an event occurring. For flexible structures, such as tall towers and long span bridges, this could be a source of serious dynamic stress-magnification which no theory based on purely statical assumptions could allow for.

One or two rules of thumb were available for avoiding the worst dynamic effect. One is that given by Irminger and Nokkentved (1936) that the natural oscillation period of radio masts should not be allowed to exceed 3 - 4 seconds. In another instance, the survival of several tall masts erected in the Far East after being struck by several fierce typhoons is credited to the fact that natural periods between 4 and 8 seconds were avoided. (see Anon. - 1937). Although these simple notions probably contain an element of truth they are unlikely to represent either sufficient or even necessary conditions for the avoidance of serious dynamic effects.

1.3.2 The Relation of the Gust Problem to the General Strong Wind Problem

Evidently, one aspect of the problem that still has to be satisfactorily answered is the prediction of the dynamic action of gusts.

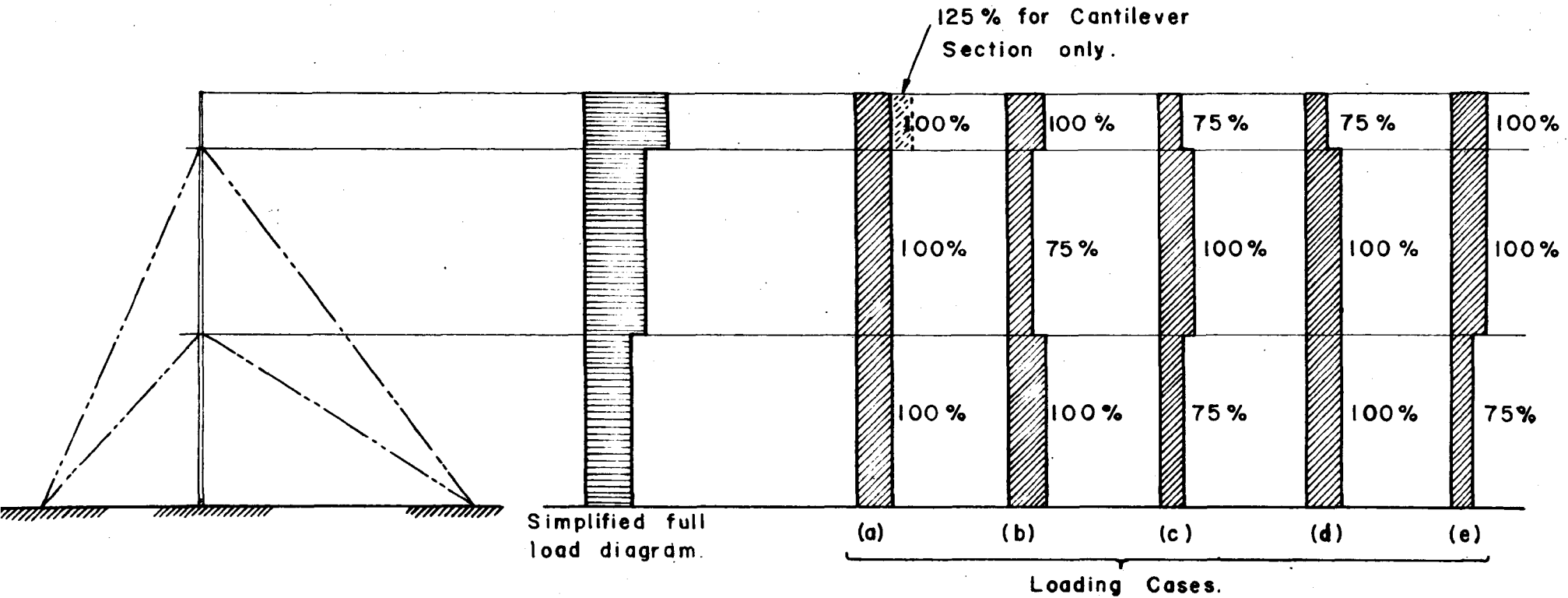


FIG. 1.1 WIND LOADING CASES FOR DESIGN OF GUYED MAST AS RECOMMENDED BY SHERLOCK (1953) AND COHEN (1958).

Expressed somewhat differently but more in line with design needs, the problem is to predict the static-equivalent gust load having a given probability of occurrence. Having found the answer to this question, it is necessary to link it with the climatological problem of predicting the extreme mean wind load at different geographical localities.

The general principles of the method suggested for answering these problems have already been described in a paper by the writer (Davenport - 1961). In it the response of a simple "one-degree of freedom" structure to gusty wind was considered. The structure was assumed to be small enough for the wind to be acting virtually at a point.

To solve the gust problem the concept of the stationary random series was introduced. This led to a "gust factor" which defined the ratio of the probable peak gust load during a given period to the mean wind load during the same period. It was shown to depend on the aerodynamic and dynamic characteristics of the structure, and also on the roughness of the site, the principle factor governing the intensity of the gustiness. The mean wind load could be determined from a theory of climatological extremes discussed earlier by Davenport (1960).

1.4 STATISTICAL CONCEPTS OF THE STATIONARY RANDOM PROCESS

The theory of the stationary, random series assumes that, although the quantities involved (wind velocity, deflexion, stresses etc.) are purely random and cannot be specified from one moment to the next, their statistical properties, nevertheless, remain stationary, that is to say constant, provided that the general conditions of the experiment stay constant. Such processes are known as stochastic processes and have the same relationship to a continuous function of time, as a random variable bears to a discrete sample value. The properties of the

stochastic process are defined by the results of a large number of individual experiments each of which yields a function of time (such as a "run" of wind).

This property of stationariness, is, it seems, generally exhibited by the wind to a highly satisfactory degree, provided that sample times are chosen suitably. A period of between one hour and five minutes appears generally to be satisfactory, largely because for such periods, general weather conditions - such as mean wind velocity and thermal stability - can normally be relied upon to remain fairly constant. Isolated samples of wind do appear to depart from this property of stationariness; these however, are seemingly unrepresentative when it comes to making an overall, long-term, prediction of wind loading, and any distortion they may cause to the statistical picture, assuming stationariness, is believed to be quite negligible.

Application of statistical concepts to physical problems are not new. They were applied to dynamic problems by Lord Rayleigh. Since then the concepts described above have been applied to the theory of Brownian motion, noise in electrical, radio and acoustical systems, noise from jet engines, certain aspects of astrophysics, ocean waves and the response of ships to these, and the response of automobiles to bumpy roads. Most significantly, from the present point of view, they form the basis of the statistical theory of turbulence developed by Taylor (1926 - 1935) and von Karman (1937). Proceeding from this, Lin (1943) determined theoretically the response of a simple pendulum to a turbulent fluid flow. The analogy of this to the gust loading of aircraft was first pointed out by Liepmann (1952). The methods would now seem eminently suitable for solving the civil engineering problem of

gust loading.

A direct consequence of the "stationariness" of the wind is that it is possible to think of the fluctuations in it as composed of a very large number of wave trains, of all frequencies, superimposed on one another. Each wave train remains the same amplitude throughout the 'run', and a "gust" will occur whenever the peaks of several wave trains arrive simultaneously; similarly a "lull" will occur whenever several troughs arrive together.

If the mean square amplitude of these wave trains are ranged accordingly to frequency, (or wave length), a form of spectrum results. A true spectrum (in which the power density or mean square amplitude per unit frequency interval is related to frequency) is obtained, if the length of the record and the number of component wave trains are increased indefinitely. The magnitude of each component wave train can, if necessary, be found by Fourier analysis of the original wind record. If this is done a remarkable result is usually obtained, in that, sampling errors excepted, the spectrum is found to be extremely regular and well ordered as can be seen from Fig. 1.2. Furthermore the form of this spectrum seems to be predictable within limits, knowing only the wind velocity, the height and the ground roughness, as is discussed in section 4.0.

If the response of the structure to each individual frequency is known, and if this is linear, then it is a simple matter to determine, first the spectrum of aerodynamic pressure, and subsequently, the spectrum of the structure's deflexion. The area under the latter is equal to the total mean square deflexion. This, together with the mean deflexion (which can be found straightforwardly) is usually enough to define the

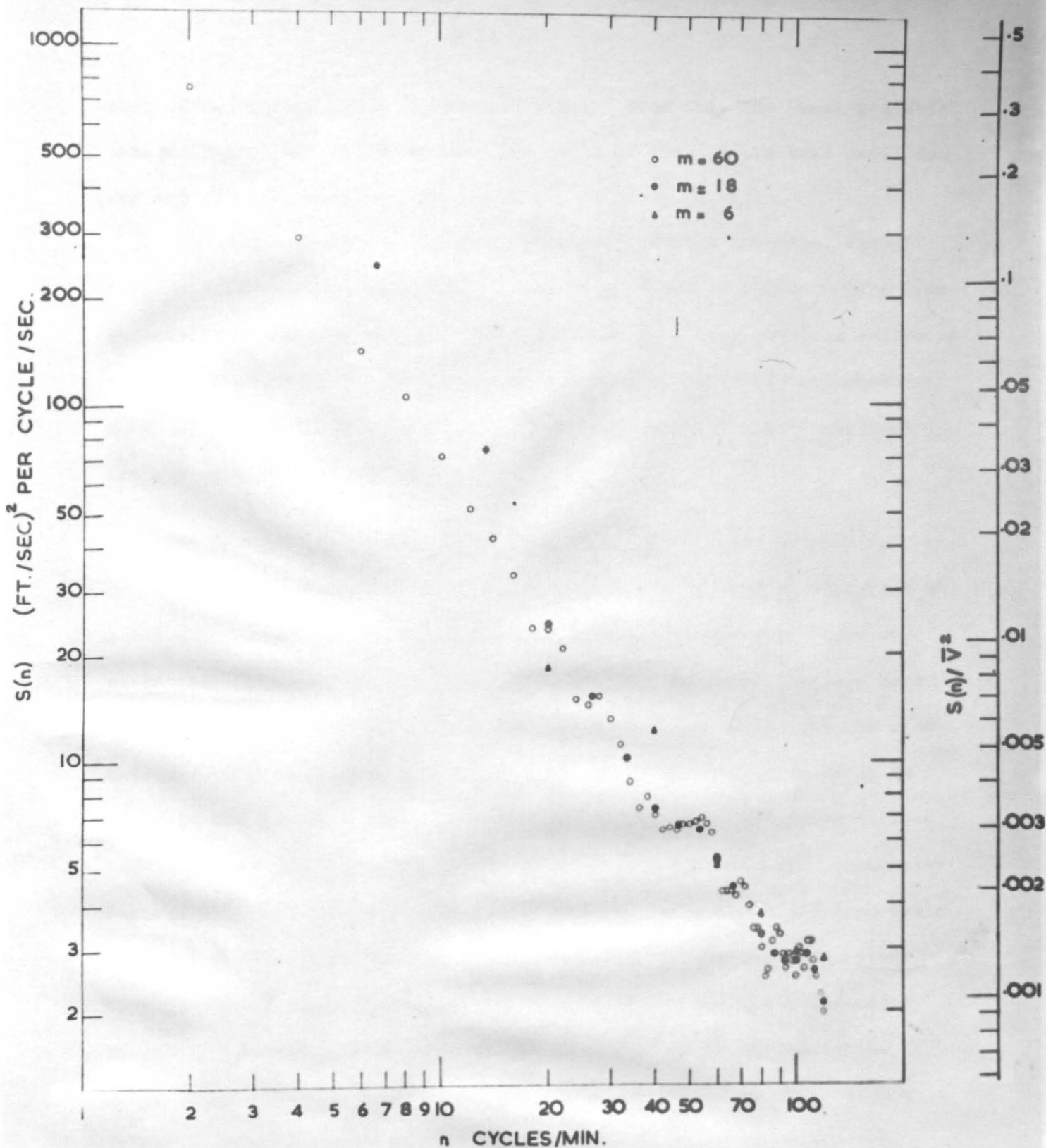


FIG. 1.2 SPECTRUM OF HORIZONTAL WIND VELOCITY

FROM A RECORD OBTAINED AT CRANFIELD, BEDFORDSHIRE USING THE ELECTRICAL RESEARCH ASSOCIATION GUST ANEMOMETER.

Date: 23 Dec. 1955 16.55 G.M.T. Duration of record: 10 min. Mean wind velocity, $\bar{V} = 46.0$ ft./sec.
 Elevation: 50 ft. above ground.

statistical distribution of the deflexions. From this the "most probable" peak deflexion can be estimated. The ratio of this to the mean deflexion defines the gust factor.

This procedure, which has been described by Davenport (1960) for the case of a simple structure, can be extended to slender, beam-like structures possessing several modes of vibration. This requires analysing the distribution of the wind velocity across the span into the component modes of the beam. The response is then determined for each mode separately, and the results superposed.

1.5 THE CLIMATE AND STATISTICS OF EXTREME WINDS

Any accurate estimate of the probable wind loading must rest on a reliable prediction of the climate of extreme winds. This forms an essential, but separate part of the wind loading problem. Use has been made recently of "extreme value" statistical methods to predict the wind extremes of climate (Shellard 1958; Thom 1960), the objective being to estimate the extreme winds typical of "flat, open country", with various recurrence periods (i.e. the "once-in-fifty-year wind etc."). Anemometer records from "suitable" stations were used for the purpose and from these contours of wind velocity were drawn. Davenport (1960) has suggested that failure to take account of the very important modifying influence of ground roughness results in mean wind velocities in cities (where, after all, most buildings are erected) being for too high. Furthermore it leads to the assumption that the exposures of the anemometers in service are far more homogeneous than they actually are.

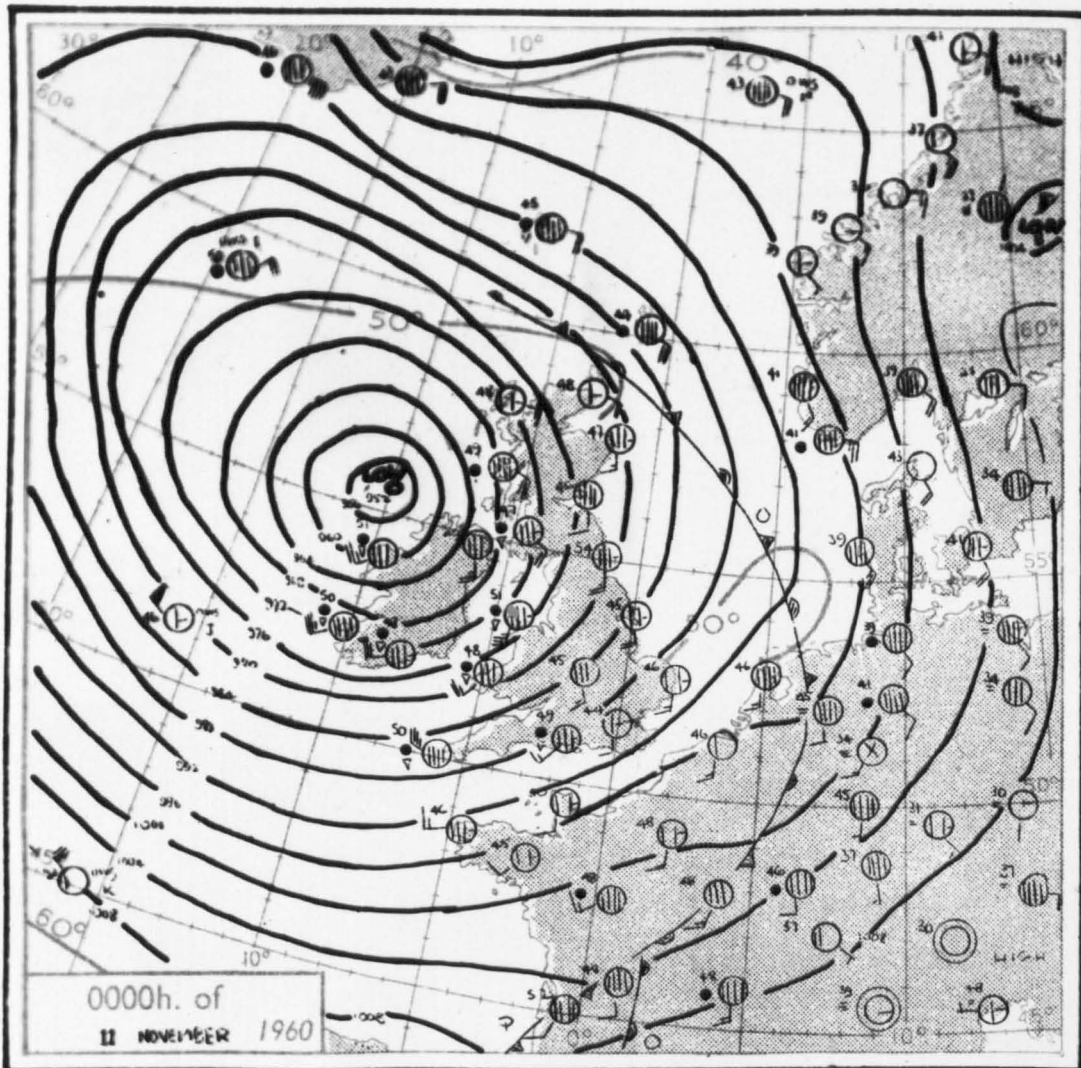
The alternative method for estimating the climate suggested by Davenport (1960) is summarised here. A possible further improvement is introduced in that gustiness is used as an 'indicator' of the roughness.

2.0 WIND STRUCTURE NEAR THE GROUND

2.1 GENERAL

It is well known that the wind is induced by the pressure differences which arise over the earth's surface. These pressure differences are indicated by the isobars (lines of equal barometric pressure) of any weather map, such as that shown in Fig. 2.1. The wind, at heights great enough for it to be unaffected by the frictional forces near the earth's surface, tends to move parallel to the isobars, and attains a velocity known as the gradient velocity. If the overall pressure patterns are stationary, this gradient velocity can be estimated quite easily from the spacing of the isobars, (i.e. the pressure gradient), their radius, and the latitude (see Sutton - 1953; Davenport - 1960). In general, the closer the spacing of the isobars, and the smaller their radius of curvature, the stronger will be the wind.

This gradient velocity, however, is only obtained at heights above about 1,000 - 2,000 ft. Below this, at heights of greater interest to the structural engineer, the airflow is influenced by the friction at the surface. The principal consequences of this are that the airflow is retarded, it becomes turbulent and gusty, and its direction is no longer parallel to the isobars. The rougher the surface the greater these effects will be. Fig. 2.2, which shows simultaneous records of windspeed at 2-second intervals at three heights on a tall mast, illustrates some of these effects.



WIND	
Symbol	Wind speed (knots)
	Calm
	1-2
	3-7
	8-12
	13-17
For each additional half-feather add 5 knots	
	48-52

FIG.2.1 WEATHER MAP SHOWING AN INTENSE DEPRESSION WITH STRONG WINDS.

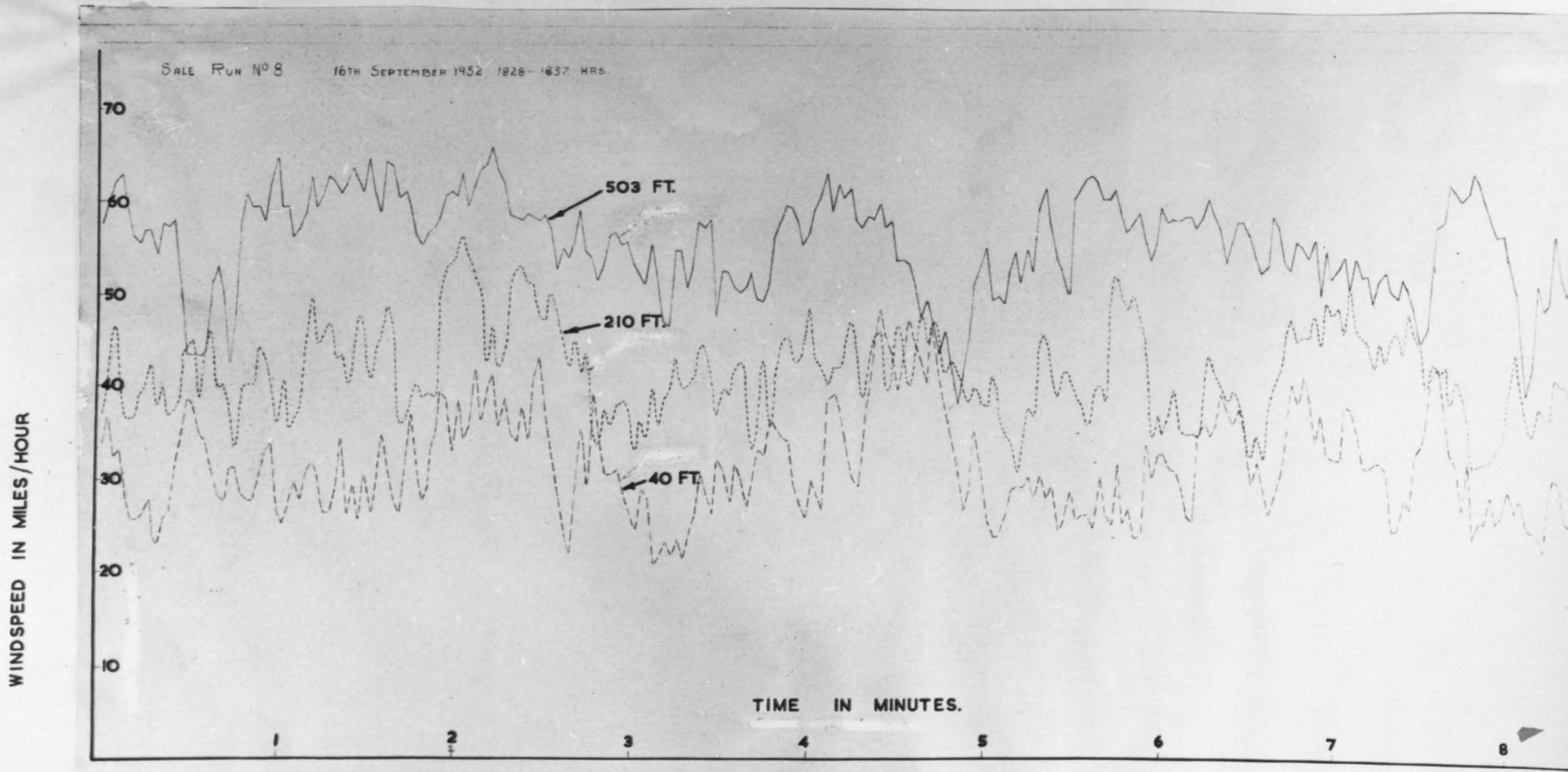


FIG. 2.2 RECORD OF WINDSPEED AT THREE HEIGHTS ON A 500FT. MAST.

2.2 VARIATION OF MEAN VELOCITY WITH HEIGHT

A number of formulae are available for describing the variation of the mean wind velocity in this lower height range. All of them are, to some extent, empirical, since, as yet, there is no established theory which accounts adequately for all the factors involved. One of the simplest and most reliable of these expressions is the power law, which can be written

$$V_Z = V_G \left(\frac{Z}{Z_G} \right)^\alpha \quad (2.1)$$

where

V_Z = mean velocity at height Z ,

V_G = gradient velocity,

Z_G = the height at which the gradient velocity is first attained (the gradient height),

and α = an exponent, applicable to the particular site and wind conditions.

In high winds it appears that the parameters of this profile are controlled almost entirely by the ground roughness. Convection - the other possible influence - is usually less important in high winds, partly because the churning action of the strong mechanical turbulence prevents the necessary thermal instabilities from arising (this is particularly true if, as is usual, clouds blanket incoming or outgoing radiation) and partly because the mechanical turbulence increases with wind-speed, whereas convective turbulence does not.

Exceptions to these statements may possibly be encountered in severe local storms, such as frontal squalls and tornadoes. However, these storms, although perhaps not infrequent when taken over a wide region, generally affect very small areas (of the order of a few square

miles) at a time and the incidence of high winds at any one place due to these "freak" storms (even in the notorious tornado belt of the American Mid-West) is probably negligibly slight compared to that due to more general large scale storm systems, to which the earlier statements refer.

In the latter, more general type of storm, it appears that both the value of α (measuring the variation of the wind velocity with height) and of Z_G (measuring roughly the thickness of the layer in which the airflow is retarded) increase with ground roughness. This can be seen from Table 2.1 giving the values of α and Z_G representative of various types of surface, as suggested by Davenport (1960). The corresponding mean wind velocity profiles (for a uniform gradient wind of 100) are shown in Fig. 2.3. From this it is seen that the mean velocity at 100 ft. in a city might be about half that in open country. This means that the kinetic pressure of the airflow in the city is a quarter that in open country.

On the other hand, the gustiness in a city is greater, also due to the greater roughness. The actual turbulent energy in the wind (at frequencies greater than about .1 cycle per minute) may be about 12 times that in open country for the same surface velocity. Consequently, large variations in the possible effective wind loads on a structure can arise, depending on whether it is erected in a city or in open country, and on whether it is susceptible to fluctuating gust loads.

It should be observed that the mean velocity profiles shown in Fig. 2.3 refer to flat terrain whose roughness characteristics extend over a sufficiently wide area for the flow regime to establish itself uniformly. Where this is not so, either due to the undulating nature of the ground or to the rapidly changing character of the surface roughness

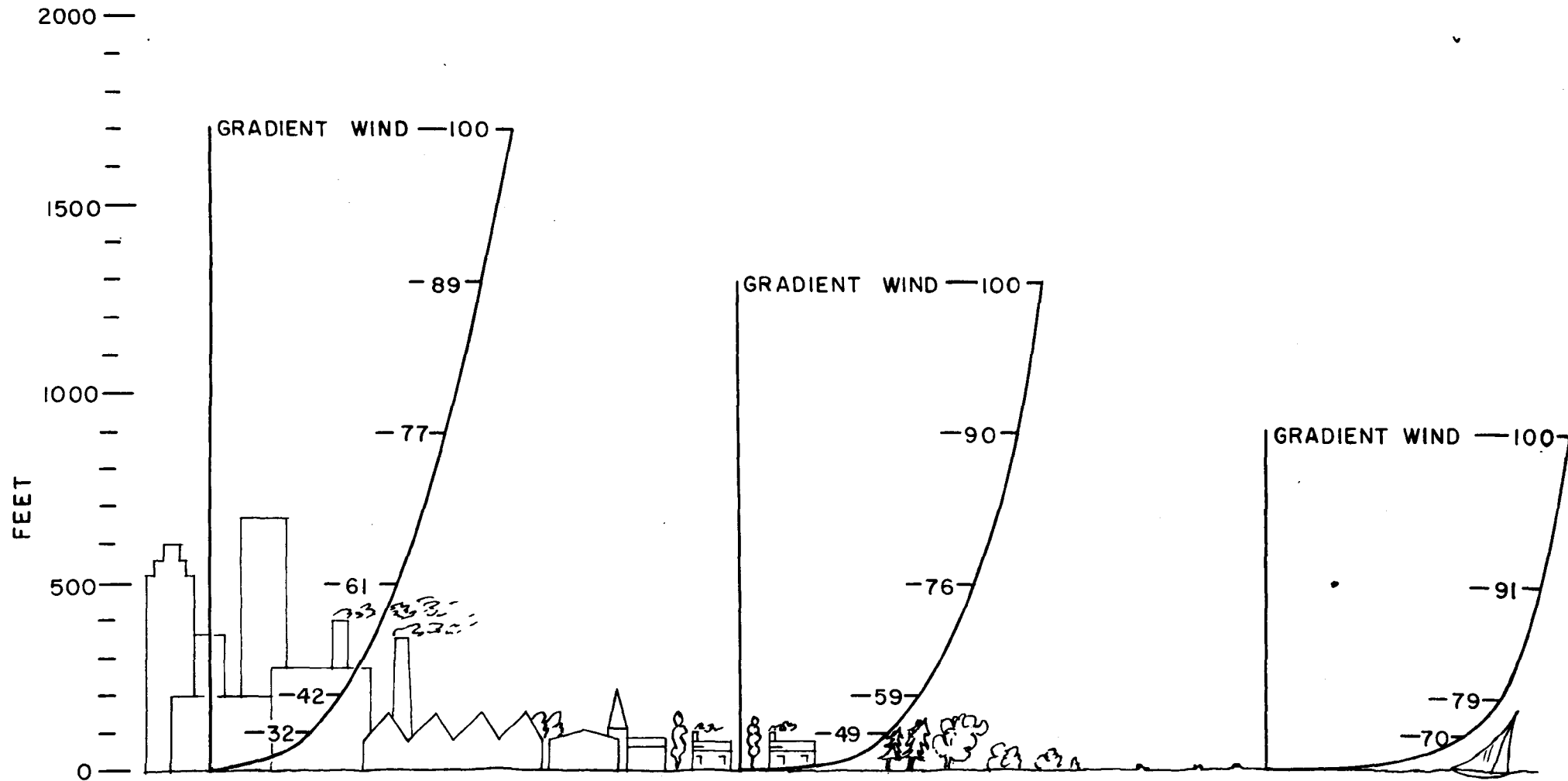


FIG.2.3 PROFILES OF MEAN WIND VELOCITY OVER LEVEL TERRAINS OF DIFFERING ROUGHNESS

TABLE 2.1

WIND STRUCTURE PARAMETERS FOR SURFACES
OF DIFFERENT ROUGHNESS

Type of surface	Power law exponent α	Gradient height Z_G	Drag Coefficient K
<p>a) Open terrain with very few obstacles:</p> <p>e.g. open grass, or farmland with few trees, hedgerows, and other barriers etc.: prairie; tundra; shores and low islands of inland lakes; desert.</p>	0.16	900	.005
<p>b) Terrain uniformly covered with obstacles 30-50 ft. in height:</p> <p>e.g. residential suburbs; small towns; wood land, and scrub; small fields with bushes, trees and hedges.</p>	0.28	1300	.015
<p>c) Terrain with large and irregular objects:</p> <p>e.g. centres of large cities; very broken country with many wind breaks of tall trees, etc.</p>	0.40	1700	.050

certain modifications will be necessary to suit the conditions. For example, in hilly regions, amplifications of wind velocity can arise near hill-tops and in funnel-shaped valleys. The former have been investigated and exploited to a limited extent, in the obtaining of power from the wind (Wax - 1956). In coastal districts, also, it seems likely that when a wind blows off the rough shore, it may take some distance (perhaps three or four miles) before the flow regime corresponding to the rougher land surface is fully established. A similar effect is likely to be present when the wind flows from the outskirts of a city to its centre. In this instance, however, the change in roughness is probably more gradual, and the wind regime may therefore establish itself sooner.

It is perhaps interesting to note that, although two of the most important applications of the study of wind structure in the lower layers (namely, the diffusion of smoke and the wind loads on buildings) refer most frequently to large urban areas, no detailed investigation has yet been carried out under these conditions. There is, however, a miscellaneous assortment of measurements available (see Davenport 1960) which all point to the conclusions referred to here.

2.3 THE CLIMATE AND STATISTICAL PROPERTIES OF EXTREME WINDS

Fundamental to the entire problem of wind loading is a satisfactory estimate of the climate and statistical properties of the mean wind velocity at the site of the structure.

Some of the difficulties encountered in determining these have been discussed by the writer (Davenport - 1960). It was pointed out that the principle source of information on wind speeds near the surface was anemometer records and that these in themselves had certain shortcomings. The siting was not always ideal (e.g. on cliffs or on city buildings)

and the period records had been kept varied from station to station. In addition the wind speed would possibly be representative of the surface roughness only in the immediate vicinity of the anemometer. This meant that to obtain an overall picture of the extreme surface winds from anemometers alone, it would be necessary not only to have anemometers situated in such a way that they reflected local variations in terrain roughness, but also to make some adjustment for the different periods of record. Clearly this would be considerable task. An alternative method for determining the climate (i.e. statistical properties) of the extreme wind velocities, suggested by Davenport (1960) is now described. This uses the gradient velocity as a reference and uses records of surface anemometers to obtain estimates of this at several points.

As a first step, the statistical properties of the surface velocities as given by anemometer records are found. To do this the annual wind velocity maxima for a number of years are extracted from records of each station and analysed statistically. It is found that their statistical distribution - in common with many other climatological and other extremes - can be satisfactorily represented by the function

$$P(V) = e^{-e^{-y}} \quad (2.2)$$

where $y = a(V-U)$,

a = the scale factor for the data (measures its dispersion),

and U = the mode of the data.

Here, $P(V)$ denotes the probability that the maximum velocity in any one year is less than V .

Some valuable results of this kind have been compiled by Shellard (1958) from the anemometer records for selected stations in the British

Isles. (A similar study has been made by Thom (1960) for the United States using a slightly different distribution.) From Shellard's values of the parameters $\frac{1}{a}$ and U for the various stations, estimates of the corresponding parameters for the gradient wind were then made (see Davenport-1960). This was done assuming a constant ratio between the velocity of the gradient wind and that at the anemometer height, determined from the wind velocity profile which seemed most appropriate to the site. Contours of the parameters of the extreme mean hourly gradient wind speed, obtained by these means are shown in Fig. 2.4 (This is a slightly improved version of the map given previously by Davenport - 1960).

From this map, the gradient wind velocity with any prescribed probability of occurring can now be predicted. For some uses - such as flood prediction - it has become customary to allude to this probability in terms of a return period which defines the average number of years before a certain value either recurs or is again exceeded. If this convention is adopted and the return period is denoted by r , the probability that a certain value is not exceeded in any one year is $(1 - \frac{1}{r})$. Hence from equation (2.2) the gradient wind velocity \bar{V}_G for which r is the return period is

$$\bar{V}_G = U - \frac{1}{a} \left[\log_e \left(-\log_e \left(1 - \frac{1}{r} \right) \right) \right] \quad (2.3)$$

For large values of r ($r \gtrsim 10$) this can be approximated by

$$\bar{V}_G = U + \frac{1}{a} \log r \quad (2.4)$$

The values of U and $\frac{1}{a}$ are read from the contours of the map. Extreme wind velocities close to the ground can now be determined from equation (2.1).

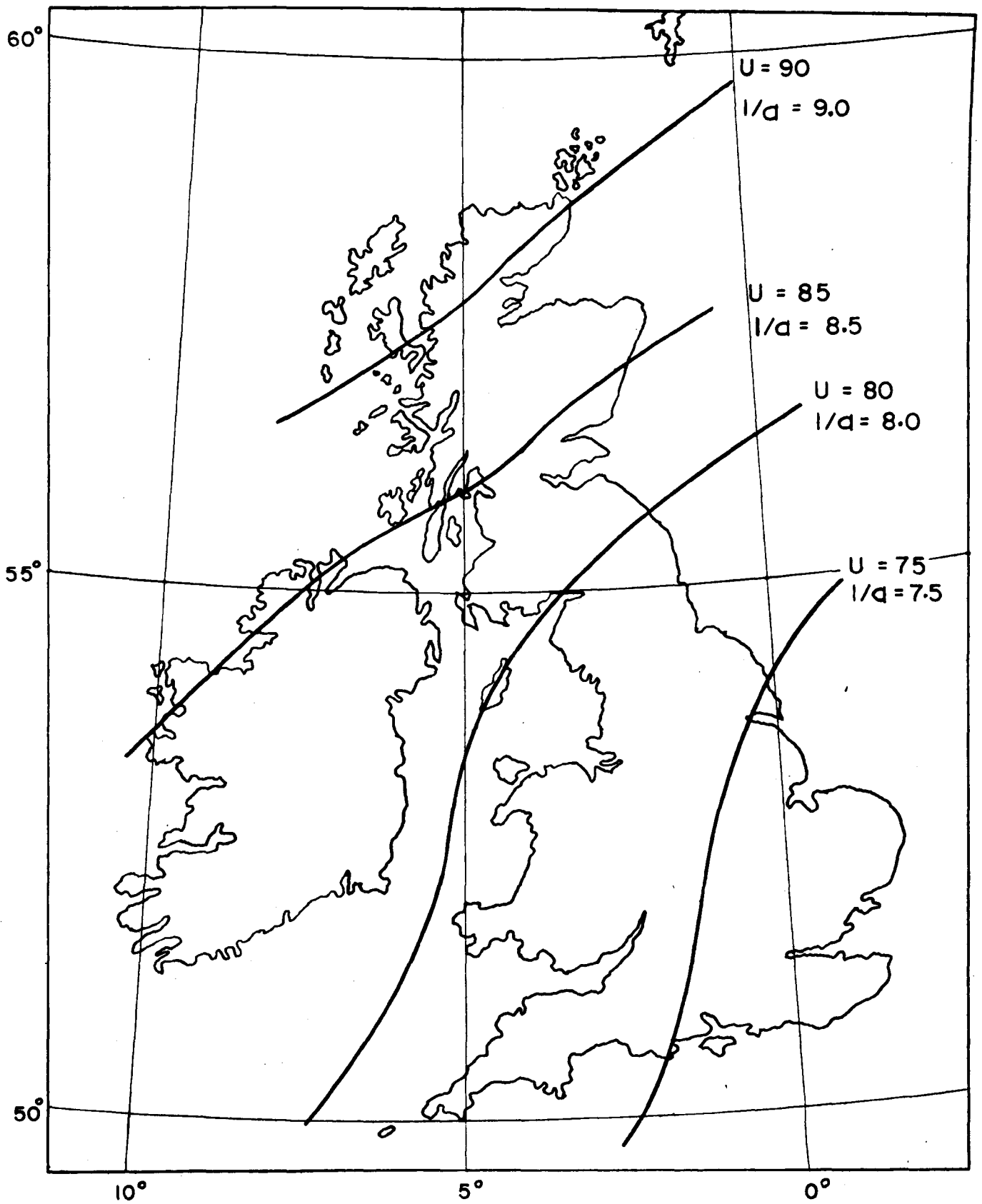


FIG.2.4 PARAMETERS OF EXTREME MEAN HOURLY GRADIENT WIND SPEED OVER THE BRITISH ISLES

UNITS: MILES PER HOUR

It is common practice for records of maximum peak instantaneous gust speed to be kept in addition to hourly mean velocities. The average ratio of the extreme gust velocities to the extreme hourly velocities gives a useful measure of the gustiness. This gustiness (as might be expected, and as is discussed in the next section) also happens to be good indication of the roughness of the site upon which the variation of the mean wind velocity with height depends. The possible use of this gust ratio as an 'indicator' of the roughness (in place of the more subjective evaluation) is discussed in the Appendix I.

3.0 THE RESPONSE OF BEAMS TO STATIC AND STOCHASTIC LOADING

3.1 INTRODUCTION

The loads imposed on a tall mast or a long span suspension bridge by a gusty wind can be separated into two parts. First, a steady component due to the mean wind, and a second, a superimposed fluctuating load, due to gusts. In principle, the response of the structure to the mean wind load presents no difficulty, since it is a simple statical problem. The loads due to gusts, however, present a more difficult problem since these are random in nature owing to the randomness of the gusts themselves. As such, they are only definable in statistical terms: to try to define them otherwise is useless.

It is hardly possible to define the statistical properties of the gust loads with any generality, since they are governed by the dynamic and aerodynamic characteristics of the particular structure. It does, however, seem to be possible to make a satisfactory statement of the statistical properties of the atmospheric turbulence (at least the more relevant ones), and then, to estimate the statistical properties of the deflexions, stresses, etc., knowing the aerodynamic and dynamic characteristics of the structure. As indicated already, this can be done using the Generalised Harmonic Analysis developed by Liepmann and others.

For the purposes of general theory, the tall mast and long span suspension bridge can be regarded simply as slender beams. The special support conditions appertaining to each structure need not be introduced until a later stage.

3.2 RESPONSE OF A BEAM TO A STATIC LOAD DISTRIBUTION

There are many methods of determining the response of a beam to a static load distribution. One of these, which happens to be in line

with the technique used later for determining the response to gust loads, uses the natural modes of the beam for representing both the deflexions and the loads.

The natural modes of a beam are given by the various solutions to the equation,

$$K(x). y + m(x). \frac{d^2 y}{dt^2} = 0 \quad (3.1)$$

where $m(x)$ and $K(x)$ are general expressions for the mass and the equivalent stiffness of the beam (taking into account such additional effects as guy supports in the mast and the support of the cable in the suspension bridge). The infinite number of solutions to this equation can usually be written in the form:

$$y_r(x, t) = \mu_r(x). \sin 2\pi n_r t \quad (3.2)$$

where n_r = the natural frequency in the r th. mode;

$\mu_r(x)$ = the r th. mode of vibration i.e. the shape of the deflexion curve during vibration.

Any static load distribution, $P(x)$, acting on the beam can be expressed in terms of these modes;

$$P(x) = \sum_r P_r. \mu_r(x) \quad (3.3)$$

The coefficients P_r can be found by multiplying both sides by $\mu_r(x)$ and integrating over the entire length of the beam, $0 - \ell$. Since it is a universal property of natural beam modes that they are orthogonal to one another,

$$\int_0^\ell \mu_r(x). \mu_s(x). dx = \begin{cases} 0 & \text{for } r \neq s \\ N_r & \text{for } r = s \end{cases} \quad (3.4)$$

and hence,

$$P_r = \frac{1}{N_r} \int_0^\ell P(x). \mu_r(x). dx \quad (3.5)$$

(A procedure similar to this is used in ordinary harmonic analysis).

It is also possible to represent the stiffness function, $K(x)$ in the same way, either directly, or by assuming an initial form for the deflexion curve.

$$K(x) = \sum_r K_r \mu_r(x) \quad (3.6)$$

where

$$K_r = \frac{1}{N_r} \int_0^l K(x) \mu_r(x) dx \quad (3.7)$$

The deflexion of the structure may be written

$$y = \sum_r \frac{P_r}{K_r} \mu_r(x) \quad (3.8)$$

Knowing the deflexion, it is then a straight forward matter to determine other quantities such as the moments and stresses.

The actual method of determining the modes is left until Section 6.0. Even if the form of the modes is difficult to express explicitly (due to changes in beam section etc.), it is usually possible to represent them sufficiently accurately by series of other simple functions, such as ordinary sine functions or the so-called Basic Functions. The analysis of the suspension bridge under static wind loading, using the former functions, has been carried out by Selberg (1944), and the tall mast, using the latter functions, by Davenport (1959).

3.3 THE RESPONSE OF BEAMS TO RANDOM LOADS

In a previous paper (Davenport 1961), the response of a simple one-degree of freedom structure to a stationary, random load was described. The equation of motion of such a system is:

$$m \frac{d^2y}{dt^2} + c \frac{dy}{dt} + Ky = P(t) \quad (3.9)$$

where y = deflexion of the structure at time t ;

m = mass of the structure;

c = velocity damping coefficient;

and K = spring stiffness (load per unit deflexion).

The solution of this equation enables the spectrum of the deflexion to be expressed in terms of the spectrum of the load. (The spectrum defines the contributions to the variance of a stochastic process made by the different frequencies.)

i.e.

$$S_y(n) = \frac{|\chi_d(n)|^2}{K^2} \cdot S_p(n) \quad (3.10)$$

where $S_y(n)$ = spectrum of deflexion at frequency n ;

$S_p(n)$ = spectrum of the load at frequency n ;

$$|\chi_d(n)|^2 = \frac{1}{\left\{1 - \left(\frac{n}{n_0}\right)^2\right\}^2 + \left(\frac{\delta}{\pi}\right)^2 \left(\frac{n}{n_0}\right)^2} ; \quad (3.11)$$

and n_0 = natural frequency

$$= 2\pi \sqrt{\frac{K}{m}} \quad (3.12)$$

$|\chi_d(n)|$ is commonly known as the dynamic magnification of the system.

It follows from the definition of a spectrum that the variance of the deflexion is:

$$\begin{aligned} \sigma^2(y) &= \int_0^{\infty} S_y(n) \cdot dn \\ &= \frac{1}{K^2} \int_0^{\infty} |\chi_d(n)|^2 \cdot S_p(n) \cdot dn \end{aligned} \quad (3.13)$$

If the structure has more than one mode of vibration - as in the case of a beam - and the load no longer acts at a point, but along the entire length of the beam, the problem is more complex. As a first approximation it is possible to consider the response in each mode

separately and then superimpose the results. This ignores any possible coupling effect between the different modes. If, however, the damping is small (as later it is shown to be), the natural frequencies are separated, and the beam modes do not involve torsion, any coupling is generally negligible and the assumption justified. (A full description of the theory taking into account the coupling has been given by Eringen (1953).)

As a first step both the load and the deflexion are represented in terms of the natural modes of the beam:

i.e.

$$P(t, x) = \sum_r P_r(t) \cdot \mu_r(x) \quad (3.14)$$

where $\mu_r(x)$ = the function defining the deflexion of the beam in the r th mode for unit deflexion at the reference point;

and $P_r(t)$ = component of the load for r th. mode. at time t .

This load will cause a deflexion $y(t, x)$ which can likewise be expressed in terms of the natural modes:

$$y(t, x) = \sum_r y_r(t) \cdot \mu_r(x) \quad (3.15)$$

Using a procedure for determining the coefficients similar to that used in the static case (see Eq. (3.5)),

$$P_r(t) = \frac{1}{N_r} \int_0^l P(t, x) \cdot \mu_r(x) \cdot dx \quad (3.16)$$

The mean square of this load component is

$$\overline{[P_r(t)]^2} = \frac{1}{N_r^2} \int_0^l \int_0^l \overline{P(t, x) \cdot P(t, x')} \cdot \mu_r(x) \cdot \mu_r(x') \cdot dx \cdot dx' \quad (3.17)$$

where the bars denote time averages. Now the quantity on the left hand side represents the variance of the quantity $P_r(t)$, and the quantity $\overline{P(t, x) \cdot P(t, x')}$ represents the co-variance of the load $P(t, x)$ at

points x and x' on the beam. Both quantities are assumed to be stationary, random functions of time, and therefore have spectra.

The spectrum of the r th. mode load component, at frequency η , is, from equation (3.17),

$$S_{P_r}(\eta) = \frac{1}{N_r^2} \int_0^l \int_0^l S_p(x, x'; \eta) \mu_r(x) \cdot \mu_r(x') \cdot dx \cdot dx' \quad (3.18)$$

where $S_p(x, x'; \eta)$ is the cross-spectrum of the loads on the beam at x and x' , for frequency η . The cross-spectrum is a complex quantity, that is to say, it is defined by two components, one in-phase and the other in quadrature. It can be normalised by dividing by the spectrum at some reference point yielding, effectively, a cross-correlation coefficient between the loads at the two points, x and x' , for the frequency η . Hence,

$$S_{P_r}(\eta) = \frac{S_{P_0}(\eta)}{N_r^2} \int_0^l \int_0^l R(x, x'; \eta) \mu_r(x) \cdot \mu_r(x') \cdot dx \cdot dx' \quad (3.19)$$

where $S_{P_0}(\eta)$ = the spectrum of the load at a reference point;

and $R(x, x'; \eta)$ = the cross-correlation coefficient of the load at x and x' at frequency η ,

$$= \frac{S_p(x, x'; \eta)}{S_{P_0}(\eta)}$$

The above expression for the r th. mode load component can be simplified by writing

$$S_{P_r}(\eta) = |J_r(\eta)|^2 \cdot S_{P_0}(\eta) \quad (3.20)$$

where

$$|J_r(\eta)|^2 = \frac{1}{N_r^2} \int_0^l \int_0^l R(x, x'; \eta) \mu_r(x) \cdot \mu_r(x') \cdot dx \cdot dx' \quad (3.21)$$

The latter is termed the "joint acceptance" for the r th mode, and is a

measure of the correlation between the form of the pressure distribution across the span and the mode.

The response of the beam to the load spectrum $S_p(n)$, is governed by equation (3.9). Resulting from this, the deflexion spectrum for the r th mode component is found to be

$$S_{y_r}(n) = \frac{|\chi_r(n)|^2}{K_r^2} \cdot S_p(n)$$

$$= \frac{|\chi_r(n)|^2}{K_r^2} \cdot |J_r(n)|^2 \cdot S_{p_0}(n)$$
(3.22)

where

$$|\chi_r(n)|^2 = \frac{1}{\left\{ 1 - \left(\frac{n}{n_r}\right)^2 \right\}^2 + \left(\frac{\delta_r}{\pi}\right)^2 \left(\frac{n}{n_r}\right)^2}$$
(3.23)

n_r = natural frequency in r th mode;

δ_r = logarithmic damping decrement in the r th mode.

If it is assumed that the small coupling effect between modes is negligible it follows from equation (3.15) that the total variance of the deflexion is

$$\sigma^2(y) = \sum_r \overline{y_r(t)^2} \cdot \mu_r^2(x)$$
(3.24)

The total spectrum of deflexion at position x is correspondingly

$$S_y(x;n) = \sum_r S_{y_r}(n) \cdot \mu_r^2(x)$$
(3.25)

where $S_{y_r}(n)$ is given by (3.20). This is the basic expression for determining the deflexion spectrum.

The variances of the shear force and bending moment on the beam at station x are given respectively by

$$\sigma_Q^2(x) = \sum_r \sigma_r^2(P_{dyn}) \cdot q_r^2(x) \quad (3.26)$$

and

$$\sigma_M^2(x) = \sum_r \sigma_r^2(P_{dyn}) \cdot m_r^2(x) \quad (3.27)$$

where $\sigma_r^2(P_{dyn})$ = the variance of the dynamically magnified mode component of load for the r th mode;

$$= \int_0^\infty |\chi_r(n)|^2 |J_r(n)|^2 S_{p_0}(n) \cdot dn$$

and $q_r(x)$ and $m_r(x)$ are the shear force and bending moment due to unit r th mode load component at station x .

Similar expressions can be written for the spectra of the shear forces and bending moments.

It is evident that the data required for evaluating the above expressions are:

1. the spectrum of the loads at some reference point;
2. the cross-spectrum of loads for pairs of points along the length of the beam;
3. the modes and natural frequencies of the beam;
4. the mechanical magnification of the beam for the various modes; (this necessitates knowing the damping in the structure).

4.0 PROPERTIES OF ATMOSPHERIC TURBULENCE

4.1 GENERAL

The properties of atmospheric turbulence required in the analysis of the wind loads on the tall mast and suspension bridge are those that arise naturally in the statistical theory of turbulence. This theory originated in an isolated paper by G. I. Taylor in 1922, discussing the problem of diffusion in the atmosphere. Part of the aim was to deduce the properties of the mean flow from the statistical properties of the turbulence, rather than by direct observation and empirical inference. It was shown that the motion of particles of air was essentially random and analogous to the Brownian motion of small particles due to molecular collisions.

In the period between the wars, very little direct use was made of the statistical theory in studying wind structure; the empirical approach still remained the principal weapon of attack. It is interesting to note, however, that one of the first applications of statistical concepts to wind structure was made by Giblett and others (including, notably, Durst) in the period 1925 - 1932 at the Royal Airship Works at Cardington. (see Giblett - 1932). Occasions of high wind were studied with the aim of obtaining basic knowledge from which the wind loads on airships might be assessed. Had interest in airships lasted, enabling these experiments to be continued, the value of statistical theory in determining the dynamic wind pressures on other structures might have been realised earlier.

In spite of this generally dormant interest in the statistical theory (at least insofar as meteorology was concerned), it nevertheless underwent considerable development during the prewar years 1935 - 1939,

due principally to the efforts of Taylor (1935) and von Karman (1937). One of the notions introduced by Taylor during this period was that of the spectrum of turbulence: this defined the contribution to the total turbulent energy made by fluctuations of different frequencies. To completely specify the turbulent fluctuations statistically it was, in general, necessary to define three velocity spectra at each point (one for each component of velocity), and also certain cross-correlation coefficients. The latter essentially measure the phase relationship between velocity components at different points, as well as the extent to which their association is random. For each particular wavelength they are defined by two components, one in-phase and the other in quadrature. For homogeneous, isotropic turbulence the picture is simplified.

Taylor also suggested that if the fluctuations are small compared to the magnitude of the mean velocity \bar{V} , then the time correlations between velocity components at a fixed point, for a time interval t , were the same as a spatial correlation between two points a distance $\bar{V}t$ apart. This fact was first demonstrated by Giblett (1932) and later by Panofsky et al (1958). Its usefulness in the present problem is that it enables certain spatial correlations to be inferred directly from their time correlations.

4.2 STATISTICAL DISTRIBUTION OF VELOCITIES

An important property of turbulence concerns the distribution of velocities. It appeared at an early stage that, in common with molecular motion, the distribution of velocities in atmospheric turbulence was Maxwellian, or very nearly so. This simply states that the probability of attaining a velocity at any instant between V and $V + dV$ is

$$f(V).dV = \frac{1}{\sqrt{2\pi}} e^{-x^2/2} . dx \quad (4.1)$$

and the probability of attaining a velocity less than V is

$$F(V) = \frac{1}{\sqrt{2\pi}} \int_{-\infty}^V e^{-x^2/2} dx. \quad (4.2)$$

where $x = \frac{V - \bar{V}}{\sigma(V)}$

and $\sigma(V) = \sqrt{V^2 - (\bar{V})^2}$

The function of the right hand side of 4.1 is the well-known "error function" and is illustrated in Fig. 8.1.

In these expressions $F(V)$ is defined as the distribution function of V , $f(V)$ the distribution density function, and $\sigma(V)$ the standard deviation of V while $\sigma^2(V)$ is the variance. From this it is seen that the distribution of velocity fluctuations can be completely defined from a knowledge of the mean and the variance.

The assumption that the velocity distribution is Maxwellian is important to the theory developed here. It has been observed to be true (or very nearly so) for sample times of the order of 10 minutes by a number of observers including Hesselberg and Bjorkdal (1929), Wagner (1929), Best (1935), Graham (1936) and Huss and Portman (1949).

4.3 PROPERTIES OF THE SPECTRA

4.3.1 General

At altitudes of 2000 ft. and greater, it is usually possible to make the simplifying assumption that the atmospheric turbulence is homogeneous and isotropic. Unfortunately the same is not true nearer the

ground. Here the turbulence is generally non-isotropic and only homogeneous in the horizontal plane if the nature of the surface is uniform. This implies that not only are the spectra of the three components of velocity all different, but that they also vary with height above ground. The same applies to the cross-correlations of the velocity components at different points. It appears that very little simplification can be made, therefore, regarding the form of the spectra.

Fortunately, however, owing to the relatively simple "line-like" form of both the tall mast and the suspension bridge, and the fact that they are only significantly affected by transverse forces, the information required is somewhat reduced. In the first place, the tall mast is only likely to be affected by the lateral and longitudinal components of turbulence. This suggests that the information required for the analysis of this structure concerns:-

- a. the spectra of the longitudinal and lateral fluctuations and their variation with height above ground;
- b. the cross-correlations between these velocity components for different vertical separations and for different heights above ground.

The suspension bridge on the other hand is only likely to be affected by the wind components in a vertical plane, normal to the bridge axis. Since the maximum effects of the wind will probably occur in a more or less beam wind it follows that the longitudinal and vertical components are of main importance. Hence the important quantities here are:-

- a. the spectra of the longitudinal and vertical fluctuations and their variation with height above ground;
- b. the cross-correlations of the longitudinal and vertical fluctuations for different lateral separations and for different heights above ground.

General expressions for all the above quantities are not yet known. However, reasonably reliable estimates can, it seems, be made of the following:-

- a. the spectrum of the horizontal components of turbulence (i.e. lateral plus longitudinal);
- b. the spectrum of the vertical components of turbulence;
- c. the cross-correlation of the horizontal components for vertical separations;
- d. the "scales" of the longitudinal lateral and vertical components for longitudinal and lateral separations.

From these data it is believed that a good estimate can be made of the response of the various structures. Details of these follow below.

4.3.2 The Spectrum of Horizontal Gustiness

An expression proposed by Davenport (1961) for the spectrum of the horizontal components of gustiness in high winds at height z is

$$S_z(n) \cdot dn = 4.0 K \bar{V}_1^2 \frac{x}{(1+x^2)^{4/3}} dx \quad (4.3)$$

where $x = 4000 \frac{n}{\bar{V}_1}$ where $\frac{n}{\bar{V}_1}$ is in cy./ft.,

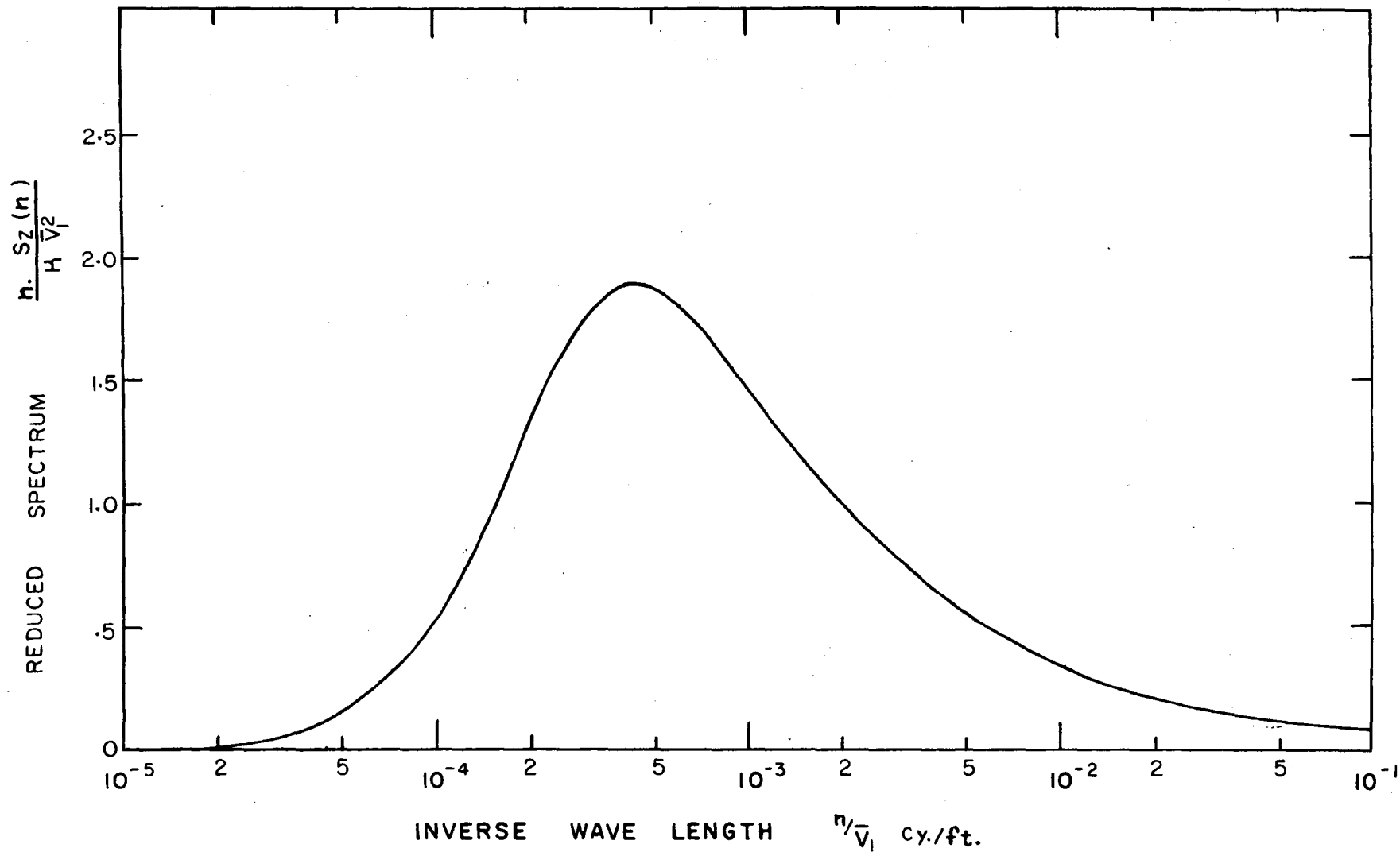
$Z_1 = 10m. (33 ft.)$ a standard reference height,

$\bar{V}_1 =$ mean (hourly) velocity at height Z_1 ;

and $K =$ the drag coefficient for the surface (referred to the mean velocity at height Z_1)

This expression was arrived at from the study of some 100 spectra for strong winds obtained at different heights and over different terrains, a large number of which are given in Appendix 2.

Values of the surface drag coefficient K are given in Table 2.1. It is found that the turbulent energy over a city might be expected to be about 12 times as great as that over open country, for the same surface velocity.



NOTE: $S_z(n)$ = SPECTRUM AT HEIGHT z AND FREQUENCY n
 \bar{V}_1 = MEAN VELOCITY AT REFERENCE HEIGHT $z_1 = 10\text{ m (33 FT.)}$
 H = SURFACE DRAG COEFFICIENT (REFERRED TO \bar{V}_1)

FIG. 4.1 SPECTRUM OF HORIZONTAL GUSTINESS

The general shape of the spectrum can be seen from Fig. 4.1, only in this instance an alternative representation is used - the product of the spectral density and the frequency. The advantage of this is that when represented on a logarithmic frequency scale - as is appropriate in the present case - the area under the curve still gives a true measure of the energy. This can be seen from the equality

$$n \cdot S(n) d(\log_e n) = S(n) \cdot dn$$

(This fact is particularly useful in planimetric integration.)

The following are particular features to note about the spectrum:

1. Almost all the energy is confined to wavelengths less than 5,000 or 10,000 ft. This implies that in a wind of about 60 mi./hr. the fluctuations with periods less than one or two minutes are small, and contribute little to the total energy.
2. The spectrum is proportional to the quantity $H \bar{V}_1^2$, which itself is proportional to the shear stress between the air and the ground. This implies that the turbulence is predominantly mechanical rather than convective in origin, which for high winds appears to be substantially true.
3. The inverse wavelength (i.e. wave number $\frac{n}{V}$) is used on the assumption that the spatial pattern of the turbulence remains invariant with change in mean wind velocity. This is true for example, of flow behind grids etc.

**PAGE
NUMBERING
AS
ORIGINAL**

4.3.3 Analysis of Severn Bridge Records

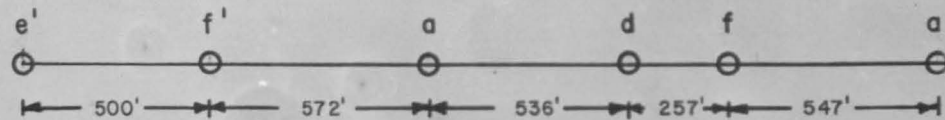
Reference has already been made to the wind-structure investigations carried out by Bailey and Vincent (1939) at the site of the Severn River railway bridge between Lydney and Sharpness. A photograph of the bridge is shown in Fig.4.2a. Fixed direction pressure-tube anemometers were mounted at intervals across the span covering a "front" of about 2,400 ft. The locations and groupings of the anemometers in the tests are shown in Fig. 4.2b, vertically below their actual locations on the bridge in the photograph above. The records obtained in these experiments provided a unique opportunity to compare the generalized spectrum of gustiness obtained above with the spectrum of gustiness at an actual bridge site. (The site is, in fact, only about four miles upstream of the projected 3,240 ft. span Severn River suspension bridge, and the wind properties there might be expected to be similar.)

In the experiments the anemometers were grouped in fours (as shown in Fig. 4.2b) and observations covered three separate recording periods each of about 4 1/2 minutes. A total of twelve anemometer runs were therefore available for analysis. From the original records, published by Bailey and Vincent, the mean wind velocity during consecutive two second intervals was estimated. Spectra were computed for each run using the auto-correlation technique (see Panofsky and McCormick - 1954; also Davenport - 1961), and the results plotted in Fig. 4.3. The mean wind velocity during the observations was 41 mi./hr. and the direction south-west - at right angles to the bridge.

Owing to the rather small number of readings in each run the statistical reliability of the spectral estimates is not high; in fact, there are no irregularities in the form of the spectra that cannot be



FIG. 4.2a VIEW OF SEVERN BRIDGE LOOKING N.E. FROM SHARPNESS.



ANEMOMETER	{ RUN 1 5.08 - 5.12 ³ / ₄ a.m. ✓ " 2 6.02 ¹ / ₂ - 6.07 a.m. " 3 6.13 - 6.17 ³ / ₄ a.m. ✓	✓			✓	✓
GROUPS		✓	✓	✓	✓	
14 JAN. 1934		✓			✓	✓

FIG. 4.2b LAYOUT OF ANEMOMETERS AND TEST GROUPINGS USED.

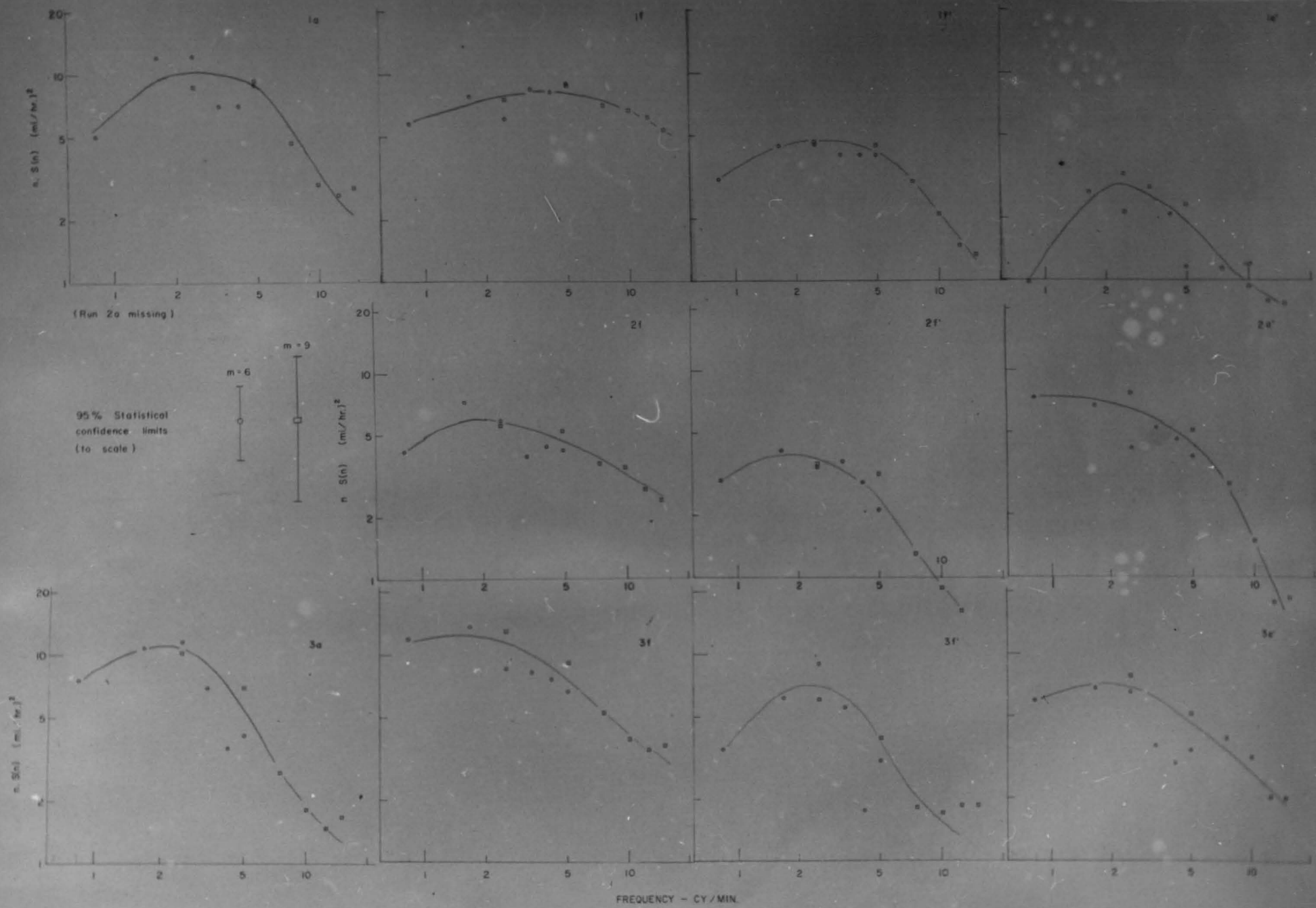


FIG. 4.3 SPECTRA OF LONGITUDINAL VELOCITY AT SEVERN BRIDGE (FROM RECORDS BY BAILEY AND VINCENT)

explained in terms of sampling errors (the 95% confidence limits are shown.). To improve the reliability, the results for all runs have been added together and averaged, and replotted in Fig. 4.4; the resulting spectrum is much smoother.

Also shown in Fig. 4.4 is the generalized spectrum of horizontal gustiness (given in equation 4.3) with the surface drag coefficient taken as .003, so as to fit the data. The agreement with the observations is seen to be most satisfactory, both with regard the general shape of the spectrum and the position of the peak.

Before going further, however, it should be observed that whereas the generalized spectrum refers to both horizontal components of gustiness, the experimental results refer to the longitudinal component only (the anemometers were fixed in the approximate direction of the mean wind). Before any comparisons are made, therefore, it is pertinent to comment on the probable nature of the two horizontal components of gustiness. Some previous results, obtained from Giblett's Cardington records (see Davenport - 1961), suggested that in high winds the lateral component contains about half or two-thirds as much energy as the longitudinal component; there was no suggestion that the general shapes of the spectra for the two components are significantly different. If this is the case, as seems reasonable, then the spectra for the combined horizontal components should be about $1 \frac{1}{2}$ - $1 \frac{2}{3}$ times the spectra of the longitudinal component only. Thus if the experimental results are augmented by this amount - as an estimate of the spectrum of both horizontal components - we would have had to choose $K \approx .005$ to make the generalized spectrum fit, and is therefore the proper value to consider. In view of the open exposure of this wide estuary in the

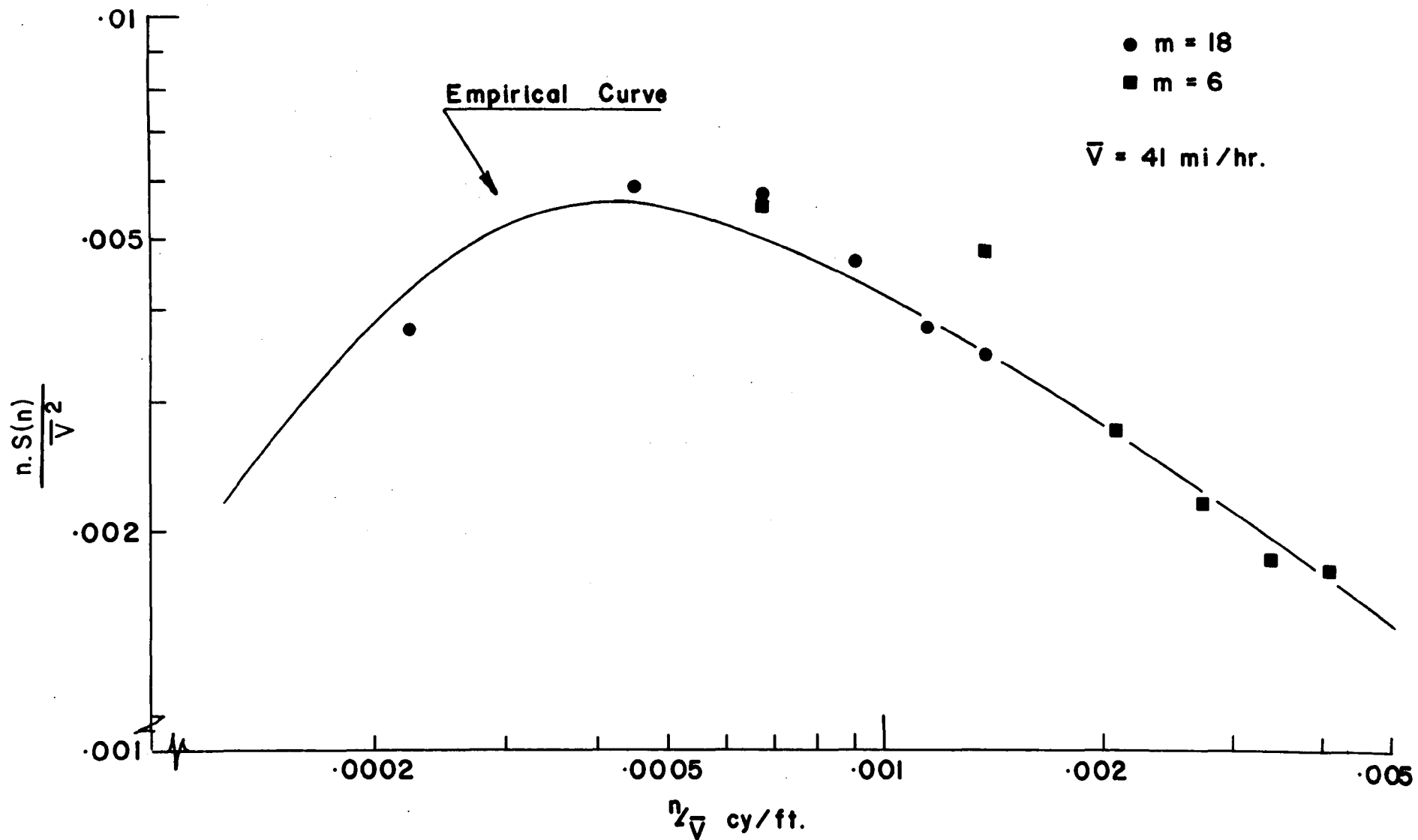


FIG. 4.4 SPECTRUM OF LONGITUDINAL VELOCITY COMPONENT AT SEVERN BRIDGE
 (AVERAGE FOR ALL RUNS) COMPARED WITH EXPRESSION FOR SPECTRUM
 OF COMBINED HORIZONTAL VELOCITY COMPONENTS ($\beta = .003$)

direction of the prevailing west to south-westerly winds, together with the rolling and treed farmland on either bank, this value for K agrees well with the values given in Table 2.1.

It seems fair to conclude from this evidence (although only obtained from one storm) that the suggested expression for the spectrum of horizontal gustiness is applicable to a site such as that at the Severn Bridge and that the appropriate value of K should be taken as approximately 0.05.

During the preliminary investigations for the new Severn suspension bridge a number of other records were made at the same site, using synchronized anemometers. These were kindly loaned to the writer by the consulting engineers for study. Unfortunately the recording apparatus was too heavily damped, and the time scale of the charts insufficiently expanded to allow any estimate to be made of the spectrum in the region of greatest energy. The records were however used to check the form of the spectrum in the region of the low-frequency "spectral gap", and did in fact confirm its existence in the instance of the very severe storm studied (mean winds 60 mi./hr. for 12 hours or so) - (see Davenport - 1961).

4.3.4 The Spectrum of Vertical Gustiness

A general expression for the spectrum of the vertical velocity component, suggested by Panofsky and McCormick (1959), is

$$S_w(n) dn = 1.1 \bar{V}_1^2 \frac{df}{(1+4f)^2 \log^2 z_1/z_0}$$

(4.4)

where $f = \frac{\pi z}{V}$ - the ratio of height to wavelength,

\bar{V}_1 = a reference velocity at height Z_1 ,

Z_0 = the roughness length.

From Prandtl velocity profile, taking von Karman's constant as 40

$$\frac{\bar{V}_1^2}{\log_e^2 Z_1/Z_0} = \frac{1}{(.40)^2} K \bar{V}_1^2$$

where K is the drag coefficient of the surface, referred to the mean velocity at the 10m. height, \bar{V}_1 , as in the horizontal spectrum.

Rewriting, the logarithmic form of the spectrum is

$$n S_w(n) \approx 6 K \bar{V}_1^2 \frac{f}{(1 + 4f)^2} \quad (4.5)$$

The form of the spectrum is shown in Fig. 4.5. The form differs somewhat from the horizontal spectrum insofar as the vertical scale of the disturbances appears to be governed by the height above ground.

4.3.5 Cross Correlation Coefficients

As already noted, both the phase relationship and the degree of association (i.e. randomness) between the velocity components at different points in the flow, are measured by the cross-correlation coefficients. These are complex quantities: that is to say they contain two components, one of which measures the in-phase correlation and the other the quadrature correlation. Only when both these components are zero or near zero is the relationship totally random. Since a structure responds differently to each frequency, it is necessary to know the cross-correlation coefficient for each frequency separately.

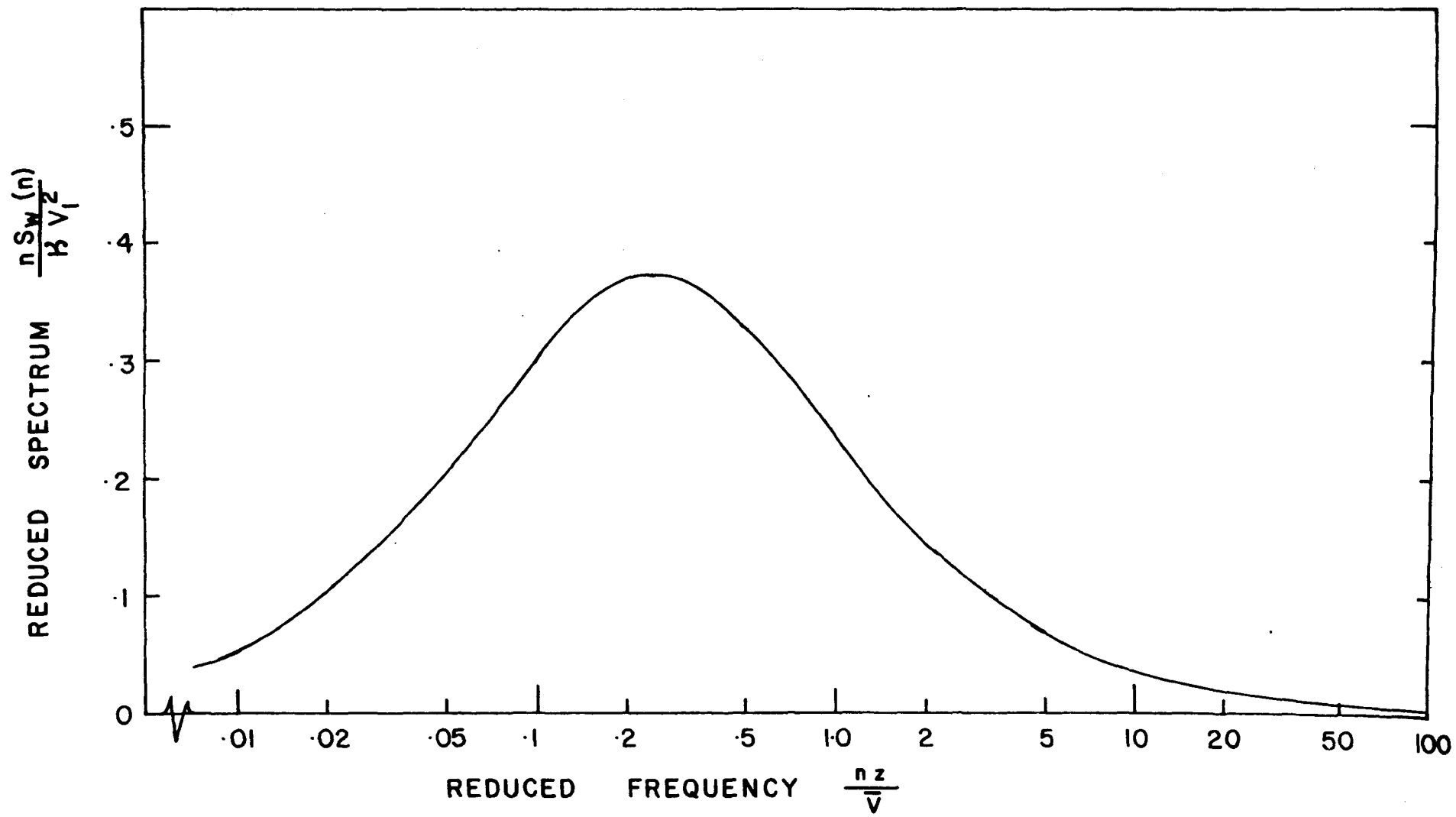


FIG. 4.5 SPECTRUM OF VERTICAL GUSTINESS (AFTER PANOFSKY)

The cross-correlation between the velocity components at two points x and x' and at frequency n is given by

$$R_{x,x'}(n) = \frac{C_{o_{xx'}}(n) + i Q_{v_{xx'}}(n)}{\sqrt{S_x(n) S_{x'}(n)}} \quad (4.6)$$

where $C_{o_{xx'}}(n)$ = co-spectrum at frequency n of velocities at x and x' (the in-phase component),

$Q_{v_{xx'}}(n)$ = the quadrature spectrum at frequency n of velocities at x and x' ,

$$i = \sqrt{-1}$$

and $S_x(n), S_{x'}(n)$ = the spectra at x and x' respectively.

It has already been noted that the spectrum of the horizontal components of turbulence is more or less invariant with height. Furthermore, although the vertical velocity spectrum does vary with height, it is only required in the suspension bridge problem in which the height of the deck is more or less uniform. Hence in the problems we are considering

$$S_x(n) = S_{x'}(n) = S(n)$$

If we write for the cross spectrum

$$S(x,x';n) = C_{o_{xx'}}(n) + i Q_{v_{xx'}}(n)$$

then

$$R_{xx'}(n) = \frac{S(x,x';n)}{S(n)} \quad (4.7)$$

which is the form in which it appeared in Section 3. The square of the modulus, $|R_{xx'}(n)|^2$, is sometimes called the "coherence".

In nearly all the problems we need to consider the mean wind is at right angles to the "beam" axis. In the case of the mast it is always so, and it represents the most serious loading condition for the suspension bridge. Under these circumstances it appears that the quadrature

component can be neglected and the cross-correlation coefficient over the region of high correlation represented by a simple expression of the type

$$R_{xx'}(r) = e^{-\frac{|x-x'|}{L(\bar{v}_n)}} \quad (4.8)$$

where $L(\bar{v}_n)$ is termed the "scale" of the turbulence and is a function of the wavelength (\bar{v}_n) .

Putting the separation $x-x' = \Delta x$ it is seen that

$$\int_0^{\infty} R_{\Delta x}(r) d(\Delta x) = L(\bar{v}_n) \quad (4.9)$$

The scale therefore can be thought of as the average dimension of a disturbance of given wavelength.

Some results quoted by Cramer (1958) for the "scales" of the horizontal components of turbulence are shown in Fig. 4.6, as functions of the wavelength \bar{v}_n . The results were obtained in open grassland. Only the cross-wind scales for stable stratification are shown: for unstable conditions the cross-wind wind scales are stated to be more or less of the same magnitude as the down wind scales. From this diagram it would appear that the crosswind wind "scales" can be represented quite adequately by

$$L\left(\frac{\bar{v}}{n}\right) \approx \frac{1}{50} \frac{\bar{v}}{n} \quad \text{in stable conditions} \quad (4.10)$$

and

$$L\left(\frac{\bar{v}}{n}\right) \approx \frac{1}{7} \frac{\bar{v}}{n} \quad \text{in unstable conditions} \quad (4.11)$$

The question of which of these expressions is the more appropriate in high winds needs to be considered. Although there is not yet much information available, the indications are that in high winds the turbulence structure tends more to resemble that in fairly stable conditions,

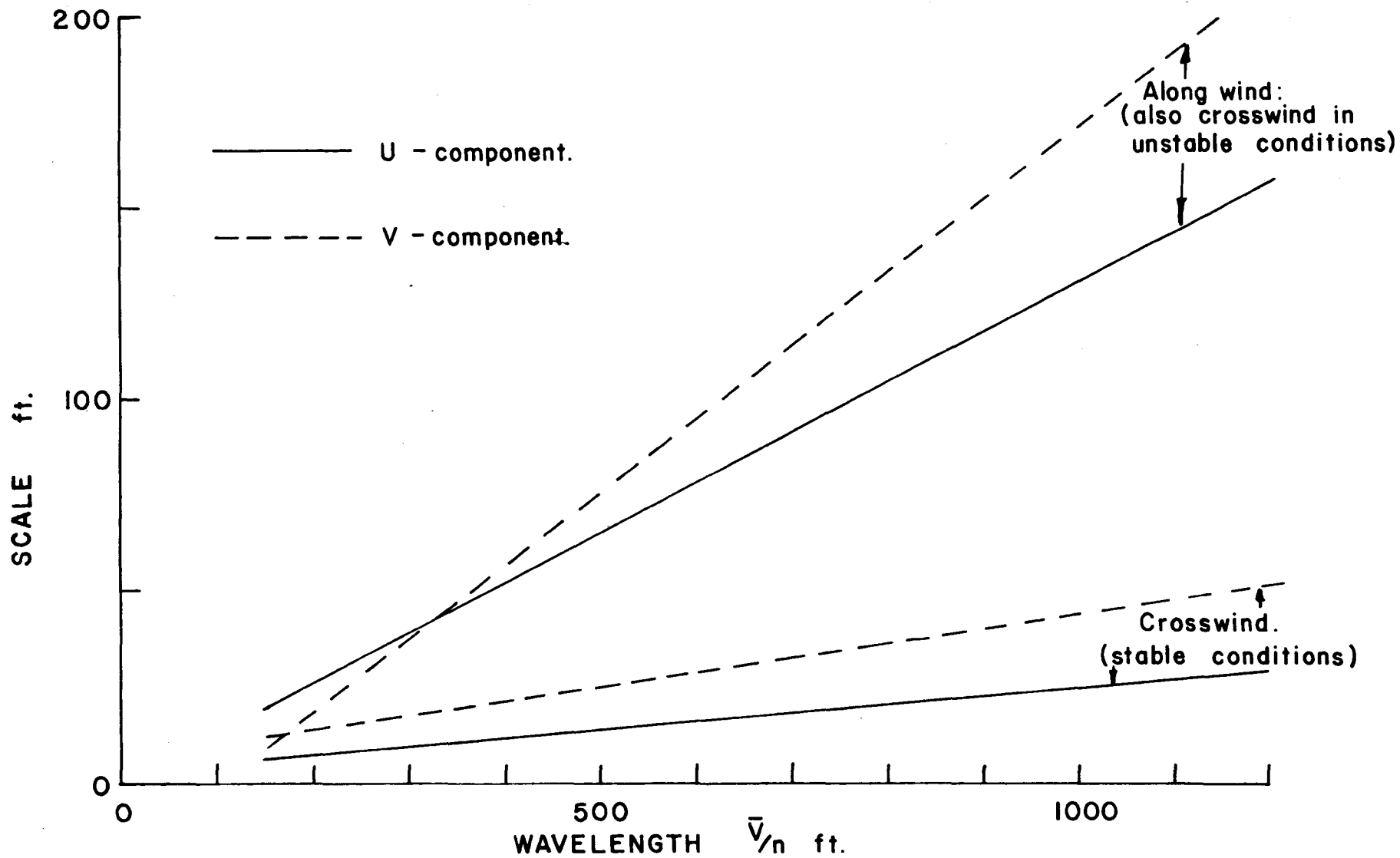


FIG. 4.6 SCALES OF TURBULENCE FOR HORIZONTAL COMPONENTS OF WIND VELOCITY AS FUNCTION OF WAVELENGTH (AFTER CRAMER)

insofar that, on the whole, the disturbances are elongated in the direction of the wind. Cross-correlation results obtained from Bailey and Vincent's (1939) Severn Bridge records of wind velocity at various points across the span, tend to suggest that the lateral scale of the longitudinal velocity component is about one third of its longitudinal scale.

However, in the present state of our knowledge it seems advisable to take the more conservative estimate (i.e. the value producing the higher correlation) and assume the value for the crosswind scale in unstable conditions. The cross-correlation coefficient then becomes

$$R_{\Delta x}(n) = e^{-7 \frac{\Delta x \cdot n}{\bar{v}}} \quad (4.12)$$

The same expression is assumed for the lateral correlation of the vertical component of turbulence.

4.3.6 The Vertical Correlation of the Horizontal Components of Turbulence

Fig. 4.7 shows the correlations for various frequencies between the horizontal velocity components at pairs of stations on a 500 ft. vertical mast. (The results are those obtained by Davenport (1961) from some records of strong wind kindly made available by Deacon of the Commonwealth of Australia Scientific and Industrial research Organization). Both the in-phase and quadrature correlations are shown. Unlike the correlation in the horizontal, crosswind direction, the correlation in the vertical direction gives rise to a non-zero quadrature component. This is not surprising since the flow is non-isotropic in the vertical direction due to the presence of the ground.

The quadrature correlation is generally much smaller than the in-phase correlation, at least, for the longer wavelengths, (i.e. smaller wave numbers) which are the only ones having a significant correlation.

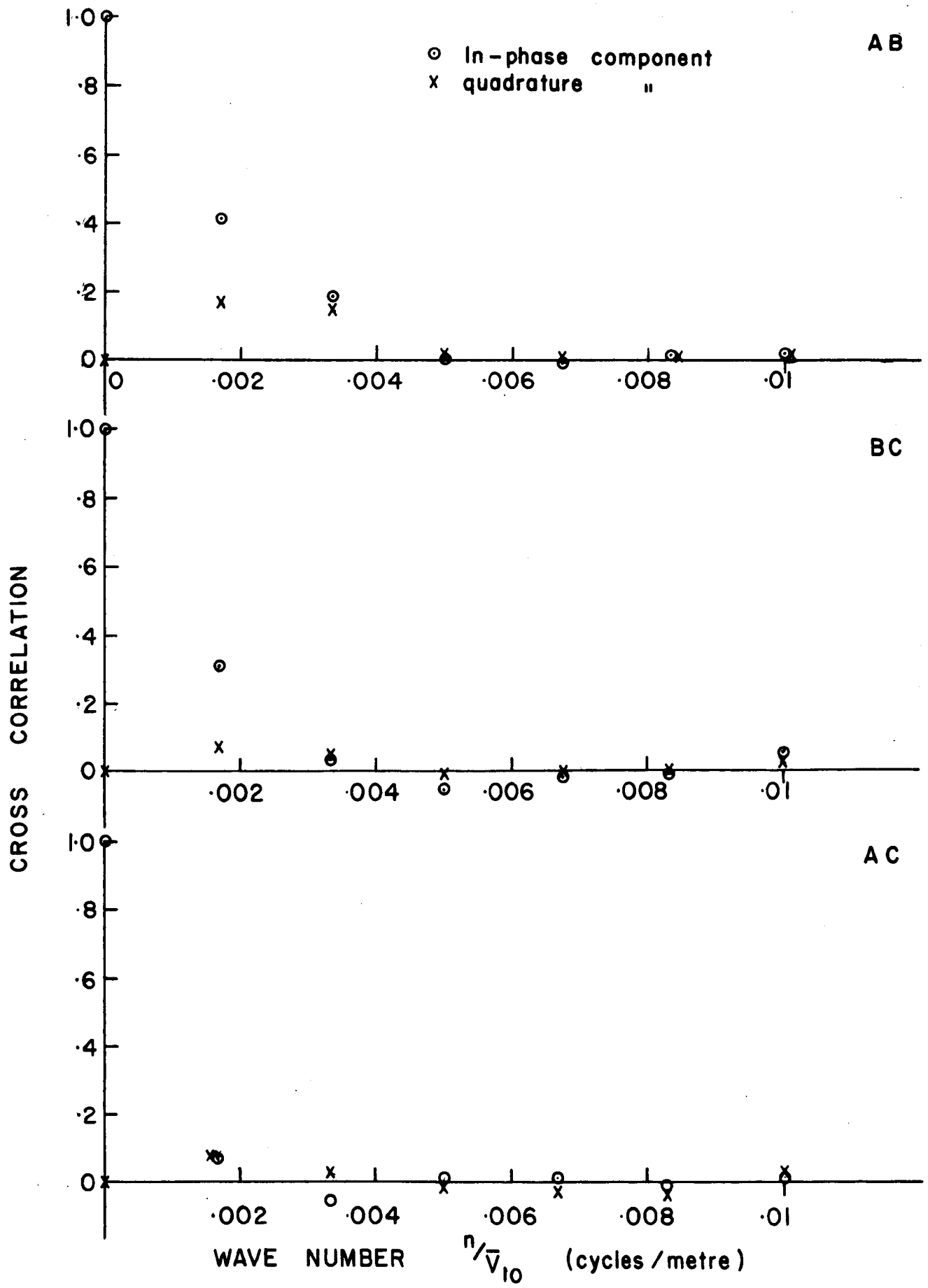


FIG. 4.7 CROSS CORRELATION SPECTRA FOR STATIONS ON A VERTICAL MAST.

It seems reasonable therefore, either to neglect the quadrature correlation (which only introduces an additional complexity into the calculations) or, better still, to use the square root of the coherence (as defined above in section 4.3.5). The square root of the coherence between the three stations on the mast are shown together in Fig. 4.8 and are expressed as a function of the separation to wavelength ratio. (i.e. $\frac{n \Delta z}{V}$). From dimensional arguments it might have been supposed that the coherence of the horizontal components in the vertical direction might also depend on the ratio of the height to the wavelength ($\frac{n z}{V}$). The results shown in Fig. 4.8, however, tend to indicate that the height variation, if present, is fairly small. The fact that there was little variation in the horizontal velocity spectrum with height would itself tend to support this. For the present purposes it would seem that over the region of significant correlation we can write

$$\sqrt{\text{Coherence}} = e^{-c \frac{\Delta z \cdot n}{V}}$$

where $c \approx 7$, as in the case of the horizontal cross-correlations in the horizontal directions. It will therefore be assumed that the "narrow-band" cross-correlation coefficient of the horizontal velocity component in the vertical direction is

$$R_{\Delta z}(n) = e^{-7 \frac{\Delta z \cdot n}{V}} \tag{4.13}$$

which is in fact the same expression as equation 4.12.

4.4 REMARKS ON THE STRUCTURE OF TURBULENCE NEAR THE GROUND

At present very little can be said with certainty regarding the structure of the turbulence near the ground. Although, as described, a

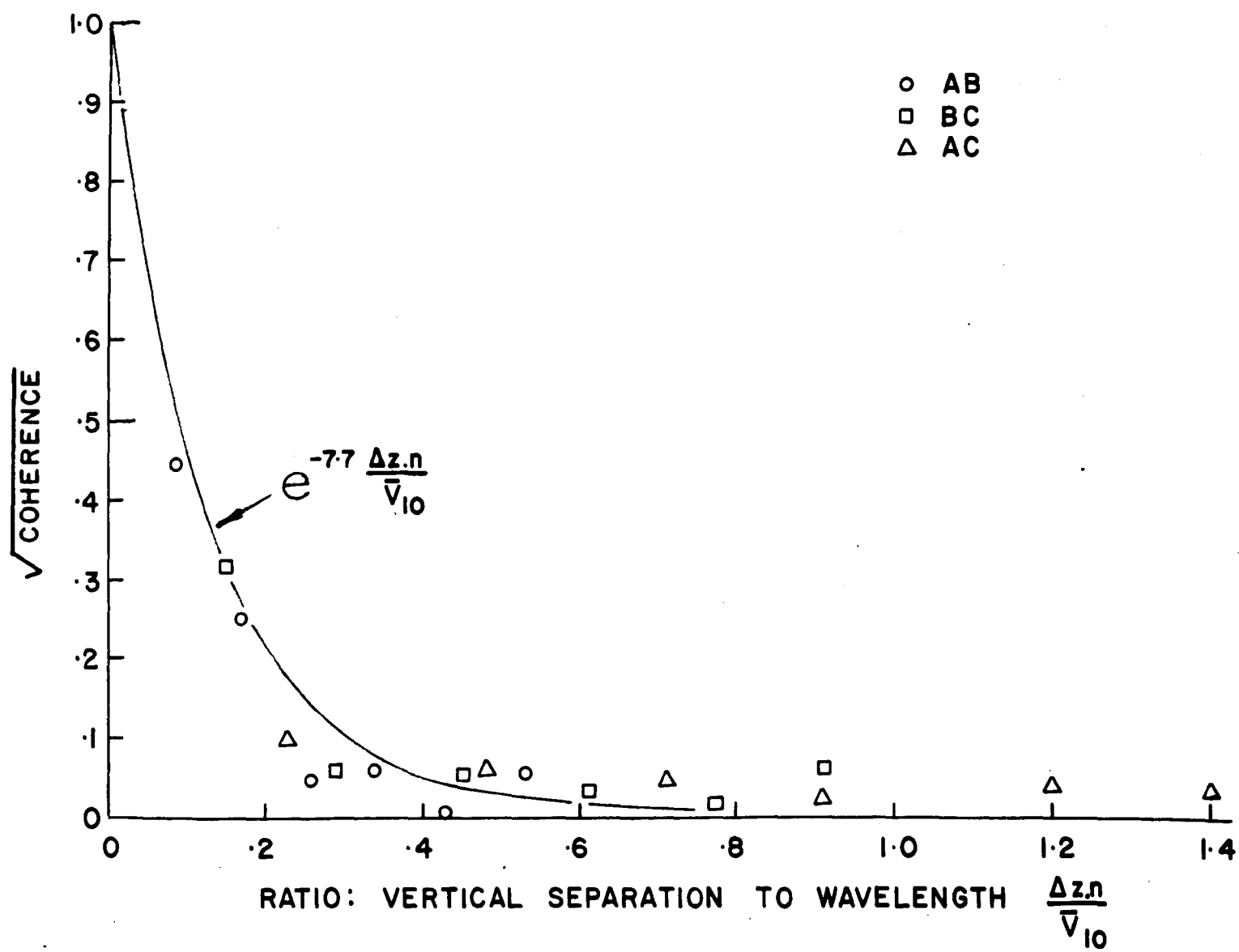


FIG. 4.8 SQUARE ROOT OF COHERENCE AS FUNCTION OF VERTICAL SEPARATION TO WAVELENGTH RATIO ($\frac{\Delta z. \eta}{\bar{V}_{10}}$)

certain amount of information is now available on the scale of the disturbances and on their spectra, this is not by any means adequate for inferring reliably the structure of the disturbances themselves. However, it is perhaps worthwhile to consider some of the possibilities, and in this respect recent wind tunnel investigations provide an interesting comparison.

In general, the similarity between turbulence in the wind tunnel and in the natural wind may be somewhat limited by the various factors, such as the thermal stability, the density gradient and the dynamic forces (e.g. the Geostrophic force due to the earth's rotation) which affect the wind but not the flow in the wind tunnel. However, in high winds, as already mentioned, thermal effects are not likely to be large and the dominant form of turbulence is likely to be mechanical in origin, as in the wind tunnel. If again we confine our attention to the so-called "constant-stress layer" the effect of the density gradient will be very small, and the dynamic forces due to the earth's rotation will be overshadowed by the shear stresses generated at the surface and transmitted upwards in the form of momentum exchange by turbulence. In the wind tunnel this "constant-stress layer" is roughly 5 - 6 cm. deep for the usual planed wooden surface: in the wind it extends to a height of 150 to 300 ft. depending on ground roughness.

Possibly the simplest notion concerning the structure of turbulence near a plane, but rough surface is that of a series of "roller-type" eddies, and this form of has been tentatively suggested by Webb (1955) in the case of the natural wind, and originally by Townsend (1956) in the case of the outer layer in the wind tunnel. More recently, however, Townsend (1957) has quoted some measurements which are

not generally consistent with this hypothesis, and has instead suggested that the motion consists of two dimensional jets which originate in the immediate neighbourhood of the wall surface. Such jets with their surrounding induced flow are shown diagrammatically in Fig. 4.9. This also indicates the deflection of the jet streamlines due to the velocity-height gradient. The slower longitudinal velocity in the jet (compared to that outside) is due to the transport upwards of the slower moving fluid near the surface. What determines the longitudinal scale of these jets is not known but possibly surface irregularities provide the principal control.

Now this postulated structure is in agreement with several observed features in the wind tunnel which the "roller" structure fails to account for. These include, inter alia:

1. the comparatively large scale of the longitudinal velocity component in the longitudinal direction and its apparent independence of height;
2. the smaller vertical velocity scale (particularly in the lateral direction) and its apparent proportionality to the height;
3. the displacement of the maximum correlation of the longitudinal velocity component in the vertical direction to a position which lies approximately along the mean of the postulated jets. In the wind tunnel this occurred along a line roughly at 45° to the mean flow which corresponds to the direction of maximum shear.

Comparing these results with those already described for high winds, a remarkable similarity is noted. First the comparatively large scale in the longitudinal (as compared to vertical) direction has already been noted, and is reflected in the different parameters used in the expressions for the spectra of the horizontal and vertical velocities.

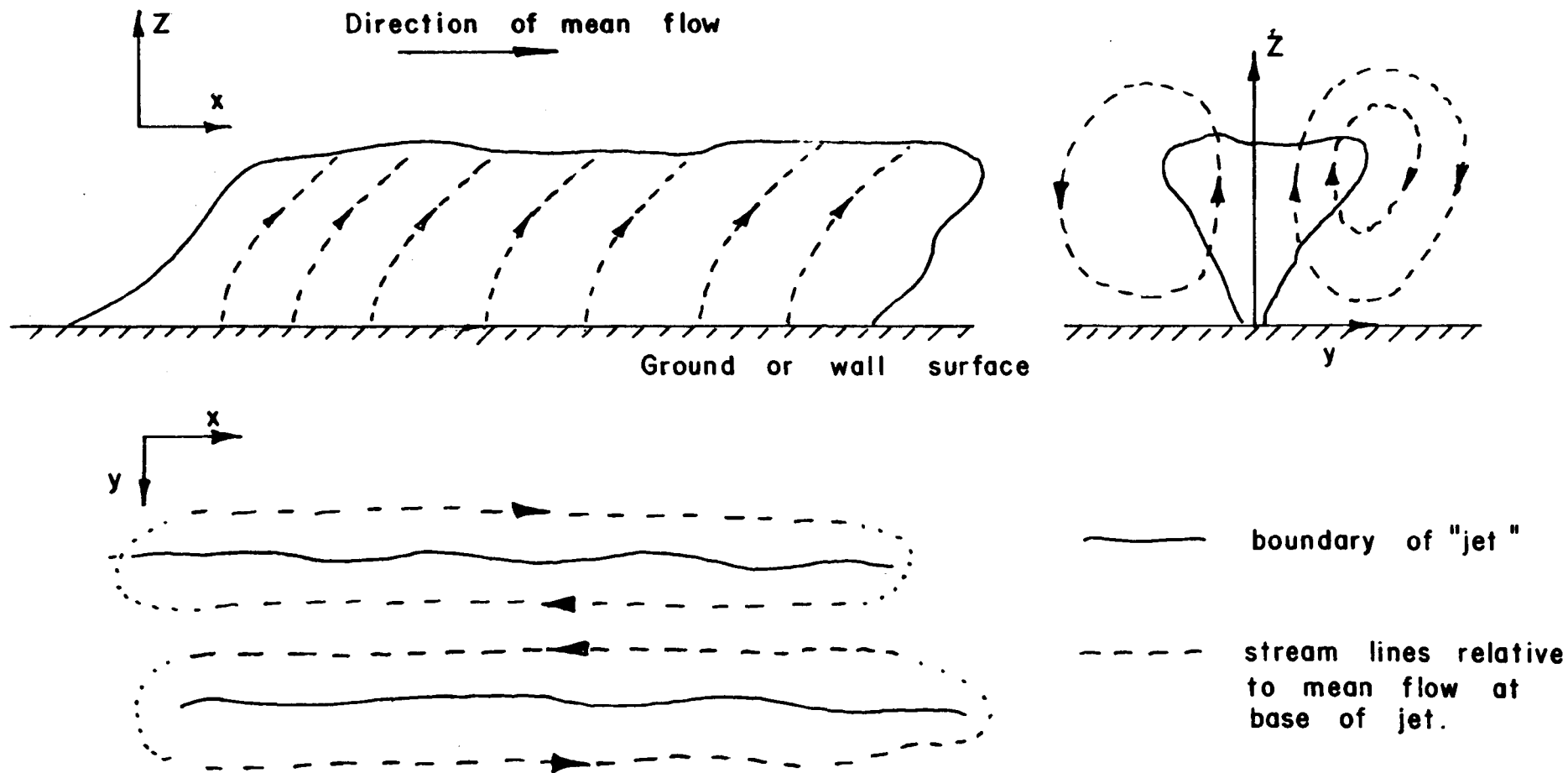


FIG. 4.9 STRUCTURE OF THE "TWO-DIMENSIONAL" JETS IN THE CONSTANT STRESS LAYER (AFTER TOWNSEND - 1957)

In the former the parameter used was $\frac{n}{V} L$, where L was another "scale" length which turned out to be about 4,000 ft. In the latter the parameter was $\frac{n z}{V}$ in which z was the height and therefore much less than 4,000 ft.

The above also indicates that the longitudinal scale is independent of height (as in 1) whereas the vertical scale is proportional to the height (as in 2). The third fact, the displacement of the position of maximum correlation of the horizontal components along approximately a 45° line, was in fact noted by Davenport (1961) in connection with correlations on a tall mast; it is the reason for the non-zero quadrature spectrum of the horizontal component in the vertical direction, which has already been noted.

These similarities between the properties of high winds, and of the flow in the wind tunnel appear hopeful from the point of view of establishing the structure of the wind under these conditions. However, when convection plays an important part, as it undoubtedly can when the wind speeds are lower, it could well be that the structure is then dominated by cellular convection cells with the general structure of roller type eddies. This would account for the very much larger lateral scales under unstable, convective conditions. (see Fig. 4.6).

Before any firm theories can be put forward, however, it would seem desirable to have a good deal more information than is at present available.

5.0 AERODYNAMIC RESPONSE TO FLUCTUATING FLOW

5.1 GENERAL

The general properties of the aerodynamic forces which arise on typical mast and bridge deck sections in a steady airflow are fairly well known and have been studied in a number of cases. Mast sections generally consist of lattice trusses of either square or triangular section, the principal members of which are usually round bars (to reduce wind drag) with flat members used for diagonal bracing. Wind tunnel tests on such structures have been described by a number of investigators (Schott et al - 1954; Cohen - 1958; Redwood - 1960). Sometimes for special reasons (usually to do with the signal pattern of the antenna mounted on the mast) circular cylindrical sections are used for the mast. Such is the case in a 700 ft. mast at Oldenburg, Germany (see Stahlban - 1956), and others in Canada described by Davenport (1959). For the cylinder, the aerodynamic characteristics in steady airflow are well known.

Since the collapse of the Tacoma Narrows Bridge, the open box truss has almost entirely replaced the plate girder as the stiffening truss of the suspension bridge. Not only does the box truss (with two levels of lateral wind bracing) provide the necessary torsional stiffness required to avoid catastrophic vibrations, but the open form of the truss is more stable aerodynamically. Static tests on bridge trusses have been described by Biggs (1954); Flachsbart (1932) and others and an exhaustive test on actual suspension bridge trusses for the Severn and Forth Bridges are described by Frazer and Scruton (1952).

5.2 RESISTANCE IN UNSTEADY FLOW

Most of the above tests have been carried out in the steady flow of a wind tunnel. There is, however, no reason why the drag (and lift) coefficients for steady flow should also apply to the fluctuating component of drag in fluctuating flow. In fact, there are good indications that under some circumstances they do not. For instance, Schwabe (1932) examined the flow induced round a cylinder started impulsively from rest, and found that the drag coefficient built up steadily to a value twice the steady state value after the mean flow had traversed nine diameters of the cylinder, as shown in Fig. 5.1. Bingham, Weimar and Griffiths (1952) obtained a somewhat similar result. In this case the cylinder was mounted in a shock tube, and the impulsive flow was induced behind a shock wave in front of an expanding body of gas. The latter found similar results with other structures such as walls and block shaped structures.

Another type of investigation into the drag of bluff objects in fluctuating flow was carried out by Keulegan and Carpenter (1958) and also McNown (1957). In the former of these experiments, the object was placed at the node of a wave generated in a wave tank. As a result the flow past the object executed almost harmonic motion with a velocity given by

$$V(t) = V_{\max} \sin 2\pi nt$$

The forces on the object were analysed and the principal component in phase with the velocity was related to the drag coefficient C_D , which was defined by the following

$$C_D = \frac{\text{Drag}}{\frac{1}{2} \rho \cdot V(t) \cdot |V(t)|}$$

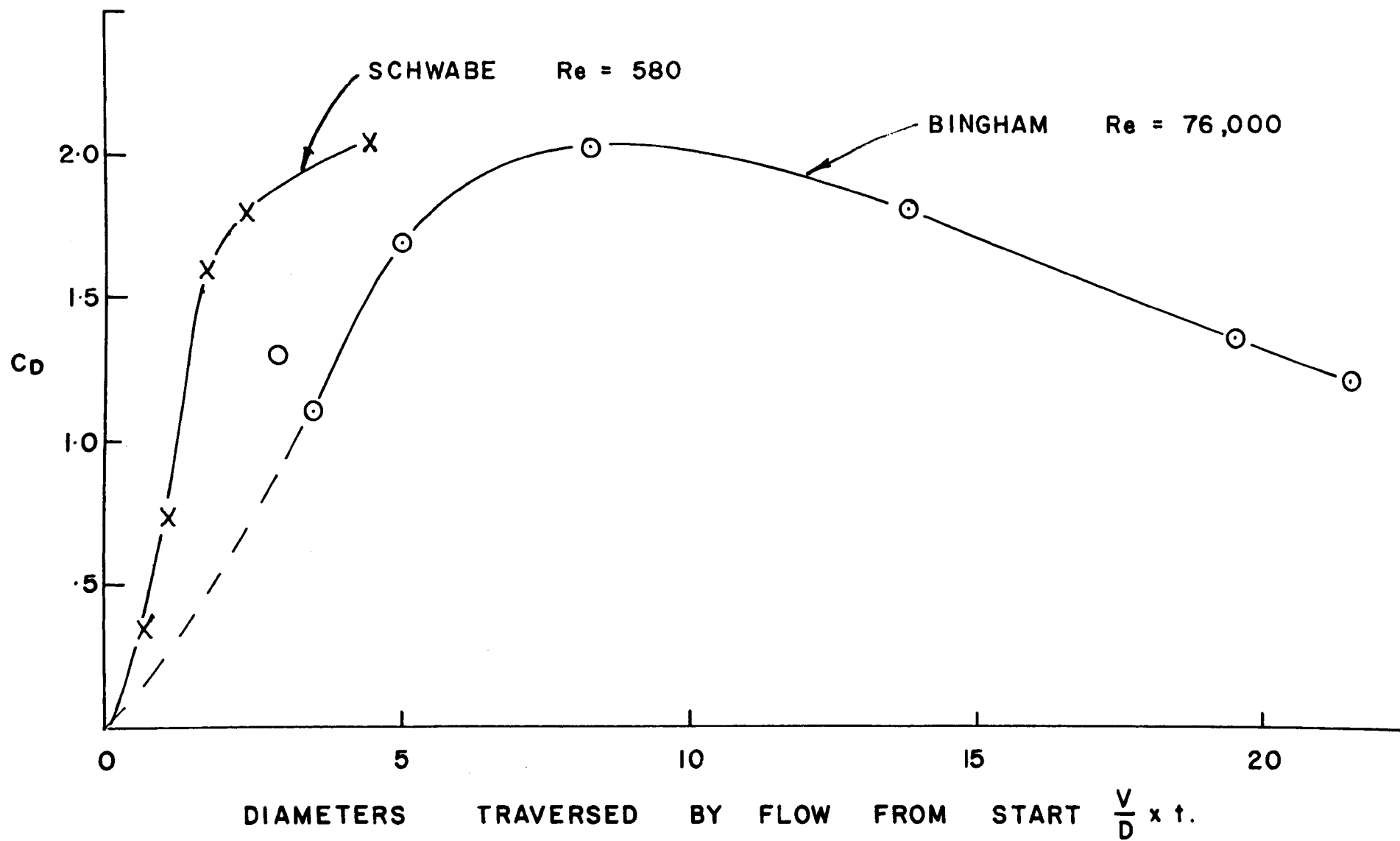


FIG. 5.1 DRAG COEFFICIENT FOR CIRCULAR CYLINDER IN IMPULSIVELY STARTED FLOW.

The values of C_D for the infinite flat plate and the circular cylinder obtained from these experiments are shown in Fig. 5.2, as a function of the dimensionless parameter $\frac{nD}{V_{max}}$.

The drag coefficient for the flat plate rises steadily with increase of this dimensionless parameter, to values three or four times as large as the steady flow values. The circular cylinder, on the other hand, rises to a maximum value of about 2.1 (twice the steady flow value) when $\frac{nD}{V_{max}} \approx .1$ and then drops off with further rise of the parameter.

It is interesting to note that if the average velocity during a half cycle is substituted for the maximum velocity, the peak is then found to occur when $\frac{nD}{V_{av}} \approx .2$. This is also the value for the frequency of eddy-shedding in a steady flow of velocity V_{av} . This hints to the possible mechanism causing this variation in the drag coefficient.

Other variations in the effective drag coefficient have been observed by O'Brien and Morison (1952) on spheres acted on by wave forces. In these experiments drag coefficients of over 3 were noted at Reynold's numbers for which the drag coefficient in steady flow is about .5.

Most significant of all, possibly, are some experiments by Schwarz and Corssin (1957) designed to test Lin's theory for the response of a simple pendulum to a turbulent flow. The latter was a straightforward application of the statistical concepts embodied in the stationary random series approach. Knowledge of the spectrum of the turbulence and of the mechanical response of the pendulum to fluctuating loads was used to predict the root mean square deflexion of the pendulum bob. This prediction was found to be some fourteen times less than the actual

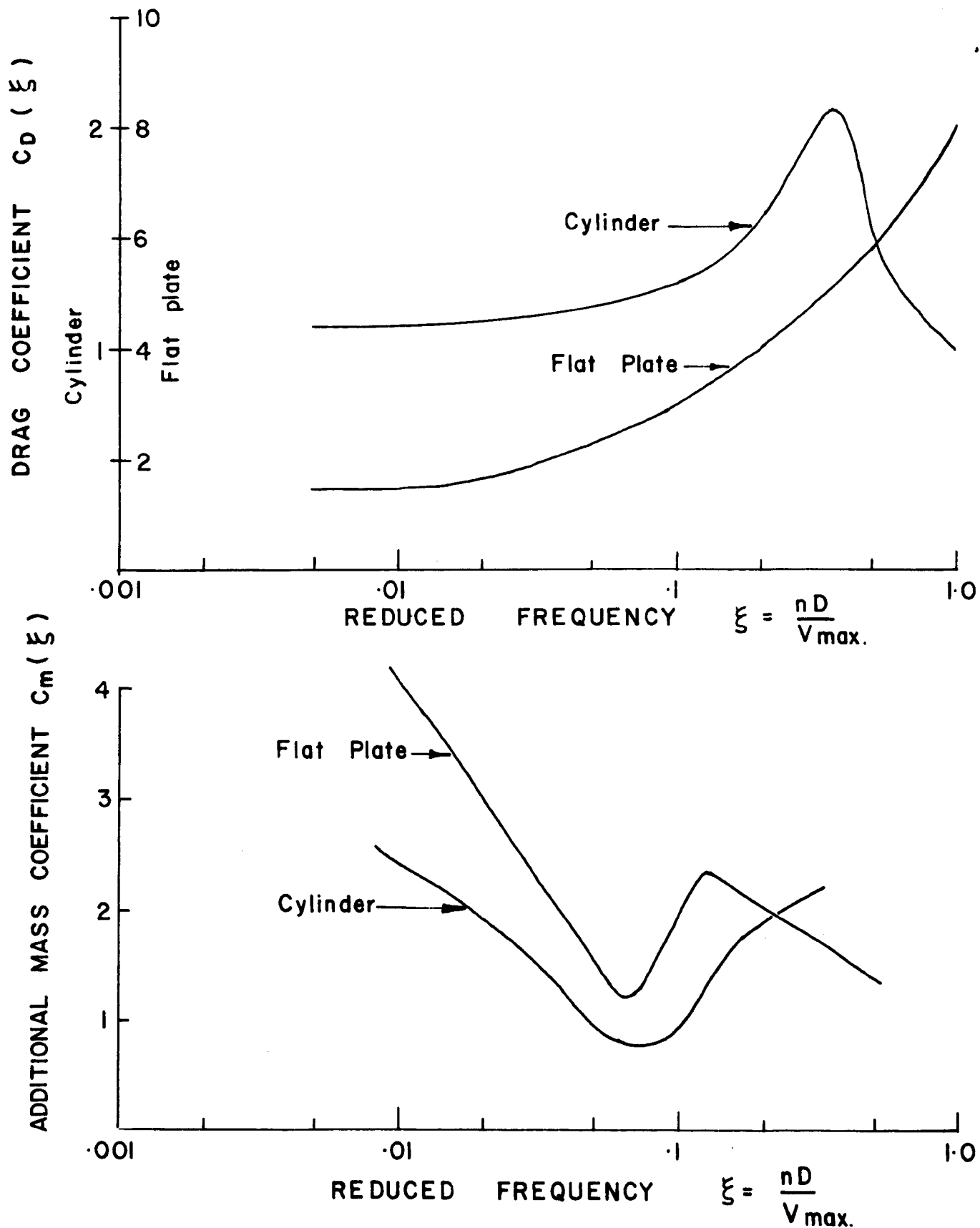


FIG. 5.2 DRAG AND ADDITIONAL MASS COEFFICIENTS FOR CYLINDER AND FLAT PLATE IN WAVE FLOW (AFTER KEULEGAN AND CARPENTER)

measured R.M.S. deflexion. This large discrepancy can no doubt be partly attributed to the fact that no account was taken of the eddy-shedding effect which would produce oscillations of the pendulum bob even in flow, free from turbulence. But more particularly it was also probably due to the fact that, in making their predictions, the steady value of the drag coefficient was used; this may very well have underestimated the response of the pendulum to certain frequencies present in the turbulence.

5.2.1 The Virtual Mass Effect

A further consequence of assuming that the wind is steady rather than fluctuating, is that the virtual (or additional) mass effect is neglected. This arises from the fact that any fluctuation in the air flow must be caused by a pressure gradient acting in the direction of the fluctuation. This pressure gradient will likewise act on the surface of any object placed in the flow, and, in addition, on a certain mass of air which effectively "clings" to the object rather than accelerate with the rest of the flow. The latter is referred to as the additional mass effect. The ratio of the effective mass of air "clinging" to the object, to the mass of a body of air equal in volume to the object itself, is known as the additional mass coefficient. For the flat plate, which theoretically has no volume, this coefficient is usually referred to the circular cylinder having the same diameter.

The importance of the additional mass effect is familiar to those concerned with such problems as the vibration of ships plating, the forces on piles under wave action, the movement of control surfaces in aircraft and in the landing resistance of flying boat hulls. Its possible bearing on the wind loading problem was first pointed out by

Feydayevsky and Belotserkovsky (1954). These authors showed that in a very sharp squall (such as one they examined which occurred in Moscow) the additional inertial forces could be just as large as the conventional drag forces. The assumptions used in this deduction, might however be regarded as somewhat severe, and as already remarked in Section 2.2 the incidence of these "freak" local storms at any particular place is small, on account of their very limited size. For these reasons it is believed that these large inertial forces are unrepresentative of general high wind-loading conditions. With the usual levels of turbulence present in high winds these inertial effects are believed to be quite small, and in the majority of cases, negligible.

A number of investigations have been carried out into the effect of acceleration on the resistance of bluff objects. (Frazer and Simmons - 1919; Stelson and Mavis - 1955). In particular, Keulegan and Carpenter also determined the virtual mass coefficient in the fluctuating flow of a wave tank. Their results are shown in Fig. 5.2 together with the drag results obtained in the same experiments, as a function of the dimensionless frequency parameter $\frac{nD}{V_{max}}$.

5.2.2 The General Problem

From the above it is evident that in considering the response of a structure to a fluctuating flow of any description, it is necessary to allow for the possible variations in the resistance not otherwise covered by simple quasi-static assumptions. In general this resistance in fluctuating flow can be expressed as

$$P(t) = \frac{1}{2} \rho \cdot C_D(n) \cdot V(t) \cdot |V(t)| + C_m(n) \rho \cdot \frac{A_o}{D} \cdot \frac{dV(t)}{dt} \quad (5.1)$$

where $P(t)$ = force per unit area and the object at time t ;
 $V(t)$ = velocity of the fluid at time t ;
 ρ = fluid density
 D = diameter of object
 A_0 = a reference area for the additional mass
 $C_D(n)$ = coefficient of drag (assumed to be a function of the
fluctuation frequency n)
 $C_m(n)$ = coefficient of additional mass (including the
equivalent mass of the fluid and the object itself) -
also assumed to be a function of n .

Clearly the problem of determining the resistance can be boiled down to that of determining the values of the effective coefficients of mass, C_m , and drag, C_D . The word effective is used since it is in fact difficult to divorce the coefficients from the characteristics of the flow itself, as is now discussed.

One of the simplest types of fluctuating flow is one in which the fluctuations are uniform throughout the fluid. This is another way of saying that the correlation of the velocity is unity for all points in the flow. For turbulent flow this is not the case, the fluctuations are both space and time dependent, and the correlation only reaches unity when the points are coincident.

Consider the response of a transverse "strip" or "salmon-slice" of a slender beam to these two distinct types of flow. The section of this beam can be represented by the bridge deck shown in Fig. 5.3, which has a breadth b and a depth D . The pressures on this slice will be determined by the flow characteristics in some limited region surrounding the section and its wake. For the sake of argument let us assume that this

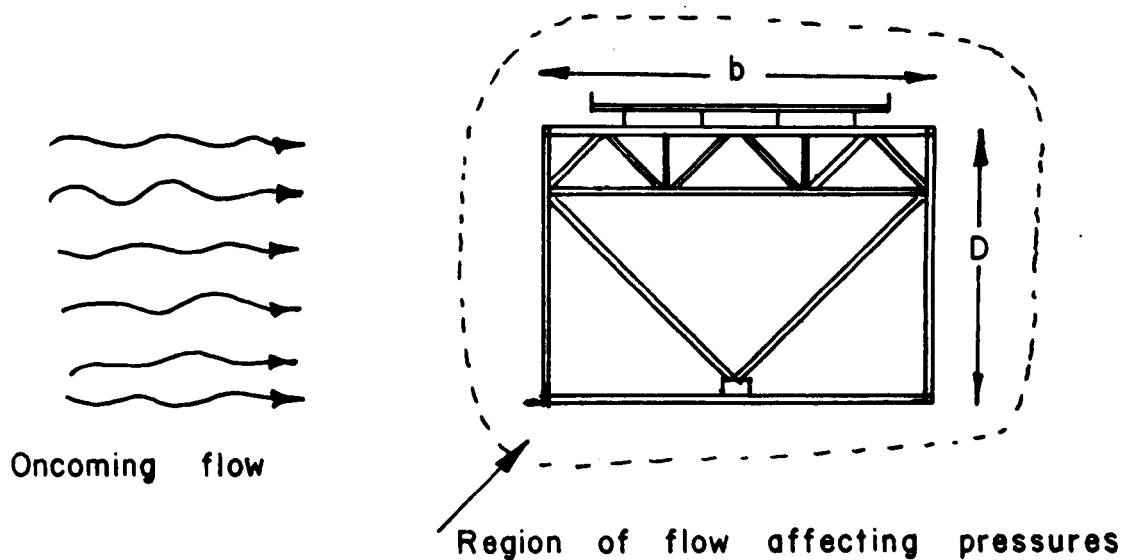


FIG. 5.3 DIAGRAM SHOWING POSTULATED REGION OF FLOW AFFECTING PRESSURE ON BRIDGE TRUSS.

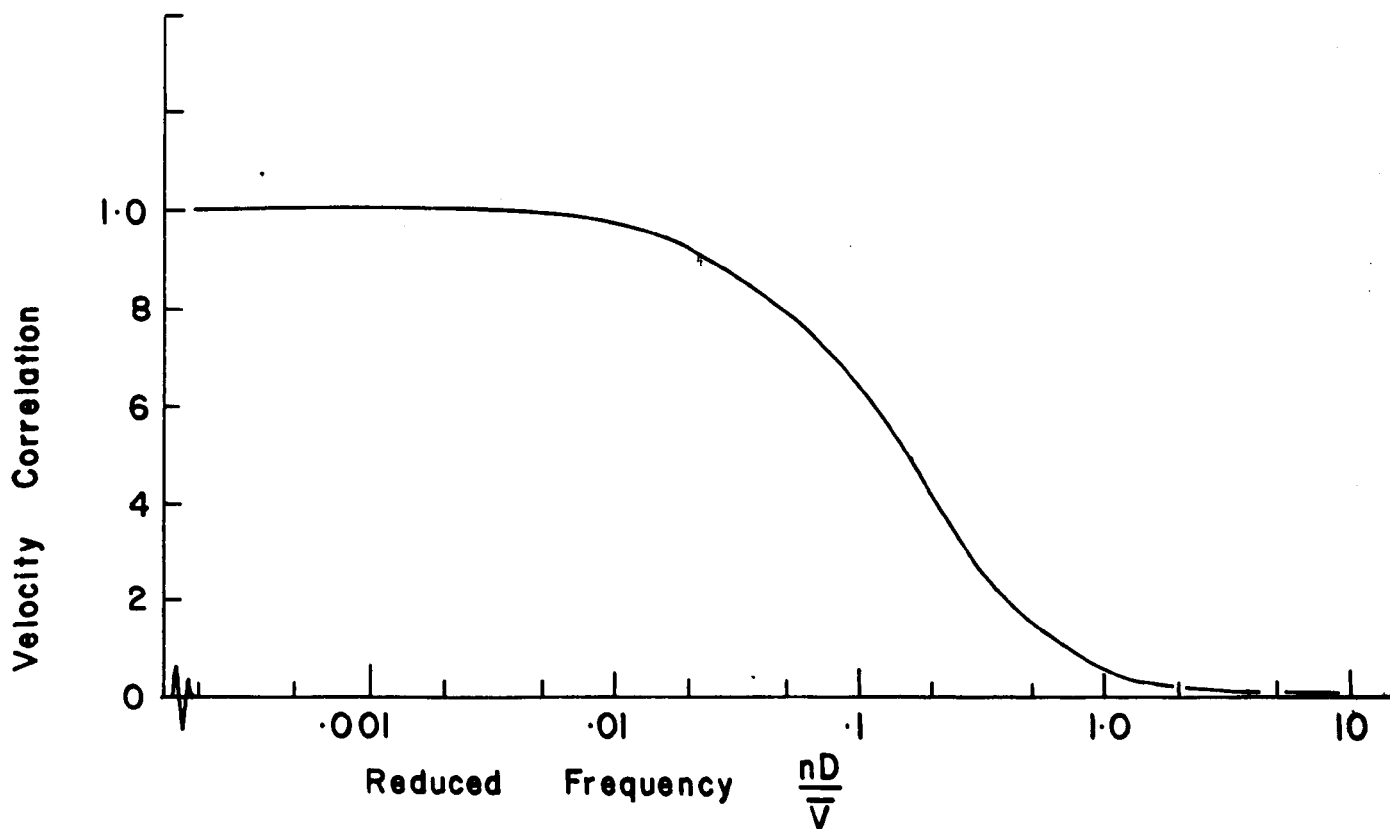


FIG. 5.4 VELOCITY CORRELATION OVER REGION OF FLOW AFFECTING PRESSURE AS FUNCTION OF REDUCED FREQUENCY.

region is approximately the size of the object itself. This is obviously conservative in the case of a "solid" body which disturbs the flow for a considerable region around, but it may be less so in a truss section, in which the drag is created by a lattice of small members each generating initially its own individual wake (which may merge later on). Let us also assume (for want of anything better) that the instantaneous force on the strip depends on the instantaneous average velocity in this region.

In uniform flow, the average velocity in the region is obviously also equal to the velocity at any point in the region. In turbulent flow, however, the average velocity differs from the velocity at a point owing to the variation in phase and randomness of the fluctuations within the region. The phase and randomness is, of course, measured by the velocity correlation of the type given in equations 4.12 and 4.13.

If we assume a correlation function of the type

$$R_{xx'}(\eta) = e^{-\frac{|x-x'|}{L(\eta)}}$$

where $L(\eta)$ is the "scale" of the fluctuations at frequency η , then the correlation over the whole area is of the form

$$C = \int_0^b \int_0^b \int_0^D \int_0^D e^{-\frac{|x-x'|}{L(\eta)}} e^{-\frac{|z-z'|}{L_z(\eta)}} dx \cdot dx' \cdot dz \cdot dz'$$

If, as in Section 4, we assume

$$L_x(\eta) \approx L_z(\eta) \approx \frac{1}{\eta} \frac{V}{\sqrt{7}}$$

and that $b = D$, then the form of the function is

$$C(\xi) = \frac{2}{(7\xi)^2} \left[7\xi - 1 + e^{-7\xi} \right] \quad (5.2)$$

where $\xi = \frac{\eta D}{V}$

This parameter $\frac{nD}{\bar{V}}$ is dimensionless and is termed the reduced frequency. The form of this function is shown in Fig. 5.4. It represents the ratio of the average mean square velocity over the entire region to the mean square velocity at a point in the region. From this it is seen that the function is negligibly small for reduced frequencies greater than about 1.0. This implies that even if the amplitude of fluctuations of this frequency are large in themselves, their effect on the bridge section as a whole is fairly small.

The conclusions that might be drawn from this are:-

1. that for reduced frequencies less than .1 the velocity fluctuations within the region of the flow likely to affect the pressures on the structure are fairly uniform: thus the resistance in turbulent flow at these reduced frequencies probably approaches that in uniform fluctuating flow;
2. that for reduced frequencies greater than 1, fluctuations in turbulent flow have negligible effect in inducing pressures on structures;
3. that for $.1 < \xi < 1$ there is a transition region in which the resistance diverges from the uniform flow result in 1, and decreases until it is negligible as in 2.

These conclusions suggested that although it might be a difficult problem to measure the fluctuating resistance in an actual turbulent flow, some useful insight might nevertheless be obtained by considering the resistance in a uniform fluctuating flow. To obtain as close an analogy as possible to the wind it would be necessary to superimpose the fluctuation on a mean flow. The resistance of bluff obstacles under these conditions does not appear to have been investigated.

As a first approach to this problem a "gust tunnel" with a 2 ft. x 3 ft. working section was built. A flow of air could be induced in the tunnel by blowing compressed air parallel to the tunnel walls through slits cut in pipes which ran the full height of the working section. It was intended to regulate the flow of compressed air in such a way as to produce controllable fluctuations in the tunnel flow itself.

It was later realized, however, that there was possibly a more direct way of determining the variation of the resistance coefficients with frequency. This was to attach the object to a heavy pendulum immersed in a steady flow, deflect the pendulum, and observe the decay of the oscillations due to the damping effect provided by the drag of the object moving through the fluid. A description of some experiments conducted on these lines now follows.

5.3 INVESTIGATION OF THE RESISTANCE OF BLUFF OBJECTS IN FLUCTUATING FLOW

5.3.1 Outline of Experiments

As noted, the aim of these experiments was to find the resistance of various bluff objects to a flow which (relative to the object) contained a fluctuating component of velocity. To produce the fluctuating component, the objects were mounted on a heavy pendulum which oscillated in a steady flow of water. The arrangement of the pendulum with the object attached is shown in Fig. 5.5, and a general photograph of the apparatus, in Fig. 5.6, shows the pendulum mounted above the long,

Fig. 5.6 Photograph showing the experimental arrangement of the pendulum suspended over the glass-sided flume with the object immersed in the flow. In the foreground can be seen the strain analyzer and oscillograph and, to the right of the object, the propellor and its supporting rod.

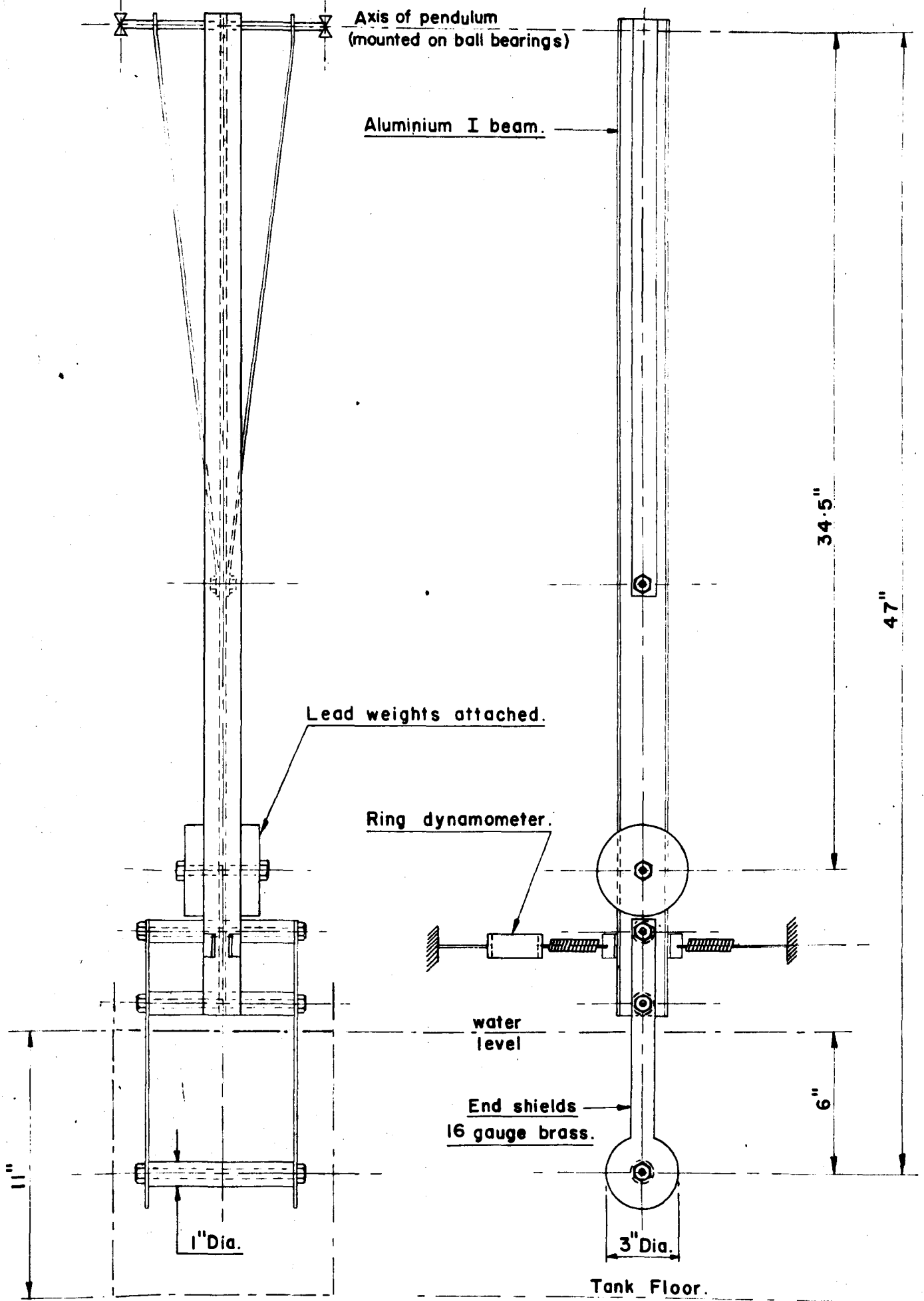


FIG.5.5 DIAGRAM OF PENDULUM FOR EXPERIMENTS ON FLUCTUATING RESISTANCE.



FIG. 5.6

glass-sided flume, (9 in. wide: 12 in. deep). The velocity and depth of flow in the flume could be adjusted by means of an inlet valve and a weir at the outflow. The water depth was kept between 10 in. and 11 in.: the object was then at the mid-depth.

The frequency of the pendulum could be altered either by adding heavy lead weights, or by varying the size of the springs fixed to the pendulum. Two stiffnesses of springs were used and two weights could be added, which, with the no-weight condition, enabled a total of six different weight-spring combinations to be arranged and thus six different pendulum frequencies. These frequencies ranged from approximately 1 cy./sec. to just over 4 cy./sec.

One of the springs attached to the pendulum was connected to a ring dynamometer as illustrated in Figs. 5.5 and 5.7. Strain gauges were attached to the ring in the conventional way, and were connected to form a bridge circuit, the output of which was amplified and fed into a pen oscillograph. The latter recorded the force in the spring which was, in fact, proportional to the deflexion of the pendulum. Thus the decay of oscillation which occurred when the pendulum was deflected and suddenly released could be recorded directly on the oscillograph. From the characteristics of the damping curve, both the additional mass and drag coefficients could be determined by a method described below. The only additional information required was the steady velocity of the water and the properties of the pendulum.

The velocity of the steady flow of water was measured by means of a small 1 inch diameter, plastic, three-bladed propellor similar to those found on miniature motor boats, (see Fig. 5.7). It ran on a

Fig. 5.7 Close-up of the lower end of the pendulum showing the object mounted between end-shields, the lead weights attached and the springs connected to the ring dynamometer.

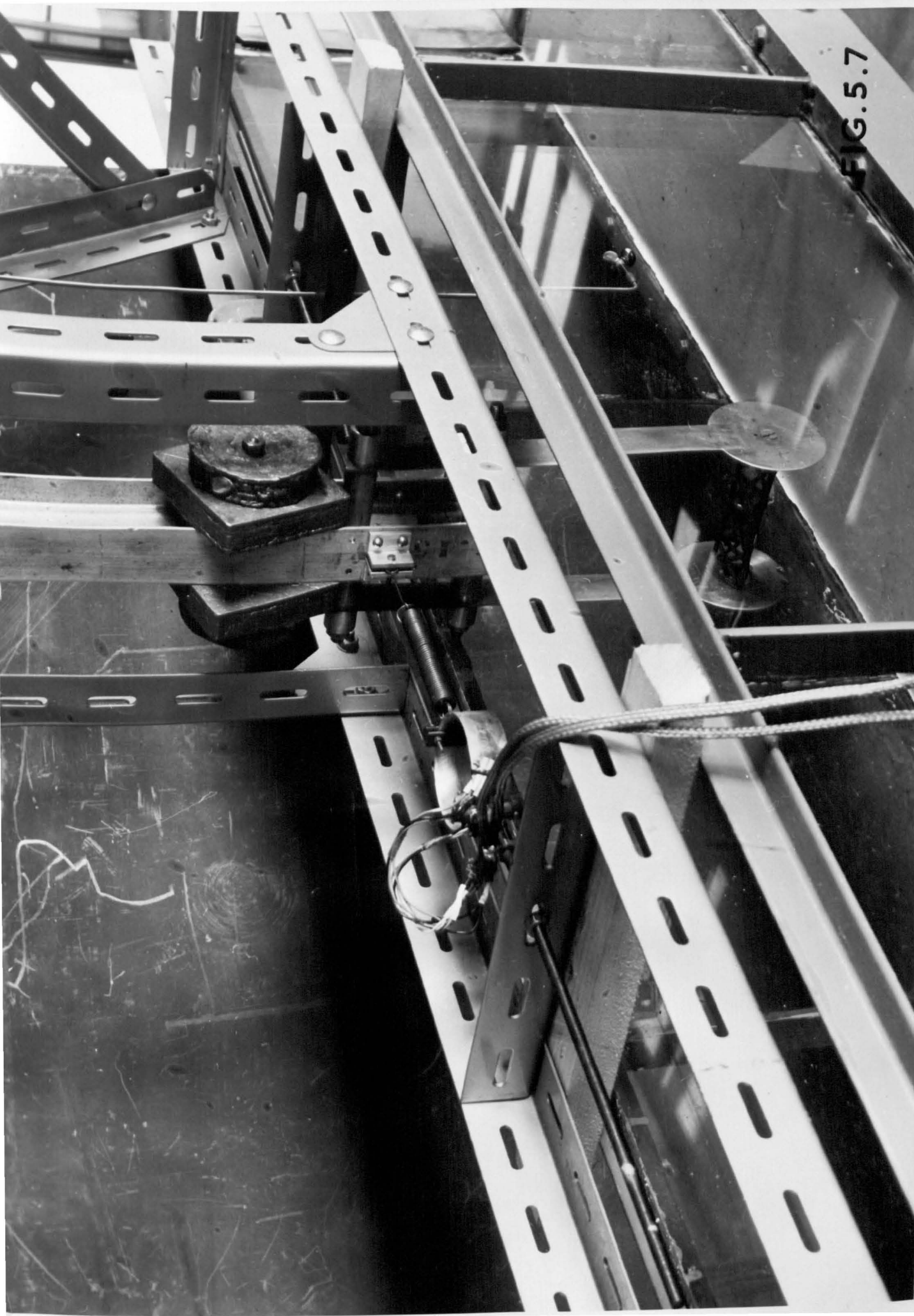


FIG. 5.7

free-running brass spindle which was mounted horizontally on a thin L-shaped, brass rod which could be lowered into the flow to the same depth as the object, but a fair distance upstream so as to avoid any interference with the flow around the object. Apart from the usual "starting velocity" (about 1 in./sec.), characteristic of most propeller instruments, the response of the propeller was linear. It was calibrated carefully in the inlet of a flume. At low velocities the speed of the propeller was determined simply by counting the revolutions against a stop-watch; at higher velocities a stroboscope was used.

The objects tested consisted of a flat plate, a circular cylinder and a triangular, lattice truss, typical of the section of many tall masts. These are illustrated in Fig. 5.8. Each had a diameter of one inch. The objects were mounted between end-shields to ensure that as far as possible the flow did not "spill" off the ends and was as uniform as possible over the span. To determine the "end effect" of the shields various lengths of object between 6 in. and 3 in. were tested. It was, in fact, found to be small.

5.3.2 Test Procedure

The method of test was simple and straight forward. After the flow had settled down and the velocity measured, the pendulum was plucked and the decay of the resulting oscillation was recorded on the oscillograph trace. As a check for consistency, three traces were obtained for each observation. Each of the 6 spring-weight combinations was investigated for mean flow velocities in the range 2 - 20 inches per second. Fig. 5.9 shows sample results.

Fig. 5.8 Photograph of the objects tested. Diameter = 1 inch.

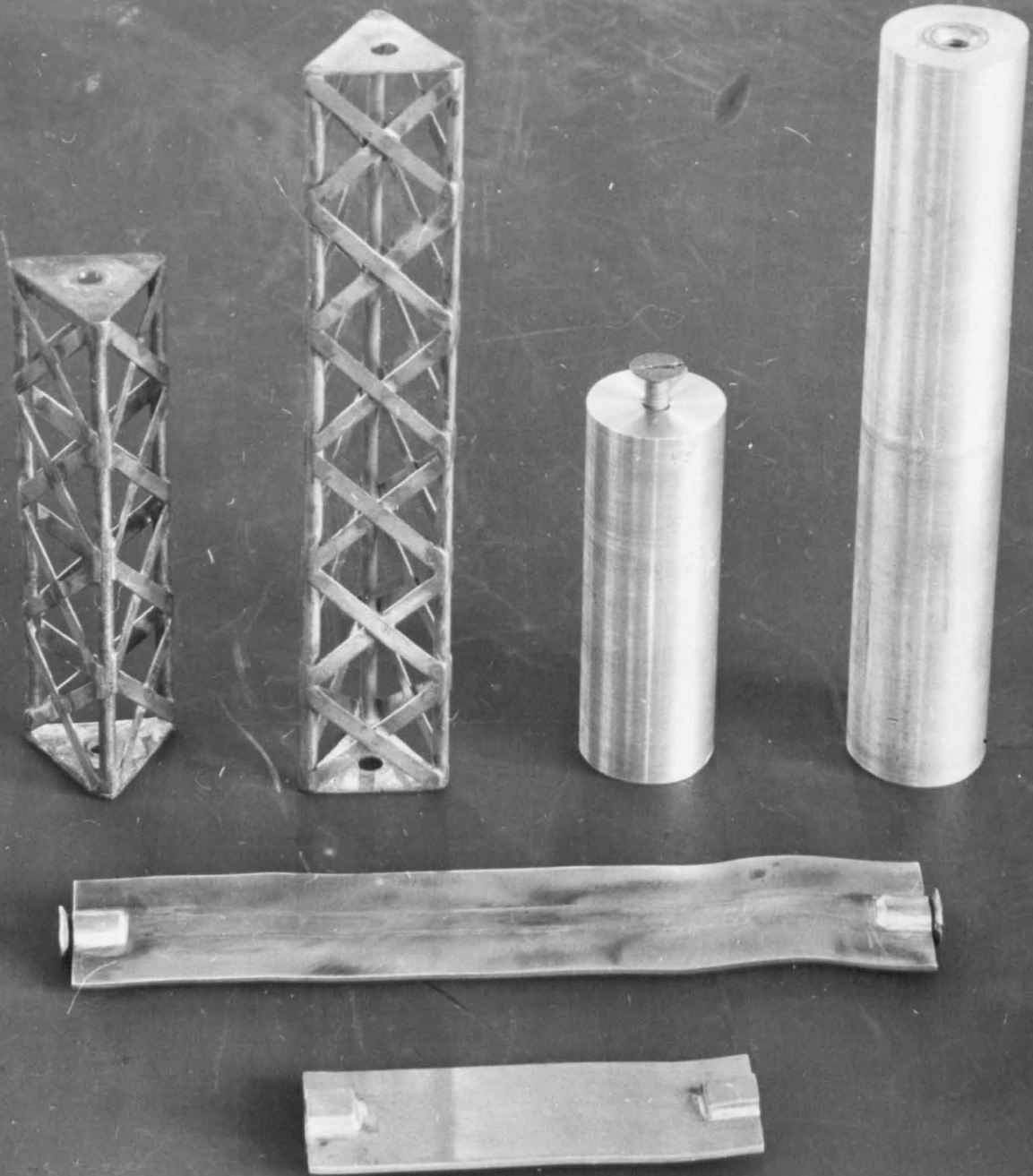


FIG. 5.8

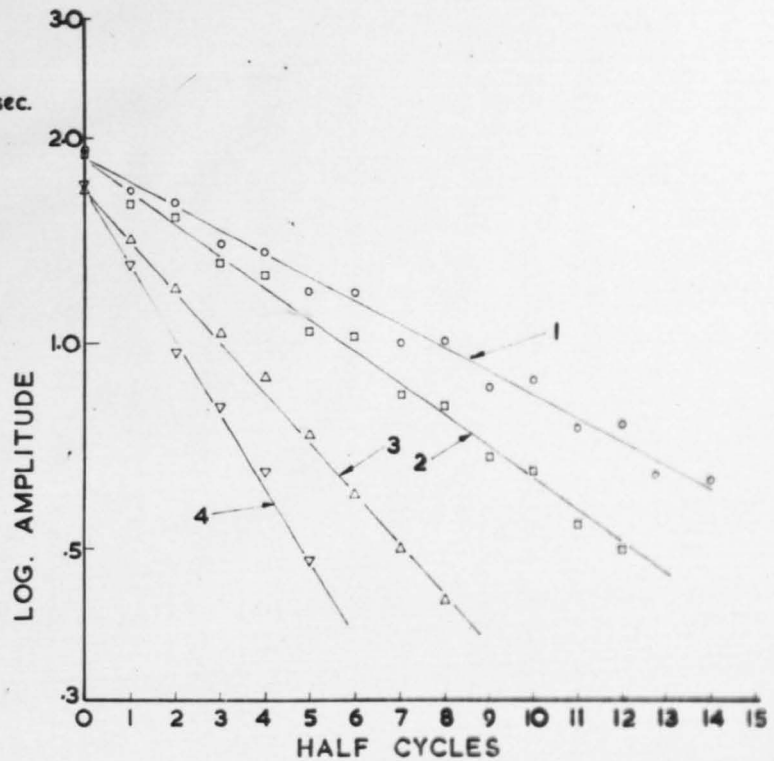
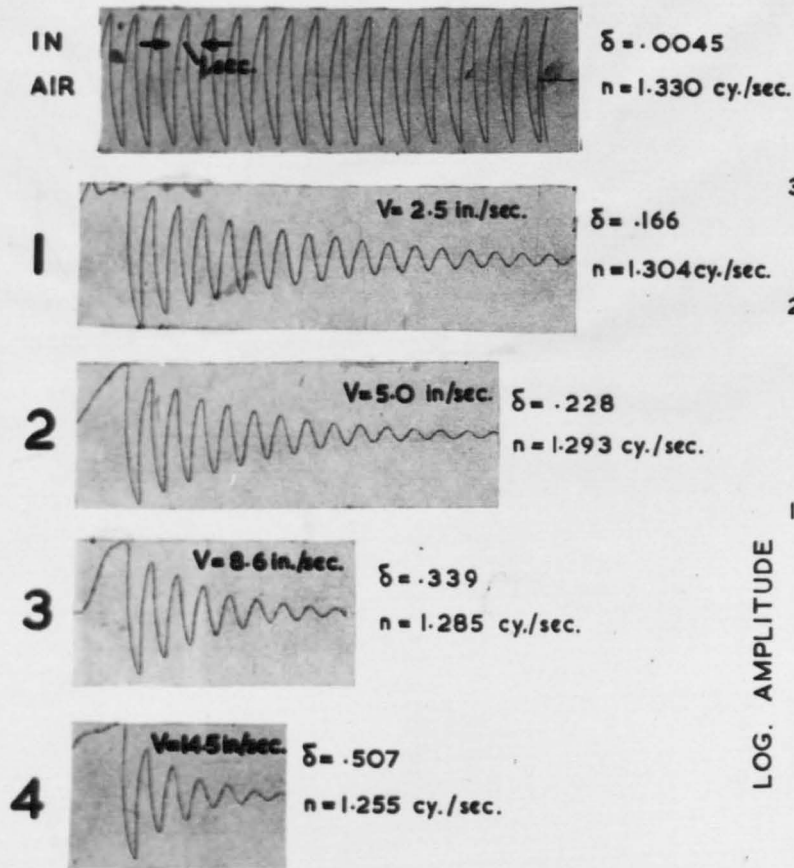


FIG 5.9 DAMPING CURVES FOR $4\frac{1}{2} \times 1$ IN. FLAT PLATE OSCILLATING IN STEADY FLOW.

5.3.3 Theory of Experiments

The velocity of the flow at time t relative to the object mounted on the pendulum is

$$V(t) = \bar{V} + L \dot{\Theta}$$

where $\dot{\Theta}$ = angular velocity of pendulum,

L = length of pendulum from axis of rotation to object centre line,

and \bar{V} = mean velocity of the flow in the flume.

Substituting in equation (5.1) the resistance of the pendulum is

$$P(t) = \frac{1}{2} \rho C_D (\bar{V} + L\dot{\Theta})^2 l.D + \rho C_m A_o l L \ddot{\Theta} \quad (5.3)$$

where C_D and C_m = the required coefficients of drag and additional mass,

A_o = reference area for additional mass,

l = length of specimen,

and D = diameter of specimen normal to the flow.

The equation of motion of the pendulum is

$$I_o \ddot{\Theta} + 2\alpha_o \dot{\Theta} + k\Theta + L.P(t) = 0 \quad (5.4)$$

where

I_o = moment of inertia of the pendulum,

α_o = velocity damping of the pendulum,

k = the restoration force due to the springs and gravity per unit angular deflexion of the pendulum.

If in eq. (5.3), the linear velocity of the pendulum is small compared to the mean flow itself so terms in $\dot{\Theta}^2$ are negligible,

then

$$P(t) = \frac{1}{2} \rho C_D \bar{V}^2 l.D + (\rho C_D \bar{V} l.D.L) \dot{\Theta} + (\rho C_m A_o l) L \ddot{\Theta} \quad (5.5)$$

Write $\Delta m = \rho C_m A_o l$ (the additional mass),

$\beta = \frac{1}{2} \rho C_D \bar{V} l.D.L$ (the velocity damping coefficient of the water),

and $\bar{P} = \frac{1}{2} \rho C_D \bar{V}^2 l.D$ (the mean resistance).

Substituting in equation (5.4)

$$(\bar{I}_0 + \Delta m L^2) \ddot{\Theta} + 2(\alpha_0 + \beta) \dot{\Theta} + k\Theta + L\bar{P} = 0 \quad (5.7)$$

From this it is seen that the effects of the water on the behaviour of the pendulum are:

1. to increase the inertia term by an amount corresponding to the additional mass,
2. to increase the damping by an amount β , which for small amplitude fluctuations can be treated as velocity damping, and
3. to exert a mean force \bar{P} on the pendulum equal to the drag due to the mean flow alone.

The solution to this equation can be written

$$\Theta(t) = \Theta_0 e^{-\delta nt} \cos 2\pi nt \quad (5.8)$$

where

$$\delta = \frac{1}{n} \cdot \frac{\alpha_0 + \beta}{(\bar{I}_0 + \Delta m L^2)} \quad (\text{the logarithmic decrement}) \quad (5.9)$$

$$n = n_1 \sqrt{1 - \frac{\delta^2}{4\pi^2}} \quad (\text{the "apparent" frequency}) \quad (5.10)$$

and

$$n_1 = \frac{1}{2\pi} \sqrt{\frac{k}{\bar{I}_0 + \Delta m L^2}} \quad (\text{the "natural" frequency in water}) \quad (5.11)$$

We also define

$$n_0 = \frac{1}{2\pi} \sqrt{\frac{k}{\bar{I}_0}} \quad (\text{the "natural" frequency in air}) \quad (5.12)$$

Equation (5.8) consists of an oscillating component with a superimposed exponential decay. Its features are well known and are seen clearly in Fig. 5.9 which shows several such curves for different water velocities. From these curves two quantities can be measured:

1. the logarithmic decrement, δ ;
- and 2. the "apparent" frequency, n ;

The decrement is obtained by picking off the peak amplitudes and plotting

these on a logarithmic scale, against time (or the number of cycles) on a linear scale. The slope then gives the decrement. The procedure is illustrated in Fig. 5.9 for the same traces. The "apparent" frequency is measured directly from the trace.

In the experiments the logarithmic decrement, was much smaller than unity. Hence expanding eq. (5.10) binomially, and neglecting terms of order greater than δ^2 ,

$$n_1 = n \left(1 + \frac{\delta^2}{8\pi^2} \dots \right) \quad (5.13)$$

and $\Delta_1 n = n_1 - n = \frac{\delta^2}{8\pi^2} n$

From (5.11) and (5.12),

$$\frac{n_0}{n_1} = \sqrt{1 + \frac{\Delta m \cdot L^2}{I_0}}$$

If $\Delta m \cdot L^2 \ll I_0$

$$\Delta_2(n) = n_0 - n_1 = \frac{1}{2} \frac{\Delta m \cdot L^2}{I_0} \cdot n_1$$

Since $n_0 \approx n_1 \approx n$

$$\frac{\Delta n}{n_0} = \frac{n_0 - n}{n_0} = \frac{1}{2} \frac{\Delta m \cdot L^2}{I_0} + \frac{\delta^2}{8\pi^2} \quad (5.14)$$

Now the "apparent" frequency in air is almost exactly equal to the natural frequency n_0 , due to the low internal damping. A typical "air damping" curve is shown in Fig. 5.9. (The frequency is seen to be somewhat higher than in water.) Since all the other quantities are measurable the additional mass Δm can be found from equation 5.14. viz.

$$\Delta m = \frac{2I_0}{L^2} \left\{ \frac{\Delta n}{n_0} - \frac{\delta^2}{8\pi^2} \right\} \quad (5.15)$$

The coefficient of additional mass is now given by equation 5.6 i.e.

$$C_m(n) = \frac{\Delta m}{\rho \cdot A_0 \cdot l} \quad (5.16)$$

Having found the additional mass coefficient it is now possible to determine the value of β , (the velocity damping coefficient due to the drag), and hence the drag coefficient. From equation 5.9

$$\beta = n \delta (I_0 + \Delta m \cdot L^2) - \alpha_0 \tag{5.17}$$

(α_0 is usually negligibly small)

If we write $\alpha_0 = n_0 \delta_0 I_0$ (where δ_0 is the logarithmic decrement in air), then from equation (5.6) the drag coefficient can be written

$$C_D(n) \approx \frac{2}{\rho \cdot L \cdot D^2} \cdot \left(\frac{nD}{V} \right) (I_0 + \Delta m L^2) (\delta - \delta_0)$$

This is the basic equation for determining the drag coefficient. All the quantities on the right hand side are measurable. The dimensionless parameter $\frac{nD}{V}$ is denoted by ξ and is the reduced frequency.

5.3.4 Results

5.3.4.1 Introduction

Dimensional analysis suggests that there are three parameters on which the values of the drag and mass coefficients might be expected to depend. These are:

1. $\frac{nD}{V} = \xi$ - the reduced frequency
2. $\frac{n\theta L}{V}$ - the velocity ratio of the object
3. $\frac{VD}{\nu} = Re$ - the "Reynold's number".

Any dependence on the second of these parameters will be revealed by the damping curves themselves, since these record the oscillation over a range of amplitudes. If the damping depends on amplitude, the plot of the damping curve on semi-logarithmic paper will be non-linear. (It was stipulated in the first place that the velocity of the object was small compared to the mean flow so no significant non-linearity could be

expected from this source.)

Dependence on the Reynold's number can be ascertained by varying the velocity (proportional to Re) but at the same time maintaining the same reduced frequency (by varying the frequency of the pendulum). In fact, with bluff, unstreamlined objects, dependence on Reynold's number might be expected to be small. This is because the most marked influence of Reynold's number is in changing the position of the 'separation points', separating the regions of laminar and turbulent flow around the body. In bodies of curved profile (such as a circular cylinder) a variation of Reynold's number can cause the separation points to move, thereby affecting the width of the wake and therefore the drag. In sharp edged bodies (such as a flat plate normal to the flow) however, the separation is almost bound to occur, at the sharp edges. This effectively fixes the size of the wake and the drag is then almost independent of the Reynold's number.

This implies that the principal parameter is likely to be the reduced frequency ξ , which is already contained in equation (5.18) for C_D . The analysis were carried out on this assumption.

5.3.4.2' Calculations

From the series of damping curves (three for each observation), obtained for various mean flow velocities and for each of the spring-weight combinations, the following data were obtained:

1. the logarithmic decrement δ . (from graphical plots such as those shown in Fig. 5.9),
2. the apparent frequency η .

By allowing the pendulum to oscillate in air the following was obtained:

3. the logarithmic decrement in air, δ_0 ,
- and 4. the natural frequency in air, n_0 ,

The moment of inertia of the pendulum, I_0 , was determined by removing the springs and timing the swing. I_0 is then given by

$$I_0 = \frac{9}{4\pi^2} M \bar{r} T^2 \quad (5.19)$$

where T is the pendulum period, M the mass and \bar{r} the distance from the pivot point to the centre of gravity (found by balancing the pendulum horizontally on a knife edge).

Values of I_0 , n_0 and δ_0 for the pendulum with various objects attached are given in Table 5.1.

It is now possible to compute the additional mass from eq. (5.15) and the additional mass coefficient from (5.16). Knowing the additional mass the drag coefficient can be computed from (5.18).

5.3.4.3 Determination of Effect of End Shields

As noted, the objects were mounted between end-shields, designed to prevent the flow 'spilling' off the ends and also to provide a means of support (see Figs. 5.5 - 5.7). The end-shields and the supporting struts were cut from 16 gauge brass sheet. In spite of the fact that the edges were sharpened so as to streamline them as far as possible, they did, nevertheless, make a small contribution to the drag, over and above that of the object itself. To determine the size of this contribution, several lengths of object were tested at the same velocity. The end effect was then determined by effectively differencing the total drag for the different lengths and assuming that the drag contribution by the end-shields was the same in each case. The procedure is illustrated in Fig. 5.10; in which the product of object length and total drag

TABLE 5.1

Properties of Pendulum for Various Tests

Spring wt.	3" Plate		4 1/2" Plate		6" Plate (Series 1)		6" Plate (Series 2)		6" Cylinder		4" Lattice Truss	
	n_o cy./sec.	I_o lb. in. ²	n_o cy./sec.	I_o lb. in. ²	n_o cy./sec.	I_o lb. in. ²	n_o cy./sec.	I_o lb. in. ²	n_o cy./sec.	I_o lb. in. ²	n_o cy./sec.	I_o lb. in. ²
A 1	1.919	4,020	1.842	4,070	1.827	4,280	1.852	4,280	1.681	4,690	1.756	3,870
A 2	1.360	8,280	1.332	8,320	1.326	8,920	1.340	8,920	1.276	9,340	1.350	8,520
A 3	1.030	16,320	1.017	16,370	1.011	16,520	1.021	16,520	.995	16,970	1.028	16,170
B 1	4.300	4,020	4.130	4,070	4.095	4,280	4.140	4,280	4.090	4,690	3.955	3,870
B 2	2.961	8,280	2.895	8,320	2.870	8,920	2.902	8,920	2.730	9,340	2.928	8,520
B 3	2.123	16,320	2.082	16,370	2.077	16,520	2.100	16,520	2.020	16,970	2.110	16,170

Damping decrement in air $\delta_o = .0050$ for all tests.

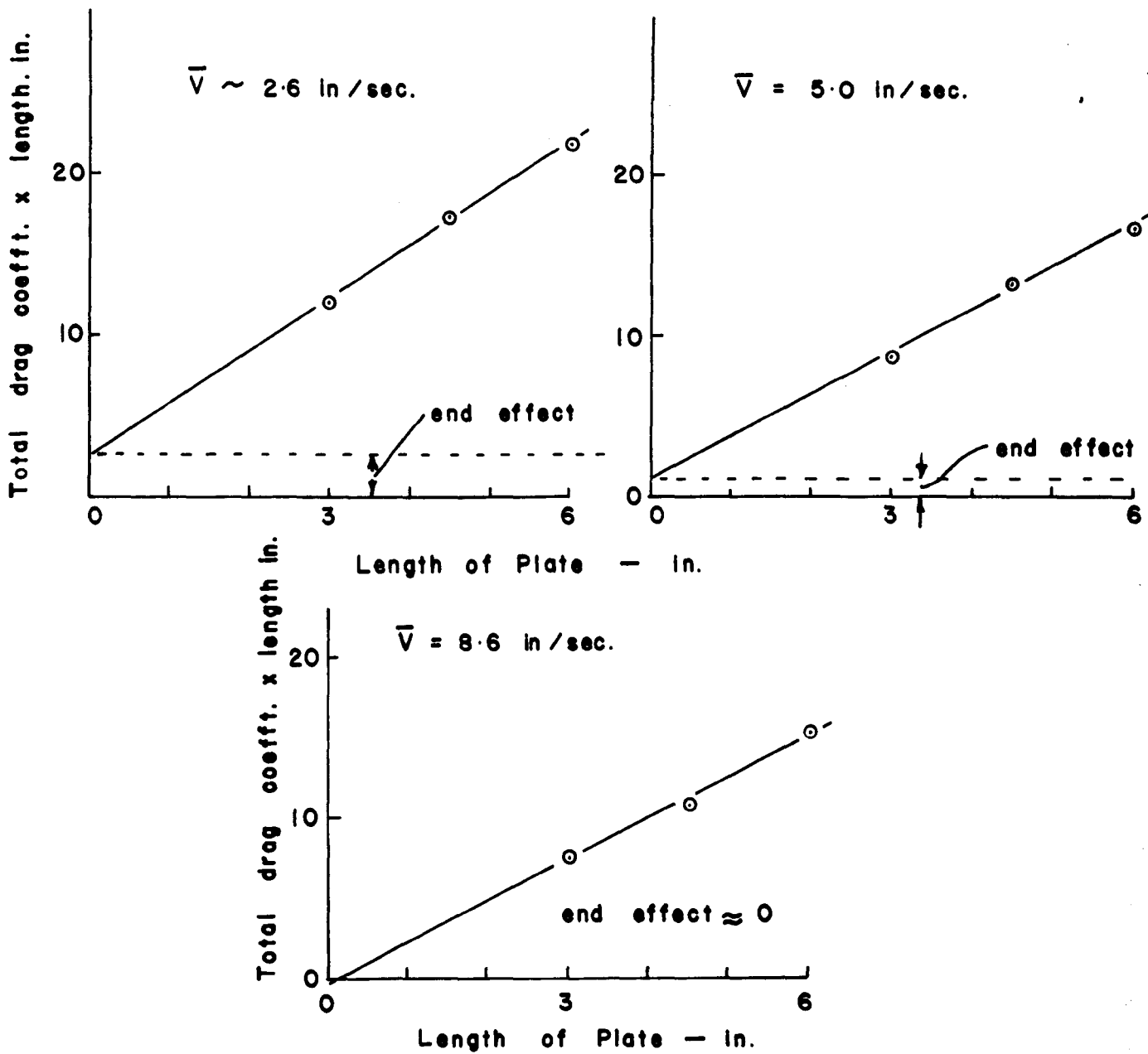


FIG. 5.10 DETERMINATION OF EFFECT OF END-SHIELDS.

coefficient (for end-shields plus object) is plotted against the object length. The gradient of these lines gives the net drag coefficient for unit length of the object alone. The intercept with the vertical axis gives a measure of the end-shield drag.

As can be seen from Fig. 5.10, the effect of the end shields decreased as the velocity increases. This can probably be explained by the difference in the drag characteristics of the object and the end shields. Whereas the drag of the former is probably almost entirely form drag, and therefore proportional to V^2 , the drag of the end shields is more likely to be viscous and therefore proportional simply to V . The drag of the latter, therefore rises less rapidly; or, put in other words, a drag coefficient computed on the basis of the drag being proportioned to V^2 will appear to decrease inversely as V . Thus the end correction appears to become less and less important as the velocity rises. In fact it only seemed necessary to correct for the end shields in the case of the lowest velocity measurements (approximately 2.5 in./sec.)

The effect of the end shields was assumed to be the same for each of the objects tested.

No allowance was made for end shields in computing the additional mass, because the crucial readings could not be made to sufficient accuracy (i.e. depended on a small increment of frequency) to warrant the attempt. That it was small, is borne out by the agreement between the results for the flat plates of different lengths shown in Fig. 5.12b.

The final results for all tests (with end-corrections made) are recorded in Tables 5.2 to 5.6 and plotted in Figs. 5.12, 5.13 and 5.14. These results are discussed in detail, following the description of the

determination of the steady-flow drag coefficient below.

5.3.4.4 Determination of Steady Flow Drag

This was accomplished by removing the springs and measuring the deflexion of the pendulum hanging freely in the flow of water, by sighting the cross-wires of a telescope on a graduated scale mounted on the pendulum itself. The drag could then be calculated from the equilibrium of the pendulum. A typical drag curve (for the lattice truss) is shown in Fig. 5.12. The drag coefficients for the three objects tested were found to be:

	Steady Flow Drag Coefficient
Flat Plate	2.0
Circular Cylinder	1.05
Lattice Truss	1.10

These values agree with those given elsewhere. The values for the flat plate and cylinder are familiar results given in text books. In the case of the lattice truss the drag coefficient is based on the gross area of the surface and not simply the net frontal area of the lattice members. For comparison with results by Cohen and Perrin (1954), Redwood (1960), Schott (1954) and others the solidity ratio (ratio of net area of members to gross area of truss) should be taken as .60.

5.3.5 Discussion

In Section 5.3.4.1 it was pointed out that the parameters on which the drag and virtual mass coefficients might be expected to depend were the reduced frequency, ξ , the velocity amplitude ratio, $\frac{n\theta L}{V}$, and the Reynold's number R_e . Independence of the velocity amplitude ratio was partially assured by using only small values of the parameter

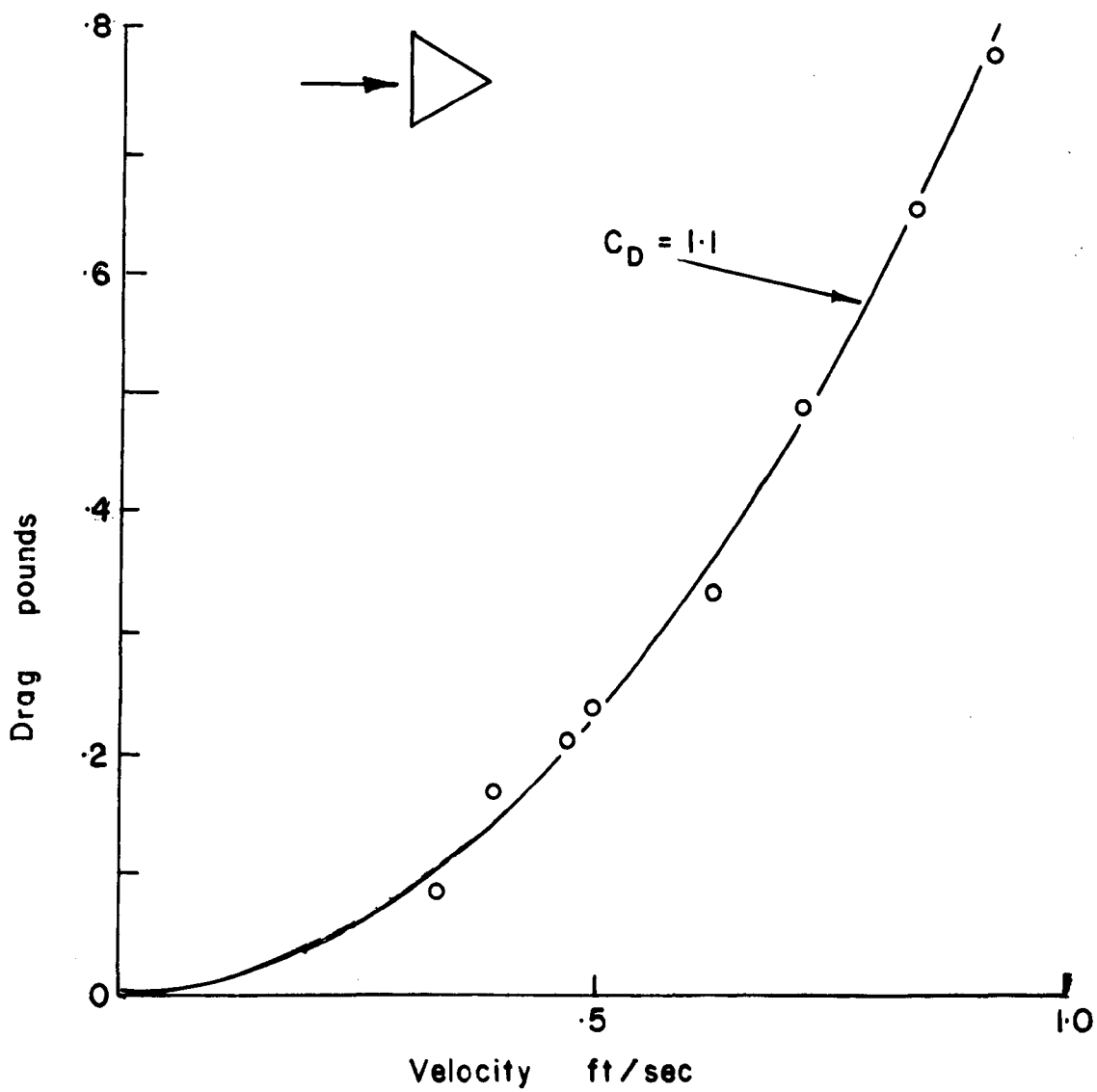


FIG. 5.11 STEADY-FLOW DRAG OF TRIANGULAR LATTICE TRUSS.

and was verified experimentally insofar as the damping curves were found to be linear (see Fig. 5.9) - a situation which would not have resulted had the coefficients been dependent on the velocity amplitude ratio. Dependence on Reynold's number was expected to be small (except possibly for the cylinder) - as is the case with the steady flow drag coefficients of most bluff objects. Hence the most influential parameter was expected to be the reduced frequency - as already pointed out. The drag and additional mass coefficients are plotted in Figs. 5.12, 5.13 and 5.14 as functions of this parameter.

Three features of these curves seem to be noteworthy

1. The drag coefficients of the flat plate and triangular lattice truss both increase steadily with reduced frequency (the truss slightly more so than the flat plate), from a value which is close to the steady state value for $\xi \approx 0.05$. The coefficient for the truss reaches about double the steady state value for $\xi = 1.5$.
2. The additional mass coefficient of the flat plate and truss both decrease with reduced frequency (the trend in the latter case being less well defined for reasons explained below).
3. The results for the circular cylinder -, insofar as they indicate any certain trends, - do not appear to exhibit either of those in 1 and 2.

It is extremely difficult in a purely quantitative experiment such as this to account for the above. Some of the same difficulty was encountered by Keulegan and Carpenter (1958) in investigating the resistance of the flat plate and cylinder to a simple periodic flow with no mean velocity. They were, however, able to obtain some insight into

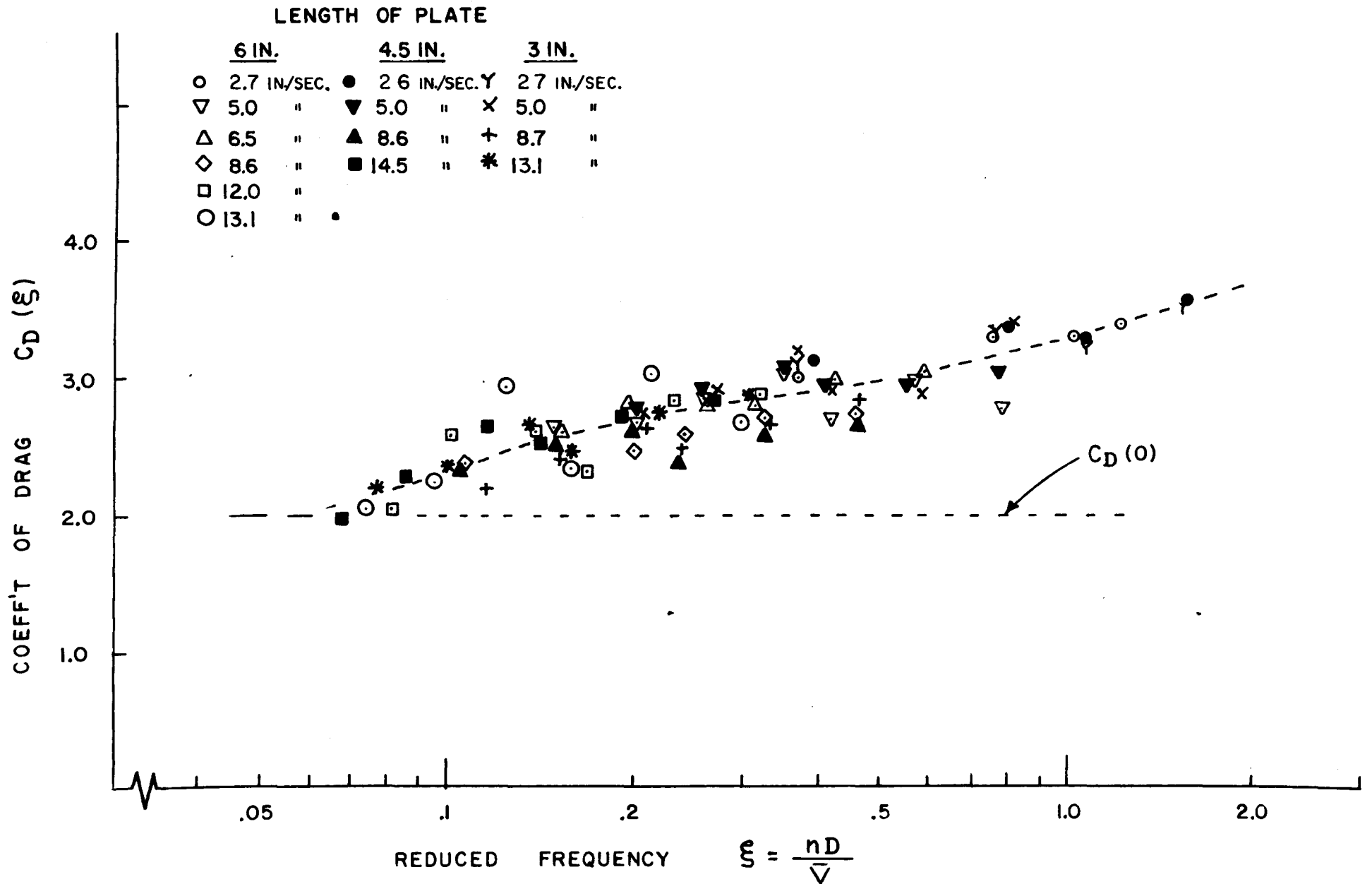


FIG. 5.12a COEFFICIENT OF DRAG OF FLAT PLATE IN FLUCTUATING FLOW

LENGTH OF PLATE

6 IN.		4.5 IN.		3 IN.	
○	2.7 IN./SEC.	●	2.6 IN./SEC.	Y	2.7 IN./SEC.
▽	5.0 "	▼	5.0 "	X	5.0 "
△	6.5 "	▲	8.6 "	+	8.7 "
◇	8.6 "	■	14.5 "	*	13.1 "
□	12.0 "				
○	13.1 "				

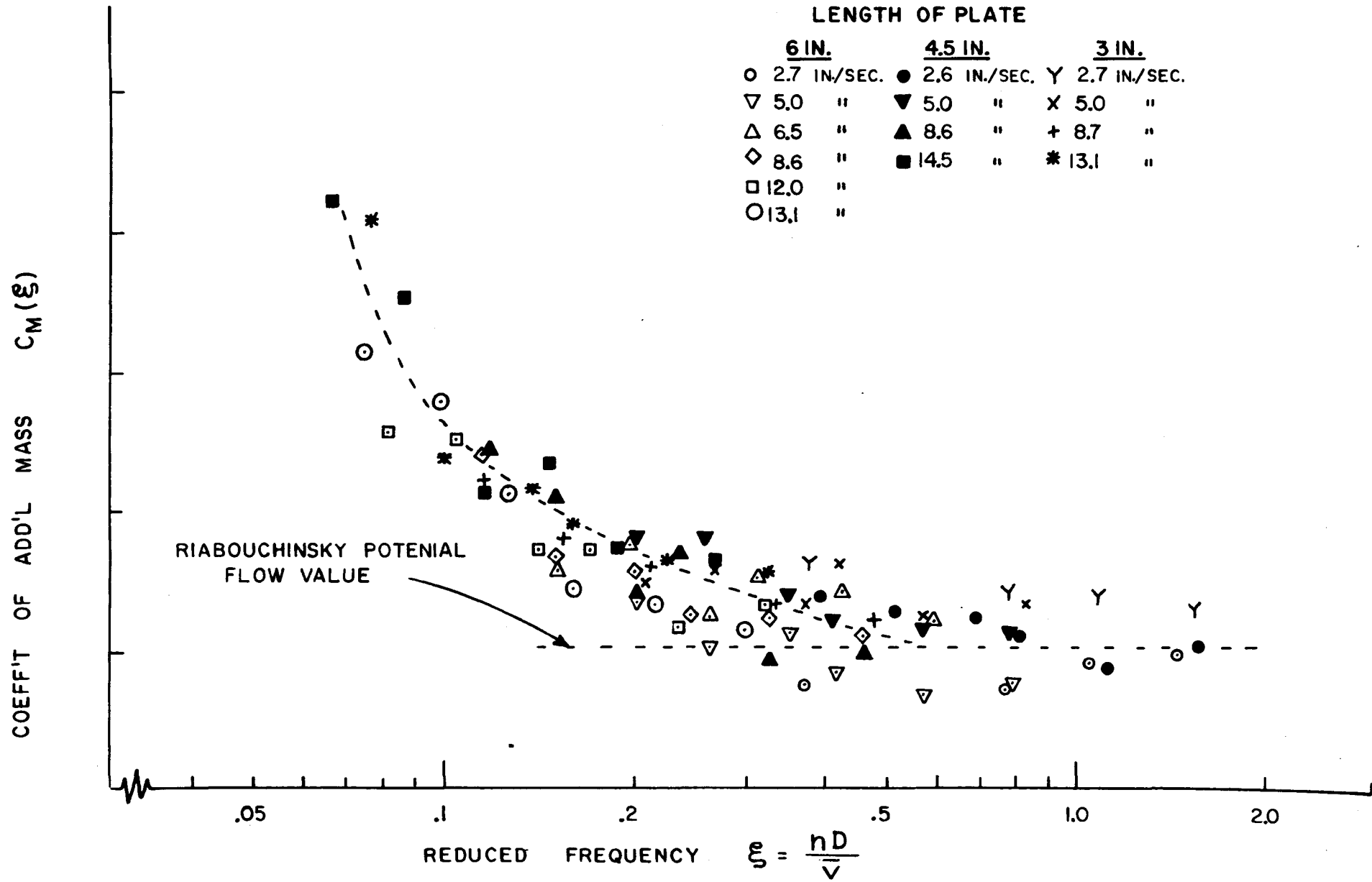


FIG. 5.12b COEFFICIENT OF ADDITIONAL MASS OF FLAT PLATE IN FLUCTUATING FLOW

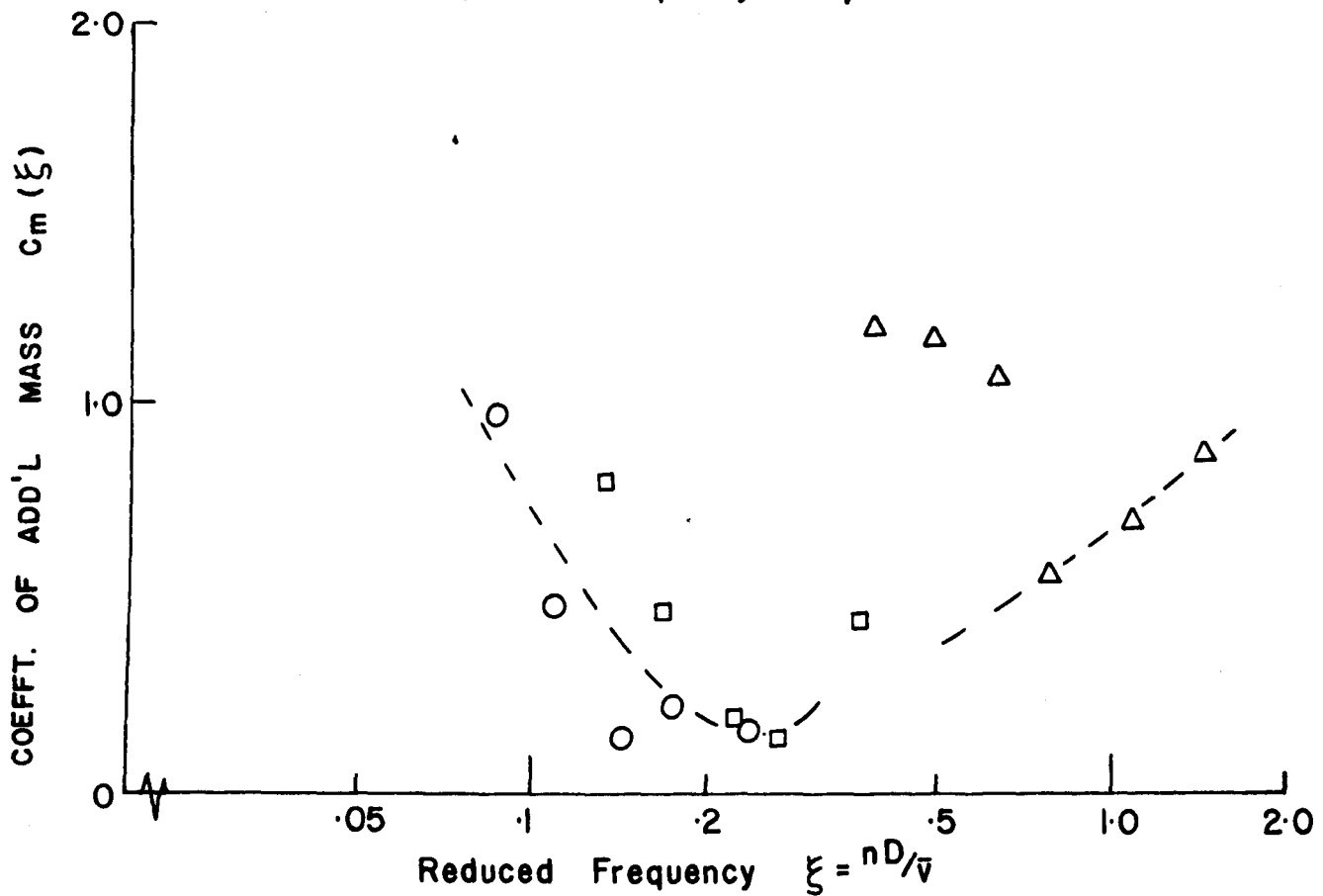
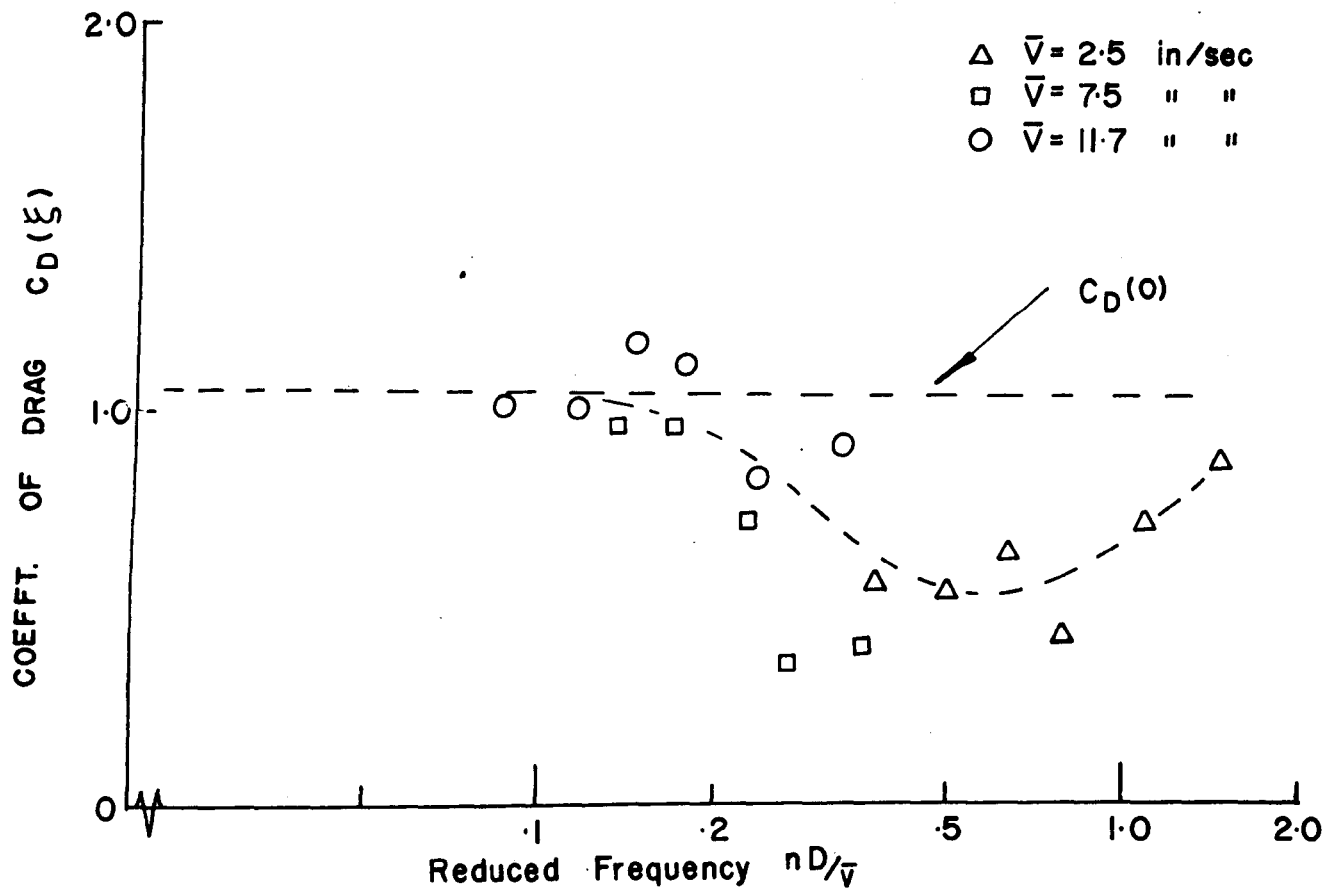


FIG. 5.13 COEFFICIENTS OF DRAG AND ADDITIONAL MASS OF CIRCULAR CYLINDER IN FLUCTUATING FLOW.

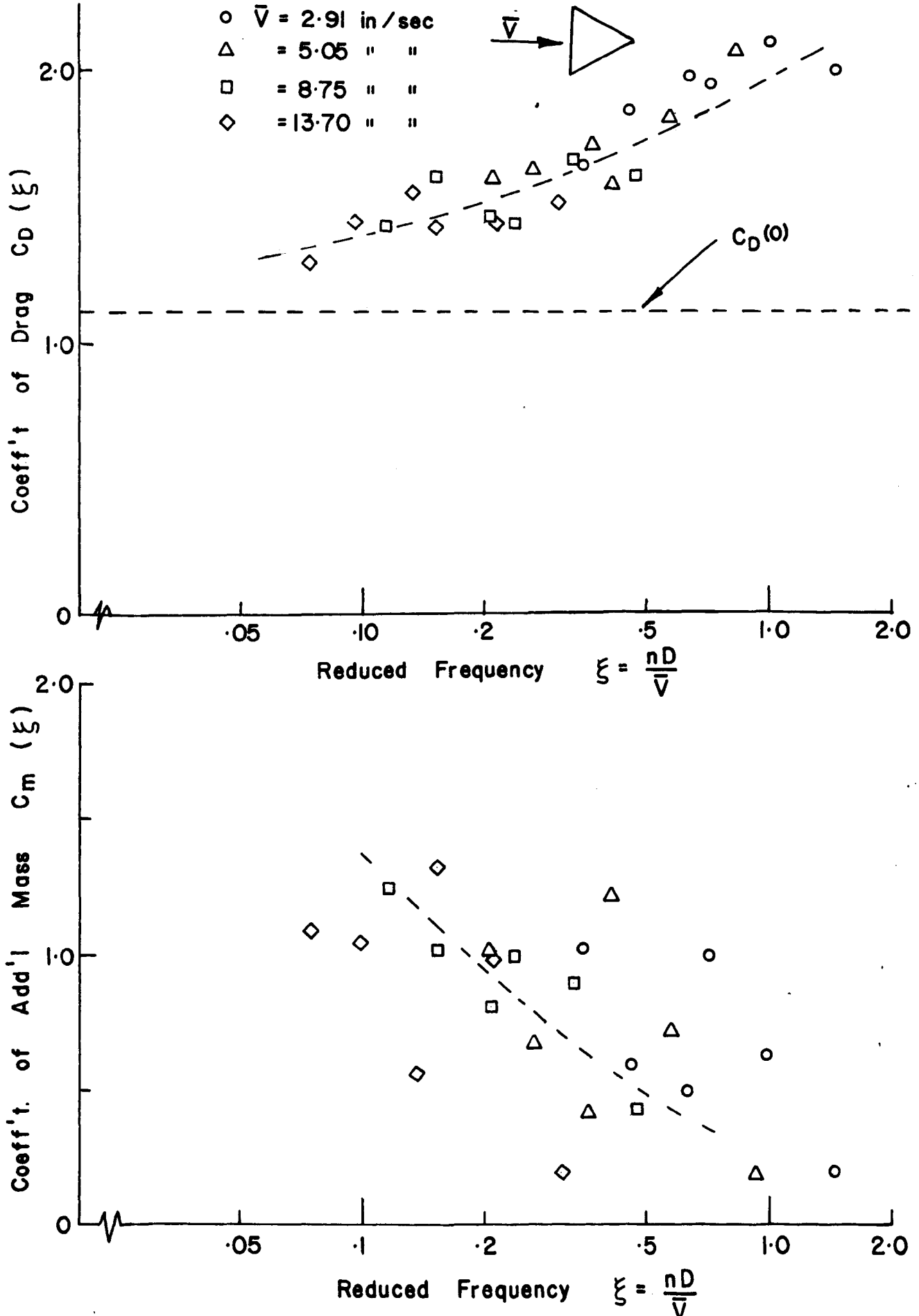


FIG. 5.14 COEFFICIENTS OF DRAG AND ADDITIONAL MASS OF TRIANGULAR LATTICE TRUSS IN FLUCTUATING FLOW

TABLE 5.2

RESULTS OF TESTS ON 3 INCH FLAT PLATE

Spring/ Weight	δ	\bar{V} in/sec	n cy/sec	ξ	C_m	C_D
A / 1	.213	2.70	1.856	0.687	1.429	(4.58)
	.249	5.00	1.860	0.372	1.303	3.30
	.342	8.75	1.846	0.211	1.601	2.61
	.512	13.10	1.818	0.139	2.173	2.65
A / 2	.113	2.70	1.342	0.497	1.421	(3.56)
	.149	5.00	1.339	0.268	1.626	2.85
	.219	8.75	1.336	0.153	1.813	2.41
	.322	13.10	1.327	0.101	2.391	2.36
A / 3	.072	2.70	1.022	0.379	1.655	3.10
	.096	5.00	1.022	0.204	1.440	2.71
	.135	8.75	1.019	0.116	2.257	2.19
	.199	13.10	1.010	0.077	4.063	2.19
B / 3	.037	2.70	2.104	0.779	1.448	3.32
	.050	5.00	2.102	0.420	1.629	2.92
	.075	8.75	2.107	0.241	1.176	2.49
	.112	13.10	2.098	0.160	1.918	2.49
B / 2	.051	2.70	2.913	1.079	1.427	3.23
	.075	5.00	2.919	0.584	1.239	3.09
	.114	8.75	2.915	0.333	1.347	2.70
	.173	13.10	2.903	0.222	1.697	2.75
B / 1	.076	2.70	4.167	1.543	1.337	3.52
	.103	5.00	4.167	0.833	1.337	3.40
	.162	8.75	4.175	0.477	1.242	2.83
	.253	13.10	4.142	0.316	1.556	2.88

TABLE 5.3

RESULTS OF TESTS ON 4-1/2 INCH FLAT PLATE

Spring/ Weight	δ	\bar{V} in/sec	n cy/sec	ξ	C_m	C_D
A / 3	.0971	2.55	1.0059	0.394	1.403	3.12
	.1532	5.00	1.0027	0.201	1.820	2.19
	.2125	8.60	.9980	0.116	2.418	2.34
	.298	14.50	.9842	0.0679	4.239	1.97
A / 2	.1656	2.55	1.3038	0.511	1.308	(3.64)
	.228	5.00	1.2931	0.259	1.812	2.90
	.339	8.60	1.2853	0.149	2.151	2.51
	.507	14.50	1.2552	0.087	3.532	2.29
A / 1	.283	2.55	1.7647	0.692	1.248	(4.37)
	.351	5.00	1.7544	0.351	1.401	3.06
	.512	8.60	1.7544	0.204	1.346	2.62
	.867	14.50	1.6948	0.117	2.145	2.64
B / 1	.1054	2.55	3.9761	1.559	1.053	3.55
	.1556	5.00	3.9682	0.794	1.102	3.02
	.2365	8.60	3.9841	0.463	0.981	2.67
	.415	14.50	3.8760	0.267	1.687	2.80
B / 2	.0702	2.55	2.8450	1.116	0.897	3.29
	.1086	5.00	2.8302	0.566	1.185	2.96
	.1619	8.60	2.826	0.329	0.951	2.55
	.285	14.50	2.800	0.193	1.763	2.70
B / 3	.0508	2.55	2.0640	0.809	1.134	3.39
	.0766	5.00	2.0619	0.412	1.240	2.93
	.1060	8.60	2.0534	0.239	1.719	2.38
	.1916	14.50	2.0408	0.141	2.375	2.56

TABLE 5.4a

RESULTS OF TESTS ON 6 INCH FLAT PLATE

Series 1

Spring/ Weight	δ	\bar{V} in/sec	n cy/sec	ξ	C_m	C_D
A / 1	.336	2.70	1.730	.640	1.176	(4.231)
	.532	6.50	1.718	.264	1.277	2.786
	.907	11.95	1.670	.140	1.726	2.608
A / 2	.209	2.70	1.296	.480	1.045	(3.811)
	.373	6.50	1.274	.196	1.780	2.817
	.631	11.95	1.250	.105	2.535	2.588
A / 3	.128	2.70	1.002	.371	.766	3.295
	.244	6.50	.992	.153	1.584	2.603
	.354	11.95	.980	.0820	2.561	2.035
B / 3	.068	2.70	2.060	.763	.713	3.642
	.1248	6.50	2.040	.314	1.549	2.802
	.189	11.95	2.035	.170	1.734	2.307
B / 2	.0907	2.70	2.815	1.043	.907	3.654
	.177	6.50	2.78	.428	1.473	2.993
	.309	11.95	2.795	.234	1.183	2.824
B / 1	.1324	2.70	3.915	1.450	.999	3.724
	.257	6.50	3.87	.595	1.233	3.022
	.452	11.95	3.85	.322	1.304	2.893

TABLE 5.4b

RESULTS OF TESTS ON 6 INCH FLAT PLATE

Series 2

Spring/ Weight	δ	\bar{V} in/sec	n cy/sec	ξ	C_m	C_D
A / 1	.439	5.00	1.756	.351	1.138	(3.023)
	.604	8.60	1.715	.200	1.580	2.453
	1.110	13.10	1.650	.126	2.132	2.961
A / 2	.280	5.00	1.310	.262	1.017	(2.846)
	.439	8.60	1.289	.150	1.696	2.625
	.564	13.10	1.256	.0959	2.788	2.248
A / 3	.187	5.00	1.005	.201	1.346	2.6767
	.284	8.60	.992	.115	2.411	2.380
	.372	13.10	.983	.0750	3.115	2.064
B / 3	.0924	5.00	2.080	.416	.829	2.705
	.150	8.60	2.070	.241	1.232	2.567
	.204	13.10	2.065	.158	1.426	2.299
B / 2	.136	5.00	2.860	.572	.679	2.977
	.210	8.60	2.825	.328	1.230	2.695
	.360	13.10	2.815	.215	1.349	3.043
B / 1	.182	5.00	3.980	.796	.871	2.781
	.304	8.60	3.935	.458	1.101	2.723
	.466	13.10	3.920	.299	1.149	2.736

TABLE 5.5

RESULTS OF TESTS ON 6 INCH CIRCULAR CYLINDER

Spring/ Weight	δ	\bar{V} in/sec	n cy/sec	ξ	C_m	C_D
A / 1	.0520	2.55	1.609	.631	1.061	.633
	.1630	7.50	1.667	.222	.198	.716
	.428	11.70	1.667	.142	.149	1.190
A / 2	.0311	2.55	1.246	.489	1.158	.523
	.1503	7.50	1.264	.169	.450	.976
	.266	11.70	1.263	.108	.458	1.120
A / 3	.0251	2.55	.982	.385	1.182	.566
	.1074	7.50	.986	.131	.796	.971
	.171	11.70	.984	.0841	.961	1.015
B / 3	.0127	2.55	2.008	.787	.530	.434
	.0181	7.50	2.017	.269	.134	.250
	.097	11.70	2.015	.172	.212	1.126
B / 2	.0213	2.50	2.692	1.077	.686	.703
	.0296	7.50	2.706	.361	.434	.352
	.0965	11.70	2.721	.233	.157	.835
B / 1	.0300	2.50	3.584	1.434	.872	.878
	-	7.50	-	-	-	-
	.132	11.70	3.854	.329	-	.912

TABLE 5.6

RESULTS OF TESTS ON 4 INCH TRIANGULAR LATTICE TRUSS

(Upstream face normal to flow)

Spring/ Weight	δ	\bar{V} in/sec	n cy/sec	ξ	C_m	C_D
B / 1	.0620	2.91	4.167	1.432	.182	2.002
	.1014	5.05	4.167	.825	.181	2.100
	.142	8.75	4.132	.472	.410	1.612
	.207	13.70	4.167	.304	.181	1.505
B / 2	.0439	2.91	2.898	.996	.623	2.106
	.0641	5.05	2.894	.573	.707	1.846
	.0978	8.75	2.885	.330	.891	1.680
	.132	13.70	2.882	.210	.951	1.466
B / 3	.0316	2.91	2.092	.719	.988	1.968
	.0423	5.05	2.088	.413	1.206	1.591
	.0637	8.75	2.092	.239	.985	1.443
	.0956	13.70	2.086	.152	1.310	1.425
A / 3	.0510	2.91	1.019	.350	1.010	1.663
	.0824	5.05	1.012	.202	1.002	1.615
	.122	8.75	1.017	.116	1.216	1.408
	.175	13.70	1.018	.0743	1.082	1.307
A / 2	.0796	2.91	1.337	.450	.584	1.863
	.119	5.05	1.335	.264	.672	1.642
	.196	8.75	1.327	.152	1.002	1.604
	.277	13.70	1.326	.0968	1.027	1.455
A / 1	.130	2.91	1.846	.634	.498	1.992
	.195	5.05	1.852	.367	.450	1.740
	.277	8.75	1.824	.208	.800	1.454
	.468	13.70	1.838	.134	.543	1.564

the mechanism governing the resistance by photographing flow patterns using dye, which led to their supposition that the variations in drag and additional mass coefficients were in some way governed by the eddy shedding in the wake. A similar photographic study in the present case would have been far more difficult to carry out, and also to interpret; the mean flow would give rise to a flow pattern of its own which would be extremely difficult to disentangle from that due to the fluctuating flow.

It seems likely that the phenomenon may be associated with the build-up and shedding of vortices at the sharp edges. Thus, the reason why the drag coefficient for the truss showed a greater rise than that for the flat plate may be due to the former's greater proportion of "edge" per unit frontal area. It should be noted that Keulegan and Carpenter (1958) in their experiments found that the drag coefficient for the flat plate rose with reduced frequency (see Fig. 5.2) just as it did in the present experiments: furthermore, the additional mass coefficient showed a similar decreasing trend. Both these facts may, however, be coincidental.

In both sets of experiments, the cylinder and flat plate registered characteristically different responses. In the present experiments the cylinder results were most irregular (see Fig. 5.13) for a number of reasons. The principal reason probably lies in the fact that the "separation points" for the cylinder do not occur at sharp edges as they do in the flat plate; this means that they are free to move - as it is well known that they do - with consequent changes in the width of the wake and in the drag. It is well known that the positions of these separation points are very sensitive to variations in the oncoming flow.

Under these circumstances it would not be surprising if the periodic fluctuations in flow imposed in the experiments were sufficient to disturb the separation points and produce widely varying results for the drag. Indeed, a very prominent feature of the investigations was that with the two highest frequency arrangements (i.e. with strong springs and the two lighter weights) the pendulum would go into a state of self-excited oscillation of such large amplitude that it precluded all possibility of obtaining damping curves. This happened over a wide range of velocities, and is probably evidence in itself of the instabilities that must exist in the drag. With these difficulties to contend with, investigation of the cylinder drag was limited to the points shown in Fig. 5.13, being those that did not exhibit self-exciting oscillations. Another reason for limiting study of the cylinder was that results for Reynold's numbers as low as these (1,000 - 10,000) have no practical relevance to the wind loading problem: and at the much higher Reynold's numbers (10^2 - 10^8 or so) encountered in tall chimneys, masts and other full-scale cylindrical structures the drag has altogether different characteristics.

It is noticed that the additional mass coefficient for the flat plate flattens out to a value close to 1 for larger reduced frequencies. This happens to be close to a theoretical value (quoted by Stelson and Mavis - 1955) determined by Riabouchinsky. He assumed two parallel flat plates placed some distance apart, with potential flow in the region surrounding the plates and the streamlines joining their opposite edges. The additional mass coefficient determined on this basis was 1.05 and is indicated by the dashed line in Fig. 5.12b.

The scatter in the results for the additional mass coefficient of the truss is much greater than that for the flat plate. The main, and probably only reason is that the additional mass effect was much smaller for the truss, and consequently, the frequency changes were more difficult to measure accurately.

One final observation concerns the value of the mean drag during the oscillations. For the truss and the flat plate (little can be said with certainty regarding the cylinder) this appeared to remain constant at the steady flow value. This fact would be verified from the oscillograph trace which showed that the mean position of the pendulum during vibration was the same as the position at rest.

5.4 THE AERODYNAMIC FORCES IN A GUSTY WIND: RECAPITULATION AND CONCLUSIONS

5.4.1 Drag Forces

To determine the gust forces on a structure such as the bridge deck shown in Fig. 5.3, or a mast section, the best we can probably do at present is assume:

1. that the gust velocity effective in creating pressures on the structure is an average velocity over some area of influence such as that suggested in Section 5.2.2 (see Fig. 5.4);
2. that the effective drag coefficients appertaining to the flow fluctuations are similar to those determined in the experiments described in 5.3 above;
- and 3. that additional mass effects are negligible.

It follows that the force per unit length of a structure due to a wind of mean velocity \bar{V} , containing a small superimposed harmonic fluctuation of frequency ω and "effective" amplitude V_e (over the region

of flow postulated in 1) will be

$$P = \frac{1}{2} \rho C_D(\omega) \bar{V}^2 + \rho C_D(\xi) \bar{V} D v_e \sin 2\pi n t$$

$$= \bar{P} + 2 \bar{P} \frac{C_D(\xi)}{C_D(\omega)} \frac{v_e}{\bar{V}} \sin 2\pi n t \quad (5.20)$$

where \bar{P} = the mean pressure = $\frac{1}{2} \rho C_D(\omega) \bar{V}^2 D$

In terms of the spectrum of the effective velocity $S_{v_e}(n)$ the spectrum of pressure $S_p(n)$, is found from this to be

$$S_p(n) = 4 \bar{P}^2 \left(\frac{C_D(n)}{C_D(\omega)} \right)^2 \frac{S_{v_e}(n)}{\bar{V}^2}$$

By the first assumption, clearly

$$S_{v_e}(n) = C S_v(n)$$

where C = velocity correlation over the postulated region of influence,

and $S_v(n)$ = spectrum of horizontal velocity at a point.

If we assume that C is given by equation 5.2 and write

$$|\chi_A(n)|^2 = C(\xi) \left[\frac{C_D(\xi)}{C_D(\omega)} \right]^2 \quad (5.21)$$

then the expression for the spectrum of pressures becomes

$$S_p(n) = 4 \bar{P}^2 |\chi_A(n)|^2 \frac{S_v(n)}{\bar{V}^2} \quad (5.22)$$

$|\chi_A(n)|^2$ will be termed the aerodynamic admittance; it is an important quantity in determining the pressures that develop. It is significant to note that, assuming the expression for $C(\xi)$ given in equation (5.2) is adopted, at the reduced frequencies for which $\frac{C_D(\xi)}{C_D(\omega)}$ becomes significantly greater than unity, $C(\xi)$ diminishes rapidly to very small values. Considering that $C(\xi)$ was not itself a precisely defined function and was based on somewhat conservative assumptions, it does not seem necessary to make any further allowance for the increase

in the drag coefficient. That is to say it seems adequate to assume that

$$|\chi_A(\xi)|^2 \approx C(\xi) \quad (5.23)$$

(with $C(\xi)$ given by eq. (5.2)).

5.4.2 Lift Forces

No examination has so far been made of the lift forces that develop on a bridge deck due to vertical gusts.

It is characteristic of most bridge decks that they will experience a vertical force when the wind is inclined to the plane of the deck. The forces that develop are large even at small angles of inclination. If the deck and the mean wind are horizontal, this angle of inclination - or angle of attack - of the deck to the wind, α is the angle between the horizontal and the instantaneous wind velocity.

Approximately,

$$\alpha = \frac{w}{V}$$

where w = the vertical component of velocity.

For most bridge decks it is possible, over a limited range, to represent the change in lift force with angle of attack by a straight line. This is true for example of the deck for the projected Severn suspension bridge, as can be seen from the results of the wind tunnel tests given in Fig. 9.2. Suppose that the slope of this line - i.e., the rate of change of lift force with α , is denoted by $\frac{dZ}{d\alpha}$, then the vertical force P is given by

$$P = \frac{dZ}{d\alpha} \cdot \frac{w_e}{V}$$

where w_e is an effective vertical velocity. The best assumption we can make regarding w_e is that, like the effective horizontal velocity, it is

the average vertical velocity over some hypothetical region of influence. If we follow the same arguments used in determining the response to horizontal gusts, the expression for the spectrum of the vertical lift force can be written

$$S_P(n) = \left(\frac{dz}{d\alpha} \right)^2 \cdot \frac{S_w(n)}{V^2} \cdot [\chi_A(n)]^2 \quad (5.25)$$

where $S_w(n)$ is the vertical velocity spectrum and

$$| \chi_A(n) |^2 = C(\xi) \quad (5.26)$$

as before.

Equations (5.22) and (5.25) now represent the necessary expressions for determining the spectra of the horizontal and vertical forces per unit length of the structure.

6.0 DYNAMIC AND STATIC BEHAVIOUR OF THE SUSPENSION BRIDGE AND TALL MAST

6.1 INTRODUCTION

Having estimated the aerodynamic pressures developed on a thin transverse "strip" of bridge, or mast, by the various frequency fluctuations in the wind, the next step is to consider how these localised pressures act collectively to excite individual modes of the structure. This can be done along the lines described in Section 3.0 provided we know the form of the cross-correlation of pressures across the span and the form of the various modes of vibration and their natural frequencies. Expressions for the cross-correlation of velocities have been given in Section 4.0, and it is reasonable to assume that for the latticed members of the mast and suspension bridge, in which the drag is generated by a large number of localised surfaces, the cross-correlation of pressures is similar. The modes and natural frequencies have not yet been discussed, however, and so represent the next aspect of the problem to be considered.

In particular we need to consider the lateral, vertical and torsional modes of the suspension bridge, and the lateral mode of the mast. Except for the lateral suspension bridge vibrations, methods already exist for determining these, and are summarized below. A method for determining the lateral modes is described in full.

6.2 VIBRATION OF THE SUSPENSION BRIDGE

6.2.1 Lateral Vibration

Suppose that the centre span of the suspension bridge is executing a simple harmonic motion laterally, and that at time t and station x across the span the deflexions of the stiffening truss and cable are given respectively by

$$y_T(x) \sin \omega t$$

and

$$y_c(x) \cdot \sin \omega t$$

Vibrations of the truss and the cable are linked by the tension that develops in the hangers as soon as one is displaced laterally relative to the other (see Fig. 6.1). If we denote the horizontal component of this hanger tension at station x as $q(x)$, (assumed uniformly distributed), then the equation of motion for the stiffening truss becomes

$$EI \frac{d^4 y_T}{dx^4} + q(x) = \frac{W_T}{g} \omega^2 y_T \quad (6.1)$$

The equation of motion for the cable is

$$H \frac{d^2 y_c}{dx^2} - q(x) = \frac{W_c}{g} \omega^2 y_c \quad (6.2)$$

where EI is the rigidity of the stiffening truss;

W_T is the dead weight of the truss;

W_c is the dead weight of the cable;

$q(x)$ is the horizontal tension in the cable;

and g is the acceleration due to gravity.

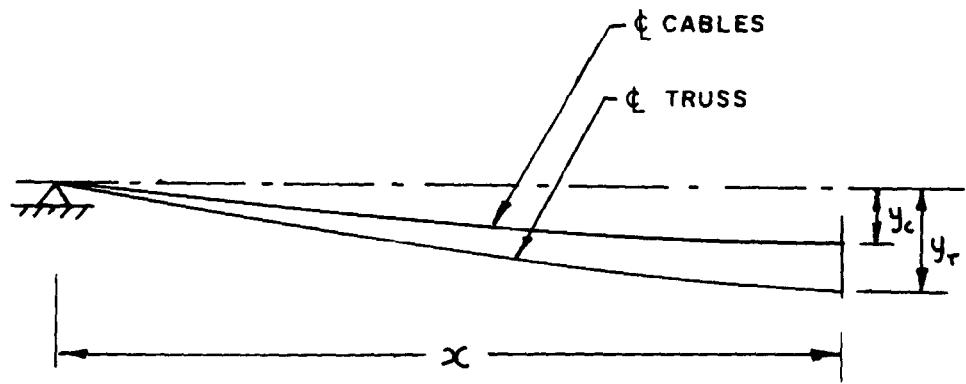
From Fig. 6.1b, by taking moments about the cable for the equilibrium of the truss, the horizontal component of tension in the cable is seen to be

$$q(x) = \frac{(y_T - y_c)}{h(x)} W_T \quad (6.3)$$

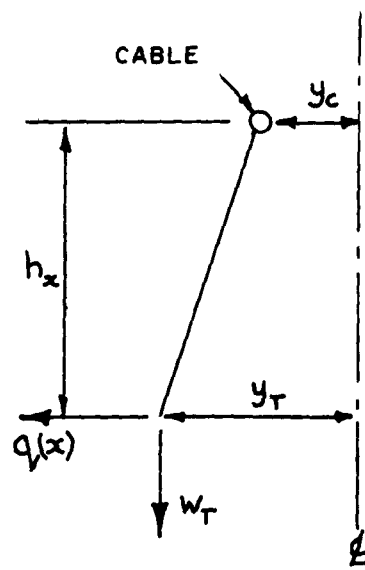
where $h(x)$ is the hanger length.

Let the deflexion of the truss and cable be represented by harmonic series of the type

$$y_T(x) = \sum_r a_r \sin \frac{r\pi x}{l} \quad (6.4)$$



PLAN



FORCES ON CABLE

FIG. 6.1 LATERAL LOADING OF SUSPENSION BRIDGE

$$y_c(x) = \sum_r b_r \sin \frac{r\pi x}{l} \quad (6.5)$$

Substituting in (6.3)

$$q(x) = w_T \sum_r (a_r - b_r) \frac{\sin \frac{r\pi x}{l}}{h(x)} \quad (6.6)$$

The quantity $\sin \frac{r\pi x}{l} / h(x)$ can be analysed harmonically as

$$\sin \frac{r\pi x}{l} / h(x) = \frac{2}{\pi} \sum_s \left[\int_0^l \frac{\sin \frac{r\pi x}{l}}{h(x)} \cdot \sin \frac{s\pi x}{l} dx \right] \sin \frac{s\pi x}{l} \quad (6.7)$$

Substituting from equations (6.4), (6.5), (6.6) and (6.7) into equations (6.1) and (6.2) and comparing the harmonic components, the following equations are obtained for the r th component:

$$EI \frac{\pi^4}{l^4} r^4 a_r + \frac{2w_T}{\pi} \sum_s (a_s - b_s) \int_0^l \frac{\sin \frac{r\pi x}{l}}{h(x)} \cdot \sin \frac{s\pi x}{l} dx = \frac{w_T}{g} \omega^2 a_r \quad (6.8)$$

$$H \frac{\pi^2}{l^2} r^2 b_r - \frac{2w_T}{\pi} \sum_s (a_s - b_s) \int_0^l \frac{\sin \frac{r\pi x}{l}}{h(x)} \cdot \sin \frac{s\pi x}{l} dx = \frac{w_c}{g} \omega^2 b_r \quad (6.9)$$

These equations can be written for all values of r , and then solved for the a 's and b 's which determine the mode shape, and for ω , which gives the frequency. In practice, only a few equations need be considered because, in any given mode, the corresponding harmonic component will always predominate over all the others and give a good first approximation to the mode. Two terms in the harmonic series generally yield all the accuracy needed. The method of numerical solution is best left until the numerical example given later.

It should be noted that, because the hanger lengths, $h(x)$ are usually symmetrical about the bridge centreline, the integrals in equations (6.8)

and (6.9) only have any value when r and s are either both even or both odd. It then follows that the equations group themselves into two families involving in the one case the odd terms only, and in the other case the even terms only.

6.2.2 Vertical Vibrations

Since the failure of the Tacoma Narrows bridge, in which coupled torsional and vertical oscillations were chiefly responsible, there has been a considerable amount of attention paid to the behaviour of the suspension bridge in these modes. Theoretical methods for determining the natural modes and frequencies have been checked experimentally. (see Bleich et al - 1950; Farquahson - 1952).

The basic equation for the vertical vibration of the suspension bridge is

$$\frac{w}{g} \omega^2 y = -\frac{d^2}{dx^2} \left[Hy + \eta \Delta H - EI \frac{d^2 y}{dx^2} \right]$$

where H is the initial horizontal cable tension;

ΔH is the increment of the cable tension during vibration;

EI is the rigidity;

η is the initial cable dip at station x ;

y is the mode deflexion;

ω is the circular frequency of vibration;

and w is the total dead weight of the span.

A simple routine method for determining the modes and frequencies from this equation has been given by Steinman (1959). It does not seem necessary to repeat the derivation of the various expressions, but for convenience of reference they are given here straightforwardly without proof. The natural frequency, n , of the suspension bridge can be expressed as

$$n = \frac{1}{2\pi} \sqrt{\frac{k.g}{w}} \tag{6.10}$$

where K is an effective stiffness for the bridge as a whole.

The effective stiffness K has to take account of a number of contributory elements such as the elastic stiffness of the stiffening truss in bending, the interaction of the side spans through flexing of the towers, the elastic extension of the cable and the gravity stiffness of the cable itself. For antisymmetric modes ($r = 2, 4, 6$ etc.) there is no side span interaction or stretching of the cable, and the expression for K is simply

$$K = r^2 \frac{\pi^2}{l^2} H + r^4 \frac{\pi^4}{l^4} EI \quad (6.11)$$

where r is the mode number,

and l is the span length as before.

Substitution of this expression in (6.10) gives the frequency directly. The mode is given by

$$y = a \sin \frac{r\pi x}{l} \quad (6.12)$$

For the symmetric modes, the expression for K is more complex, since side span interaction and cable stretching are both bound to occur. In this case K is given as the solution to an expression of the type

$$\sum' \frac{C \frac{f}{l}}{r^2 \left(K - \frac{w_0}{w} K_r \right)} \quad (6.13)$$

where the summation covers all odd values of r in each of the several spans of the bridge. In this expression

$$K_r = r^2 \frac{\pi^2}{l^2} H + r^4 \frac{\pi^4}{l^4} EI \quad (6.14)$$

f = the central dip of the cable (measured vertically from the chord joining the two ends of the cable span);

l = length of the particular span in the summation;

w = dead weight of span;

w_0 = dead weight of main span.

The quantity $C = \frac{512}{\pi^2} \cdot \frac{f}{l^2} \cdot \frac{E_c A_c}{L_s}$ (6.15)

where E_c = the elastic modulus,

A_c = the cross sectional area of the cable,

and L_s = the total length of cable (all spans),

$$= \sum \left(1 + \frac{8f^2}{l^2} \right) \sec^3 \gamma$$

where γ = the inclination of the cable chord,

and the summation covers all the spans. Solving equation (6.13) for K is not difficult and can be determined rapidly using successive approximations as shown in the worked example.

The mode forms are not given simply by single harmonic terms (as in the antisymmetric modes) but by a series of harmonic terms in which the dominating term will, however, always correspond to the particular mode being considered (i.e. in the r th mode the r th harmonic term will always predominate). If the mode shape for the main span is

$$y_0 = a_1 \sin \frac{\pi x}{l_0} + a_3 \sin \frac{3\pi x}{l_0} + \dots$$

and for the side spans is

$$y_s = a_{s1} \sin \frac{\pi x}{l_s} + a_{s3} \sin \frac{3\pi x}{l_s} + \dots$$

then the relative amplitudes of the coefficients are given by the proportionality,

$$a_r \propto \frac{1}{r \left(K - \frac{w_0}{w} K_r \right)} \quad (6.16)$$

which holds for both main and side spans.

Determination of the vertical modes by this method is illustrated in the worked example.

6.2.3 Torsional Oscillations

Similar expressions for determining the torsional modes and frequencies have also been given in the same paper by Steinman (1959).

The formulae are not repeated here, however, partly because they cannot be stated with quite the same conciseness as in the case of vertical oscillations, and partly because torsional oscillations have not been considered in the worked example given later - mainly because the necessary numerical data was not available at the time of writing. This omission of the torsional modes does not imply that they are less critical than either the lateral or vertical modes.

6.3 THE VIBRATION OF THE GUYED MAST

6.3.1 General

The vibration of the tall mast was first analysed by Kolousek (1947). The method he employed was based on the 'slope-deflexion' technique, and required solving simultaneously a number of equations for the slope and deflexion of each point of discontinuity on the mast, where either a change of section or a guy attachment point occurred. For very tall masts, with many guy levels and incorporating several changes of section, the work involved quite soon becomes laborious, and better suited for electronic, rather than desk computation. With the additional complication of large axial loads, the solution along these lines is still more difficult.

An alternative method was suggested by Davenport (1959) using a development of the so-called Basic function technique first used by Inglis for determining the whirling speed of turbine shafts. These functions represent the natural modes of uniform beams possessing similar end conditions to the beam under consideration. For example, the Basic function for a simply supported beam is the sine function. For the "hinged-free" and "fixed-free" beams, which have end conditions similar

to the two types of guyed mast found in practice, the Basic functions are composed of both trigonometrical and hyperbolic functions. The mast can be analysed as a whole by simply representing the deflexion, bending moments etc. in terms of series of these functions and their derivatives. The number of terms used in the series depends only on the accuracy required.

It is usual to regard the guyed mast as an elastic beam resting on flexible supports. These supports (provided by the guys) can, for limited deflexions, be regarded as having linear characteristics. Under static loads the stiffness of the guys is due principally to the elastic stiffness of the cable stretching as a taut wire; this is partially offset, however, by a gravity effect due to the raising and lowering of the cable mass during the deflexion process. Under dynamic loading this stiffness contains a third element due to the inertia effect of the cable mass which, as was shown by Davenport (1959), can be large when the excitation frequency is close to the natural frequency of the cable vibrating as a taut wire. The dynamic behaviour of the guy cable is now considered.

6.3.2 The Influence of the Guys

It is well known that the shape the guy cable will adopt when it hangs at rest is the arc of a catenary. If however the tension is large enough so that the change in tension due to the weight of the cable is small, this arc will be almost exactly parabolic. In practice this is almost always the case for the simple reason that a slack cable is a most ineffective support. This assumption, that the arc will be

almost exactly parabolic, is made here.*

Consider the guy illustrated in Fig. 6.2. The notation is defined as follows:

- T is the average tension in the cable,
 - $\Delta T(t)$ is the change in this tension at time t during a cycle due to the movement of the upper guy attachment point in vibration,
 - S is the length of the cable, at rest,
 - σ is the inclination of the chord joining the two ends of the guy,
 - w is the weight per unit length of the cable,
 - A_g is the cross sectional area of the cable,
 - E_g is the elastic modulus of the cable material,
- and ρ is the mean radius of curvature of the guy cable at rest.

The case in which the stack is vibrating in the same plane as the guy, is examined first.

Consider an element of length dx at distance x from the lower end. Suppose that when the stack is stationary the deflection from the chord is y ; suppose, further, that when the upper end of the cable is displaced horizontally during vibration by an amount $v(t)$, that the deflection of the same element becomes $y + \eta(t)$ measured now from the chord in its new position ON' . The additional displacement of the element due to the rotation of the chord is $\frac{x}{S} \cdot v(t) \cdot \sin \sigma$ and the normal acceleration of the element is therefore

*At the time of writing, a paper by Dean has appeared ("The static and dynamic characteristics of guy cables" - J. Str. Div. Proc. Am. Soc. Civ. Eng. Jan. 1961) in which this assumption is not made and the derivation based on the catenary. Although the results for fairly shallow guys are not likely to differ greatly, for steep, slack guys, Dean's derivation is clearly preferable.

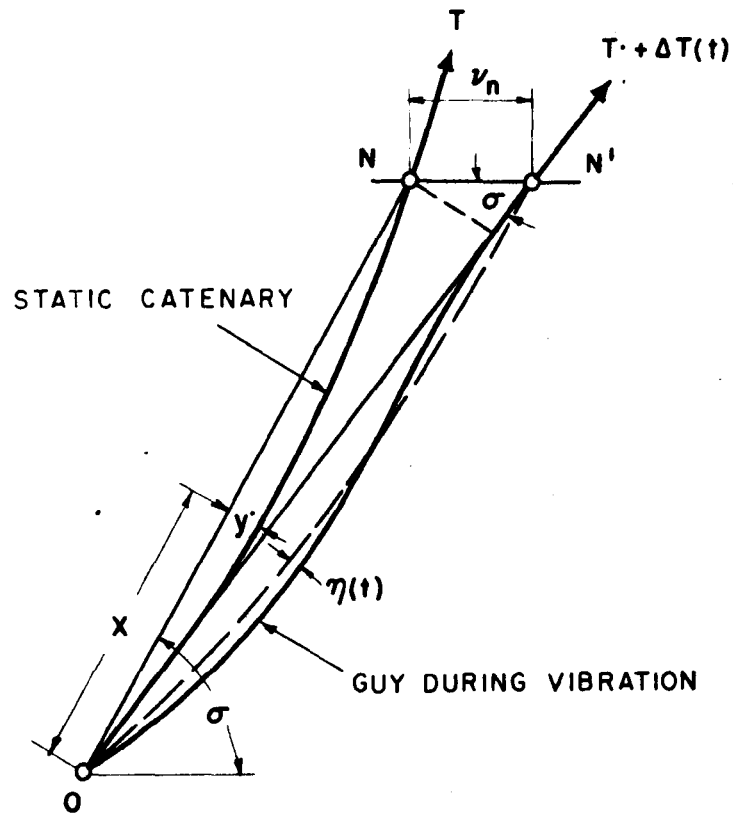


FIG. 6.2 DISPLACEMENT OF GUY DURING VIBRATION

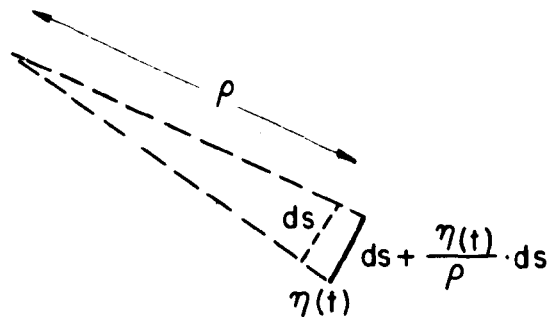


FIG. 6.3 EXTENSION OF GUY ELEMENT DURING VIBRATION

$$\frac{x}{s} \ddot{v}(t) \cdot \sin \sigma + \ddot{\eta}(t)$$

The total force causing this acceleration is

$$\left[T \cdot \eta''(t) + \Delta T \cdot y'' + \Delta T(t) \eta''(t) \right] dx$$

where y'' signifies $\frac{d^2 y}{dx^2} \approx -\frac{1}{e}$.

The quantity $\Delta T(t) \cdot \eta''(t)$ is of second order if the vibration is small, and the equation of motion therefore becomes

$$\frac{W}{g} \left(\frac{x}{s} \sin \sigma \ddot{v}(t) + \ddot{\eta}(t) \right) = \Delta T(t) \cdot y'' + T \eta''(t) \quad (6.17)$$

The change in length between the ends of the guys due to the additional deflection $\eta(t)$ is given by $\int_0^s y'' \cdot \eta(t) \cdot dx$ (This result can be seen from the elementary diagram in Fig. 6.3). The elastic extension due to the additional tension $\Delta T(t)$ is $\frac{\Delta T \cdot s}{A_g \cdot E_g}$. Equating this with the longitudinal displacement of the upper end of the guy

$$v(t) \cdot \cos \sigma = \frac{\Delta T \cdot s}{A_g \cdot E_g} + \int_0^s y'' \cdot \eta(t) \cdot dx$$

From the theory of taut wires, the curvature

$$y'' = -\frac{1}{e} = -\frac{W}{T} \cos \sigma$$

Hence

$$\Delta T(t) = \frac{E_g \cdot A_g \cdot \cos \sigma}{s} \left[v(t) + \frac{W}{T} \int_0^s \eta(t) \cdot dx \right] \quad (6.18)$$

Equation (6.18) shows that $\Delta T(t)$ and $\eta(t)$ are linear functions of $\nu(t)$. Therefore if $\nu(t)$ varies harmonically with circular frequency ω , then so will $\Delta T(t)$ and $\eta(t)$. That is, if $\nu(t) = \nu \cdot \sin \omega t$ then $\Delta T(t) = \Delta T \cdot \sin \omega t$ and $\eta(t) = \eta \cdot \sin \omega t$. Substitution in equation (6.18) gives

$$\frac{W}{g} \cdot \omega^2 \left(\frac{x}{s} \cdot \sin \sigma \cdot \nu + \eta \right) + T \cdot \eta'' + \Delta T \cdot y'' = 0$$

Substituting from (6.18) into this last equation,

$$\begin{aligned} \frac{W}{g} \cdot \omega^2 \sin \sigma \nu + \frac{W}{g} \cdot \omega^2 \eta + T \eta'' + \frac{E_g A_g \cos^2 \sigma}{s} \frac{W}{T} \nu \\ + \frac{E_g A_g \cos^2 \sigma}{s} \frac{W^2}{T^2} \int_0^s \eta \cdot dx = 0 \end{aligned} \quad (6.19)$$

To solve this equation, η is represented by the Fourier series

$$\eta = \nu \left[a_1 \sin \frac{\pi x}{s} + a_2 \sin \frac{2\pi x}{s} + \dots + a_n \sin \frac{n\pi x}{s} + \dots \right] \quad (6.20)$$

Likewise each term of equation (6.19) can be broken down into a series of harmonic components. Since equation (6.19) must be satisfied for each component separately, as many equations can be formed as there are harmonic components. From these, the various coefficients a_1, a_2, \dots etc. may be determined. Equation (6.18) then gives the so-called guy modulus K , which, after some further simplification, can be written

$$K = \frac{\Delta T(t)}{\nu(t)} = k \left[1 - \frac{F \cdot \Omega^2 - 1}{G \cdot \Phi(\Omega) - 1} \right] \quad (6.21)$$

where

$$k = \frac{E_g A_g \cos^2 \sigma}{s}$$

$$F = \frac{\pi^2 T^2}{W \cdot s^2 \cdot k} \cdot \frac{\sin \sigma}{2}$$

$$G = \frac{\pi^2 T^3}{s^3 w^2 k}$$

$$\Omega = \frac{\omega}{\frac{\pi}{8} \sqrt{\frac{Tg}{w}}}$$

$$\text{and } \bar{\Phi}(\Omega) = \Omega^2 \left\{ 1 - \frac{\tan \frac{\pi \Omega}{2}}{\frac{\pi \Omega}{2}} \right\}^{-1}$$

The quantity Ω , in fact, is the ratio of the impressed frequency ω , to the fundamental frequency of the guy cable vibrating as a taut wire. Values of $\bar{\Phi}(\Omega)$ have been given by Davenport (1959).

If the mast is vibrating at an angle Θ inclined to the plane of the guy, the expression for the guy modulus is

$$K_{\Theta} = k \cos^2 \Theta \left[1 - \frac{\cos \Theta}{\cos \phi} \frac{F \cdot \Omega^2 - \cos^2 \phi}{G \cdot \bar{\Phi}(\Omega) - \cos^2 \phi} \right] \quad (6.22)$$

where
$$\cos \phi = \frac{\cos \Theta \cos \sigma}{\sqrt{1 - \cos^2 \Theta \cos^2 \sigma}}$$

The static modulus can be found by putting $\omega = 0$ (or $\Omega = 0$), for which $\bar{\Phi}(\Omega) = -\frac{12}{\pi^2}$. Equation 6.22 then gives

$$K = k \cos^2 \Theta \left[1 - \frac{\cos \Theta \cdot \cos \phi}{\frac{12 T^3}{s^3 w^2 k} - \cos^2 \phi} \right] \quad (6.23)$$

Since $\frac{12 T^3}{s^3 w^2 k}$ is usually much greater than $\cos^2 \phi$ the static modulus can be written

$$K = k \cos^2 \Theta \left[1 - \cos \Theta \cos \phi \frac{s^3 w^2 k}{12 T^3} \right] \quad (6.24)$$

a familiar result obtained otherwise from purely static considerations.

It is significant to consider the general behaviour of the dynamic guy modulus given by equation 6.21 (or 6.22).

For small values of Ω (i.e. impressed frequencies much less than the fundamental frequency for the guy cable), the modulus is quasi-static: that is to say, dynamic effects are not felt. As Ω approaches

unity (impressed frequency equal to the fundamental for the guy) the modulus falls to the value $\frac{\pi^2 T^2}{W S^2} \cdot \frac{\sin \sigma}{2}$, which is independent of elastic terms. For a very small further increase in frequency the guy modulus becomes first negative, and then goes through a series in infinities (positive and negative) as $G \cdot \ddot{\phi}(\Omega) \rightarrow \omega \sigma^2 \phi$. The infinities are found to occur whenever the impressed frequency is slightly greater than the odd-mode natural frequency of the cable. Between these frequencies, i.e. for $1 > \Omega > 3$, $3 > \Omega > 5$ etc., the guy modulus is generally constant at a value close to the simple elastic stiffness for the cable - k . This implies that there is practically no gravity or inertia contribution to the dynamic cable modulus at frequencies above the fundamental for the cable - except in the immediate vicinity of the odd-mode natural frequencies of the guy cable, when the inertia stiffness dominates almost completely.

In considering these results it must be remembered that no allowance has been made for the damping of the cable which is inevitably present whenever the guy cable is forced into oscillation. This explains the somewhat anomalous result that the modulus is infinite when the frequency is close to the odd-mode natural frequency of the guy cable. This behaviour is analogous to that of any undamped dynamic system which when excited at its own natural frequency theoretically builds up to an infinite amplitude. It is to be expected, therefore, that if damping is taken into account, the modulus will remain finite at all frequencies and the anomaly thereby removed. A further factor is that, as the impressed frequency approaches the odd-mode natural frequency of the guy cable, the amplitudes probably become large, and the strictly linearised theory adhered to above no longer holds. Non-linear effects will usually

tend to inhibit the amplitude somewhat and in effect, to damp the vibration.

The modifications necessary to the guy modulus when velocity damping is acting (not previously considered by the writer (Davenport - 1959)) are now discussed.

6.3.3 Effect of damping on the Guy Modulus

The equation of motion for the guy cable with damping is the same as equation (6.19) with the addition of the velocity damping term,

$$c \left(\frac{x}{s} \sin \sigma \cdot \dot{v} + \dot{\eta} \right) \quad (6.25)$$

where c is the velocity damping coefficient. The effect of damping is to produce a phase difference between the force $\Delta T(t)$ and the mast deflexion $v(t)$.

Thus if $\eta(t) = \eta \sin \omega t$

then $v(t) = (u + i v) \sin \omega t$

Following the previous procedure we express the cable deflexion as a Fourier series, which this time must be taken as complex. Assume therefore

$$\eta = u \left(a_1 \sin \frac{\pi x}{s} + a_2 \sin \frac{2\pi x}{s} + \dots \right) \\ + i v \left(b_1 \sin \frac{\pi x}{s} + b_2 \sin \frac{2\pi x}{s} + \dots \right)$$

If substitution is made for $\eta(t)$ and $v(t)$ in the equation of motion, the equation is found to consist of a real, and an imaginary part, both of which must be satisfied independently. If each term of these two equations is broken down (by Fourier analysis) into its harmonic components

then the equations must hold for each harmonic component separately. From these equations so formed, the coefficients a_1 , a_2 , etc. and b_1 , b_2 etc. may be determined.

Equation (6.18) is again used to determine the guy modulus, which this time is found to consist of a real (i.e. in-phase) and an imaginary (i.e. quadrature) component. After some manipulations, the in-phase component is found to be

$$K = k \left[1 - \frac{(F.\Omega^2 - 1)(G.\psi_1(\Omega) - 1) + 2G.F.\Omega.\alpha.\psi_2(\Omega)}{(G.\psi_1(\Omega) - 1)^2 + (G.\psi_2(\Omega))^2} \right] \quad (6.26)$$

The quadrature component of the guy modulus is

$$K' = -k \left[\frac{2F.\Omega.\alpha(G.\psi_1(\Omega) - 1) + (F.\Omega^2 - 1)G.\psi_2(\Omega)}{\{G.\psi_1(\Omega) - 1\}^2 + \{G.\psi_2(\Omega)\}^2} \right] \quad (6.27)$$

where k, F, G and Ω are the same as before and

$$\alpha = c s \sqrt{\frac{g}{WT}} \cdot \frac{\sin \sigma}{2} \quad (6.28)$$

$$\psi_1(\Omega) = \frac{8s^2}{\pi^4 T} \frac{\phi_1}{\phi_1^2 + \phi_2^2} \quad (6.29)$$

and

$$\psi_2(\Omega) = \frac{8s^2}{\pi^4 T} \frac{\phi_2}{\phi_1^2 + \phi_2^2} \quad (6.30)$$

The functions ϕ_1 and ϕ_2 denote

$$\phi_1 = \sum_{n \text{ odd}} \frac{\Omega^2 - n^2}{n^2 [(\Omega^2 - n^2)^2 + 4\Omega^2\alpha^2]} \quad (6.31)$$

$$\phi_2 = \sum_{n \text{ odd}} \frac{2\Omega\alpha}{n^2 [(\Omega^2 - n^2)^2 + 4\Omega^2\alpha^2]} \quad (6.32)$$

where the summations cover all odd values of n .

If the velocity damping coefficient is zero (i.e. $\alpha = 0$) it is found that the quadrature component of the guy modulus, given in equation 6.27, has no value and the in-phase component of equation (6.26) reverts to the undamped form of equation (6.21), as might be expected.

The denominators in the expressions for the guy modulus are seen to consist of the sum of two squared terms. Provided the damping coefficient is non-zero, the second of these is always positive and greater than zero and so the guy modulus can never become infinite as in the undamped case.

In a high wind the velocity damping will arise in two ways. First from the natural mechanical damping produced by the rubbing of strands of the cable against one another, and second due to the aerodynamic, drag damping (corresponding to the fluctuating drag component of the pendulum in the experiments discussed in Section 5) of the cable moving against the strong air flow.

It is evident from the analysis of Section 5.3.3 (of the damping of the pendulum) that the value of the damping coefficient is given by

$$c = \rho \cdot C_D \cdot D \cdot \bar{v}$$

6.3.4 Vibration of the Mast with Guys

As noted, the method used for determining the vibration of the guyed mast is that described by Davenport (1959). This uses the Basic functions which describe the natural modes for the uniform beam having end restraints similar to the mast. For the mast ball-jointed at the

base and unsupported at the top, the first four Basic functions of the lowest order, labelled $B_1(x)$, $B_2(x)$, $B_3(x)$ and $B_4(x)$ are

$$\begin{aligned} B_1(x) &= \frac{x}{l} \\ B_2(x) &= -2.787495 \times 10^{-2} \sinh \frac{\alpha_2 x}{l} + \sin \frac{\alpha_2 x}{l} \\ B_3(x) &= 1.2041205 \times 10^{-3} \sinh \frac{\alpha_3 x}{l} + \sin \frac{\alpha_3 x}{l} \\ B_4(x) &= -5.20346 \times 10^{-5} \sinh \frac{\alpha_4 x}{l} + \sin \frac{\alpha_4 x}{l} \end{aligned} \quad (6.33)$$

where $\alpha_2 = 3.92660$

$$\alpha_3 = 7.06583 \quad (6.34)$$

$$\alpha_4 = 10.21018$$

and $l =$ the overall span length.

These functions are illustrated in Fig. 6.4 and have been tabulated by Davenport (1959).

For the beam cantilevered at the base and unsupported at the top, the first three Basic function are given by

$$\begin{aligned} B_1(x) &= 1.362221 \left[\cosh \alpha_1 \frac{x}{l} - \cos \alpha_1 \frac{x}{l} \right] - \left[\sinh \alpha_1 \frac{x}{l} - \sin \alpha_1 \frac{x}{l} \right] \\ B_2(x) &= 0.9818676 \left[\cosh \alpha_2 \frac{x}{l} - \cos \alpha_2 \frac{x}{l} \right] - \left[\sinh \alpha_2 \frac{x}{l} - \sin \alpha_2 \frac{x}{l} \right] \\ B_3(x) &= 1.000776106 \left[\cosh \alpha_3 \frac{x}{l} - \cos \alpha_3 \frac{x}{l} \right] - \left[\sinh \alpha_3 \frac{x}{l} - \sin \alpha_3 \frac{x}{l} \right] \end{aligned} \quad (6.35)$$

where $\alpha_1 = 1.875104$

$$\alpha_2 = 4.694092 \quad (6.36)$$

$$\alpha_3 = 7.854757$$

These functions are illustrated in Fig. 6.5 and again have been tabulated by Davenport (1959).

Two subsidiary functions are also required (termed the second and third Basic functions) and these are defined respectively by

$$b_n(x) = \frac{1}{\alpha_n} \frac{d B_n(x)}{d x/l} \quad (6.37)$$

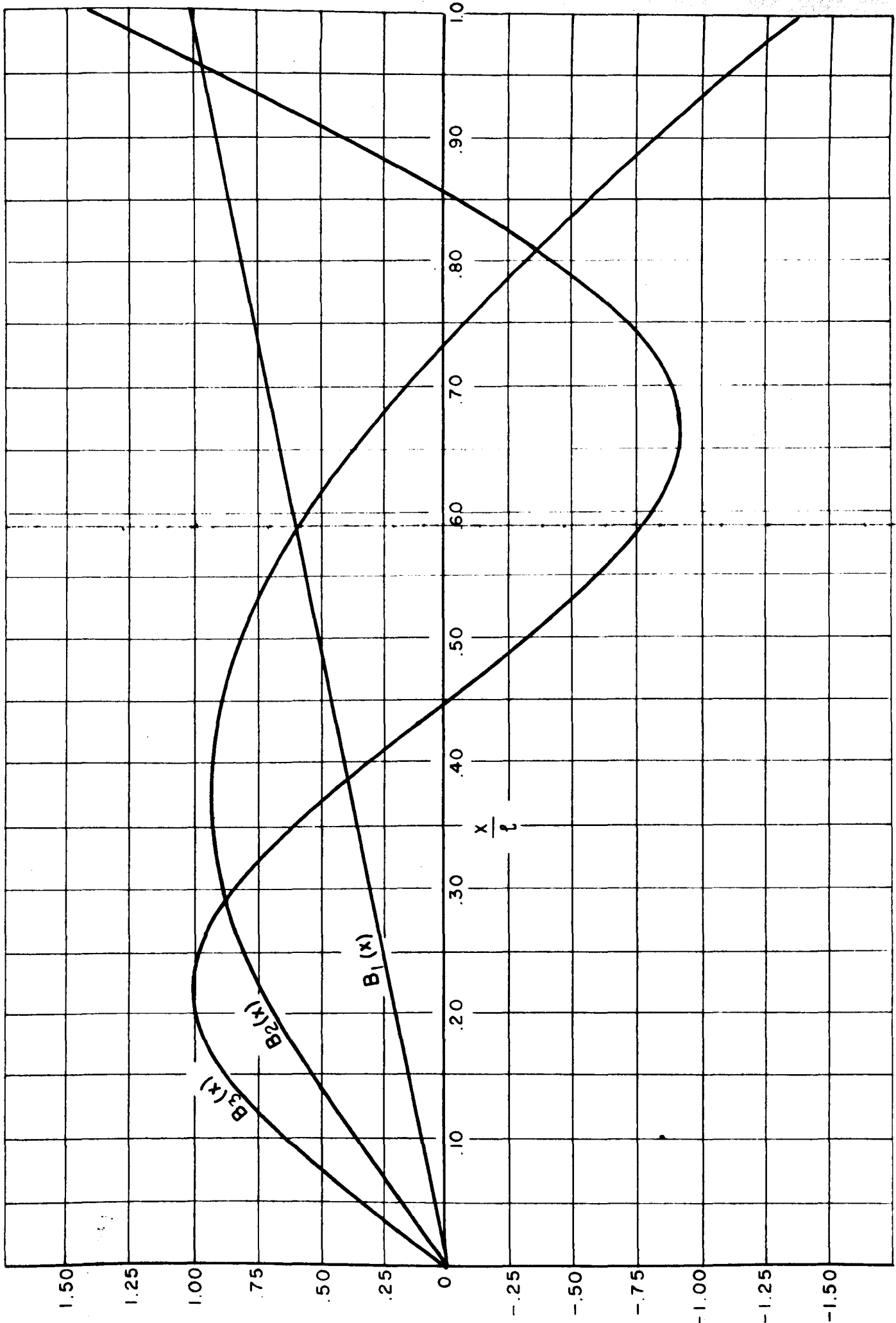


FIG 6.4 BASIC FUNCTIONS FOR HINGED-FREE BEAM

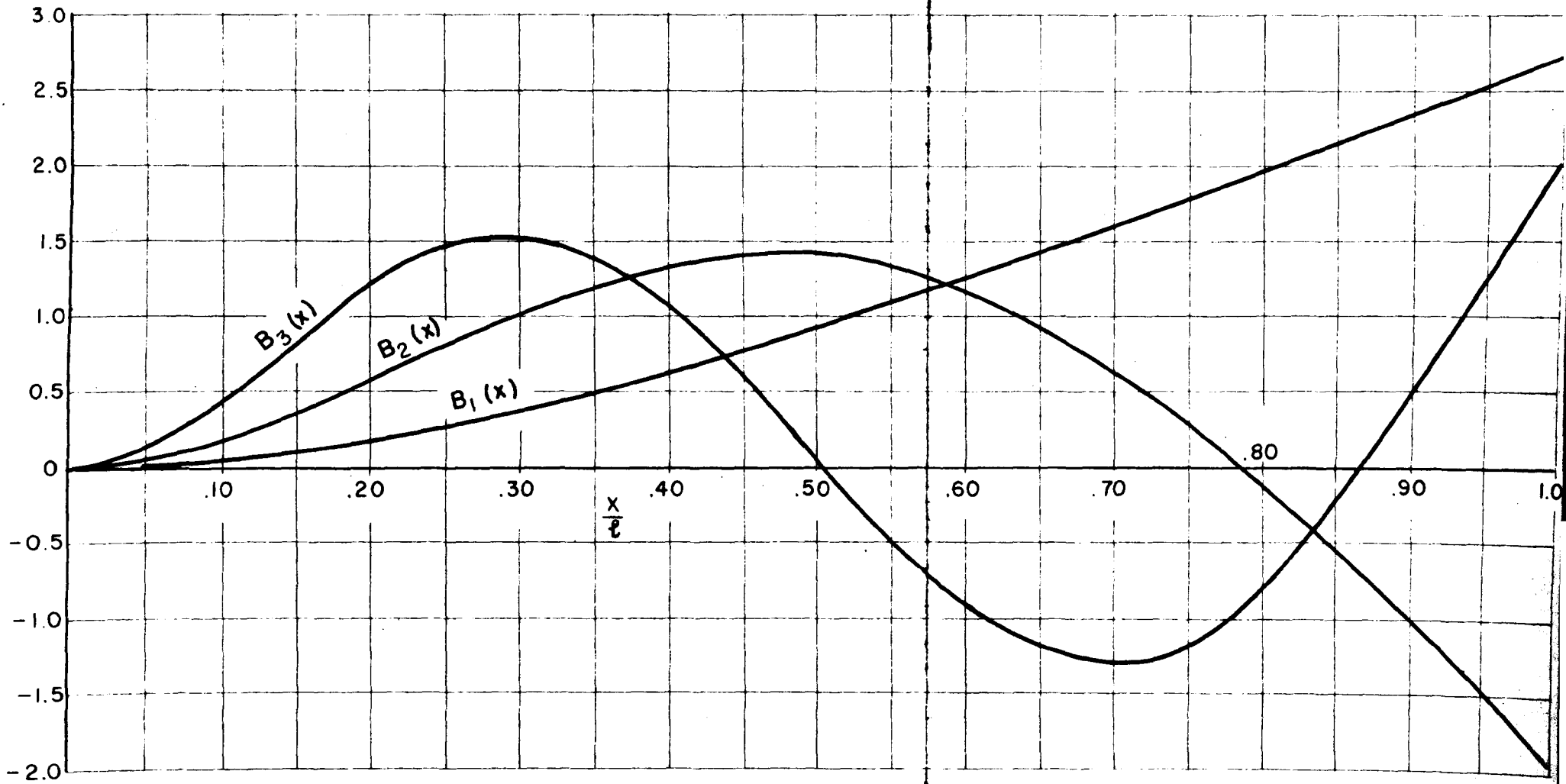


FIG.6.5 BASIC FUNCTIONS FOR CANTILEVER BEAM

and

$$\beta_n(x) = \frac{1}{\alpha_n^2} \frac{d^2 B_n(x)}{d^2 x/l} \quad (6.38)$$

These functions have also been tabulated (Davenport - 1959)

The method of solution using Basic functions is now described.

Consider a mast of total height l , for which the rigidity and mass (which may be irregular or discontinuous) have values EI_x and m_x at height x above the base. Suppose that the tower is supported by guys at several levels, the j^{th} level being at a height c_j and having a total dynamic modulus for the guy system at this level of K_j . It is not necessary at this point to specify whether the tower is fixed at the base or pinned.

The deflection (or mode) of the tower during vibration may be represented by the series

$$y = \sum_r a_r B_r(x) \quad (6.39)$$

The determination of the natural frequencies and modes of vibration can now proceed by an energy method. This consists of determining the total elastic energy stored up by the tower and the guys at its point of extreme deflexion when it is momentarily at rest, and equating this with the kinetic energy of the tower and the change in potential energy of the axial loads, as the tower passes through the mid-position.

The total elastic energy stored up by the guys, U_g , is given by

$$U_g = \frac{1}{2} \sum_j K_j y_j^2$$

where the summation includes all the guys. From equation (6.39)

$$y_j = \sum_r a_r B_r(c_j)$$

and so

$$U_g = \frac{1}{2} \sum_j K_j \sum_r a_r B_r(c_j) \quad (6.40)$$

The total elastic energy stored up by the tower U_t (if the shear energy is neglected) is given by

$$U_t = \frac{1}{2} \int_0^l EI_x \left(\frac{d^2 y}{dx^2} \right)^2 dx$$

Differentiating equation (6.39) twice and substituting third Basic functions, $\beta_r(x)$ for $\frac{d^2 y}{dx^2}$, we have

$$U_t = \frac{1}{2} \int_0^l \frac{EI_x}{l^4} \left[\sum_r a_r \cdot \alpha_r^2 \cdot \beta_r(x) \right]^2 dx \quad (6.41)$$

The change in potential energy ΔV of the axial loads S_x due to the deflection of the tower and its consequent small foreshortening, is given by

$$\Delta V = \frac{1}{2} \int_0^l S_x \cdot \left(\frac{dy}{dx} \right)^2 dx$$

$\frac{dy}{dx}$ can be expressed in terms of second Basic functions and

$$\Delta V = \frac{1}{2} \int_0^l \frac{S_x}{l^2} \left[\sum_r a_r \cdot \alpha_r \cdot b_r(x) \right]^2 dx \quad (6.42)$$

If the mast is vibrating with circular frequency ω such that at time t

$$y(t) = y \cdot \sin \omega t$$

the kinetic energy W of the stack at its mid position ($t = \frac{n\pi}{\omega}$) is given by

$$W = \frac{1}{2} \int_0^l m_x \omega^2 y^2 dx$$

which, from equation (6.39) is

$$W = \frac{1}{2} \omega^2 \int_0^l m_x \left[\sum_r a_r \cdot B_r(x) \right]^2 dx \quad (6.43)$$

by the conservation of energy

$$Q = U_g + U_t - \Delta V - W = 0 \quad (6.44)$$

By the calculus of small variations

$$\frac{\partial Q}{\partial a_1} = \frac{\partial Q}{\partial a_2} = \dots = \frac{\partial Q}{\partial a_r} = 0 \quad (6.45)$$

Substituting equations (6.40), (6.41), (6.42) and (6.43) into (6.44) and applying (6.45) the following basic equation can be written for all values of r

$$\begin{aligned} & \frac{EI_0}{l^4} \alpha_r^2 \left\{ a_1 \cdot \alpha_1^2 \int_0^l \frac{EI_x}{EI_0} \beta_1 \beta_r d\frac{x}{l} + a_2 \cdot \alpha_2^2 \int_0^l \frac{EI_x}{EI_0} \beta_2 \beta_r d\frac{x}{l} \dots \right\} \\ & - \frac{S_0}{l^2} \alpha_r \left\{ a_1 \cdot \alpha_1 \int_0^l \frac{S_x}{S_0} b_1 b_r d\frac{x}{l} + a_2 \cdot \alpha_2 \int_0^l \frac{S_x}{S_0} b_2 b_r d\frac{x}{l} \dots \right\} \\ & + \sum_j \frac{K_j}{l} B_j(c_j) (a_1 B_1(c_j) + a_2 B_2(c_j) + \dots) \\ & = \omega^2 m_0 \left\{ a_1 \int_0^l \frac{m_x}{m_0} B_1 B_r d\frac{x}{l} + a_2 \int_0^l \frac{m_x}{m_0} B_2 B_r d\frac{x}{l} \dots \right\} \end{aligned} \quad (6.46)$$

where EI_0 , S_0 and m_0 are reference values.

Usually, it is quite sufficient to represent the deflexion by three or perhaps four terms of the series given by equation (6.39), so that equation (6.46) is written only for $r = 1, 2, 3$ and 4 . The four equations enable the natural frequency and the three ratios of the coefficients to be found. This can be done by a method of continuous approximation. The deflexion is first approximated by the dominant term of the series which invariably is the term corresponding to the number of the mode to be determined. (i.e. the second term if the second mode is being determined). The equation in which this term is dominant (in this case the second) then yields a first approximation to the frequency, ω , which can be

substituted in the other equations, to give the ratio of the a's. These in turn can be substituted into the original dominant equation to give a better approximation to the frequency. The procedure is repeated until all the values settle down, which usually requires either one or two cycles.

The determination of the various integrals involved in equation (6.46) is best accomplished by numerical integration, and for this purpose values of the various Basic function products have been tabulated at intervals of $\frac{x}{l} = .05$ by Davenport (1959). The procedure is further simplified by the use of certain fundamental properties of Basic functions given in Table 6.1, including the orthogonal property that for $r \neq s$

$$\int_0^1 B_r(x) \cdot B_s(x) dx = \int_0^1 \beta_r(x) \beta_s(x) dx = 0$$

6.4 Determination of Moments and Shears

From the point of view of design it is important to determine the moments and shears. If the mode form is known, these can be found directly from the basic property that the shear force

$$Q(x) = \int w \cdot dx \quad (6.47)$$

and the moment

$$M(x) = \int Q(x) \cdot dx \quad (6.48)$$

where w is a general expression for the loading on the beam.

In the case of the lateral suspension bridge modes the loading is provided by

1. the inertia loading of the deck $- \frac{w_T}{g} \cdot \omega^2 \cdot \mu(x)$,

TABLE 6.1

NUMERICAL QUANTITIES USED IN BASIC FUNCTION ANALYSIS

Hinged-free beam		Fixed-free beam
1.00000	α_1	1.875104
3.92660	α_2	4.694092
7.06583	α_3	7.854757
10.21018	α_4	--
1.00000	α_1^2	3.516015
15.41819	α_2^2	22.035000
49.92595	α_3^2	61.697208
104.24777	α_4^2	--
0.33333	$\int_0^1 B_1^2(x) dx$	1.855645
0	$\int_0^1 \rho_1^2(x) dx$	
0.50000	$\int_0^1 B_2^2(x) dx = \int_0^1 \theta_2^2(x) dx$	0.964065
0.50000	$\int_0^1 B_3^2(x) dx = \int_0^1 \beta_3^2(x) dx$	1.001553
0.50000	$\int_0^1 B_4^2(x) dx = \int_0^1 \rho_4^2(x) dx$	--

and 2. the cable reaction $q(x)$ (given by equation 6.3)).

For the vertical modes of vibration the loading is provided by

1. the inertia loading, $\frac{W}{g} \cdot \omega^2 y(x)$
2. the cable reaction $H \frac{d^2 y}{dx^2} + \Delta H \frac{d^2 \eta}{dx^2}$

where ΔH is the increment of cable tension given by

$$\Delta H = C \frac{\pi}{4} \sum \frac{a^4}{r^4}$$

the other quantities being given by equations (6.14) and (6.15)

The loading of the guyed mast is supplied by

1. the inertia loading $\frac{W}{g} \cdot \omega^2 y$
2. the guy reactions $K_j y_j$
3. the axial loads $\frac{d}{dx} (S_x \frac{dy}{dx})$

Knowing the form of the mode, the loadings can each be found and the moments and shears evaluated straight forwardly.

It should be noted that double differentiation of the deflexion to obtain $EI \frac{d^2 y}{dx^2}$, is not a satisfactory method for determining the moments. This is because differentiation of the serial representation of the mode deflexion is often non-convergent. The same argument applies to the shear forces.

6.5 THE RESPONSE OF THE MAST AND SUSPENSION BRIDGE TO STEADY WIND LOADING

6.5.1 General

In Section 3.2 the response of a beam to a static load distribution was analysed by expressing the deflexion and loading in terms of the natural modes of the structure. However, since the modes have been expressed in terms of series of either sine functions or Basic functions, it is in fact more direct to represent both the static load distribution and the deflexion in terms of these functions rather than the natural modes.

6.5.2 The Suspension Bridge

For the suspension bridge the mean wind may be taken as uniform across the span. This mean wind load acts laterally and consists of two components, \bar{P}_T and \bar{P}_C acting on the stiffening truss and cable respectively. The static analysis follows the dynamic analysis of Section 6.2.1 closely, only instead of inertia loading, the harmonic components of the static loading are substituted. Equations 6.8 and 6.9 now read

$$EI \frac{\pi^4}{l^4} r^2 a_r + \frac{2w_r}{\pi} \sum_r (a_s - b_s) \int_0^l \frac{\sin r\pi x}{h(x)} \sin \frac{s\pi x}{c} dx = \frac{4}{r\pi^2} \bar{P}_T \quad (6.49)$$

$$H \frac{\pi^2}{l^2} r^2 a_r + \frac{2w_r}{\pi} \sum_r (a_s - b_s) \int_0^l \frac{\sin r\pi x}{h(x)} \sin \frac{s\pi x}{c} dx = \frac{4}{r\pi^2} \bar{P}_C \quad (6.50)$$

From the above equations the coefficients a_r and b_r may be found, enabling the deflexion and the cable load, $q(x)$ to be found from equations 6.4, 6.5 and 6.6. Knowing the uniform wind loading \bar{P}_T and the proportion of this load taken directly by the cable, the lateral bending moments and shears induced in the stiffening truss may be found.

A method similar to the above has been described by Selberg, who also introduced into his analysis one or two secondary effects such as the deflexion of the tower tops. The value of including detailed secondary effects here, when the wind loading problem as a whole can only be sketched in broad outline is debatable, and can perhaps lead to a false impression of the accuracy of the final result.

6.5.3 The Tall Mast

In considering the mean wind loadings of the tall mast it is necessary to allow for the variation of the mean wind velocity with height. With this observation, the static wind load analysis, broadly

speaking, follows the dynamic analysis. The mean wind load is broken down into its Basic function components which are substituted for the inertia terms in the dynamic analysis. Equation (6.46) now is modified to

$$\frac{EI_0}{l^4} \alpha_r^2 \left\{ \sum_s a_s \alpha_s^2 \int_0^l \frac{EI_x}{EI_0} \beta_s \beta_r d\frac{x}{l} \right\} - \frac{S_0}{l^2} \alpha_r \sum_s a_s \alpha_r \int_0^l \frac{S_x}{S_0} b_s b_r d\frac{x}{l} + \sum_j \frac{K_j}{l} B_r(c_j) \sum_s a_s B_s(c_j) = \bar{P}_1 \int \frac{\bar{V}_1^2}{V_1^2} B_r(x) d\frac{x}{l} \quad (6.51)$$

where \bar{P}_1 , is the mean wind load of the reference height and \bar{V}_1 , the corresponding mean wind velocity.

From these equations (written for each value of r) the coefficients a_1, \dots, a_r may be determined and hence the deflexion. Knowing the deflexion, the guy reactions and the effect of the axial loads can be determined, and hence, the moments and shears. It should be noted that the static values for the guy moduli should be used, given by equation (6.24).

7.0 MECHANICAL AND AERODYNAMIC DAMPING

7.1 GENERAL

The damping of a structure vibrating in a high wind arises from two sources. First there is the mechanical damping occurring at joints of the structure and within the material itself, and second the aerodynamic damping due to the motion of the object through the strong current of air. Some estimate of these damping parameters is vital on account of the strong control they have over the attainable amplitudes of oscillation.

7.2 MECHANICAL DAMPING

The mechanical damping present in a structure appears to be an extremely variable quantity dependent on such factors as the material it is made of, the foundations, the mode of vibration and its construction - whether it is prestressed or reinforced in the case of concrete structures, or whether it has welded, rivetted or bolted joints in the case of metallic structures.

This mechanical damping can be determined experimentally by deflecting the structure, releasing it and recording the resulting decay of vibration, either by strain gauges or photographically. Several such experiments have been performed on full scale chimney stacks and masts, (see Davenport - 1959). The logarithmic damping decrement found from these experiments ranged from .01 for an unlined, welded steel structure to .10 for a welded aluminum structure. Two guyed steel masts, 120 ft. and 500 ft. high, both gave a value of .05. Two, 240 ft.-high, rivetted steel chimneys with brick linings gave values between .03 and .07.

Very little information is available on the mechanical damping of full scale suspension bridges although some experiments were performed on short span suspension bridges for light traffic (mostly wooden) by the University of Washington. These are reported by Farquahson et. al. (1954), from which it would seem that the logarithmic damping decrement can be expected to be at least .02.

There is bound to be difficulty in predicting exactly the mechanical damping in a structure. However, from what little information is available, it seems reasonable to assume that the damping will give a logarithmic decrement for the fundamental mode of vibration of at least .01 or .02. To assume a value of this magnitude for all modes is, of course, likely to underestimate the actual mechanical damping present, particularly in the higher modes. Fortunately the lack of precision will not, it seems, significantly affect the outcome because in this instance the mechanical damping is apparently overshadowed by the aerodynamic damping due to the high wind, which can be estimated fairly accurately.

The importance of the aerodynamic damping in the wind has been previously overlooked by the writer (see Davenport - 1959) and also by others discussing the aeroelastic vibration of the suspension bridge.

7.3 THE AERODYNAMIC DAMPING

A structure vibrating in air will be subject to certain aerodynamic forces tending to damp the vibration. In still air, the forces will be due mainly to the viscosity of the air disturbed by the oscillating object. The damping is not likely to be large and probably insignificant compared to the mechanical damping. If, however, the air is flowing past the object, the principal aerodynamic forces acting will be from drag and

lift. If the object is moving, fluctuating components of these lift and drag forces will be induced, tending to oppose, and hence damp out the motion. This form of damping is precisely that investigated in the pendulum experiments described in Section 5.3.

An alternative definition for the logarithmic damping decrement to that used before is

$$\delta = \frac{\Delta E}{2 E}$$

where ΔE is the work done per cycle against the drag (or lift), and E is the total energy stored in the system.

Suppose the mode of the beam (i.e. mast or suspension bridge) is $y = \mu(x)$, then the velocity of the beam at station x is

$$\dot{y} = 2\pi n_r \mu_r(x) \sin 2\pi n_r t$$

where n_r is the natural frequency in the r th mode.

The drag on a slice of the beam of thickness dx , in a steady wind of velocity \bar{V}_x is

$$d\bar{R} = \frac{1}{2} \rho C_D \bar{V}_x^2 D dx$$

where D is the diameter of the beam.

The fluctuating component of this drag, when the velocity of the object is \dot{y} , is

$$d(\Delta R) = dx \cdot \frac{2\dot{y}}{\bar{V}_x} \left(\frac{1}{2} \rho C_D \bar{V}_x^2 D \right)$$

The work done per cycle on the slice is then

$$d(\Delta E) = \oint d(\Delta R) dy$$

where the integral is taken over one cycle.

The total energy in the system is given by the kinetic energy at the mid-position of the oscillation. For the same slice of the beam this is

$$d(E) = dx \cdot \frac{1}{2} m_x \dot{y}^2$$

where $m(x)$ is the mass per unit length at station x .

For the entire beam, the logarithmic decrement is therefore

$$\begin{aligned} \delta &= \frac{\int_0^l d(\Delta E)}{\int d(E)} \\ &= \frac{(\frac{1}{2} \rho C_D D \bar{V}_1^2)}{n_r} \frac{\int_0^l \frac{\bar{V}_x}{\bar{V}_1} \mu_r^2(x) dx}{\int_0^l m(x) \mu_r^2(x) dx} \end{aligned} \quad (7.1)$$

This is the basic expression for the logarithmic decrement due to aerodynamic drag damping.

In the above form the expression applies principally to the tall mast, in which allowance has to be made for variations in the wind velocity with height and in the section of the mast. In the suspension bridge both of these generalities are unnecessary and both the wind velocity and the section can be assumed constant across the span. The expression then becomes simply

$$\delta = \frac{(\frac{1}{2} \rho C_D \bar{V}^2 D)}{n_r \bar{V} m} \quad (7.2)$$

Here the numerator represents the drag per unit length in a steady wind of velocity \bar{V} (provided that the drag coefficient can be taken as for quasi-steady flow).

For the vertical vibrations the expression is found to be

$$\delta = \frac{dZ}{d\alpha} \frac{1}{2 n_r \bar{V} m} \quad (7.3)$$

where $\frac{dZ}{d\alpha}$ is the rate of change of the lift force per unit length of the deck with the angle of attack α (in radians).

Evidently, the damping varies directly as the mean wind velocity and inversely as the frequency of vibration. The latter implies that the higher modes of vibration are more lightly damped.

The values these formulae give for the fundamental-mode, logarithmic decrement for the tall mast considered later in the worked example, are .4 and .7, for open country, and city conditions respectively: for the suspension bridge the values are .4 for the first vertical mode and .18 for the first lateral mode. These results (which are presumably typical) suggest that the aerodynamic drag and lift damping makes a far larger contribution to the total damping than does the inherent mechanical damping.

8.0 TIME-HISTORY RELATIONSHIPS

8.1 GENERAL

The aims of this discussion so far have been to estimate the spectra of the bending moments, shears and deflexions at all points on the span. In addition methods for determining the bending moments, shears and deflexions under the action of the mean wind load have been described. The problem now is to estimate the critical quantities needed in design from this basic information.

The question first to be considered is what quantities are critical? Answers to this may be several. If the structure is liable to failure through brittle fracture, then probably peak values of stress are most important. If on the other hand the structure is more vulnerable to fatigue failure the number of stress repetitions will be more vital. It will again depend to some extent on the design precepts; that is to say whether the structure is being analysed for ultimate collapse conditions or for a more limiting condition such as the onset of plastic yield of the material, with resulting permanent plastic set.

The particular criteria most relevant to the design of the suspension bridge and tall mast are again debatable. For the sake of argument, however, it will be assumed that the instantaneous peak values of stress are those that are most important in determining the sufficiency of the structural members.

A number of expressions are available for predicting, not only the peak values, but also such items as the number of excesses and maxima of a random series occurring in a given time. Several of these were arrived at in studies of noise in communications (Rice - 1945) and in ocean waves (Longuet Higgins - 1952). Three which seemed relevant

to civil engineering problems were given by Davenport (1961), and are now repeated here for convenience.

As noted elsewhere, the statistical distributions of all the stochastic variables considered here are assumed to be normal i.e. Gaussian. This follows immediately from the normal or near-normal distribution of the wind velocity and from the quasi-linear relationships which have been assumed to exist with all other variables - pressure, deflexion, shear, moment etc.

8.2.1 The Number of Excesses per Unit Time

Rice (1945) has shown that for a stationary random series of the normally distributed stochastic variable x that the number of times, $N(x_0)$, a given value x_0 is exceeded in unit time is

$$N(x_0) = \frac{\sigma'(x)}{\sigma(x)} e^{-\frac{x_0^2}{2\sigma^2(x)}} \quad (8.1)$$

where $\sigma(x)$ = standard deviation of x ;

$$\begin{aligned} &= \left[\int_0^{\infty} S_x(n) dx \right]^{1/2}, \\ \sigma'(x) &= \left[\int_0^{\infty} n^2 \cdot S_x(n) \cdot dx \right]^{1/2} \end{aligned} \quad (8.2)$$

and $S_x(n)$ = spectrum of x .

8.2.2 The Distribution of the Peak Values Occurring Within a Given Period

If a number of periods, each of duration T , are chosen from the same stationary random series, the proportion of them in which the largest values are less than x_0 is $1 - T \cdot N(x_0)$ ($0 \leq N \leq \frac{1}{T}$). Using Rice's expression for $N(x_0)$ it follows that the distribution of the peak, or largest, instantaneous values η for all the periods is

$$Q(\eta) = 1 - \nu T e^{-\frac{\eta^2}{2\sigma^2(x)}} \quad (8.3)$$

where $Q(\eta)$ = the probability that the maximum value during period
is less than η ,

$\sigma(x)$ = the standard deviation of the parent population of variable x ,

and $\nu = \frac{\sigma'(x)}{\sigma(x)}$.

The frequency density function is

$$q(\eta) = \frac{\nu T}{\sigma(x)} \cdot \eta \cdot e^{-\frac{\eta^2}{2\sigma^2(x)}} \quad (8.4)$$

νT will be termed the response factor. The mean of the distribution is found to be

$$\bar{\eta} = \sigma(x) \left[\sqrt{2 \log_e \nu T} + \frac{1}{\sqrt{2 \log_e \nu T}} \dots \right] \quad (8.5)$$

and the standard deviation

$$\sigma(\eta) = \frac{\sigma(x)}{\sqrt{2 \log_e \nu T}}$$

The form of the distribution and its relation to the parent

population can be seen from Fig. 8.1.

8.2.3 The Distribution of Largest Average Values Occurring Within a Given Period

If, instead of the peak values, the largest value averaged over a finite interval of time, ΔT , is required, the same formulae as above in Section 8.2.2 are used, only a modified form of spectrum for determining $\sigma(x)$ and $\sigma'(x)$ is adopted, namely,

$$S'_x(n) = S_x(n) \left[\frac{\sin n\pi\Delta T}{n\pi\Delta T} \right]^2 \quad (8.6)$$

8.3 THE GUST FACTOR

The expression derived for the probability distribution of the peak values (equation 8.3), is seen to be a function of $\sigma(x)$, the r.m.s. fluctuation, which, for the wind depends on the mean value, \bar{x} . Due to

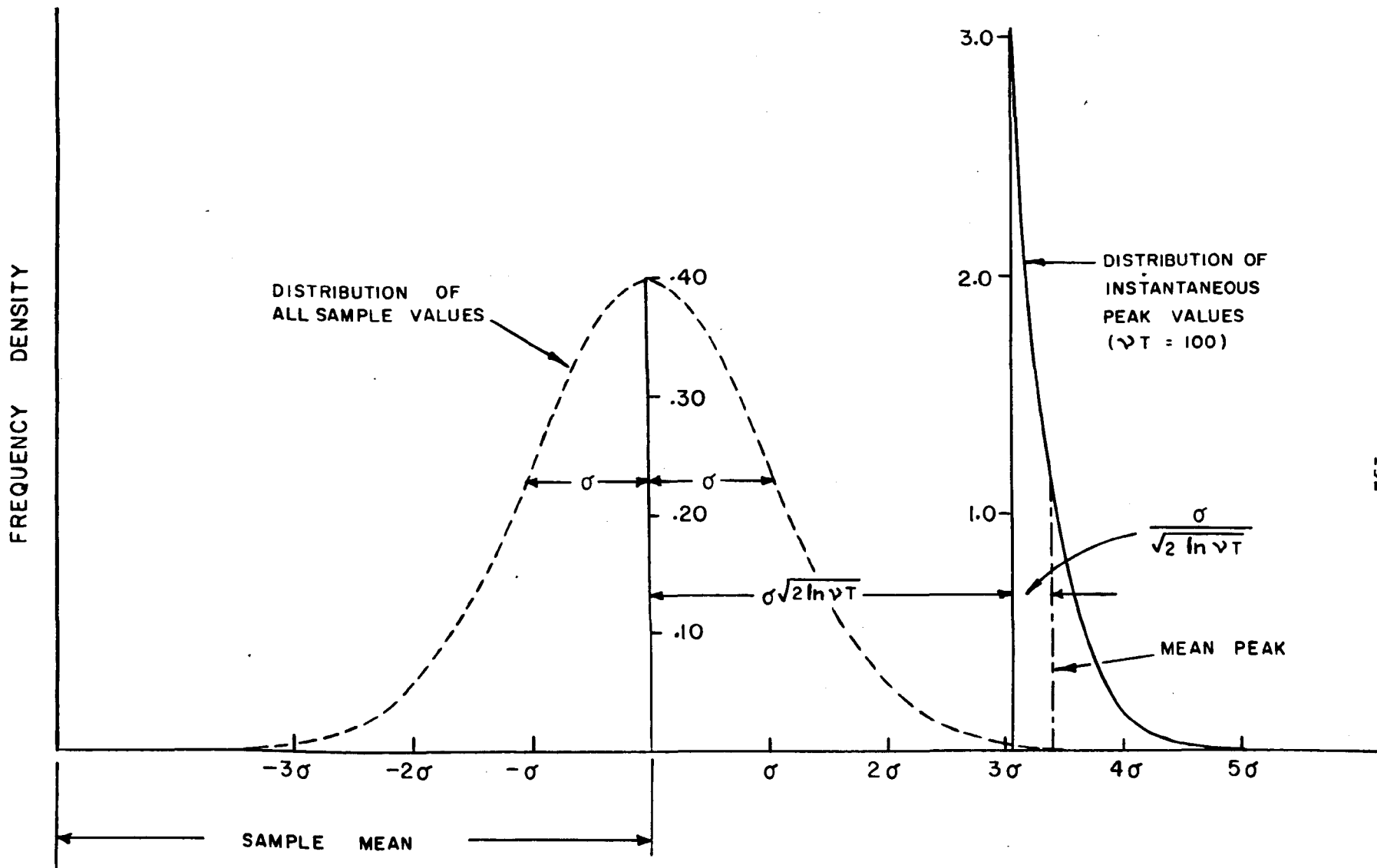


FIG. 8.1 FREQUENCY DISTRIBUTIONS OF ALL SAMPLE VALUES AND OF MAXIMUM INSTANTANEOUS (PEAK) VALUES FOR γT (i.e. RESPONSE FACTOR \times SAMPLE DURATION) = 100

climatological variations the mean value is itself likely to be a chance occurrence with its own probability distribution (as discussed in Section 2.3) To find the absolute probability of a given peak value, therefore, requires knowing the combined probability of the mean values as well as their associated peaks. This is not impossible to determine knowing the properties of each distribution separately. In practice, however, the labour involved is hardly justified, and it is felt that in most cases perfectly adequate estimates can be made using certain approximations which enable the complications to be avoided.

As can be seen from Fig. 8.1, the distribution of maximum values is narrow one, and in practical cases 95% of the peak values lie within an interval much less than half the standard deviation of the parent population on either side of the mean peak value. This suggests that not much error will be involved if this slight spread of peak values is disregarded and the peak value in any given period is taken equal to the mean peak value. The total peak value X_p (referred to the true origin) can then be written

$$X_p = \bar{x} \left\{ 1 + g(\nu T) \frac{\sigma(x)}{\bar{x}} \right\}$$

where \bar{x} = mean value of population and (from equation (8.5) and Fig. 8.1)

$$g(\nu T) = \sqrt{2 \log_e \nu T} + \frac{1}{\sqrt{2 \log_e \nu T}} \quad (8.7)$$

($g(\nu T)$ is plotted as a function of νT in Fig. 8.2)

$g \cdot \frac{\sigma(x)}{\bar{x}}$ is not necessarily constant, and may have a slightly different value for every value of \bar{x} : in practical cases, however, the variation is not likely to be great and it will normally be adequate to choose a suitably conservative value corresponding to a value of \bar{x} close to the mean value of the \bar{x} distribution. The absolute peak values will then

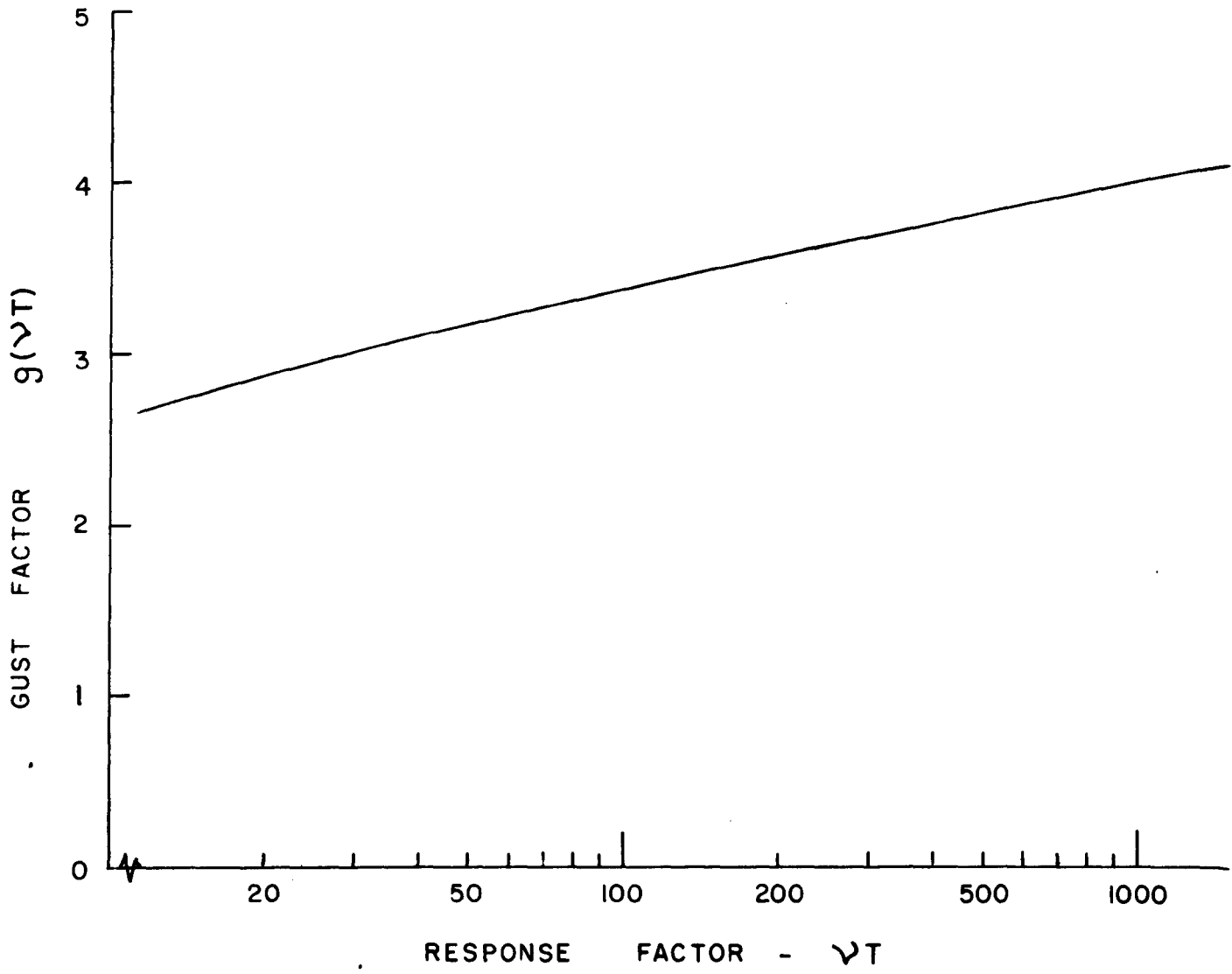


FIG. 8.2 PEAK GUST FACTOR AS FUNCTION OF RESPONSE FACTOR

have a distribution similar to the mean values, except that the variable will be increased by the factor $\left[1 + g \frac{\sigma(x)}{\bar{x}} \right]$

The assumptions this involves are not severe. Measurements of peak gust velocities for example appear to follow the extreme value distribution (equation 2.2) just as well as the mean velocities themselves, and the two velocities are in more or less a constant ratio to one another for all return periods.

The quantity g will be defined as the gust factor, since it measures the additional deflexion, force, velocity, moment, shears etc. which can be attributed to the gustiness of the wind. It is a crucial quantity in estimating wind loads. In beam like structures it will vary across the span and with the variable being considered.

9.0 APPLICATIONS

9.1 THE WIND LOADING OF A SUSPENSION BRIDGE

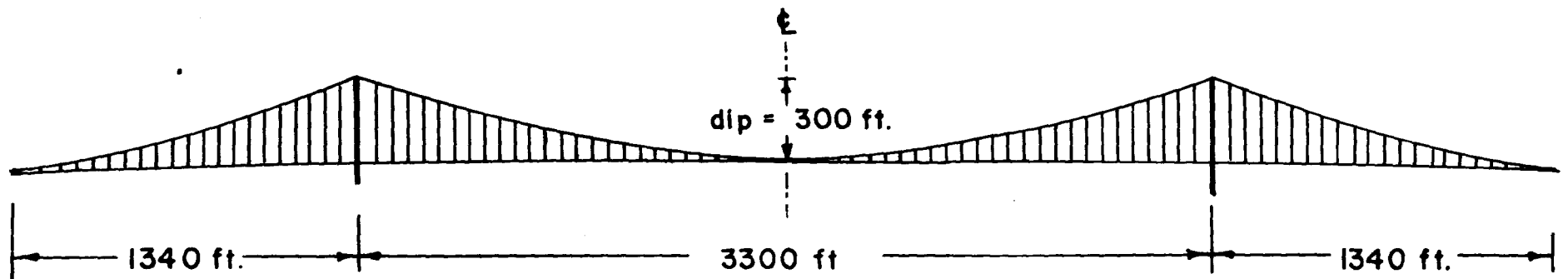
9.1.1 Description of Bridge

The suspension bridge analysed is illustrated in Fig. 9.1. The essential structural details are also given. This bridge (on which construction began in 1958) is typical of modern trends in suspension bridge design: the stiffening girder consists of a box-shaped, open lattice truss with two levels of horizontal wind bracing, one being at deck level, the other below. Due to the closed box-shape, the torsional rigidity of the stiffening girder is high: this fact, together with the open lattice construction, contribute towards a bridge section that is aerodynamically stable against catastrophic forms of aeroelastic vibration.

9.1.2 Aerodynamic Properties

Although the aerodynamic properties of the Forth Bridge were not available, those for the Severn River Bridge, a sister project of almost identical span, were published in a detailed report by Frazer and Scruton (1952), and these are taken to be representative of the Forth Bridge also. Summarized results of the lift, drag and pitching moment on a 180 ft. section of the deck in a 100 mi./hr. wind for various angles of yaw and attack are given in Fig. 9.2.

It is seen that the horizontal drag force in a beam wind remains almost constant for changes in wind direction up to 20° and for changes in angle of attack of up to about 10° . The variation of lift force with angle of attack is more or less linear for all wind directions.



	SPAN:	CENTRE	SIDE
Effective EI of truss about vertical axis about horizontal axis	lb. ft. ²	18.42×10^{12} 2.29×10^{12}	13.43×10^{12} 1.67×10^{12}
Average dead load (including cables)	lb/ft	10.9×10^3	15.0×10^3
Weight of both cables	lb/ft	2.52×10^3	2.56×10^3
Horizontal force per cable	lb	24.67×10^6	
Vertical curve radius of truss	ft	90,757	62,167

FIG. 9.1 DETAILS OF SUSPENSION BRIDGE OVER FIRTH OF FORTH.
(By courtesy of Freeman Fox and Partners)

9.1.3 Description of Site and Ground Roughness

The bridge is situated in approximately a North-South direction across the Firth of Forth which itself, runs approximately East-West. The fetch of the prevailing westerly wind is probably somewhat rougher than the Severn Bridge site owing to the fact that the latter has open water to the westward, whereas at the Forth Bridge the river narrows to the westward and is flank/by hilly country. It was concluded in Section 4.3.3 that the surface drag coefficient at the Severn Bridge site might be taken as $K = .005$; on account of the slightly greater roughness, a value of $K = .010$ has been assumed for the Forth Bridge. Site investigation would improve this estimate. X^{ad}

9.1.4 Estimation of Design Mean Wind Velocity

From Fig. 2.4 the parameters of the extreme hourly gradient wind speed at the Firth of Forth are seen to be approximately ($U_a = 84$; $\frac{1}{a} = 8.4$) The extreme hourly gradient wind speed occurring on average once every r years is then

$$\bar{V}_G(r) = 84 + 8.4 \log_e r \quad \text{mi/hr}$$

where r is known as the return period. For a return period of 50 years the gradient wind speed is 117 mi./hr., for 500 years, 136 mi./hr. From Table 2.1 the gradient height Z_G , and power law exponent α , corresponding to a terrain having a roughness factor of $K = .01$ are seen to be approximately 1000 ft. and .20 respectively. The elevation of the stiffening girder is about 200 ft. above mean sea level at which height the design hourly wind velocity for a 50 year return period is found from equation (2.1) to be 85 mi./hr. (124 ft./sec.), and for a 500 year return period, 99 mi./hr. (145 ft./sec.)

The question of what return period is appropriate cannot, of course, be decided without reference to a number of factors, such as the duration the structure is expected to last, the design stress limitations, the cost of insurance, and the cost to the community if the structure fails. (For a discussion of these points see Pugsley - 1951; Freudenthal - 1954.) For arguments sake, the gust and mean wind loading have been determined in this example for a mean wind velocity of 100 ft./sec. The wind loading at other mean wind velocities will be approximately in proportion to the mean wind loads (i.e. to the square of the mean velocities).

9.1.5 The Response to Horizontal Winds

The determination of the response of the suspension bridge to horizontal winds falls into two parts - the response to gusts and to mean winds. The quantities that need to be determined are as follows:

Part I Gust response:

1. The horizontal gust spectrum,
2. The aerodynamic admittances and hence, the spectrum of pressure on a "strip",
3. The lateral modes of the bridge and natural frequencies of vibration.
4. The joint mode acceptances and of the spectra of pressure in phase with the modes.
5. The damping and dynamic magnification for each mode.
6. The dynamically magnified mode components of pressure.
7. The shears and bending moments in each mode of vibration.
8. The total R.M.S. shears and bending moments across the span by superposition of the shears and bending moments due to individual modes.

9. The response factors and gust factors and hence the peak values of the bending moments and shears due to gusts.

Part 2 Response to mean wind:

1. The relative deformations of the cable and deck and hence the proportion of the mean wind load taken by truss.
2. The shear and bending moments.

These steps are now amplified and illustrated.

9.1.5.1 The Lateral Modes and Natural Frequencies of Vibration

To determine the lateral modes of vibration the analysis of Section 6.2.1 is followed.

The hanger length $h(x)$ at mid span is 9 ft. Assuming the cable is parabolic the hanger length at any other station x is

$$h(x) = 9 + 12.6 \left(\frac{x}{l} - .5 \right)^2$$

From this the following integrals are soon found (by numerical integration)

$$W_T \int_0^1 \frac{\sin^2 \pi \frac{x}{l}}{h(x)} d \frac{x}{l} = 187.5 \quad \text{lb/ft}^2$$

$$W_T \int_0^1 \frac{\sin^2 2\pi \frac{x}{l}}{h(x)} d \frac{x}{l} = 67.6 \quad "$$

$$W_T \int_0^1 \frac{\sin^2 3\pi \frac{x}{l}}{h(x)} d \frac{x}{l} = 164.8 \quad "$$

$$W_T \int_0^1 \frac{\sin^2 4\pi \frac{x}{l}}{h(x)} d \frac{x}{l} = 94.7 \quad "$$

$$W_T \int_0^1 \frac{\sin \pi \frac{x}{l} \sin 2\pi \frac{x}{l}}{h(x)} d \frac{x}{l} = -57.0 \quad "$$

$$W_T \int_0^1 \frac{\sin 2\pi \frac{x}{l} \sin 4\pi \frac{x}{l}}{h(x)} d \frac{x}{l} = -47.0 \quad "$$

$$W_T \int_0^1 \frac{\sin r\pi \frac{x}{l} \cdot \sin s\pi \frac{x}{l}}{h(x)} dx = 0$$

for $(r+s) = \text{odd numbers.}$

Substituting in equations 6.8 and 6.9, the equations for determining the first and third modes are found to be

$$\begin{aligned} 15.1 a_1 + 119.2 (a_1 - b_1) - 36.3 (a_3 - b_3) &= 262. a_1 \cdot \omega^2 \\ 44.4 b_1 - 119.2 (a_1 - b_1) + 36.3 (a_3 - b_3) &= 78.7. b_1 \cdot \omega^2 \\ 1223 a_3 - 36.3 (a_1 - b_1) + 104.9 (a_3 - b_3) &= 262. a_3 \cdot \omega^2 \\ 399 b_3 + 36.3 (a_1 - b_1) - 104.9 (a_3 - b_3) &= 78.7 b_3 \omega^2 \end{aligned}$$

The equations for the second (and fourth) modes are

$$\begin{aligned} 241.6 a_2 + 43.0 (a_2 - b_2) - 29.9 (a_4 - b_4) &= 262. a_2 \cdot \omega^2 \\ 177.6 b_2 - 43.0 (a_2 - b_2) + 29.9 (a_4 - b_4) &= 78.7. b_2 \cdot \omega^2 \\ 3860 a_4 - 29.9 (a_2 - b_2) + 60.4 (a_4 - b_4) &= 262 a_4 \omega^2 \\ 710 b_4 + 29.9 (a_2 - b_2) - 60.4 (a_4 - b_4) &= 78.7. b_4 \cdot \omega^2 \end{aligned}$$

The equations may be solved by successive approximation. For example, a first approximation to the first mode may be found by assuming that the deck and cable move integrally. Adding the first two equations then gives a first approximation to ω^2 which may be used to solve the remaining equations simultaneously to find the ratios of the coefficients $a_1 : a_3 : b_1 : b_3$. These in turn lead to an improved estimate of ω^2 . The procedure is repeated until no further changes take place in the value of ω^2 and the coefficients. The results are tabulated below:

— centreline of deck.
- - - centreline of cables.

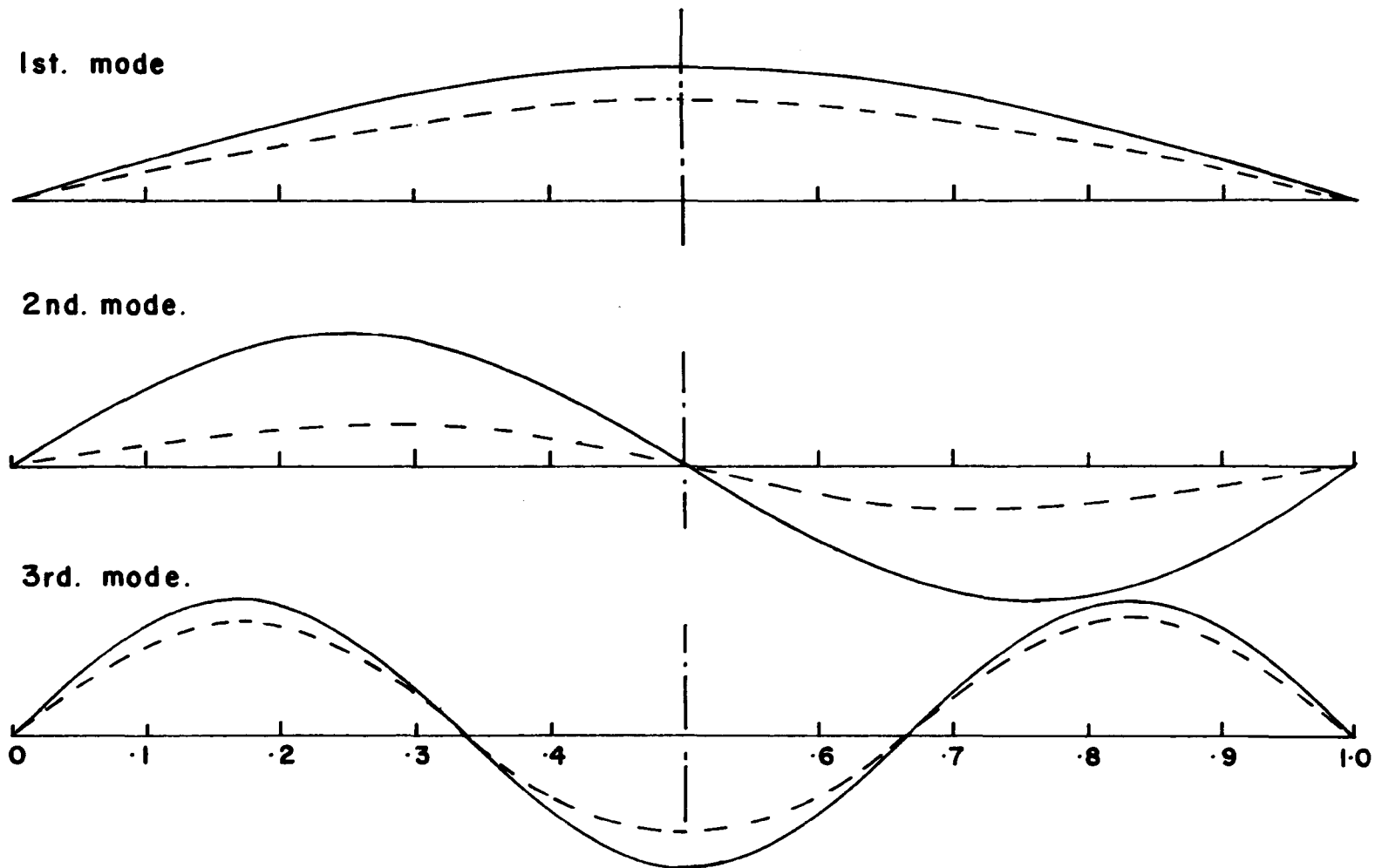


FIG 9.3 FIRST THREE LATERAL MODES OF SUSPENSION BRIDGE CENTRE SPAN.

TABLE 9.1

LATERAL MODES AND NATURAL FREQUENCIES OF SUSPENSION BRIDGE

Harmonic	Frequency cy./sec.	Period secs./cy.	Mode
1st	.0636	15.7	$y_T = \sin \frac{\pi x}{l} + .00452 \sin \frac{3\pi x}{l}$ (truss) $y_C = .74 \sin \frac{\pi x}{l} - .014 \sin \frac{3\pi x}{l}$ (cable)
2nd	.164	6.10	$y_T = \sin \frac{2\pi x}{l} + .00523 \sin \frac{4\pi x}{l}$ (truss) $y_C = .314 \sin \frac{2\pi x}{l} - .030 \sin \frac{4\pi x}{l}$ (cable)
3rd	.348	2.88	$y_T = -.0179 \sin \frac{\pi x}{l} + \sin \frac{3\pi x}{l}$ (truss) $y_C = .066 \sin \frac{\pi x}{l} + .806 \sin \frac{3\pi x}{l}$ (cable)

The forms of these modes are illustrated in Fig. 9.3.

The period of the 1st lateral mode of the Golden Gate Bridge (4,200 ft.) was observed to be between 23 - 18 secs., (Vincent - 1959). Thus the spans and periods of the two bridges are in roughly the same ratio, as might be expected.

9.1.5.2 Determination of Lateral Response to Horizontal Gusts

The basic procedure in determining the response to horizontal gusts is shown diagrammatically in Fig. 9.4.

The first step is to specify the spectrum of horizontal gustiness. The expression suggested in equation 4.3 (see Fig 4.1) is used and is repeated in the top right hand of Fig. 9.4 (a logarithmic scale is used to enable the multiplications incurred to be done graphically).

The next step is to determine the pressure acting on a transverse "strip" or "slice" of the bridge. The velocity correlation function given in Fig. 5.4 (see also equation 5.3) in conjunction with equation 5.25 gives the Aerodynamic Admittance, (top left hand diagram) which when multiplied by the gust spectrum gives the spectrum of pressure on a "slice" or "strip" of the bridge deck (eq. 5.22), (right hand centre diagram).

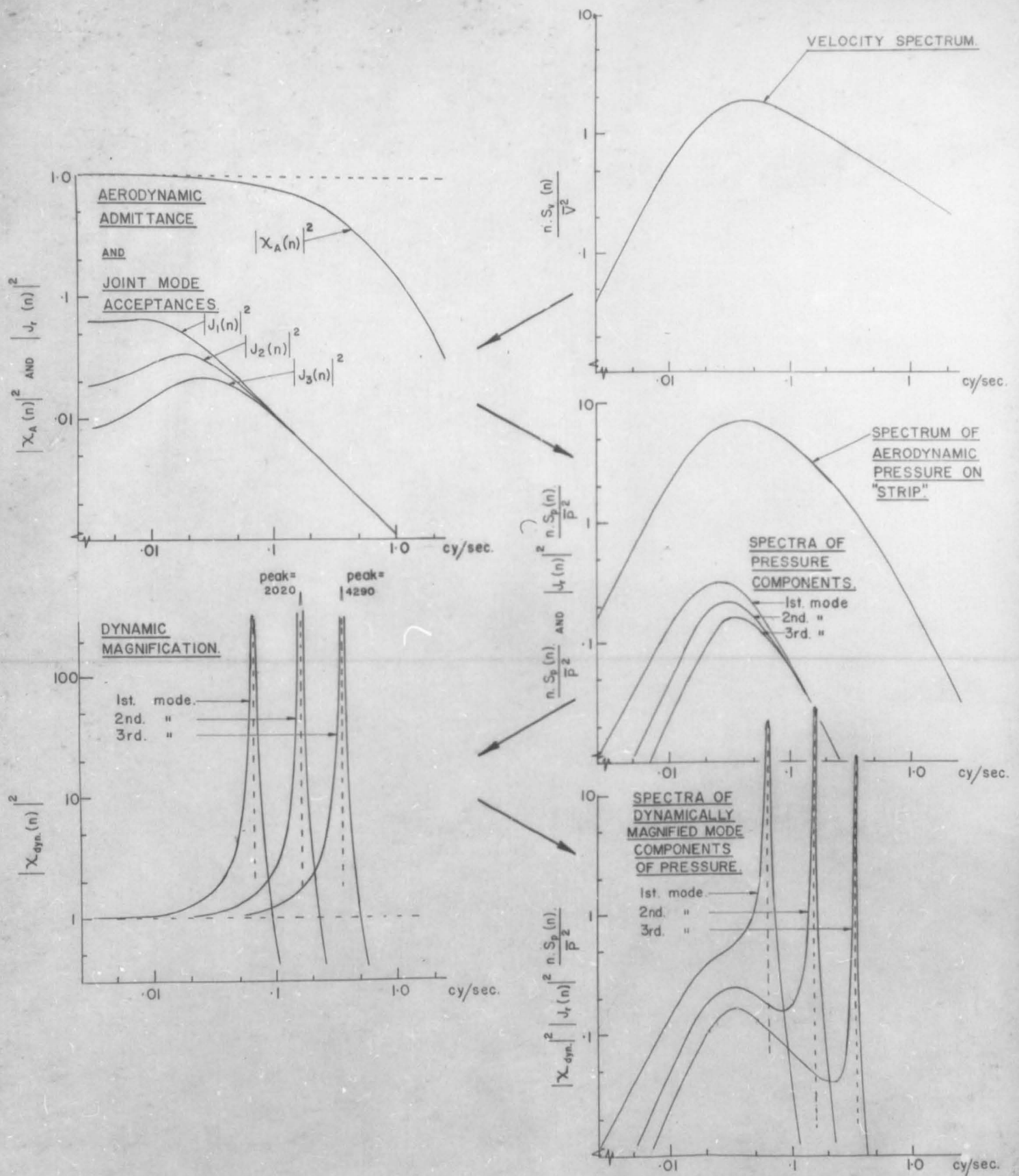


FIG. 9.4 LATERAL RESPONSE OF CENTRE SPAN OF SUSPENSION BRIDGE TO HORIZONTAL GUSTS. ($\bar{V} = 100$ FT./SEC. : $K = \dots$)

The spectra are also drawn on a linear ordinate scale in Fig. 9.5.

The third step is to determine the spectra of the components of pressure acting in phase with the various modes of the bridge. The joint mode acceptances are given in the form

$$|J_r(n)|^2 = \frac{1}{N_r^2} \int_0^l \int_0^l R_{xx'}(n) \cdot \mu_r(x) \cdot \mu_r(x') \, dx \cdot dx'$$

in which the cross correlation coefficient, $R_{xx'}(n)$ has been given

by equation (4.12),

$$R_{xx'}(n) = e^{-\frac{7|x-x'|n}{V}}$$

Since the mode forms have been derived in Section 9.1.5 in terms of sine functions, the above expression for the joint mode acceptance can be rewritten in terms of integrals of the type

$$\int_0^l \int_0^l e^{-c \frac{|x-x'|}{l}} \sin \frac{r\pi x}{l} \cdot \sin \frac{s\pi x'}{l} \, dx \cdot dx'$$

where $c = 7 \frac{n}{V} l$. From Fig. 4.1 it is seen that over the important range of the horizontal gust spectrum, the wave number $\frac{n}{V}$, is greater than about 2×10^{-4} cy./ft. The main span of the Firth of Forth suspension bridge is 3,300 ft., consequently in the range of interest $c \gtrsim 5$, for which values, the correlation is concentrated over fairly short intervals of the span. As c increases, the average correlation over these intervals tends towards $\frac{2}{c}$. Furthermore, since these intervals are small, x and x' will not be widely separated over regions of significant correlation, and consequently for larger values of c the above integral tends towards

$$\frac{2}{c} \int_0^l \sin \frac{r\pi x}{l} \sin \frac{s\pi x}{l} \, dx$$

This integral has a value only for $r=s$ when it tends to the value $\frac{1}{c}$.

Hence the only significant terms in the joint mode acceptance will be of the type

$$\int_0^l \int_0^l e^{-c \frac{|x-x'|}{l}} \sin \frac{n\pi x}{l} \cdot \sin \frac{n\pi x'}{l} \, dx \cdot dx'$$

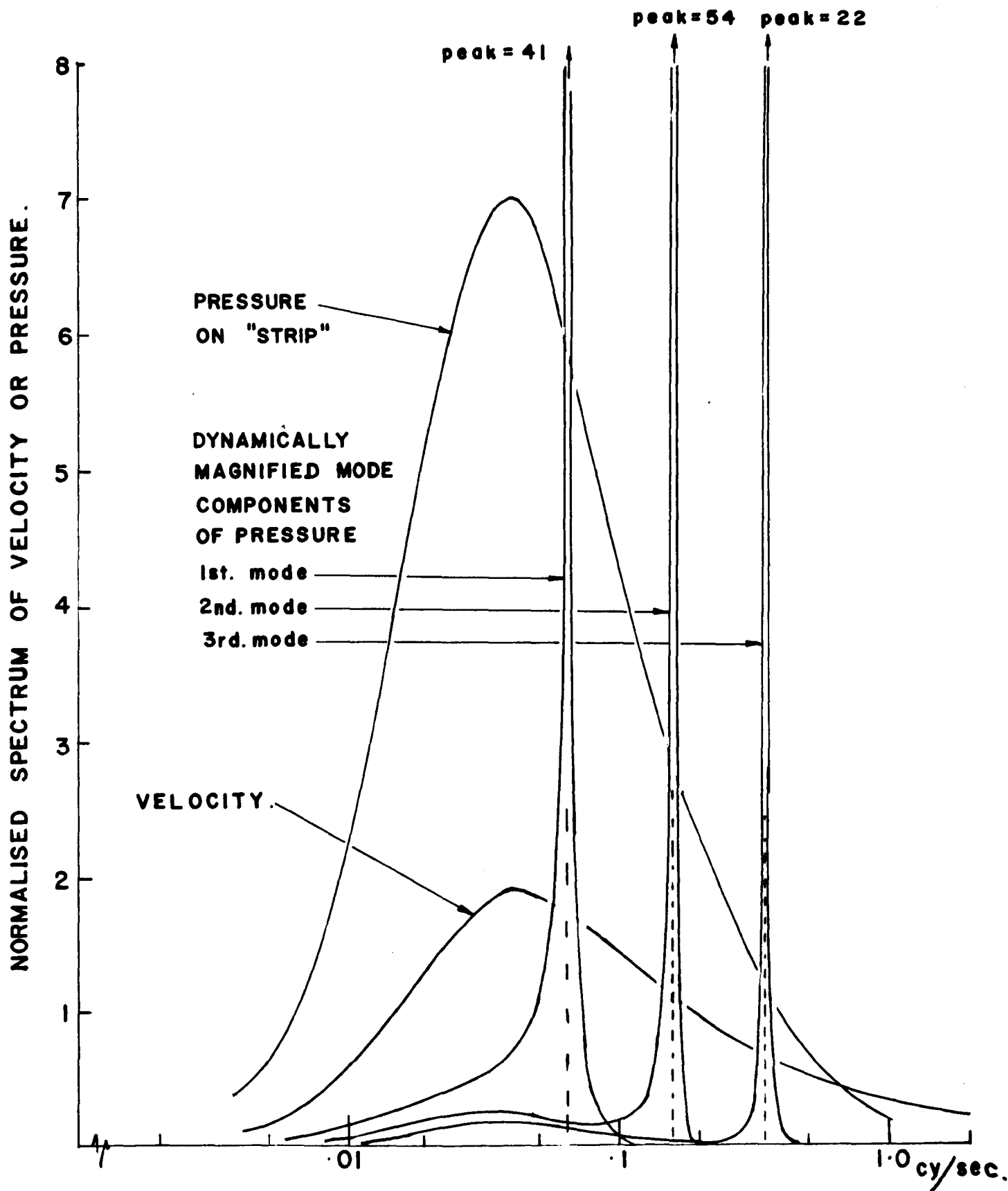


FIG. 9.5 SPECTRA OF VELOCITY AND PRESSURE FOR LATERAL LOADING OF SUSPENSION BRIDGE DUE TO HORIZONTAL GUSTS.

Exact values of this integral for $n = 1, 2, 3$ are given in Fig. 9.6. The joint mode acceptances found directly from this (making use of the mode forms given in Section 9.1.5) are shown in Fig. 9.4. The spectra of the mode components of pressure are shown in the middle right diagram of Fig. 9.4.

The next step is to determine the dynamic magnification for each mode, and a crucial part of this is the determination of the damping. The expression necessary for determining the logarithmic decrement of the aerodynamic damping is given in equation 7.2,

$$\delta = \frac{(\frac{1}{2} \rho C_D \bar{V}^2 D)}{n_r \bar{V} m}$$

The numerator is simply the horizontal wind load in the 100 ft./sec. mean wind and is found from Fig. 9.2 to be approximately 336 lb./ft. With the mass $m = 341$ slugs/ft. and the natural frequencies given in Section 9.1.5, the aerodynamic damping in the various modes are found to be as follows:

Logarithmic damping decrements

for suspension bridge in lateral modes

Mode	Aerodynamic damping	Mechanical damping	Total damping
1st	.155	.02	.175
2nd	.060	.02	.080
3rd	.028	.02	.048

The values of the mechanical damping decrement are minimum values suggested in the discussion of Section 7.2. The aerodynamic damping is seen to be far more important than the mechanical damping. The dynamic magnification factors are calculated from equation 3.21,

$$|X_r(n)|^2 = \left[\left(1 - \left\{ \frac{n}{n_r} \right\}^2 \right)^2 + \left\{ \frac{\delta_r}{\pi} \right\}^2 \left\{ \frac{n}{n_r} \right\}^2 \right]^{-1}$$

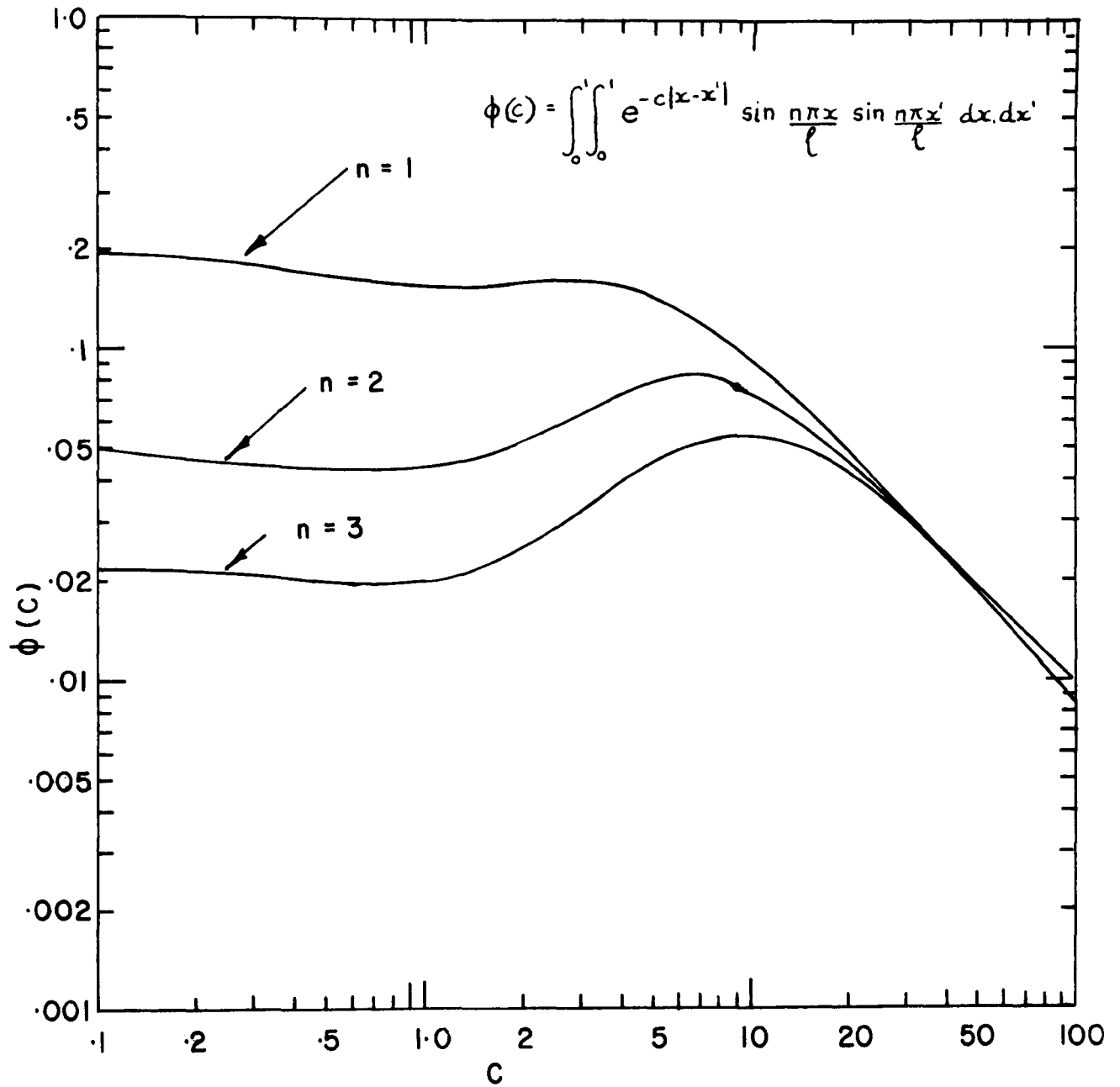


FIG. 9.6 VALUES OF $\int_0^l \int_0^l e^{-c|x-x'|} \sin \frac{n\pi x}{l} \sin \frac{n\pi x'}{l} dx dx'$ FOR SIMPLY SUPPORTED BEAM.

and are plotted in the lower left diagram of Fig. 9.4. These factors are used as multipliers, and the resulting spectra of the dynamically magnified pressures for the various modes are shown in the bottom right hand diagram. The spectra are redrawn on a linear ordinate scale in Fig. 9.5.

It is noticed that almost all the energy of the spectrum is concentrated in the immediate neighbourhood of the natural frequency. This enables the areas of the spectra to be computed from the following simple expression, which is valid for small values of δ and for values of $S(n)$ which do not vary rapidly over the neighbourhood of the peak.

$$\int_0^{\infty} \frac{S(n) \, dn}{\left\{ 1 - \left(\frac{n}{n_r}\right)^2 \right\}^2 + \left(\frac{\delta_r}{\pi}\right)^2 \left(\frac{n}{n_r}\right)^2} = \frac{\pi^2}{2 \delta_r} n_r \cdot S(n_r)$$

Applying the formula, the normalized variance of the dynamically magnified mode components of pressure,

$$\frac{\sigma_r^2(P)}{\bar{p}^2} = \int_0^{\infty} |\chi_r(n)|^2 \cdot |J_r(n)|^2 \cdot \frac{S_p(n)}{\bar{p}^2} \cdot dn$$

are found to be:

<u>Mode</u>	<u>Normalized Variance of Pressure</u> $\sigma_r^2(P) / \bar{p}^2$
r	
1	.936
2	.502
3	.128

Evidently the higher modes are less important which gives some (but not complete) justification for neglecting modes higher than the third.

Applying the same formula, the second moments of the pressure spectra,

$$\frac{\sigma_r'^2(P)}{\bar{p}^2} = \int_0^{\infty} n^2 \left(|\chi_r(n)|^2 \cdot |J_r(n)|^2 \cdot \frac{S_p(n)}{\bar{p}^2} \right) dn.$$

required in calculating "the response factors", ψ_T , of equation 8.2, are found to be:

<u>Mode</u>	<u>Normalized 2nd Moment of Pressure Spectrum</u>
r	$\sigma_r'^2(P) / \bar{P}^2$
1	.00358
2	.01313
3	.01547

The estimation of the peak bending moments and shears can now be considered. In Fig. 9.7 the bending moments and shears arising from unit load distributions for the first three lateral modes are plotted: the lateral load taken directly by the cable (found from equation 6.6) is also shown. These shears and bending moments are repeated in Table 9.2. To determine the total mean square bending moments and shears arising across the span, the squares of the shears and bending moments for unit mode load distributions are combined in proportion to the mean square intensity of each of these load components, found above. Thus the root mean square shear and bending moment at station x , $\sigma_Q(x)$ and $\sigma_M(x)$ can be written

$$\sigma_Q(x) = \sqrt{\sum_r \sigma_r'^2(P) \cdot q_r^2(x)}$$

and

$$\sigma_M(x) = \sqrt{\sum_r \sigma_r'^2(P) \cdot m_r^2(x)}$$

where $q_r(x)$ and $m_r(x)$ = shear force and bending moment at station x due to unit r th mode load distribution (from Fig. 9.7). Similarly, the second moments of the shear and bending moment spectra are given by

$$\sigma_Q^2(x) = \sum_r \sigma_r'^2(P) \cdot q_r^2(x)$$

and

$$\sigma_M^2(x) = \sum_r \sigma_r'^2(P) \cdot m_r^2(x)$$

Details of the calculations appear in Table 9.2.

The response factor, γ , is found from the ratio of the second moment of the spectrum to the root mean square fluctuation (i.e. $\frac{\sigma^2(x)}{\sigma(x)}$)

1 ST. MODE

2 ND. MODE

3 RD. MODE

LOAD — LB/FT. (— Inertia load — — — Load taken by cable)

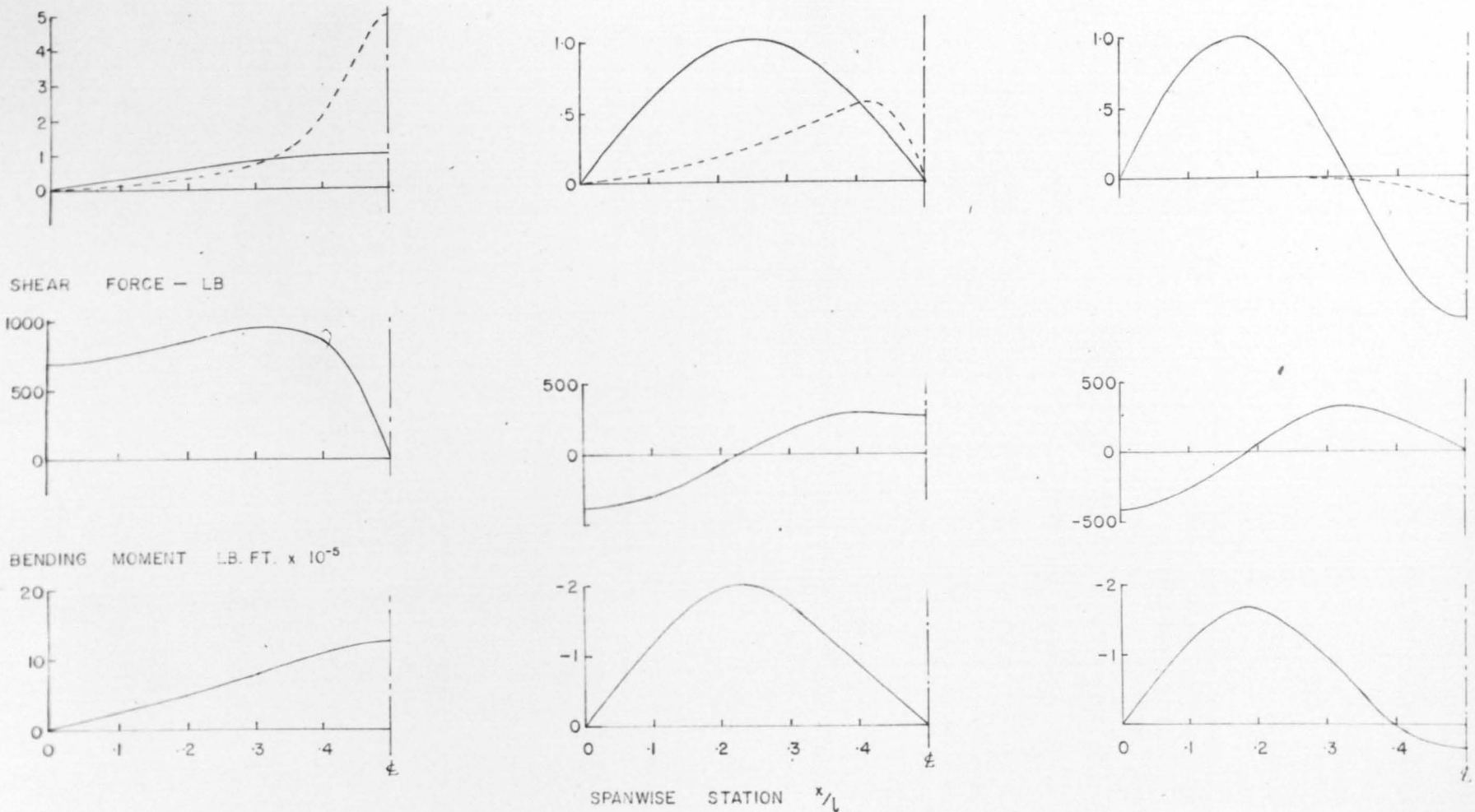


FIG. 9.7 SHEAR FORCE AND BENDING MOMENT DIAGRAMS FOR UNIT MODE LOAD DISTRIBUTIONS FOR FIRST THREE LATERAL MODES OF VIBRATION OF SUSPENSION BRIDGE CENTRE SPAN.

TABLE 9.2

ANALYSIS OF LATERAL WIND-LOADING OF SUSPENSION BRIDGE

Mean Wind-load $\bar{P} = 336 \text{ lb./ft.}$
 Mean Wind Velocity $\bar{V} = 100 \text{ ft./sec.}$
 Roughness factor $k = .01$

SHEAR LB. $\times 10^{-5}$

$\frac{x}{L}$	"Unit mode load" factors			$\frac{\sigma_Q(x)}{\bar{P}}$	$\frac{\sigma'_Q(x)}{\bar{P}}$	Response factor $\gamma = \frac{\sigma'_Q(x)}{\sigma_Q(x)}$	Gust factor $g(\gamma T)$	Peak gust shear $g \cdot \sigma_Q(x)$	Mean shear	Total peak shear
	q_1	q_2	q_3							
0	680	-390	-408	728	79	.108	3.75	.91	3.20	4.11
.1	746	-315	-258	761	65	.085	3.69	.95	2.10	3.05
.2	848	-84	56	824	52	.063	3.60	1.00	1.05	2.05
.3	937	170	294	920	70	.076	3.65	1.13	.10	1.23
.4	858	290	238	860	68	.079	3.65	1.05	.45	1.50
.5	0	250	0	177	29	.162	3.86	.23	0	.23

$$\frac{\sigma_Q(x)}{\bar{P}} = \sqrt{.936 q_1^2(x) + .502 q_2^2(x) + .128 q_3^2(x)} \quad ; \quad \frac{\sigma'_Q(x)}{\bar{P}} = \sqrt{.358 q_1^2(x) + 1.313 q_2^2(x) + 1.547 q_3^2(x)} \times 10^{-1}$$

BENDING MOMENT LB.FT. $\times 10^{-5}$

$\frac{x}{L}$	"Unit mode load" factors			$\frac{\sigma_M(x)}{\bar{P}}$	$\frac{\sigma'_M(x)}{\bar{P}}$	Response factor $\gamma = \frac{\sigma'_M(x)}{\sigma_M(x)}$	Gust factor $g(\gamma T)$	Peak Gust Moment $g \cdot \sigma_Q(x)$	Mean Moment	Total peak Moment
	m_1	m_2	m_3							
0	0	0	0	0	0	-	-	0	0	0
.1	2.26	1.19	1.19	2.39	.243	.102	3.75	301	892	1,193
.2	4.85	1.95	1.62	4.93	.418	.085	3.69	610	1,404	2,014
.3	7.86	1.70	.96	7.73	.523	.068	3.63	945	1,586	2,531
.4	10.93	.85	-.06	10.60	.660	.062	3.60	1,281	1,503	2,784
.5	12.58	0	-.32	12.18	.755	.062	3.60	1,472	1,403	2,875

$$\frac{\sigma_M(x)}{\bar{P}} = \sqrt{.936 m_1^2(x) + .502 m_2^2(x) + .128 m_3^2(x)} \quad ; \quad \frac{\sigma'_M(x)}{\bar{P}} = \sqrt{.358 m_1^2(x) + 1.313 m_2^2(x) + 1.547 m_3^2(x)} \times 10^{-1}$$

as outlined in Section 8.1. The gust factor, $g(\sqrt{T})$ is found from Fig. 8.2. (T is taken as 3600 secs. since we are interested in the hourly gust factor). The peak shears and bending moments due to gust action only are found by multiplying the R.M.S. values by the appropriate gust factors. (The calculations again appear in Table 9.2).

9.1.5.3 Response to Mean Wind

The response to the mean wind is carried out according to the method described in Section 6.5.3.

The quantities appearing on the left hand sides of equations 6.49 and 6.50 have been evaluated already in Section 9.1.5.1 in connection with the determination of the modes and natural frequencies. The mean wind loading on the truss and cable are $\bar{P}_T = 336$ lb./ft. and $\bar{P}_C = 38$ lb./ft. respectively (for a 100 ft./sec. mean wind). Substituting in 6.49 and 6.50 the equations for determining the deflected form of the truss and cable are:

$$\begin{array}{rcl} 15.1 a_1 + 119.2 (a_1 - b_1) - 36.3 (a_3 - b_3) & = & 1360 \\ 44.4 b_1 - 119.2 (a_1 - b_1) + 36.3 (a_3 - b_3) & = & 15.4 \\ 1223 a_3 - 36.3 (a_1 - b_1) + 104.9 (a_3 - b_3) & = & 45.3 \\ 399 b_3 + 36.3 (a_1 - b_1) - 104.9 (a_3 - b_3) & = & 5.1 \end{array}$$

From these equations the static deflexion of the bridge (in feet) is found to be given by

$$y = 3.12 \sin \frac{\pi x}{l} + .0520 \sin \frac{3\pi x}{l} \quad \text{ft.}$$

(i.e. a mid span deflexion of 3.17 ft.)

It is also found that

$$a_1 - b_1 = .77 \text{ ft} \quad ; \quad a_3 - b_3 = .089 \text{ ft.}$$

The wind load taken directly by the cable, $q(x)$, can now be found from equation 6.6 viz.

$$q(x) = w_T \sum_r (a_r - b_r) \sin \frac{r\pi x}{l}$$

The distribution of the load taken by the cable is shown in Fig. 9.8. It is seen to be concentrated around the mid-span region, where, in fact, the counteraction by the cable is found to be greater than the wind load itself for a short region.

The moments and shears produced by these loads on the stiffening truss are found straight forwardly and are also shown in Fig. 9.8. It is noticed that one effect of the cable load is to displace the positions of maximum bending moment from the mid-span to nearer the quarter points and at the same time to produce a central zone (nearly three quarters the span in length) having nearly constant bending moment. (This fact is referred to again in the discussion below).

The moments and shears shown in Fig. 9.8 are repeated in Table 9.2.

9.1.5.4 Discussion of the Effects of Horizontal Wind

Final results of the bending moments and shears due to both gust and mean wind loading are combined in Fig. 9.9 to show the maximum peak bending moments and shears across the span of the bridge. Certain features of the diagram seem noteworthy.

In the first instance it should be emphasized that the magnitude of the gust loading is dependent on the surface roughness (proportional to $K^{1/2}$). Thus if the bridge under discussion was situated in a more open site, such as the Severn River, where we have seen $K \approx .005$, the gust loading would be roughly 70% of that shown, (for the same mean wind loading). At rougher sites - such as those occupied by the Thames bridges in London, the Clifton Bridge at Bristol, or the East River

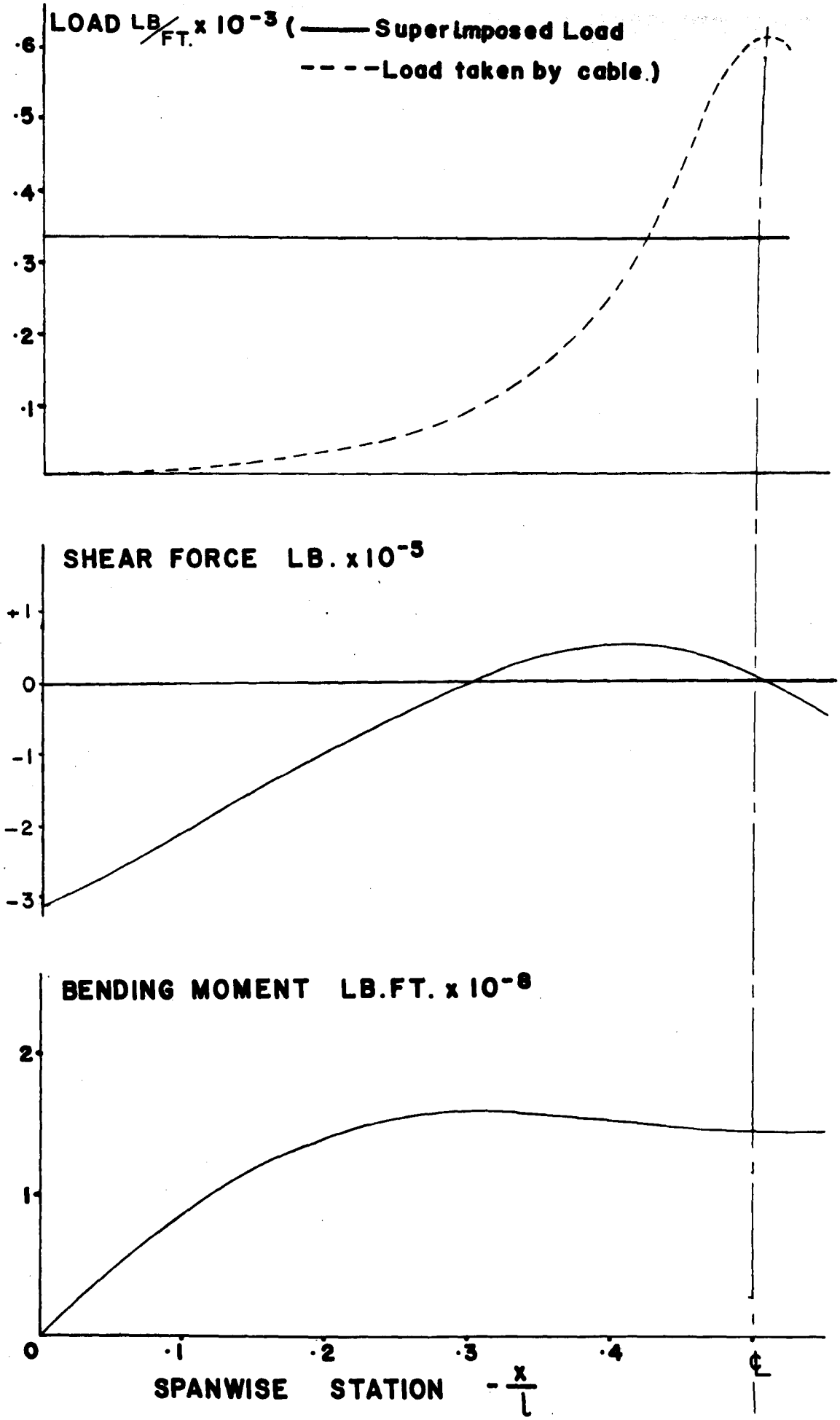
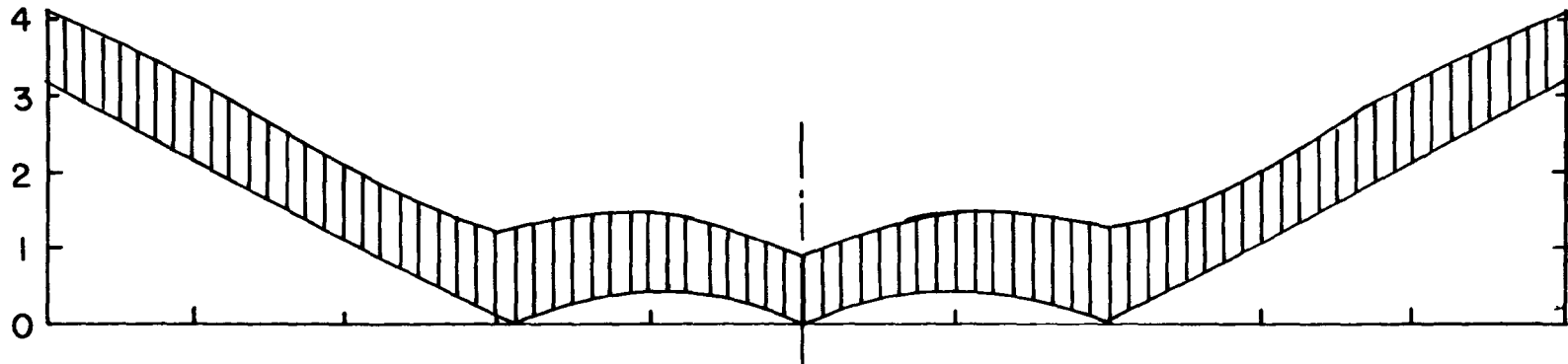
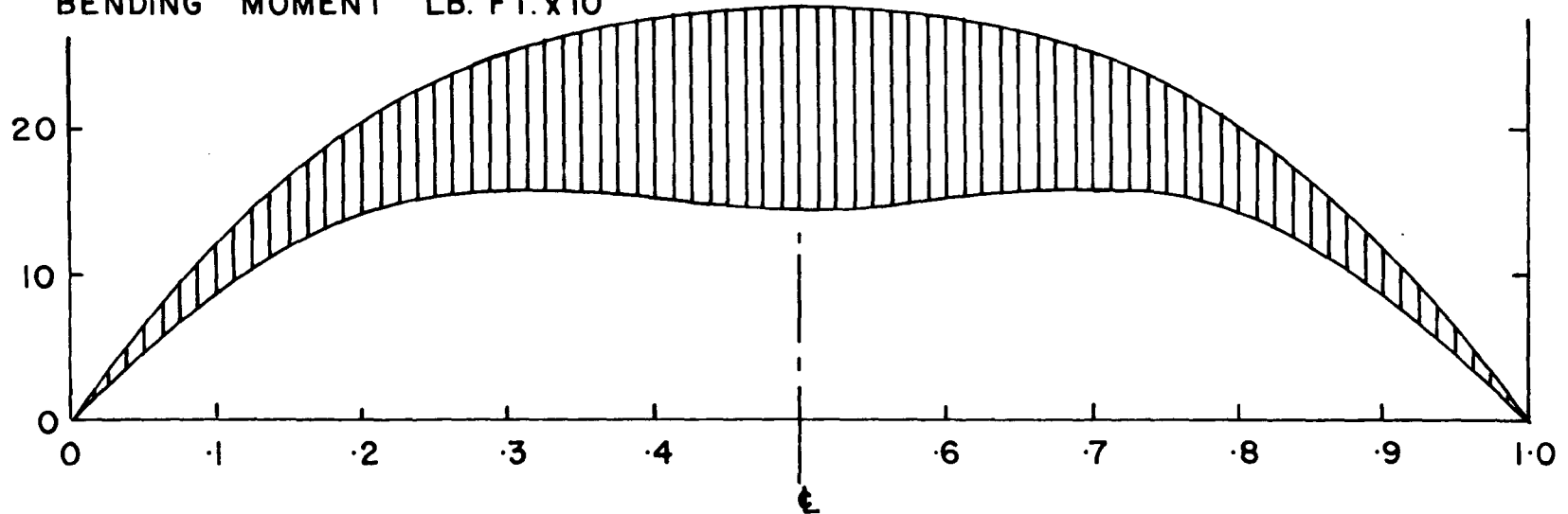


FIG.9.8 MEAN WIND LOADING OF FORTH BRIDGE. $\bar{V} = 100\text{ft./sec.}$

SHEAR FORCE LB x 10⁻⁵



BENDING MOMENT LB. FT. x 10⁻⁷



due to mean (hourly) wind



due to gusts

FIG. 9.9 ENVELOPES OF MAXIMUM PEAK HOURLY LATERAL SHEAR FORCE AND BENDING MOMENT ON CENTRE SPAN STIFFENING TRUSS OF SUSPENSION BRIDGE DUE TO LATERAL WIND. ($\bar{V} = 100$ FT./SEC.: $K = .01$)

bridges in New York - a value of μ nearer .04 might be appropriate and the gust load, consequently, twice as great (for the same mean wind load). On the other hand it must be remembered that the roughness of the surface also governs the attainable mean wind loads. Thus at the smoother Severn bridge site, although the gust loading may be relatively less, the mean loading will be higher and as a consequence the total loading may be higher. Conversely, the rougher city sites the mean wind loading will be less.

It should also be noted that the mean wind velocity of = 100 ft./sec. was chosen arbitrarily. At any other wind velocity the wind loading (gust as well as mean) will be in proportion to the squares of the velocities, or very nearly so. Thus if the once-in-five-hundred year wind was felt appropriate, which for the Forth Bridge site was shown to be approximately 99 mi./hr. or 145 ft./sec. (see Section 9.1.4), the values of the wind loading would be $\left(\frac{145}{100}\right)^2$, or 2.1, times those shown in Fig. 9.9.

It is also seen that the effects of the gust and mean wind-loading on the shear and bending moment diagrams are not similar. Whereas the shear due to the mean wind loading varies considerably across the span, from a maximum at the ends to no value at the mid-span, the shear due to gusts is almost constant across the span except very close to the centre where only the second mode vibration makes any contribution.

The bending moments due to the mean and gust loads are again dissimilar. Whereas the mean bending moment is relatively constant over a broad central region, with slight maxima near the quarter points; the bending moment due to gusts, is peaked with a maximum at the mid-span.

It is worth observing that the form of the bending moment and shear diagrams are dependent on the proportion of the load taken by the cables. The latter is determined by the length of the hangers; in other words, the dip to span ratio and the distance the deck is hung below the lowest point of the cable. In fact it would seem that the shorter the central hanger and the smaller the dip to span ratio, the greater is the lateral load taken by the cable and consequently the smaller need be the lateral stiffening truss.

9.1.6 Response of Suspension Bridge to Vertical Gusts

In broad outline, the procedure for determining the response of the suspension bridge to vertical and to horizontal gusts are similar. Certain details, however, such as the expression used for vertical gusts, and the method for determining the vertical modes of vibration differ, and the aerodynamic forces developed depend on variations in wind-inclination rather than velocity. There is, of course, no mean wind effect to consider unless the vertical forces happen to be asymmetrical.

9.1.6.1 The Vertical Modes and Natural Frequencies

The procedure used is due to Steinman and is described in Section 6.2.2. From the data of Fig. 9.1 the following are calculated:

		<u>Main Span</u>	<u>Side Span</u>
$\frac{EI\pi^4}{L^4}$	lb/ft ²	1.875	50.5
$\frac{H\pi^2}{L^2}$	lb/ft ²	44.4	269.0
$\frac{W}{g}$	slugs/ft	341	469

From these data the equivalent stiffness, K , the natural frequency, η , and the mode for each antisymmetric mode can be found from

equations (6.11), (6.10) and (6.12) respectively. The results are as follows:

TABLE 9.3 a

ANTISYMMETRIC VERTICAL MODES AND NATURAL FREQUENCIES OF SUSPENSION BRIDGE

Harmonic	K lb./ft. ²	n cy./sec.	Period sec./cy.	Mode
2nd	207	.124	8.10	$y = a \sin \frac{2\pi x}{l}$
4th	1190	.293	3.38	$y = a \sin \frac{4\pi x}{l}$

To determine the symmetric modes it is necessary to compute the following:

$$C = \frac{512}{\pi} \cdot \frac{f}{l^2} \cdot \frac{E_c A_c}{L_s} = 5170 \text{ lb/ft}^2$$

	<u>Main Span</u>	<u>Side Spans</u>
$C \frac{f}{l^2} \text{ lb/ft}^2$	470	223
$\frac{W_0}{W} K_r$	(r=1) 46.3	(r=2) 552
		(r=1) 233

Substituting, the basic equation for determining the stiffness (equation 6.13) now reads

$$\frac{470}{l^2(K-46.3)} + \frac{470}{3^2(K-552)} + \frac{2 \times 223}{l^2(K-233)} = 1$$

This equation can be solved rapidly as follows. Suppose we require to find K for the 1st mode. Assume a good approximation to K is K_r - in this case 46.3. Substitute this for K in the 2nd and 3rd fractions on the left hand side (the less significant ones) but still leaving K as an unknown in the first fraction. Solve for K thus obtaining a better approximation. Repeat the procedure until K settles down to a constant value.

Once K has been found the relative sizes of the coefficients of the mode expressions can be found from equation (6.16). The following

results were found:

TABLE 9.3 b

SYMMETRIC VERTICAL MODES AND NATURAL FREQUENCIES FOR
SUSPENSION BRIDGE

Harmonic	K lb./ft. ²	n cy./sec.	Period sec./cy.	Mode	
				<u>Main Span</u>	<u>Side Spans</u>
1st	132	.098	10.02	$y = \sin \frac{\pi x}{l_0} - .068 \sin \frac{3\pi x}{l_0}$	$y = -.458 \sin \frac{\pi x}{l_s}$
3rd	518	.196	5.10	$y = -.209 \sin \frac{\pi x}{l_0} + \sin \frac{3\pi x}{l_0}$	$y = -.347 \sin \frac{\pi x}{l_s}$

These modes are depicted (to a somewhat exaggerated vertical scale) in Fig. 9.10. It is noted that only the symmetric modes involve side-span and tower participation.

The inertia loading and the loading taken by the cables are now determined from the expressions given in Section 6.4. The shear forces and bending moments (with loading diagrams) for unit mode load distributions are shown in Fig. 9.11, and are repeated in Table 9.4.

9.1.6.2 Response to Vertical Gusts

As in the case of horizontal gusts the first step in estimating the gust loading is to define the spectrum of gustiness. Panofsky's spectrum (see Fig. 4.5 and equation 4.5) is used with the height taken as the deck height of approximately 200 ft. This is shown in Fig. 9.12. The aerodynamic admittance function is assumed to be the same as in the case of horizontal gusts, and the vertical force is calculated according to equation 5.25. The resulting spectrum of the pressure on a transverse strip is also shown in Fig. 9.12. The joint mode acceptances are almost precisely the same as those for the lateral modes.

Before the dynamic magnifications can be computed it is necessary

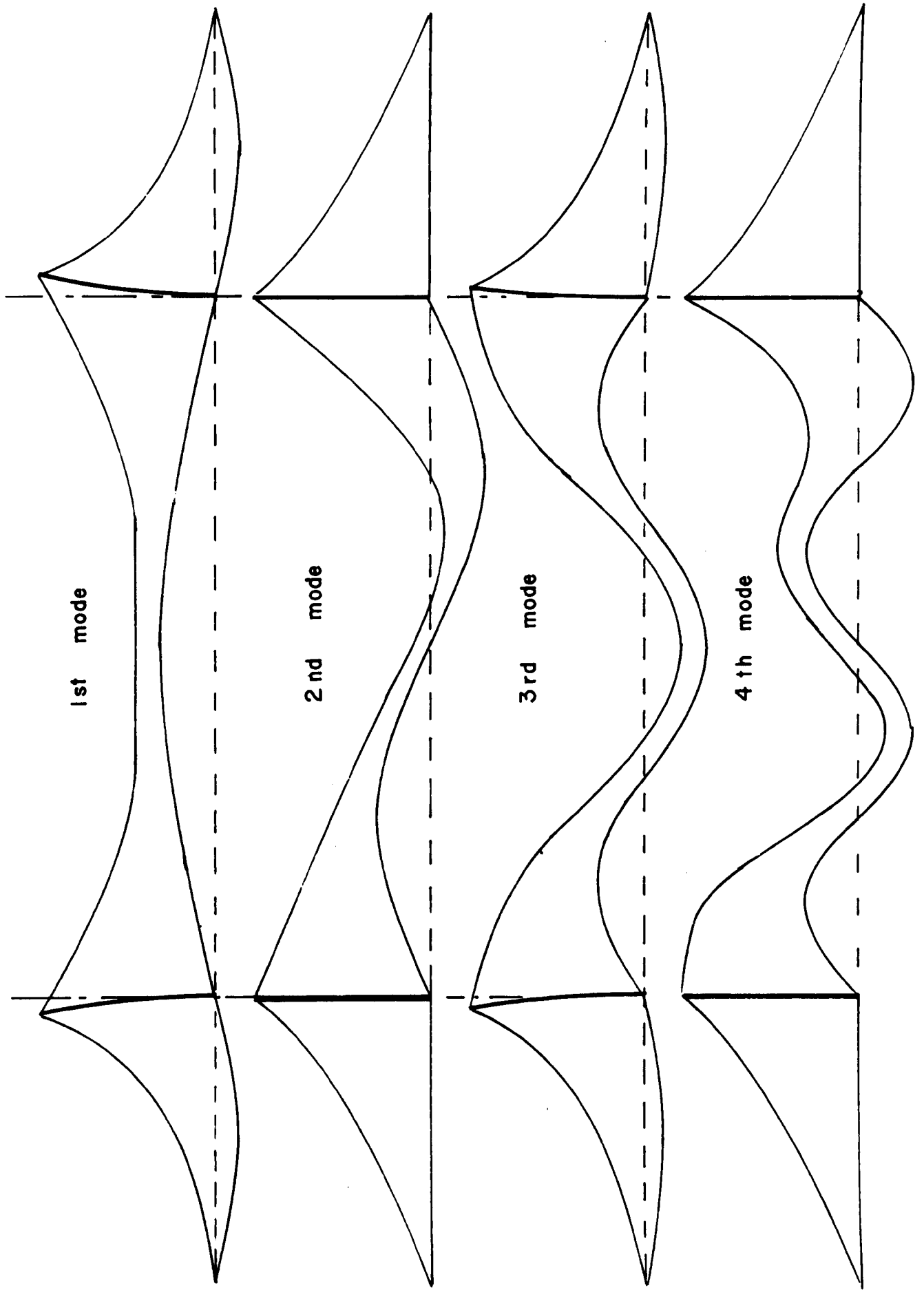


FIG. 9.10 FIRST FOUR VERTICAL MODES OF SUSPENSION BRIDGE.

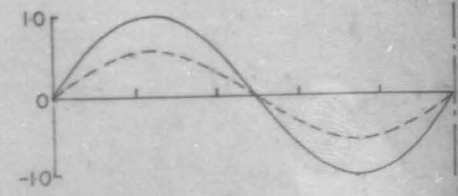
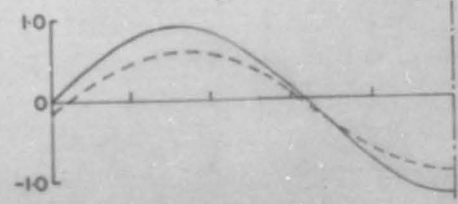
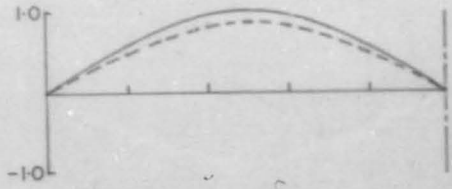
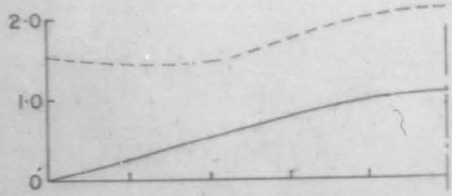
1 ST. MODE

2 ND. MODE

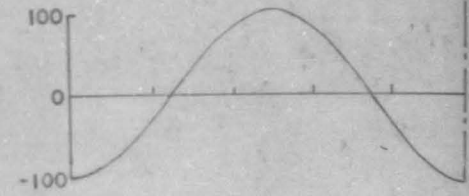
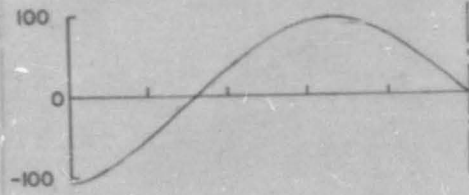
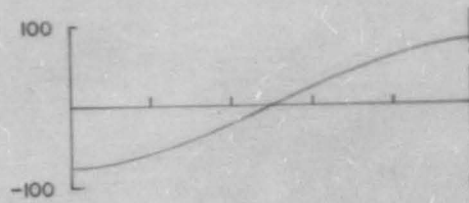
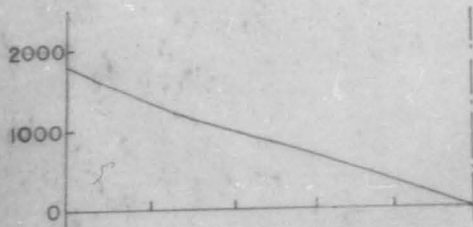
3 RD. MODE

4 TH. MODE

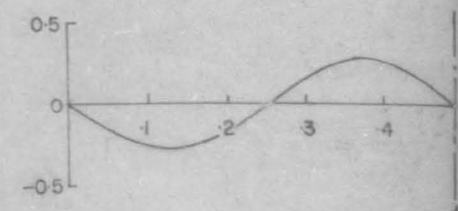
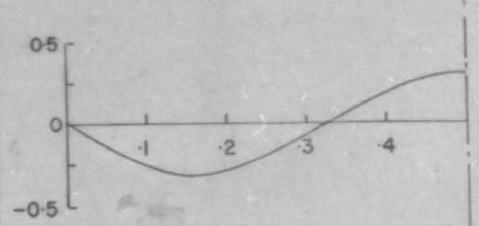
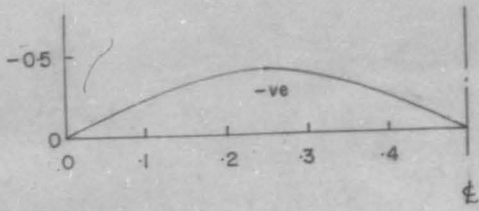
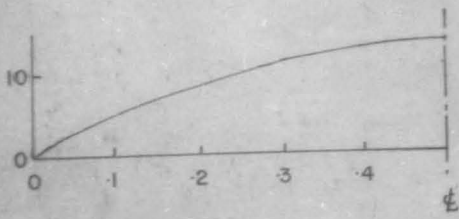
LOAD - LB / FT. (— Inertia load - - - Load taken by cable)



SHEAR FORCE - LB.



BENDING MOMENT LB. FT. x 10⁻⁵



SPANWISE STATION x/L

FIG. 9.11 SHEAR FORCE AND BENDING MOMENT DIAGRAMS FOR UNIT MODE LOAD DISTRIBUTIONS FOR FIRST FOUR VERTICAL MODES OF VIBRATION OF SUSPENSION BRIDGE CENTRE SPAN.

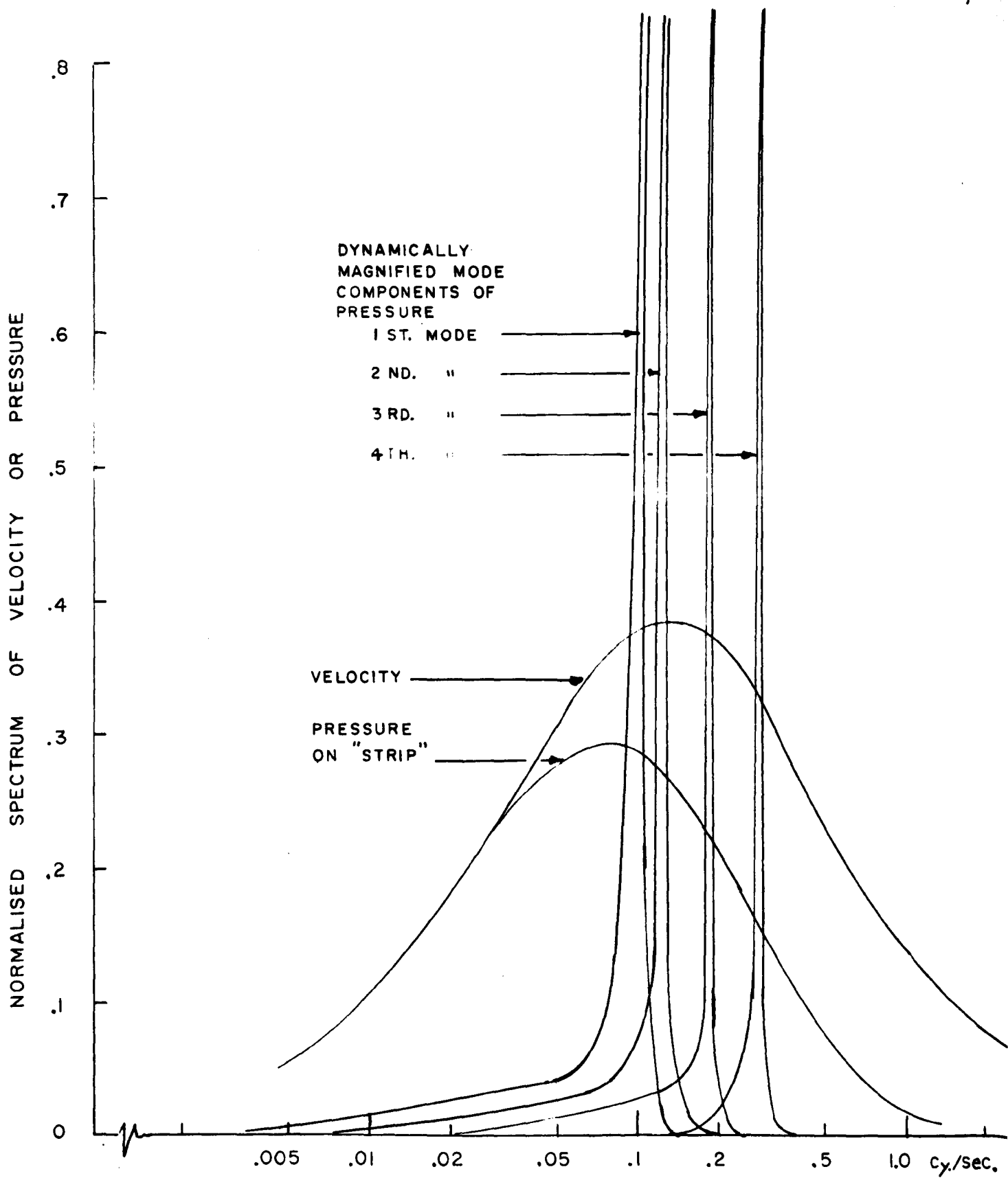


FIG. 9.12 SPECTRA OF VELOCITY AND PRESSURE FOR VERTICAL LOADING OF SUSPENSION BRIDGE DUE TO VERTICAL GUSTS

to determine the damping. These are computed from equation 7.3. The quantity $\frac{dz}{d\alpha}$ is found from Fig. 9.2 to be 2,730 lb./ft./rad. in a beam wind of 100 ft./sec. mean velocity. This results in the following logarithmic damping decrements (allowing .02 for mechanical damping)

LOGARITHMIC DAMPING DECREMENTS FOR
VERTICAL MODES OF SUSPENSION BRIDGE

Harmonic	δ (aerodynamic)	δ (mechanical)	δ (total)
1st	.408	.02	.428
2nd	.323	.02	.343
3rd	.210	.02	.230
4th	.137	.02	.157

The mechanical damping is seen to be small compared to the aerodynamic damping.

The dynamic magnification factors can now be calculated from equation 3.23 and the resulting spectra of the dynamically magnified mode components of load are shown in Fig. 9.12. Again all the energy is seen to be concentrated at or near the natural frequency, n_r , which enables the simple approximate formula to be used for determining the variance, viz.

$$\sigma^2 = \int_0^{\infty} \frac{S(n) \cdot dn}{\left\{ 1 - \left(\frac{n}{n_r}\right)^2 \right\}^2 + \left(\frac{\delta}{n}\right)^2 \left(\frac{n}{n_r}\right)^2} = \frac{\pi^2}{2\delta} \cdot n_r \cdot S(n_r)$$

We find from this that the normalised variance of the dynamically magnified mode components of pressure, $\sigma^2(P)/\left(\frac{dz}{d\alpha}\right)^2$ and the normalised second moments of the spectra $\sigma^2(P)/\left(\frac{dz}{d\alpha}\right)^2$ have the following values:

VALUES OF $\sigma^2(P)/(\frac{dZ}{d\alpha})^2$ AND $\sigma'^2(P)/(\frac{dZ}{d\alpha})^2$
(VERTICAL RESPONSE OF SUSPENSION BRIDGE)

Harmonic	$\sigma^2(P)/(\frac{dZ}{d\alpha})^2$	$\sigma'^2(P)/(\frac{dZ}{d\alpha})^2$
1st	.0132	.000128
2nd	.0126	.000194
3rd	.0108	.000414
4th	.0053	.000452

When combined with the unit mode load factors of shear and bending moment, the variance of shears and bending moments (and the second moments of the spectra) are obtained for all points on the beam as indicated in the Table 9.4. The response factor, ψ , enables the gust factor, ψ^T , to be found which in turn determines the peak values of shear and bending moment. These peak values of shear and bending moment (given in Table 9.4) are plotted in Fig. 9.13.

9.1.6.3 Discussion

From a comparison of Fig. 9.9 and 9.13 it appears that the peak vertical and lateral shear forces and bending moments are of a similar magnitude. This result may seem surprising in view of the generally much smaller depth to span ratio of the vertical stiffening truss. Fig. 9.11, and the unit mode load factors of Table 9.4 indicate that by far the largest contribution to the moments and shears in the stiffening truss is made by the first mode component. Further examination of Fig. 9.11 shows that the reaction developed in the cable is mainly responsible for this.

It was shown in Section 6.4 that the cable reaction was composed of two components, one of which was due to a change in the geometry

TABLE 9.4

ANALYSIS OF VERTICAL GUST-LOADING OF SUSPENSION BRIDGE

Mean Wind = velocity = .100 ft./sec.

$\frac{dZ}{d\alpha}$ (from Fig. 9.2) = 2730 lb./ft./rad.

Roughness factor $R = .01$

SHEAR

$\frac{x}{l}$	Unit mode load factors				$\frac{\sigma_Q(x)}{(\frac{dZ}{d\alpha})}$	$\frac{\sigma'_Q(x)}{(\frac{dZ}{d\alpha})}$	$\nu = \frac{\sigma'_Q(x)}{\sigma_Q(x)}$	$g(\nu T)$	Peak shear lb $\times 10^{-5}$
	q_1	q_2	q_3	q_4					
0	1731	-75	-119	-105	199	19.6	.099	3.72	2.02
.1	1295	-60	-50	-33	149	14.7	.099	3.72	1.51
.2	955	-22	37	85	110	10.7	.099	3.72	1.12
.3	657	22	90	85	76	7.4	.099	3.72	.77
.4	337	60	73	-33	39	4.2	.108	3.75	.40
.5	0	75	0	-105	11	2.5	.227	3.95	.12

$$\frac{\sigma_Q(x)}{dZ/d\alpha} = \sqrt{1.32q_1^2 + 1.26q_2^2 + 1.08q_3^2 + .53q_4^2} \times 10^{-1}$$

$$\frac{\sigma'_Q(x)}{dZ/d\alpha} = \sqrt{1.28q_1^2 + 1.34q_2^2 + 4.14q_3^2 + 4.52q_4^2} \times 10^{-2}$$

BENDING MOMENT

$\frac{x}{l}$	Unit mode load factors				$\frac{\sigma_M(x)}{(\frac{dZ}{d\alpha})}$	$\frac{\sigma'_M(x)}{(\frac{dZ}{d\alpha})}$	$\nu = \frac{\sigma'_M(x)}{\sigma_M(x)}$	$g(\nu T)$	Peak moment lb. ft. $\times 10^{-7}$
	m_1	m_2	m_3	m_4					
0	0	0	0	0	-	-	-	-	-
.1	5.00	-.23	-.23	-.26	.57	.57	.099	3.72	5.8
.2	8.71	-.37	-.30	-.16	1.00	.99	.099	3.72	10.2
.3	11.37	-.37	-.09	.16	1.31	1.29	.099	3.72	13.3
.4	13.01	-.23	.18	.26	1.50	1.47	.099	3.72	15.2
.5	13.56	0	.30	0	1.56	1.53	.099	3.72	15.6

$$\frac{\sigma_M(x)}{dZ/d\alpha} = \sqrt{1.32m_1^2 + 1.26m_2^2 + 1.08m_3^2 + .53m_4^2} \times 10^{-1}$$

$$\frac{\sigma'_M(x)}{dZ/d\alpha} = \sqrt{1.28m_1^2 + 1.34m_2^2 + 4.14m_3^2 + 4.52m_4^2} \times 10^{-2}$$

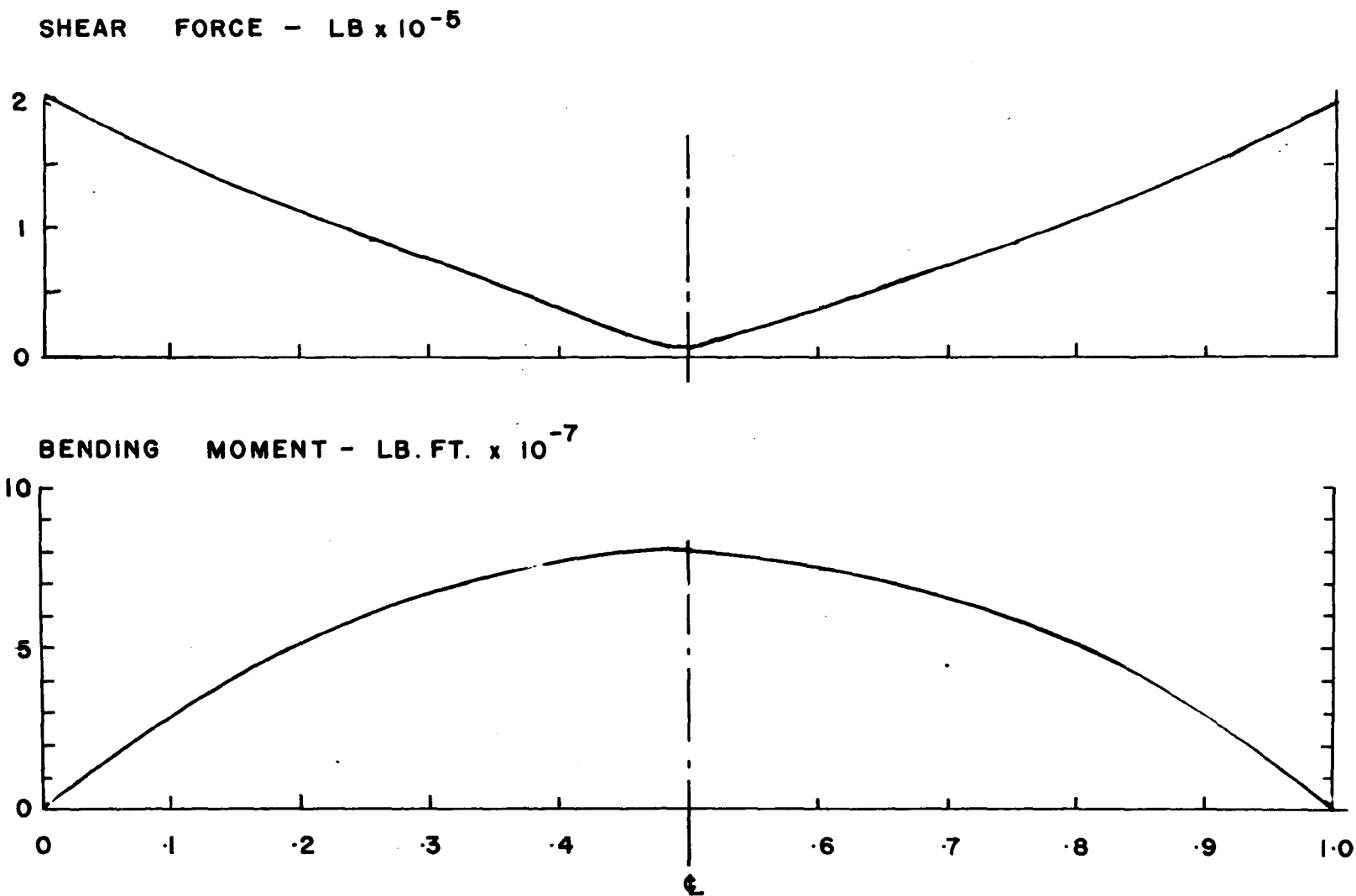


FIG.9.13 ENVELOPES OF MAXIMUM PEAK HOURLY VERTICAL SHEAR FORCE AND BENDING MOMENT ON CENTRE SPAN STIFFENING TRUSS OF SUSPENSION BRIDGE DUE TO VERTICAL GUSTINESS. ($\bar{V} = 100$ FT./SEC.; $K = .01$)

of the cable $\left(H \frac{d^2 y}{dx^2} \right)$ and the other due to a change in cable tension $\Delta H \frac{d^2 \eta}{dx^2}$ (η being the original coordinate of the cable). The symmetric modes of vibration involve both tower and side span participation, as well as stretching of the cable, accompanied by an increase in tension. The latter has the effect of inducing a uniformly distributed load across the deck which, in the first vertical mode, is relatively large. In all other modes the change in cable tension is either small or, in the asymmetric modes, non-existent.

This predominance of the first mode oscillations in producing moments and shears suggests that consideration of more than two modes is superfluous, and makes calculation of the peak values relatively simple. The distributions of maximum shears and bending moments are similar to those for the lateral modes, insofar as the maximum shear forces occur at the ends of the span and the maximum moments at the centre.

It is worthwhile to consider the peak vertical deflexions under the same wind conditions. These are given by

$$\frac{\sigma(\bar{P}) \cdot g(vT)}{K}$$

For the first mode, $g(vT) = 3.72$; $\sigma(\bar{P}) \frac{dz}{d\alpha} = \sqrt{1.32} \times 10^{-1}$;
 $\frac{dz}{d\alpha} = 2730 \text{ lb./ft./rad.}$ and $K = 132 \text{ lb./ft.}^2$

Hence the peak deflexion is found to be approximately 9.0 ft. (from centre line). The peak second mode deflexion is found to be about 5 ft. It seems quite likely that oscillations of this magnitude could be mistakenly ascribed to an aeroelastic phenomenon of the flutter type instead of to the lift induced by the vertical components of gustiness. In the past, this has been largely due to the fact that there has been no satisfactory method for estimating the effects of vertical changes in wind direction.

9.2 THE WIND LOADING OF A TALL MAST

9.2.1 Description of the Mast

The mast, illustrated in Fig. 9.14, is 500 ft. high and consists of a slender elastic column supported at three levels by guys spread around the base at 120° horizontal spacing. All the guys in the same vertical plane terminate in common anchorages. The top section of the mast is cantilevered and, as a consequence, is considerably stiffened at the top guy level as indicated in Fig. 9.14. The base of the mast rests on a ball seating, enabling the mast to pivot freely. All relevant statistics of the mast and guys are given in Table 9.5.

9.2.2 Wind Loading Conditions

The wind load on the mast in a steady wind of 100mph is taken as 200 lb./ft. The ground roughness is significant because it determines both the gust intensity, the mean wind velocity variation with height, and, consequently, the mean wind load distribution. To study the effects of both extremes of surface roughness the wind loading in both city and open country conditions is investigated. For illustrative purposes it is assumed that the mast is situated on the $U = 80 ; \frac{1}{\alpha} = 6$ contour of Fig. 2.4 and that it is to be designed to resist the once-in-fifty year wind load. The mean wind loads at a 30 ft. datum are then 89 lb./ft. and 10 lb./ft. in open country and city conditions respectively.

9.2.3 Behaviour of the Guys

From the data of Table 9.5 the following are evaluated:

	<u>Bottom Guy</u>	<u>Middle Guy</u>	<u>Top Guy</u>
$k = \frac{E_g A_g \cos^2 \sigma}{s}$ lb/ft $\times 10^{-4}$	2.97	2.39	3.21
$\cos \phi = \frac{\cos \theta \cos \sigma}{\sqrt{1 - \cos^2 \theta \cos^2 \sigma}}$.500	.395	.308
$F = \frac{\pi^2 T^2}{s^2 W K} \cdot \frac{\sin \sigma}{2}$.0339	.0675	.0915
$G = \frac{\pi^2 T^3}{s^3 W^2 K}$	2.74	2.72	2.37

RIGIDITY
& MASS.

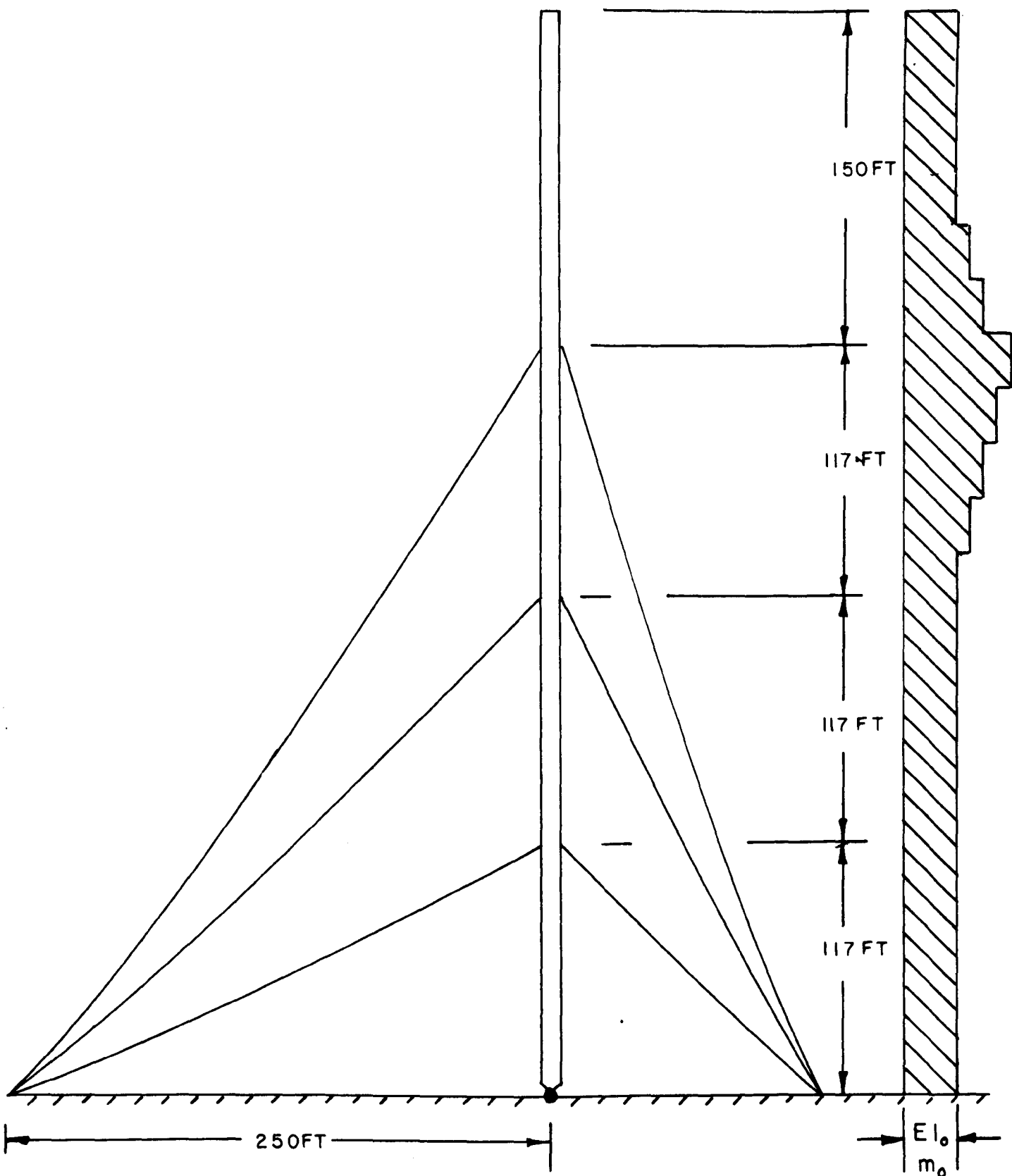


FIG. 9-14 500FT. GUYED MAST.

TABLE 9.5

DETAILS OF GUYED MAST

Rigidity at reference section $EI_0 = 1.4 \times 10^9 \text{ lb. ft}^2$
Mass per unit length at reference section $m_0 = 8.0 \text{ slugs/ft.}$

Guy data:		Bottom	Middle	Top
Guy length	s ft.	278	341	426
Inclination	σ	24°45'	42°45'	54°00'
Wt./unit length	w lb/ft	1.7	2.57	6.73
Cross section	$A_g \text{ in}^2$.500	.755	1.98
Modulus	$E_g \text{ lb/in}^2$		20 x 10 ⁶	
Tension	T lb	8,000	12,000	30,000

	<u>Bottom Guy</u>	<u>Middle Guy</u>	<u>Top Guy</u>
$\omega_0 = \frac{\pi}{S} \sqrt{\frac{Tg}{W}}$ rad/sec	4.39	3.56	2.79
n_0 cy/sec	.698	.567	.444

The guy moduli are calculated, for a vibration coplanar with one of the guy sets and therefore inclined at 60° to the other two guy sets. The modulus for the guy in the plane of vibration is calculated from equation 6.21 and, for the other two guys, from equation 6.22. These expressions make no allowance for damping. The combined moduli for each set of guys in the frequency range 0 - 2.5 cy./sec. are shown in Fig. 9.15 by the dashed lines, which, except in the vicinity of the odd numbered modes, coincide with the full line. If damping is taken into account the modulus is calculated from equation (6.27). For 10 per cent critical damping the moduli are given in Fig. 9.15 by the full lines. Damping is seen to be significant only in the vicinity of the odd modes. For practical purposes it would seem to be adequate to assume that the modulus is approximately equal to its static value for frequencies less than the fundamental, and approximately equal to the "taut wire" value k , at higher frequencies.

9.2.4 Determination of the Natural Modes

It is assumed that the modes can be adequately represented by four Basic functions as follows:

$$y = a_1 \cdot B_1(x) + a_2 \cdot B_2(x) + a_3 \cdot B_3(x) + a_4 \cdot B_4(x)$$

The first step in determining the natural modes is to calculate the integrals appearing in equation 6.46, written for each value of r from 1 to 4. Using Simpson's integration formula and the tables of Basic function products given by Davenport (1959), together with the Basic

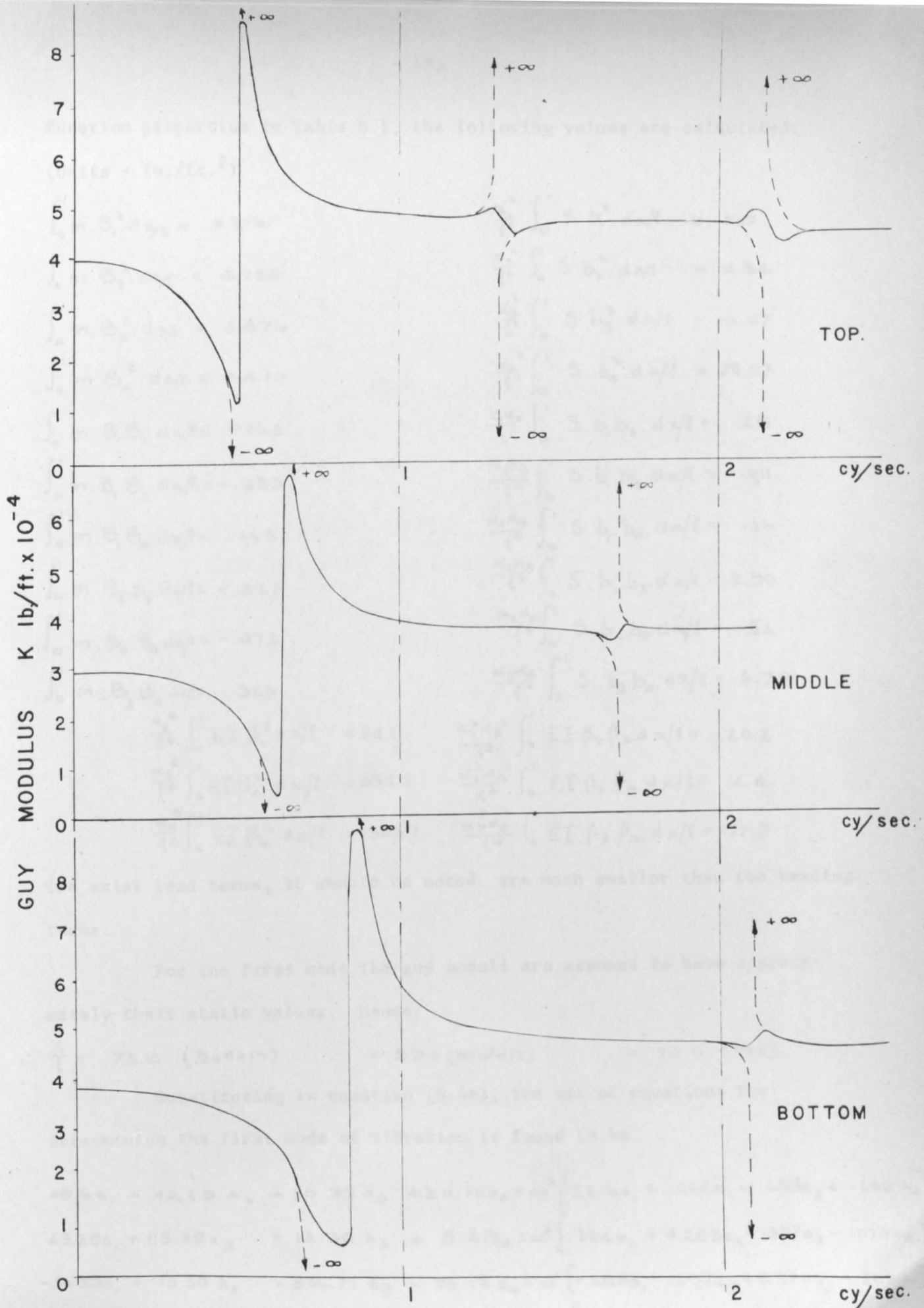


FIG. 9.15 VARIATION OF GUY MODULUS WITH FREQUENCY OF VIBRATION.

———— 10% CRITICAL DAMPING. - - - - - NO DAMPING.

function properties in Table 6.1, the following values are calculated:

(Units - lb./ft.²)

$\int_0^1 m. B_1^2. dx/l = 3.216$	$\frac{\alpha_1^2}{l^2} \int_0^1 S. b_1^2. dx/l = .510$
$\int_0^1 m. B_2^2. dx/l = 4.253$	$\frac{\alpha_2^2}{l^2} \int_0^1 S. b_2^2. dx/l = 4.34$
$\int_0^1 m. B_3^2. dx/l = 4.876$	$\frac{\alpha_3^2}{l^2} \int_0^1 S. b_3^2. dx/l = 13.07$
$\int_0^1 m. B_4^2. dx/l = 4.470$	$\frac{\alpha_4^2}{l^2} \int_0^1 S. b_4^2. dx/l = 28.57$
$\int_0^1 m. B_1. B_2. dx/l = .264$	$\frac{\alpha_1 \alpha_2}{l^2} \int_0^1 S. b_1. b_2. dx/l = .28$
$\int_0^1 m. B_1. B_3. dx/l = -.685$	$\frac{\alpha_1 \alpha_3}{l^2} \int_0^1 S. b_1. b_3. dx/l = -.011$
$\int_0^1 m. B_1. B_4. dx/l = .265$	$\frac{\alpha_1 \alpha_4}{l^2} \int_0^1 S. b_1. b_4. dx/l = .06$
$\int_0^1 m. B_2. B_3. dx/l = -.357$	$\frac{\alpha_2 \alpha_3}{l^2} \int_0^1 S. b_2. b_3. dx/l = 2.90$
$\int_0^1 m. B_2. B_4. dx/l = -.073$	$\frac{\alpha_2 \alpha_4}{l^2} \int_0^1 S. b_2. b_4. dx/l = -.52$
$\int_0^1 m. B_3. B_4. dx/l = -.303$	$\frac{\alpha_3 \alpha_4}{l^2} \int_0^1 S. b_3. b_4. dx/l = 6.78$
$\frac{\alpha_1^4}{l^4} \int_0^1 E.I. \beta_1^2. dx/l = 34.1$	$\frac{\alpha_2^2 \alpha_3^2}{l^4} \int_0^1 E.I. \beta_2. \beta_3. dx/l = -20.2$
$\frac{\alpha_2^4}{l^4} \int_0^1 E.I. \beta_2^2. dx/l = 394.5$	$\frac{\alpha_2^2 \alpha_4^2}{l^4} \int_0^1 E.I. \beta_2. \beta_4. dx/l = 12.4$
$\frac{\alpha_3^4}{l^4} \int_0^1 E.I. \beta_3^2. dx/l = 1509.7$	$\frac{\alpha_3^2 \alpha_4^2}{l^4} \int_0^1 E.I. \beta_3. \beta_4. dx/l = -72.5$

The axial load terms, it should be noted, are much smaller than the bending terms.

For the first mode the guy moduli are assumed to have approximately their static values. Hence:

$$\frac{K}{l} = 73.0 \text{ (bottom)} \quad = 59.0 \text{ (middle)} \quad = 70.0 \text{ (top)}$$

Substituting in equation (6.46), the set of equations for determining the first mode of vibration is found to be

$$49.6a_1 + 43.29a_2 + 30.35a_3 + 20.16a_4 = \omega^2 \{ 3.216a_1 + .264a_2 - .685a_3 + .265a_4 \} \text{ (i)}$$

$$43.29a_1 + 115.39a_2 + 13.30a_3 + 8.47a_4 = \omega^2 \{ .264a_1 + 4.253a_2 - .357a_3 - .073a_4 \} \text{ (ii)}$$

$$-30.35a_1 + 13.30a_2 + 506.70a_3 - 70.18a_4 = \omega^2 \{ -.685a_1 - .357a_2 + 4.876a_3 - .303a_4 \} \text{ (iii)}$$

$$20.16a_1 + 8.47a_2 - 70.18a_3 + 1642.4a_4 = \omega^2 \{ .265a_1 - .073a_2 - .303a_3 + 4.470a_4 \} \text{ (iv)}$$

These equations can be solved by successive approximations. Initially it is assumed that $a_2 = a_3 = a_4 = 0$ and a first approximation for ω^2 is obtained from equation (1). This is then substituted in the remaining three equations to obtain values for a_2/a_1 , a_3/a_1 , and a_4/a_1 . Substitution of these ratios into (1) leads to a new estimate of ω^2 which may or may not agree with the first estimate. If it does agree the approximation is completed; if a discrepancy still exists the process is repeated. (Sometimes a better estimate can be obtained by assuming only a_3 and $a_4 = 0$ and solving for ω^2 from the first two equations). The result of this analysis gives for its first mode: $n = .456$ cy/sec. The mode form (normalised to give unit deflexion at the top) is

$$u(x) = .540 B_1(x) - .284 B_2(x) + .038 B_3(x) - .003 B_4(x)$$

For calculating the higher modes the guy moduli assumed above, are unlikely to be appropriate (this will be established when the frequencies are determined). Instead the taut wire moduli (i.e. elastic stiffness) are assumed: These give

$$\frac{K}{l} = 92.0 \text{ (bottom)} \quad = 74.0 \text{ (middle)} \quad = 94.0 \text{ (top)} \quad \text{lb/ft}^2$$

The resulting equations are:

$$\begin{aligned} 67.06 a_1 + 57.54 a_2 - 42.01 a_3 + 28.03 a_4 &= \omega^2 [3.216 a_1 + .264 a_2 - .685 a_3 + .265 a_4] \\ 57.54 a_1 + 142.70 a_2 + 24.20 a_3 + 7.12 a_4 &= \omega^2 [.264 a_1 + 4.253 a_2 - .357 a_3 - .073 a_4] \\ -42.01 a_1 + 24.20 a_2 + 548.70 a_3 - 65.40 a_4 &= \omega^2 [-.685 a_1 - .357 a_2 + 4.876 a_3 - .303 a_4] \\ 28.03 a_1 + 7.12 a_2 - 65.40 a_3 + 1642.40 a_4 &= \omega^2 [.265 a_1 - .073 a_2 - .303 a_3 + 4.470 a_4] \end{aligned}$$

Solving these in the fashion described above, the 2nd and 3rd natural frequencies are formed to be respectively 1.012 cy./sec and 1.710 cy./sec. The mode forms (having unit mast top deflexions) are:

$$\begin{aligned} \mu_2(x) &= .877 B_1(x) + 1.260 B_2(x) - .113 B_3(x) - .037 B_4(x) \\ \mu_3(x) &= .100 B_1(x) + .164 B_2(x) + .899 B_3(x) + .025 B_4(x) \end{aligned}$$

The forms of these modes are shown in Fig. 9.16. The next step is to determine the shears and bending moments corresponding to these deflexions. This requires integrating the loading acting on the mast. As discussed in section (6.4) this loading is supplied by the inertia loading $\frac{W}{g} \cdot \omega^2 \mu(x)$ the guy reactions, $K \mu(x)$ and the axial loading $-\frac{d}{dx} \left\{ S_x \frac{d\mu}{dx} \right\}$. Each of these can now be evaluated, and the moments and shears formed in the usual way. The shear and bending moment diagrams for the first three modes for unit mast - top deflexion are shown in Fig. 9.17.

9.2.5 Response to Static Windload

The mean wind pressure at height x ft. is

$$\bar{P}_x = \bar{P}_1 \frac{\bar{V}_x^2}{\bar{V}_1^2}$$

where \bar{P}_1 = mean wind pressure at a 30 ft. reference height.

From equation (2.1) this can be written

$$\bar{P}_x = \bar{P}_1 \left(\frac{x}{x_1} \right)^{2\alpha}$$

Substituting for α from Table 2.1, in open country,

$$\bar{P}_x = \bar{P}_1 \left(\frac{x}{x_1} \right)^{.32}$$

and in city conditions,

$$\bar{P}_x = \bar{P}_1 \left(\frac{x}{x_1} \right)^{.80}$$

These loadings are shown in Fig. 9.18.

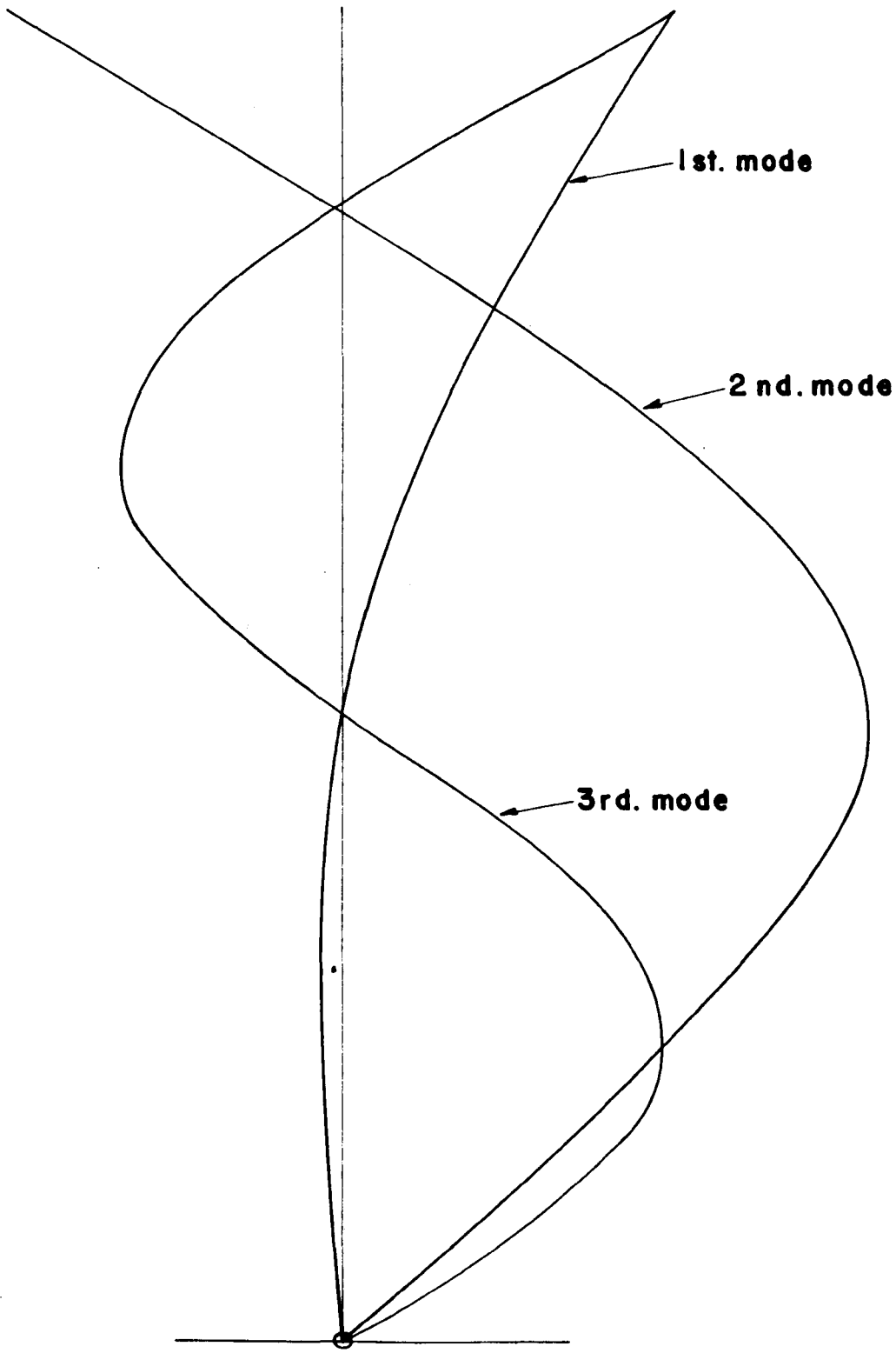


**FIG.9.16 NATURAL MODES OF VIBRATION
OF GUYED MAST.**

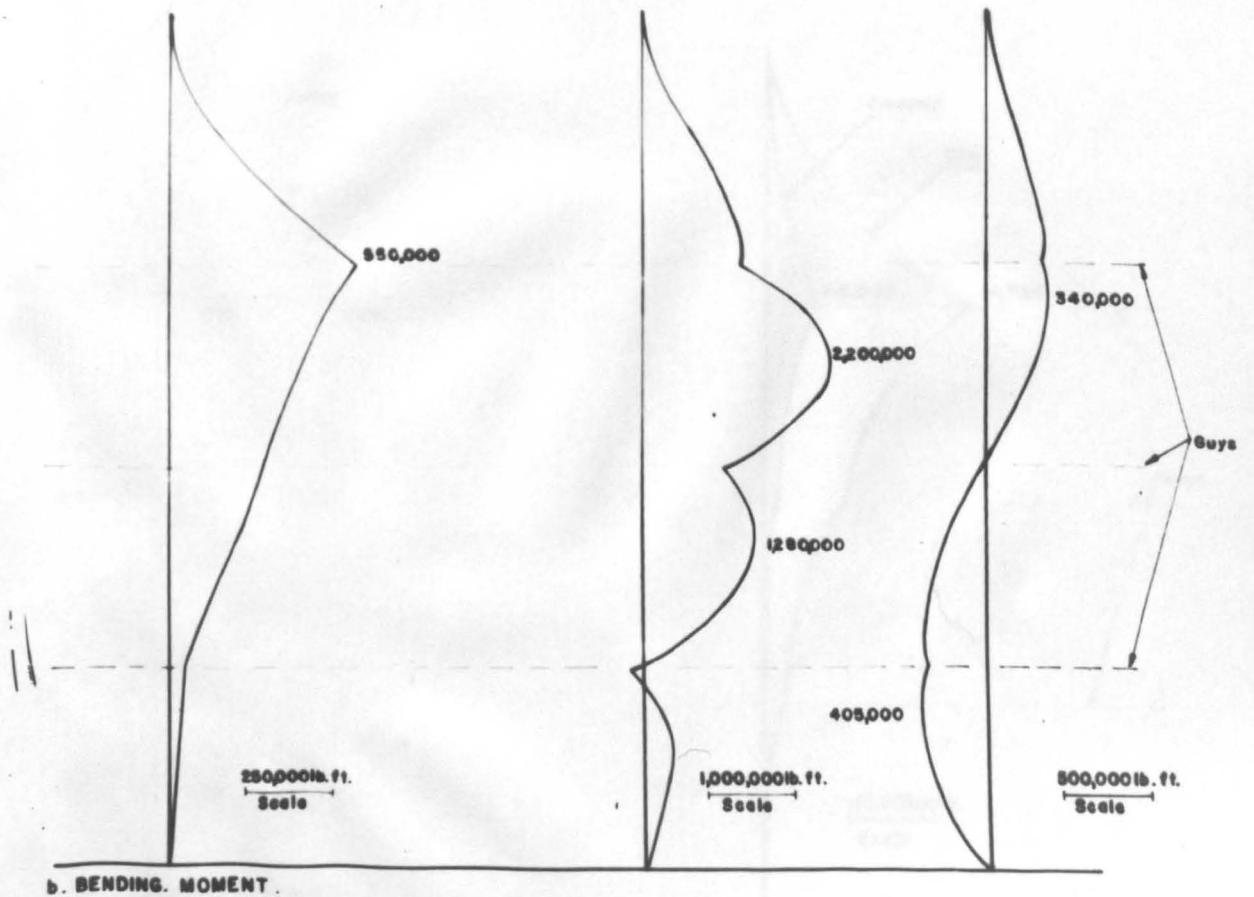
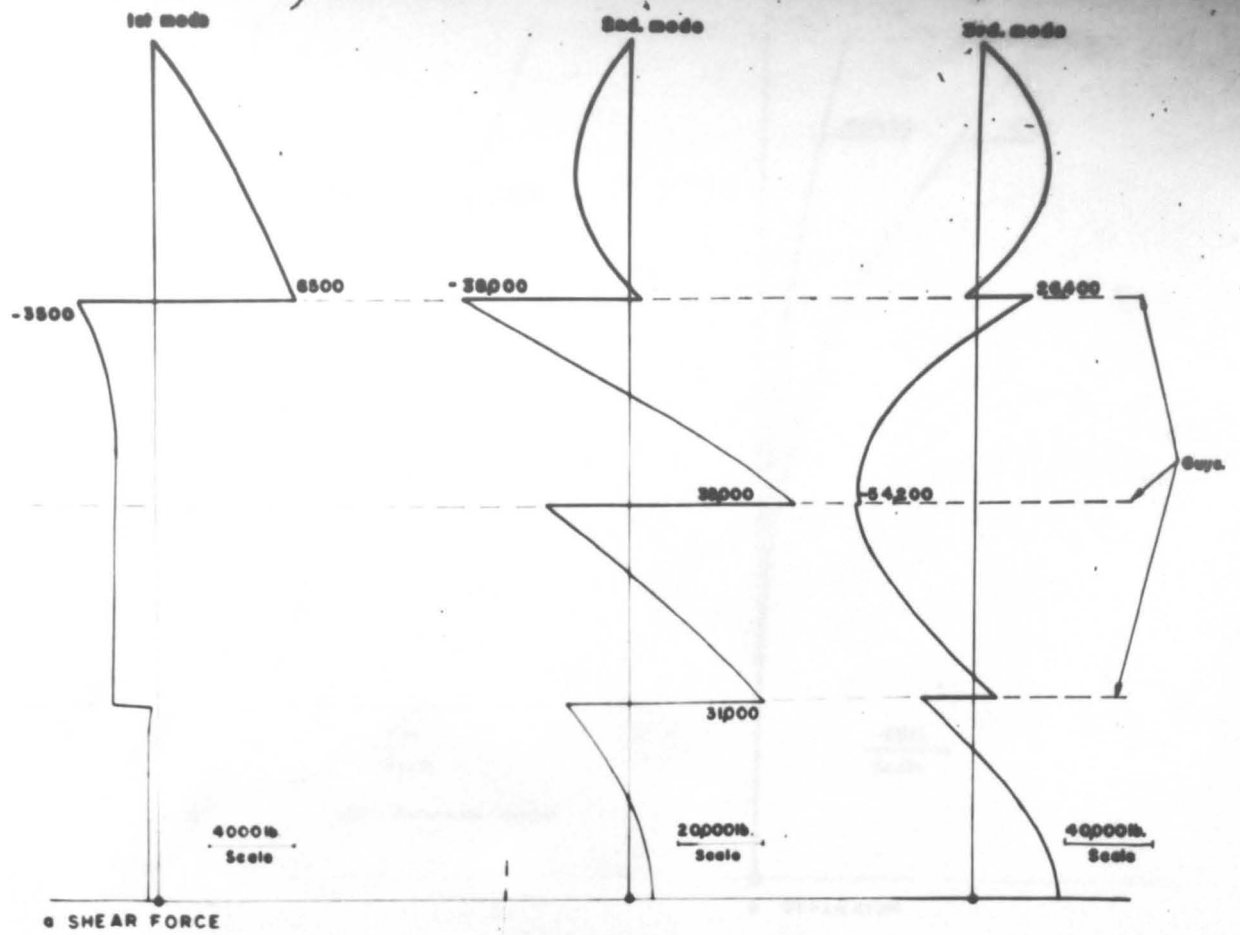


FIG. 9.17 SHEAR AND MOMENT DIAGRAMS FOR THE FIRST THREE MODES FOR UNIT DEFLEXION AT MAST-TOP.

N.B. DIAGRAMS NOT TO SAME SCALE.

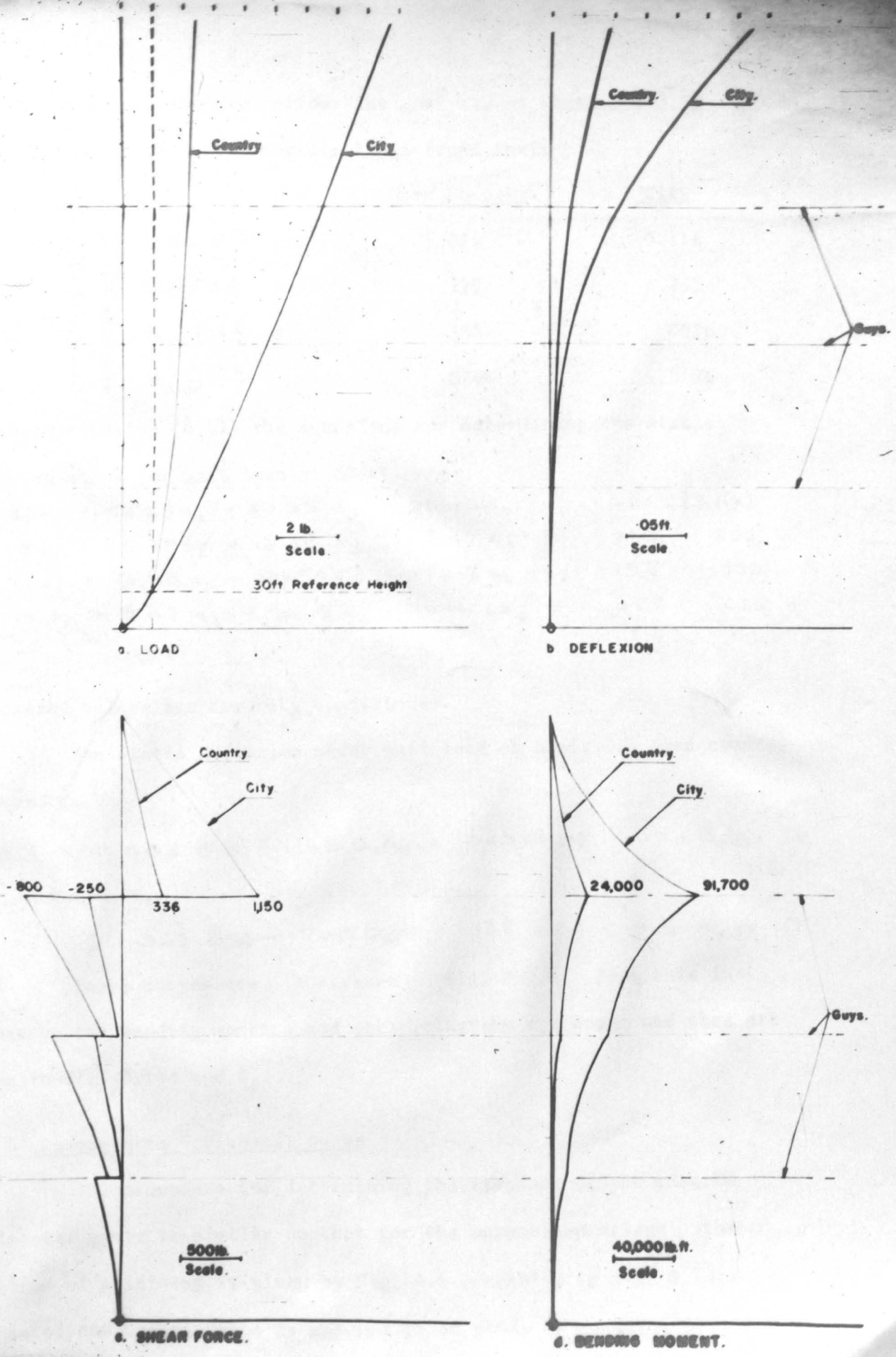


FIG. 9.18 MEAN WIND LOADING OF GUYED MAST UNDER OPEN COUNTRY AND CITY CONDITIONS.

The solution now follows the analysis of Section 6.5.3.

Evaluating the necessary integrals it is found that:

	<u>Open Country</u>	<u>City</u>
$\int_0^1 \frac{\bar{P}_x}{P_1} B_1(x) d\frac{x}{l} =$	1.021	3.116
$\int_0^1 \frac{\bar{P}_x}{P_1} B_2(x) d\frac{x}{l} =$.329	.255
$\int_0^1 \frac{\bar{P}_x}{P_1} B_3(x) d\frac{x}{l} =$.138	.0928
$\int_0^1 \frac{\bar{P}_x}{P_1} B_4(x) d\frac{x}{l} =$.0768	.0198

Following equation (6.51) the equations for determining the static deflected shape for unit load at 30 ft. are

$$\begin{aligned}
 49.60a_1 + 43.29a_2 - 30.35a_3 + 20.16a_4 &= 1.021 \quad (3.116) \\
 43.29a_1 + 115.39a_2 + 13.30a_3 + 8.47a_4 &= .329 \quad (.255) \\
 -30.35a_1 + 13.30a_2 + 506.70a_3 - 70.18a_4 &= .138 \quad (.093) \\
 20.16a_1 + 8.47a_2 - 70.18a_3 + 1642.4a_4 &= .077 \quad (.020)
 \end{aligned}$$

(Bracketed values are for city conditions).

The static deflexion under unit load at 30 ft. in open country is found to be

$$y = .583 B_1(x) - .168 B_2(x) + .045 B_3(x) - .004 B_4(x) \text{ ft.}$$

and, in the city,

$$y = 1.965 B_1(x) - .708 B_2(x) + .138 B_3(x) - .015 B_4(x) \text{ ft.}$$

These curves are illustrated in Fig. 9.18b. From this information the bending moments and shear diagrams are drawn and they are shown in Fig. 9.18c and d.

9.2.6 Response to Horizontal Gusts

The procedure for determining the response of the mast to horizontal gusts is similar to that for the suspension bridge. The spectrum of gustiness is given by Fig. 4.1 (repeated in Fig. 9.19). The aerodynamic admittance is assumed to be given by equation (5.23)

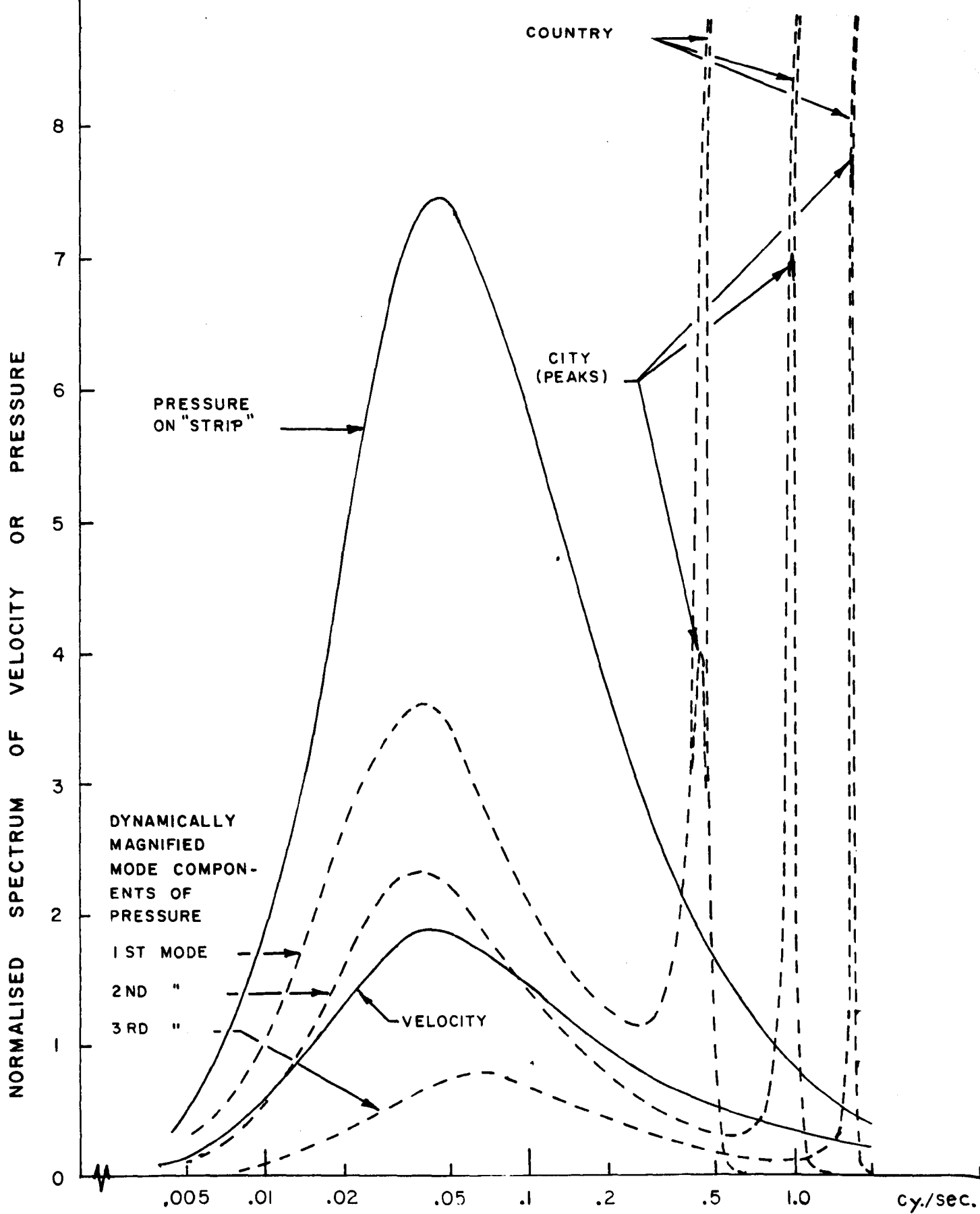


FIG. 9.19 SPECTRA OF VELOCITY AND PRESSURE FOR GUST LOADING OF GUYED MAST

and resulting spectrum of aerodynamic pressure on a transverse strip is given in Fig. 9.19 also. The joint mode acceptances also take a similar form to those for the suspension bridge. The major contributions are

made up of terms of the type;

$$\int_0^1 \int_0^1 e^{-c \frac{|x-x'|}{t}} B_n(x) B_n(x') dx dx'$$

Values of this integral for $n=1, 2$ and 3 are shown in Fig. 9.20. Using the known values of the constituents of the Basic functions, the Joint Mode acceptances are calculated and from these the mode components of pressure. The next step is to compute the damping in each mode so that the dynamic magnification can be found. At this stage it is necessary to specify the mean wind velocity, and for purposes of illustration a mean wind velocity of 100 ft./sec. at a 30 ft. datum has been chosen in both city and country. In practice it would be better to use the actual design mean wind velocity, corresponding to the return period considered appropriate for the structure.

The basic expression for the aerodynamic damping is given by equation 7.1. The integrals involved are found to be

	<u>City</u>	<u>Country</u>
$\int_0^1 m(x) \mu_1^2(x) dx = 1.196 \text{ slugs/ft}$	$\int_0^1 \frac{Vx}{V_1} \mu_1^2 dx = .423$	$.226$
$\int_0^1 m(x) \mu_2^2(x) dx = 9.81$	$\int_0^1 \frac{Vx}{V_1} \mu_2^2 dx = 2.638$	1.497
$\int_0^1 m(x) \mu_3^2(x) dx = 4.15$	$\int_0^1 \frac{Vx}{V_1} \mu_3^2 dx = .90$	$.555$

Hence the logarithmic damping coefficients are found to be as follows:

LOGARITHMIC DAMPING DECREMENTS FOR GUYED MAST

Mode	δ_{aero}		δ_{mech}^*	δ_{total}	
	<u>Country</u>	<u>City</u>		<u>Country</u>	<u>City</u>
1st	.397	.745	.02	.417	.765
2nd	.140	.246	.02	.160	.266
3rd	.082	.153	.02	.102	.173

*assumed minimum

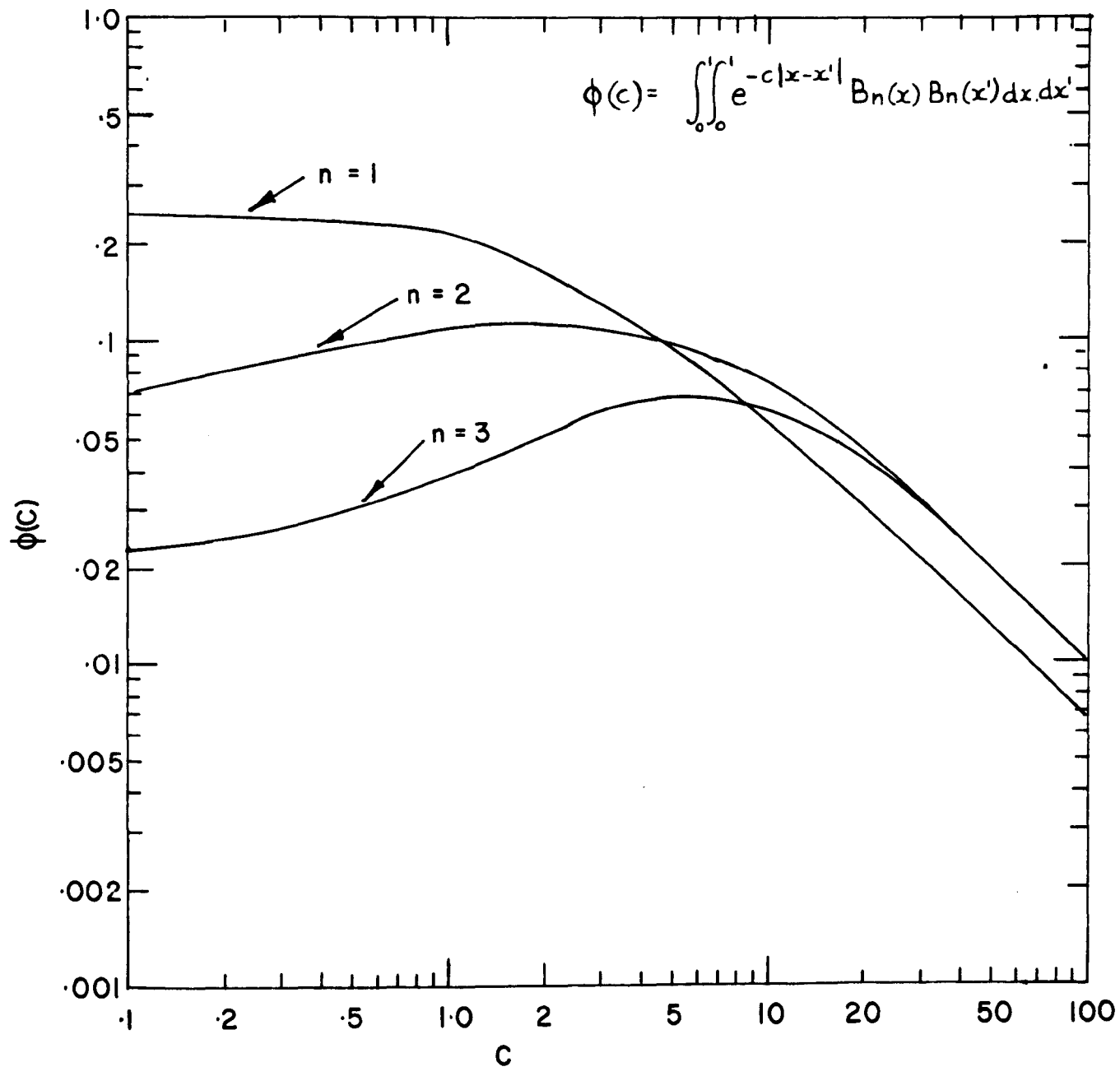


FIG. 9.20 VALUES OF $\phi(c) = \int_0^1 \int_0^1 e^{-c|x-x'|} B_n(x) B_n(x') dx dx'$
FOR HINGED - FREE BEAM.

The dynamic magnification for each mode is now calculated from equation (3.23). The resulting spectra of the dynamically magnified mode components of pressure are given in Fig. 9.19. The areas under the spectra were measured planimetrically and found to be as follows:

Mode	VALUES OF $\frac{\sigma_r^2(P)}{\bar{p}^2}$ FOR GUYED MAST	
	Country	City
1st	.420	4.50
2nd	.033	.36
3rd	.036	.39

The above values take into account the different roughness coefficients, viz. $K = .005$ in open country and $K = .060$ in the city. The second moment of the spectra are as follows:

MODE	VALUES OF $\frac{\sigma_r'^2(P)}{\bar{p}^2}$ FOR GUYED MAST	
	Country	City
1st	.0207	.136
2nd	.0072	.052
3rd	.0258	.187

The peak values of the bending moments and shears due to the gustiness are calculated in Table 9.6 and combined with the bending moments and shears due to the mean wind. As noted already the values calculated in this table refer to a mean velocity at the 30 ft. datum of 100 ft./sec. In practice it would be logical to calculate the peak gusts for the chosen design mean velocity at the site (e.g. the "once-in-50-years" mean velocity). As mentioned in Section 9.2.2 it was the intention to compare the "once-in-50-year" wind loads in open country and city conditions for a site where the parameters of the extreme hourly gradient wind velocity are ($U_G = 80; \frac{1}{\Delta} = 8$)

TABLE 9.6 a

ANALYSIS OF WIND LOADING OF GUYED MAST (SHEAR FORCE)

Mean wind at 30 ft. $\bar{V}_1 = 100$ ft./sec.

Mean wind load at 30 ft. $\bar{P}_1 = 95$ lb./ft.

Roughness $k = .005$ (open country): $= .040$ (city)

$\frac{x}{L}$	Unit mode load factors			OPEN COUNTRY							CITY						
	q_1	q_2	q_3	$\frac{\sigma_Q(x)}{\bar{P}_1}$	$\frac{\sigma_Q'(x)}{\bar{P}_1}$	v	$g(vr)$	$g\sigma_Q$ lb.	Mean shear lb.	Total peak shear lb.	$\frac{\sigma_Q(x)}{\bar{P}_1}$	$\frac{\sigma_Q'(x)}{\bar{P}_1}$	v	$g(vr)$	$g\sigma_Q$ lb.	Mean shear lb.	Total peak shear lb.
1.0	0	0	0	0	0	-	-	0	0	0	0	0	-	-	0	0	0
.9	40.1	-27.6	28.0	27.0	7.7	.28	4.00	108	100	208	88.5	20.1	.23	3.95	350	418	768
.8	69.3	-27.9	26.5	45.5	11.1	.24	3.97	180	228	409	148.8	28.7	.19	3.91	582	800	1382
.7	92.9	+6.5	-3.5	60.6	14.5	.24	3.96	240	336	576	198.2	37.5	.19	3.90	773	1150	1923
.6	-50.0	-98.8	24.9	37.3	11.8	.32	4.02	150	-250	400	122.5	31.0	.25	4.00	490	-800	1290
.5	-30.0	-10.9	-28.2	20.3	6.3	.31	4.01	81	-145	226	66.4	16.7	.25	4.00	265	-490	755
.47	-27.9	72.3	-48.7	24.2	10.7	.44	4.13	100	-51	151	79.4	28.7	.36	4.07	323	-230	553
.4	-27.1	98.7	-48.7	26.8	12.1	.45	4.15	111	-25	136	88.0	32.4	.36	4.07	358	-150	408
.3	-27.1	-51.5	-50.2	22.1	10.0	.45	4.15	92	-200	292	72.5	27.2	.27	4.07	295	-670	965
.23	-27.9	-12.4	-45.0	20.1	8.3	.42	4.10	82	-140	222	65.9	22.2	.34	4.05	267	-418	785
.2	-28.6	46.8	-16.8	20.6	6.3	.31	4.00	82	-75	157	67.6	16.7	.25	3.98	269	-227	496
.1	-28.6	80.1	12.3	23.7	8.2	.35	4.05	96	0	195	77.7	21.7	.28	4.50	311	-120	431
.0	-3.6	-38.8	-28.3	9.2	5.6	.61	4.20	39	-130	169	30.2	15.2	.50	4.17	126	-261	387
.0	-3.6	-27.0	-15.8	6.2	3.5	.56	4.18	26	-80	106	20.4	9.3	.45	4.12	84	-200	284
.0	-5.0	4.6	20.1	5.1	3.3	.65	4.21	21	-20	42	16.7	8.9	.54	4.20	70	-70	140
.0	-5.7	4.0	34.0	7.5	5.5	.74	4.25	32	30	62	24.6	14.9	.61	4.21	103	-50	153

$$\frac{\sigma_Q(x)}{\bar{P}_1} = \sqrt{42.0q_1^2 + 3.3q_2^2 + 3.6q_3^2} \times 10^{-1}; \quad \frac{\sigma_Q'(x)}{\bar{P}_1} = \sqrt{4.50q_1^2 + .36q_2^2 + .39q_3^2}$$

$$\frac{\sigma_Q'(x)}{\bar{P}_1} = \sqrt{2.07q_1^2 + .72q_2^2 + 2.58q_3^2} \times 10^{-1}; \quad \frac{\sigma_Q(x)}{\bar{P}_1} = \sqrt{13.6q_1^2 + 5.2q_2^2 + 18.7q_3^2} \times 10^{-1}$$

TABLE 9.6 b

ANALYSIS OF WIND LOADING OF GUYED MAST (BENDING MOMENT)

Mean wind at 30 ft. $\bar{V}_1 = 100$ ft./sec.

Mean wind load at 30 ft. $\bar{P}_1 = 95$ lb./ft.

Roughness $k = 0.005$ (open country)

$H = 0.040$ (city)

$\frac{x}{t}$	Unit mode Load factors			OPEN COUNTRY							CITY						
	m_1	m_2	m_3	$\frac{\sigma_M(x)}{\bar{P}_1}$	$\frac{\sigma'_M(x)}{\bar{P}_1}$	v	$g(\nu T)$	$g \cdot \sigma_M$ lb. ft. $\times 10^{-3}$	Mean moment lb. ft. $\times 10^{-3}$	Total peak moment lb. ft. $\times 10^{-3}$	$\frac{\sigma_M(x)}{\bar{P}_1}$	$\frac{\sigma'_M(x)}{\bar{P}_1}$	v	$g(\nu T)$	$g \cdot \sigma_M$ lb. ft. $\times 10^{-3}$	Mean moment lb. ft. $\times 10^{-3}$	Total peak moment lb. ft. $\times 10^{-3}$
1.0	0	0	.00	0	0	-	-	0	0	0	0	0	-	0	0	0	0
.9	1.04	.75	.08	.69	.16	.24	3.98	2.7	3.1	5.8	2.25	.42	.19	3.90	8.8	14.1	22.9
.8	3.84	2.28	.23	2.52	.59	.23	3.96	10.0	10.1	20.1	8.26	1.51	.18	3.90	32.2	43.2	75.2
.7	7.71	2.88	.30	5.02	1.14	.23	3.96	19.9	24.0	43.9	16.43	2.92	.18	3.90	64.1	91.7	155.8
.6	5.80	5.66	.28	3.90	.96	.25	3.99	15.6	12.0	27.6	12.77	2.50	.20	3.91	49.9	55.0	104.9
.5	4.29	4.11	.19	2.88	.71	.25	3.99	11.5	6.5	18.0	9.43	1.84	.20	3.91	36.9	39.5	76.4
.47	3.73	2.40	0	2.46	.57	.23	3.96	9.7	6.0	15.7	8.04	1.48	.18	3.90	31.4	38.0	69.4
.4	3.11	3.31	.18	2.10	.53	.25	3.99	8.4	4.3	12.7	6.89	1.37	.20	3.91	26.9	23.0	49.9
.3	1.61	2.43	.34	1.14	.31	.28	4.00	4.6	3.1	7.7	3.72	.83	.22	3.92	14.6	13.0	27.6
.23	.59	.45	.35	.40	.11	.27	4.00	1.6	2.2	3.8	1.30	.28	.22	3.92	5.1	10.4	15.5
.2	.54	.06	.38	.36	.10	.28	4.00	1.4	1.0	2.4	1.17	.26	.22	3.92	4.6	6.2	10.8
.1	.32	.71	.32	.25	.09	.36	4.07	1.0	.5	1.5	.67	.24	.36	4.07	2.7	1.0	3.7
0	0	0	0	0	0	0	0	0	0	0	0	0	0	0	0	0	0

$$\frac{\sigma_M(x)}{\bar{P}_1} = \sqrt{42.0 m_1^2 + 3.3 m_2^2 + 3.6 m_3^2} \times 10^{-1}$$

$$\frac{\sigma_M(x)}{\bar{P}_1} = \sqrt{4.50 m_1^2 + .36 m_2^2 + .39 m_3^2}$$

$$\frac{\sigma'_M(x)}{\bar{P}_1} = \sqrt{2.07 m_1^2 + .72 m_2^2 + 2.58 m_3^2} \times 10^{-1}$$

$$\frac{\sigma'_M(x)}{\bar{P}_1} = \sqrt{13.6 m_1^2 + 5.2 m_2^2 + 18.7 m_3^2} \times 10^{-1}$$

mi./hr. For such a locality, the mean wind loads at 30 ft. are 89 lb./ft. and 10 lb/ft. in open country and city conditions respectively. The wind loads adjusted to correspond to these values, are plotted in Fig. 9.21.

9.2.7 Discussion

The results of Fig. 9.21 indicate some of the differences between the wind loads on a tall mast in open country and city conditions, the probability of occurrence being the same in both localities. Both the peak shear forces and bending moment envelopes are seen to be less in the city - the maximum peak shear force in open country is three times as large as that in the city while the maximum peak bending moment is $2 \frac{1}{2}$ times as large. The relative contributions to the peak shears and bending moments made by gusts and mean wind are seen to be different: for instance, of the total peak bending moment in open country only a third is attributable to gusts which in a city the proportion is nearer to a half.

There are two main reasons for these differences. In the first place the mean wind load at 30 ft. in the city is only 10 per cent of that in open country while at the top of the mast (500 ft.) it is nearer 66 per cent. Secondly, in spite of the fact that the drag coefficient in the city is taken to be .060 whereas in open country it is only .005, the drag force between the air and the ground generating the gustiness is only $1 \frac{1}{2}$ times that in open country. This means that the R.M.S. gust velocities are only about 20 per cent greater in the city and the R.M.S. gust loads actually smaller, being probably only 40 per cent of that in open country.

Because the mean wind velocities in the city are less, the damping is also less meaning that the dynamic magnification is larger: however, this is largely offset by the fact that the natural frequencies of the mast

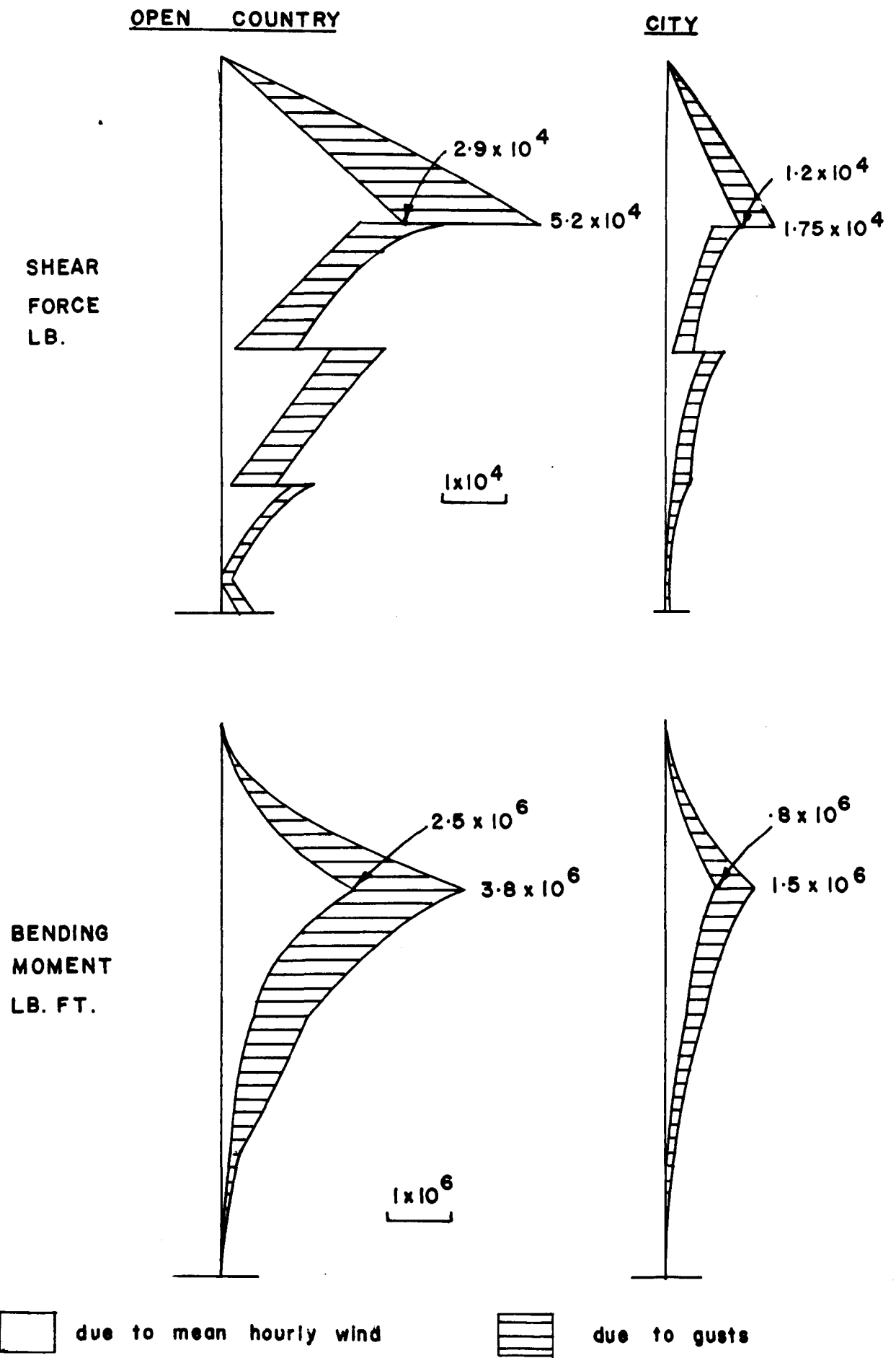


FIG. 9.21 COMPARISON OF ONCE-IN-FIFTY YEAR WIND LOADING ON A TALL GUYED MAST UNDER OPEN COUNTRY AND CITY CONDITIONS ($U_G = 80 \text{ mi/hr.} ; \frac{1}{q} = 8 \text{ mi/hr.}$)

then correspond to higher wave numbers $\frac{n}{V}$, for which the gust spectrum generally contains less energy.

Since the gust spectrum has been assumed invariant with height, the height of the mast is not likely to greatly affect the ratio of the gust loading in city and country. On the other hand a taller mast generally means that the natural frequencies are slower so that the dynamic magnification occurs at lower wave numbers and hence higher gust energies. (In this connection it should perhaps be mentioned that the mast considered in the worked example is probably somewhat stiffer in relation to its mass than the majority of masts of a similar height, and consequently the natural frequencies tend to be somewhat higher). In contrast, the effect of increasing the height will be to make the mean wind effects in city and open country more nearly equal.

The envelopes of peak bending moment are seen to be more or less similar to the distribution of mean wind bending moment (in both city and country). The same is not however so true of the shear forces. Here it would appear that the additional shear due to gusts is nearly constant between guy points (except for the top cantilevered section) whereas the mean shear is more or less triangular. Since the bending moment is probably more critical, it seems that with proper selection of the ratio of peak to mean moments the peak moments can be satisfactorily estimated from the moments due to the mean wind load only. The study of various mast configurations would be necessary to determine the value of this ratio for masts of various types and for specified roughness conditions.

No comparison was made with the peak shear and moment envelopes obtained from loading patterns such as those shown in Fig. 1.1, used in conjunction with the "gust profiles" suggested by Sherlock (1947) and

Deacon (1954). (The characteristic of the latter being a steeper slope than the mean velocity profile, the suggested power law index being .085 instead of .14 - .16 for open country). It is to be expected that any similarity would be largely fortuitous.

10.0 EVALUATION AND SUGGESTIONS FOR FUTURE RESEARCH

10.1 GENERAL

The aims of this study have been to provide first, some understanding of the physical processes involved in the wind loading of two slender beam-like structures, second a comprehensive, rational treatment of the problem on which engineering design might be based, and third the data needed to apply the latter. We now consider briefly to what extent the goals have been achieved.

Although it is believed that there is a satisfactory framework of ideas upon which a physical understanding of wind-loading can be based, much is unknown about the details. At the root of the wind-loading problem is the question of the climate of extreme winds. Although some of the characteristics are recognizable - it not explainable - the problem of finding a general statement of the climate of a territory suitable for adaptation to particular localities still remains largely unsolved. An empirical method for doing so has been suggested, (to demonstrate the need as much as for any other reason): it is, however, based on limited evidence and experience and may later prove to be imperfect. Although knowledge of the structure of turbulence near the ground is steadily improving, it is, nevertheless, still deficient. In investigations on this subject, the statistical theories of turbulence undoubtedly provide the necessary framework. A third area, about which possibly even less is properly understood, is the formation of aerodynamic forces on bluff objects in turbulent flow.

By comparison, the mechanical aspects of the wind-loading problem, concerning the behaviour of the structure under dynamic and static loads, are better understood, although some of the more far reaching questions -

such as what form of loading is most critical in these structures - have scarcely been touched.

The statistical treatment of wind loading has revealed several facts not previously widely recognized or possibly even suspected. The worked examples for instance have shown that gusts of wind are relatively ineffectual in producing large momentary pressures on a structure (contrary to what common design precepts would suggest). The regularity with which they occur, however, is such as to maintain oscillations over a fairly wide range of frequencies, those near the natural frequencies being particularly large, resulting in large inertia forces. The most important role of the gust loads is to overcome the damping. The treatment has also enabled the vertical gust forces on the suspension bridge to be evaluated in a way that has not hitherto been managed.

The worked examples have indicated that only the first and second modes cause significant stresses and deflexions. This suggests that simplifications are possible leading to adaptations of the method to meet design needs. (The question has not yet been considered in detail). On the whole, the merits of the statistical approach are that it is rational, it gives a true reflection of the physical processes involved, and is suitable for practical application.

For applying the method it has only been possible to provide a bare minimum of data. Where information has been uncertain or imprecise - as in the determination of cross-correlation coefficients and the forces in fluctuating flow - values have been suggested in the belief they are slightly on the conservative side, although this might not necessarily be so. In this respect it is worth noting that many of the quantities introduced (cross-correlation coefficients, spectra, aerodynamic admittance etc.)

appear finally in square root form which appreciably reduces any initial errors. In general, the aim has been more to evaluate the probable value of the wind loading rather than a value circumscribed by natural design-office cautiousness.

A few selected topics for research now follow.

10.2 SUGGESTIONS FOR FUTURE RESEARCH

Wind Structure and Climate

1. The investigation of high-wind structure up to 1000 ft. in rougher regions such as the centres of large cities. This has never been thoroughly studied, it appears, although it is obviously of interest for many applications.
2. The amalgamation of the results of 1 with those for more open regions to improve estimates of climate made from anemometer records.
3. The investigation of the spectra and cross-correlation coefficients (both vertical and horizontal) under different roughness conditions - with particular reference to strong winds.

Aerodynamics

1. Investigation of the buildup of aerodynamic forces in turbulent flow.

Structural

General

1. Investigation of the modes of failure of flexible beam-like structures due to wind-type loading.

Suspension Bridges

2. Investigation of the lateral modes and natural frequencies of the complete suspension bridge, including the possibility of coupled vertical-lateral oscillations.

3. Observation of the behaviour of full scale structures including study of their internal structural damping.

Mast

1. Investigation of the behaviour of guy wires under dynamic load, (experimental and theoretical).
2. Investigation of the behaviour of full scale structures including a study of their internal damping and modes of vibration.

APPENDIX I

USE OF THE PEAK GUST RATIO AS AN INDICATOR OF SURFACE ROUGHNESS

Reference was made in Section 2.4 to the possibility of using the ratio of peak gust velocity to mean velocity as an indicator of the surface roughness of an anemometer site - or for that matter the site for a structure at which exploratory wind investigations have been made. The premises for this are as follows.

In Section 8.3 it was shown that the average peak fluctuation of a random process during a period T was $g(vT) \cdot \sigma$, where $g(vT)$ was the "gust factor" and σ , the R.M.S. fluctuation. The random process in this instance is the indicated wind speed. If the "admittance" of the anemometer (defining its response to different frequencies) is $|\chi_A|$ then the spectrum of the indicated velocity will be $|\chi_A|^2 \cdot S(n)$ where $S(n)$ is the velocity spectrum of the actual wind. Hence the indicated R.M.S. fluctuation is

$$\sigma = \left[\int_0^{\infty} |\chi_A(n)|^2 \cdot S(n) \cdot dn \right]^{1/2}$$

and the "response factor", $v = \frac{\sigma'}{\sigma}$

where

$$\sigma' = \left[\int_0^{\infty} n^2 \cdot |\chi_A(n)|^2 \cdot S(n) \cdot dn \right]^{1/2}$$

The expression for the horizontal gust spectrum suggested in Section 4.2 is of the form

$$S(n) \cdot dn = K \cdot \bar{V}_1^2 \cdot f(x) \cdot dx$$

where x was proportional to the wave-number.

Using the power law to relate the mean velocity at reference height, \bar{V}_1 , to that at anemometer height \bar{V}_A we can write

$$S(n) \cdot dn = K \cdot \bar{V}_A^2 \cdot \left(\frac{z_1}{z_A} \right)^{2\alpha} \cdot f(x) \cdot dx$$

If the anemometer response is not too sensitive to changes in mean wind velocity the R.M.S. fluctuation can be written

$$\begin{aligned}\sigma &= K^{\frac{1}{2}} \cdot \bar{V}_A \cdot \left(\frac{z_1}{z_A}\right)^{\alpha} \left\{ \int_0^{\infty} |\chi_A(\tau)|^2 \cdot f(x) \cdot dx \right\}^{\frac{1}{2}} \\ &= K^{\frac{1}{2}} \cdot \bar{V}_A \cdot \left(\frac{z_1}{z_A}\right)^{\alpha} \cdot \phi\end{aligned}$$

where ϕ is the value of the definite integral. The peak gust ratio is now found to be

$$\begin{aligned}\frac{V_{\text{peak}}}{\bar{V}_A} &= \frac{1}{\bar{V}_A} \left[1 + g(vT) \cdot \sigma \right] \\ &= 1 + g(vT) \cdot K^{\frac{1}{2}} \cdot \left(\frac{z_1}{z_A}\right)^{\alpha} \cdot \phi\end{aligned}$$

Provided again that the anemometer response is moderately insensitive to changes in wind velocity, then $g(vT)$ and ϕ will both be constants for the anemometer and for the sampling period T . Hence the peak gust ratio is seen to be more or less independent of wind speed, but dependent on the anemometer height z_A , and on α and K which are functions of the roughness of the site.

Thus, it appears that if the gust factor $g(vT)$ and the response characteristics of the instrument are known, the peak gust ratio can be used to define a function of K and α , from which the roughness can be ascertained. Another function of K and α can be formed by interpolation of the values given in Table 2.1. K and α can then be evaluated by simultaneous solution of the two expressions. Once the value of α is established the roughness factor, k_A , for the anemometer site (the ratio of the gradient velocity to the mean velocity at the anemometer height) can be found from

$$k_A = \frac{\bar{V}_G}{\bar{V}_A} = \left(\frac{z_G}{z_A}\right)^{\alpha}$$

Z_G can be expressed as a function of α using the values in Table 2.1. A nomogram for the complete solution of the roughness factor from the peak gust ratio is given in Fig. A-1. The dashed line illustrates the solution for an anemometer installation at which

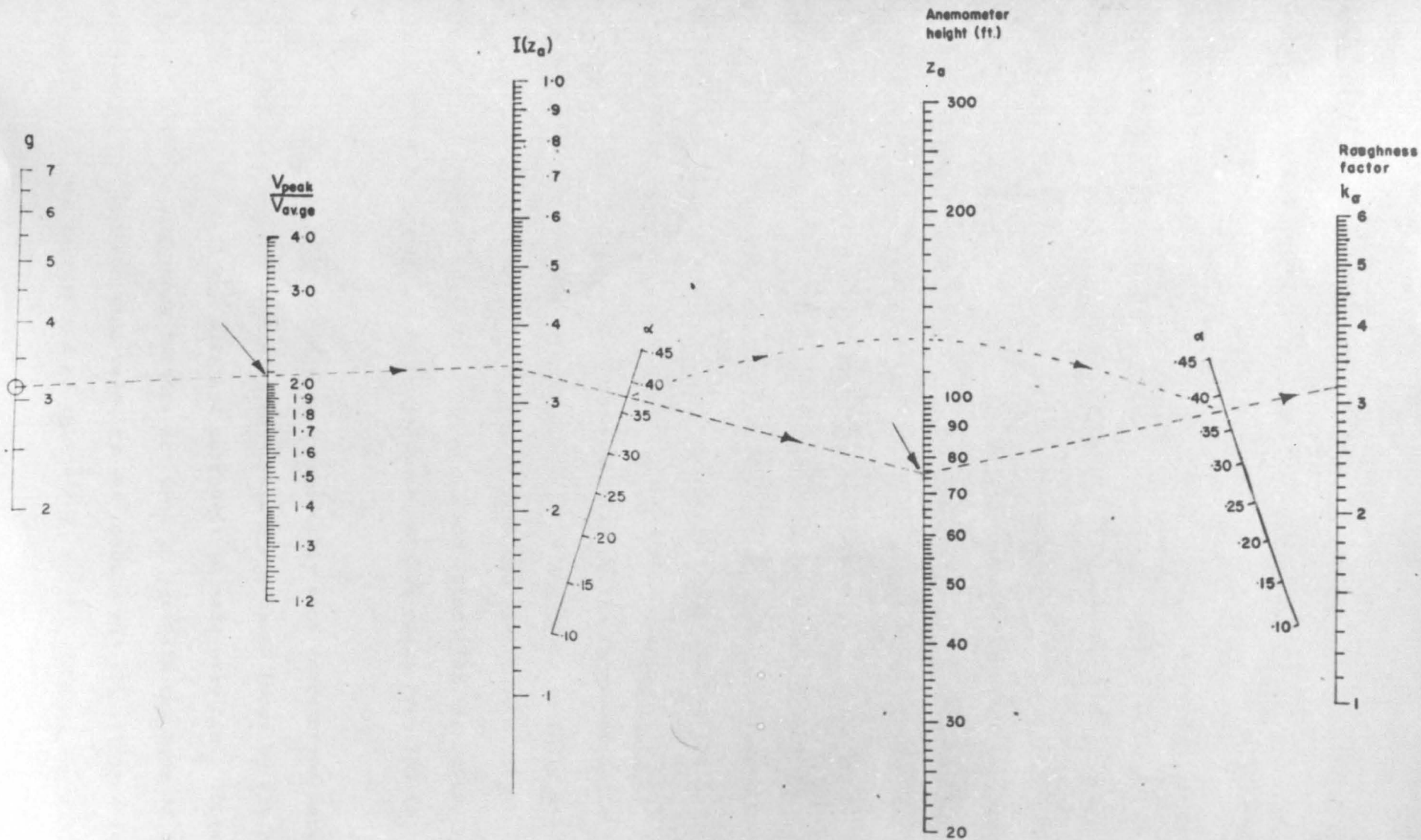
$$Z_A = 75 \text{ ft.}, \quad g(v_T) = 3.2$$

and the peak gust ratio = 2.06. It is found that $\alpha = .37$ and $k_A = 3.2$.

In applying these results the question arises as to how best to estimate the peak gust ratio appropriate to an anemometer installation. Fortunately, in the United Kingdom it is the practice at most meteorological stations to record not only the maximum mean hourly wind speeds but also the peak gust speeds.

Values of the peak gust ratio determined from individual observations of peak and hourly speeds will obviously vary from one estimate to the next. Possibly a better way to estimate the peak gust ratio is to determine the ratio of the parameters (mean, mode, etc.,) of the statistical distributions of both extreme hourly wind speeds and of extreme gust speeds. From an examination of Shellard's data (1958), for example, it appears that the modes of the two distributions are in approximately the same ratio as the "once-in-50-year" quantiles. (This can be seen from the few sample values given in Table A-1). This ratio is probably as representative a value for the peak gust ratio as can be obtained.

The gust recording anemometers installed at most British meteorological stations would appear to be of the Dine's pressure-tube variety. Some frequency response data for this instrument are given in the "Handbook of Meteorological Instruments", from which it appears that the response is "flat" up to a critical frequency (about 2 cy./sec. in a



FIGA-1 NOMOGRAM FOR DETERMINING THE ROUGHNESS FACTOR OF AN ANEMOMETER INSTALLATION FROM THE RATIO OF PEAK GUST SPEED TO MEAN WINDSPEED.

60 mi./hr. wind) at which point the falling-off of the response to higher frequencies is so rapid that it might almost be regarded as a high frequency "cut-off". This cut-off frequency increases with wind speed and over the range of extreme wind speeds encountered in practice it seems reasonable to assume that it occurs at constant wave-number. The length and cross-section of the pressure tubing connecting the instrument head to the recording gear has a large effect on the instrument response. For this reason the response characteristics of the Dines anemometers in service at meteorological stations may vary. However, if it is assumed that the "high-frequency cut-off" referred to above is reasonably representative of the installed anemometers then it is found that the "gust factor" is approximately 3.83. It is also assumed that the Dines anemometer indicates the instantaneous value of the horizontal wind speed (and not merely the velocity component in the mean wind direction), so that the spectrum of horizontal gustiness cited above is applicable.

Using the nomogram, some estimates of the roughness factors for a few anemometer stations in Southern England are given in Table A-1. The stations are seen to range in roughness from the centre of a city (Kingsway-London) to the open sites of Lympne (airfield) and Dover (on a pier over the sea). The instrument heights range from 160 ft. to 36 ft.

It is seen that there is a reasonably good correlation between the "roughness factors" found by these means and those found by the subjective evaluation of the site and surroundings made previously (Davenport - 1960). When the roughness factors are used to estimate the mode of the extreme hourly gradient wind velocity the results all lie within a few miles/hour of one another and of the 70 - 75 mi./hr. contour for this

TABLE A-1

DETERMINATION OF ROUGHNESS FROM PEAK GUST RATIO

Station	Ht. z _A ft	Mean hr'ly velocity mi./hr		Peak gust velocity mi./hr		Peak Gust Ratio		α	Roughness Factor k _A †	Gradient Velocity mi/hr k _A · U _H	Exposure
		U _H	$\frac{1}{a_H}$	U _g	$\frac{1}{a_g}$	$\frac{U_g}{U_H}$	$\frac{V_g(5g)}{V_H(5g)}$				
Shoeburyness	104	45	4.5	66	6.8	1.46	1.48	.12	1.30 (1.57)	60*	Flat lowland on coast
Birmingham	118	34	4.1	63	7.4	1.85	1.84	.31	2.15 (2.40)	74	City Suburb
London Kw (Kingsway)	160	28	4.1	56	9.9	1.98	2.13	.33	2.44 (-)	70	City centre
Croydon	105	37	4.3	65	6.5	1.74	1.68	.26	1.93 (2.15)	72	Suburban airfield
Kew Obs'ty	75	30	2.4	61	5.3	2.06	2.09	.32	2.60 (2.75)	76	City park
Dover	36	42	2.9	63	6.2	1.51	1.65	.12	1.45 (-)	61*	Pier on sea front
Lympne	76	43	3.7	69	6.0	1.61	1.60	.18	1.62 (1.75)	70	Open airfield
Manston	46	40	3.7	67	5.7	1.68	1.64	.18	1.79 (2.00)	71	Open shore
Calshot	80	42	4.6	64	7.7	1.51	1.57	.15	1.48 (1.60)	63*	Lowland verging on Solent
Boscombe D.	55	39	3.7	65	6.2	1.66	1.66	.18	1.72 (1.90)	67	Military station in open grassland
Larkhill	51	39	3.1	68	4.8	1.72	1.68	.18	1.75 (1.60)	68	Military station in open grassland

† Bracketed values previously obtained from subjective evaluation of site and surroundings (Davenport - 1960)

*It would appear that stations on the coastline give somewhat lower estimates.

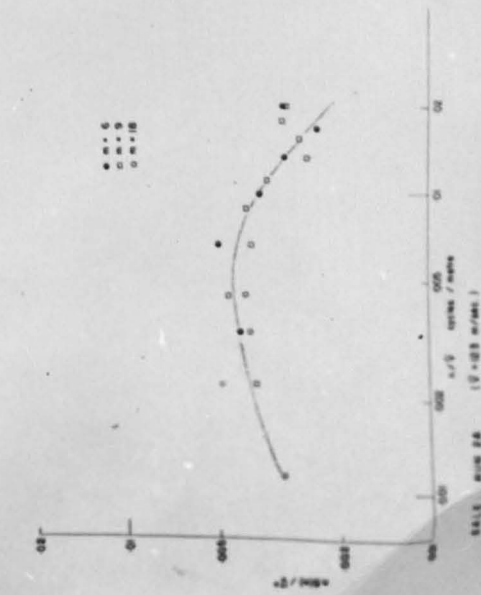
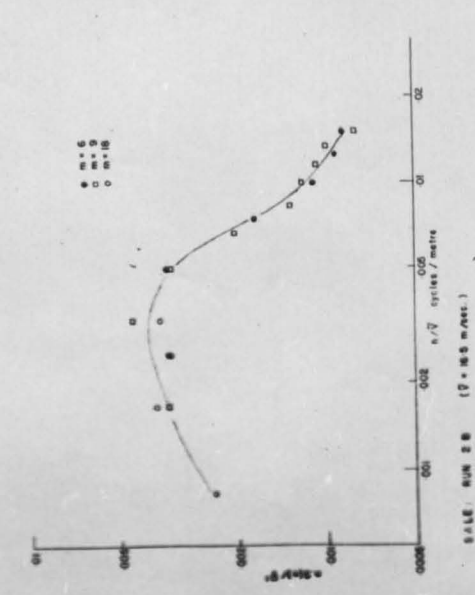
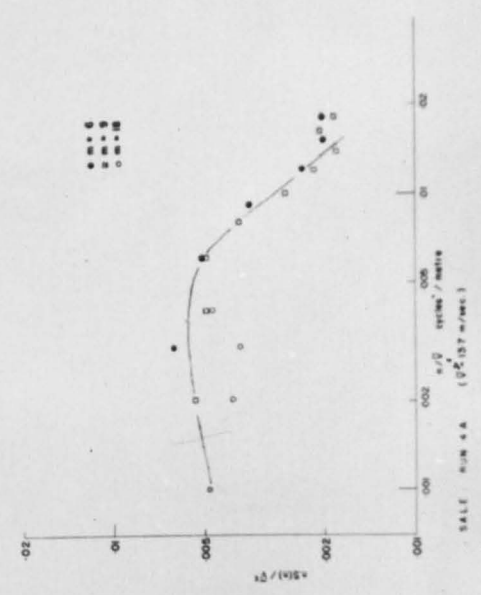
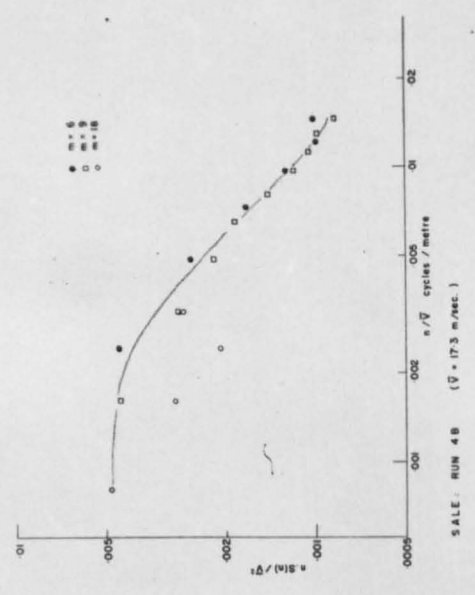
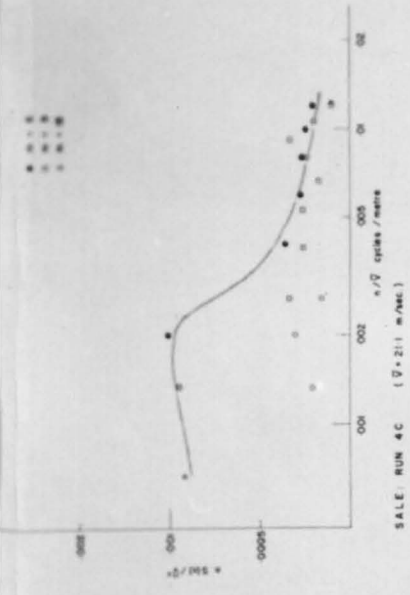
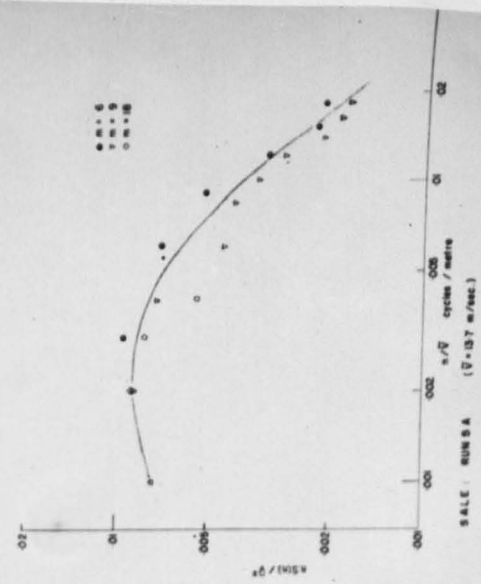
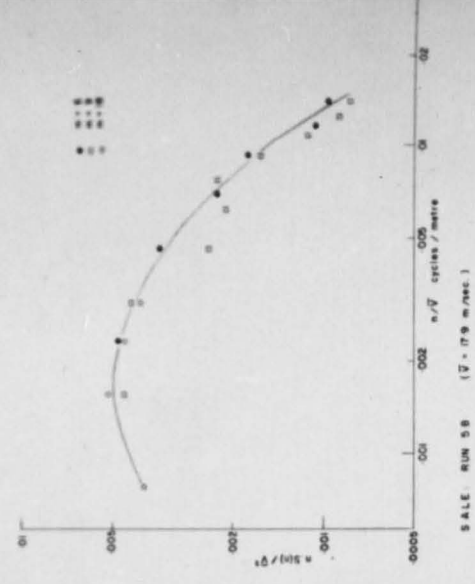
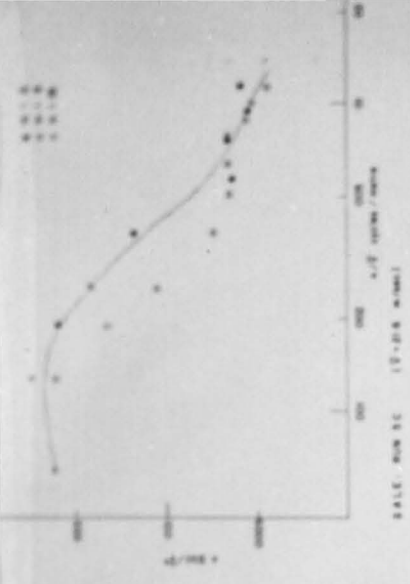
general region given in Fig. 2.4

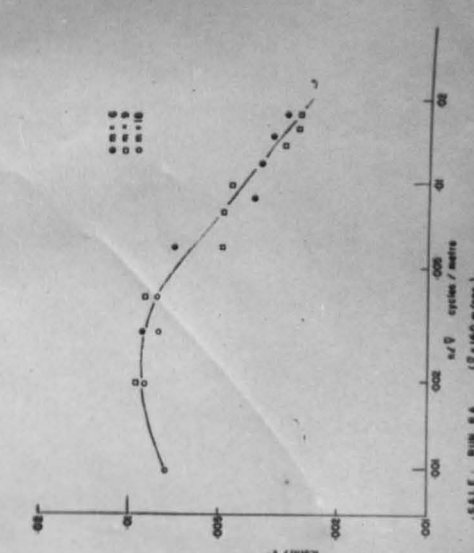
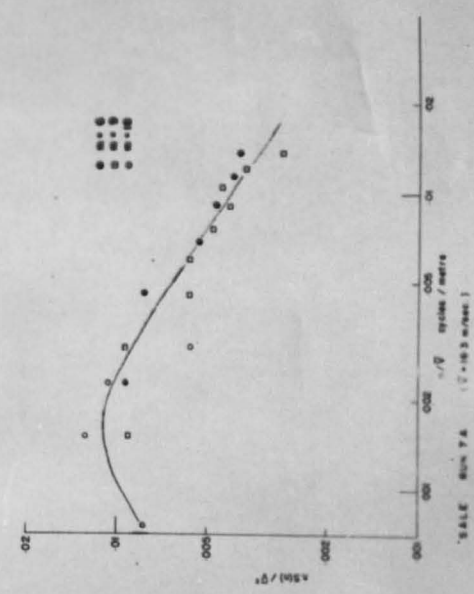
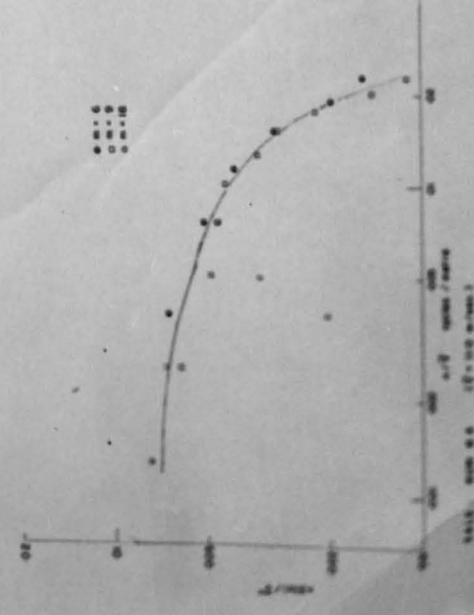
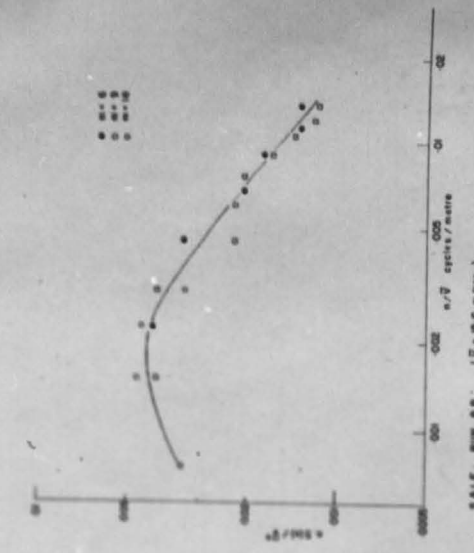
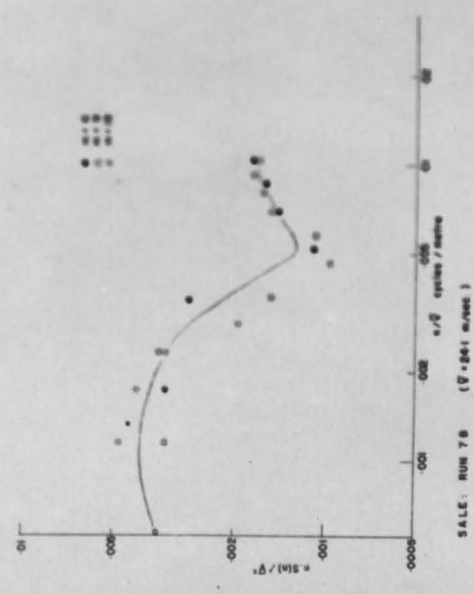
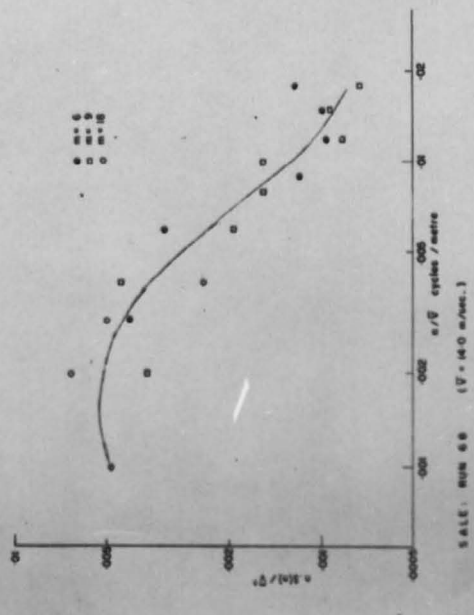
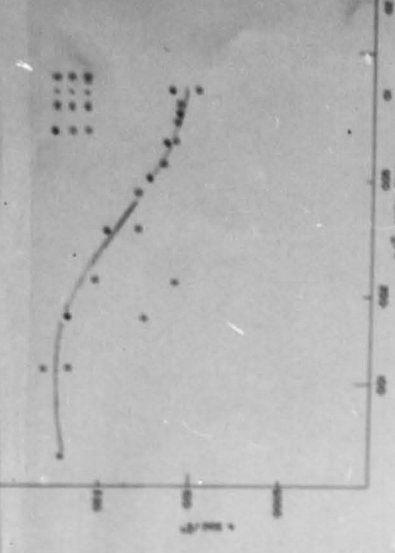
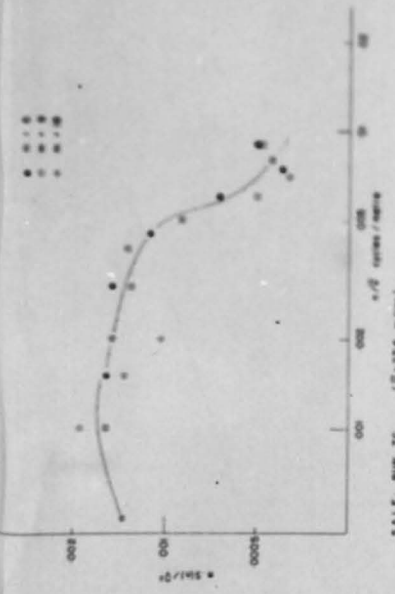
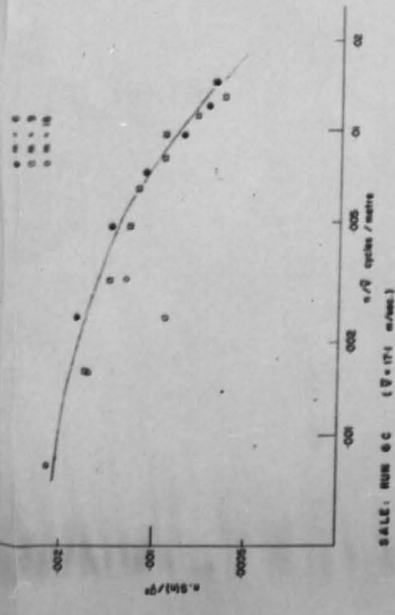
Thus it would seem that the peak gust ratio may prove to be a useful predictor for determining the roughness parameters of anemometer sites. With further confirmation regarding the response of the anemometers in service and with the analysis of extreme winds extended to include the records of more recent years, it might prove profitable to make a wider survey of the extreme wind climate along these lines.

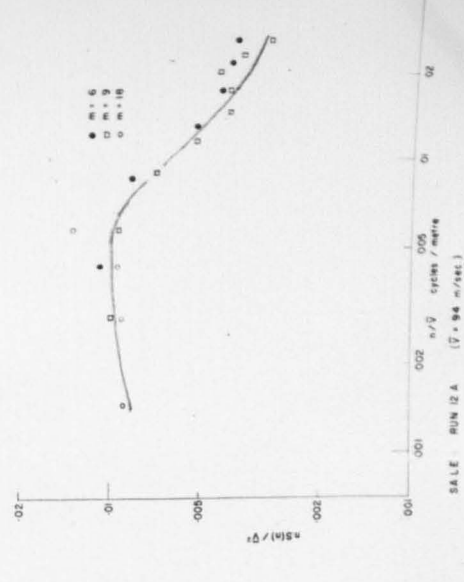
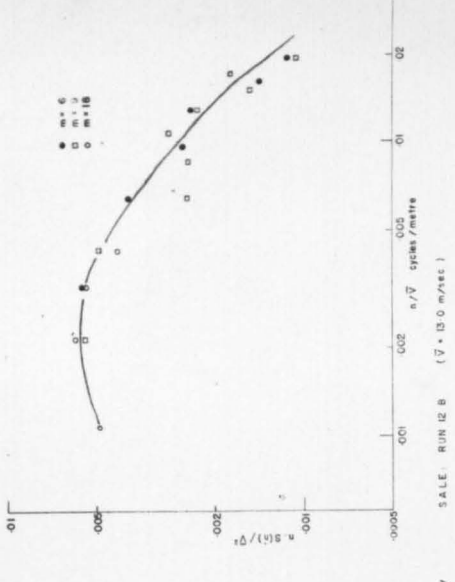
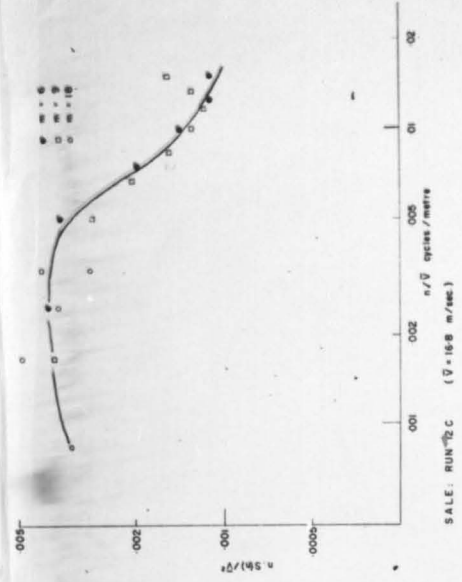
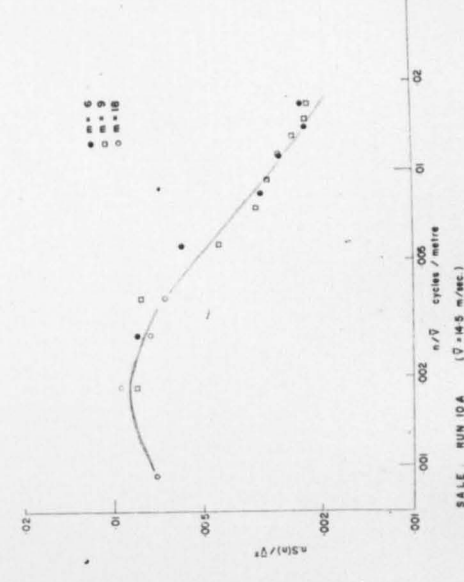
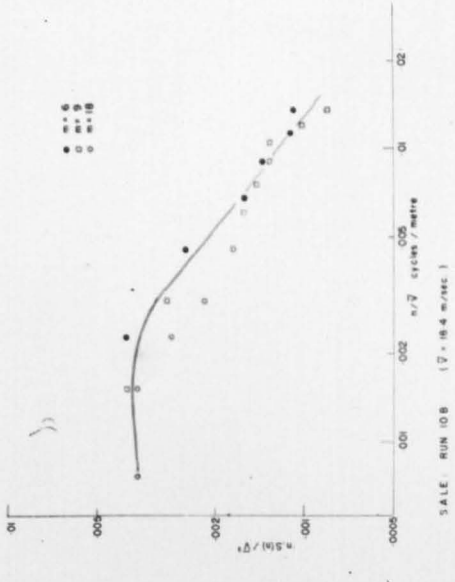
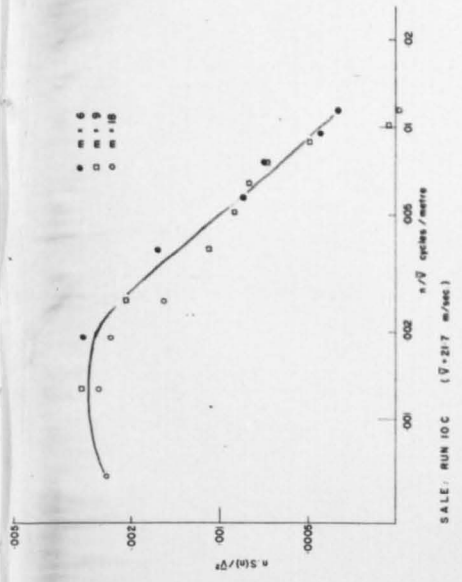
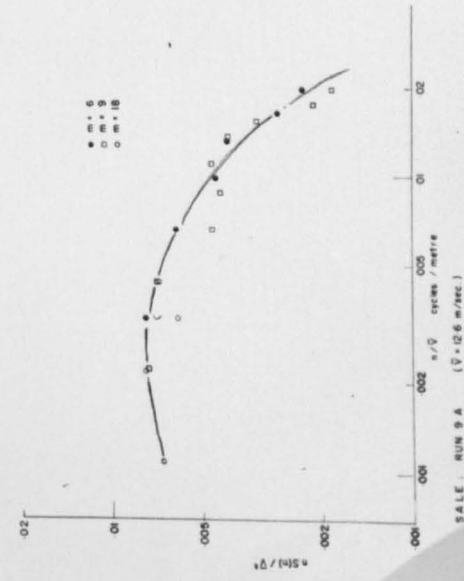
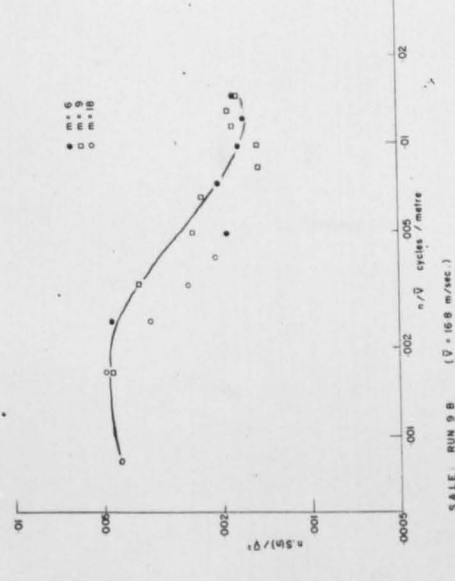
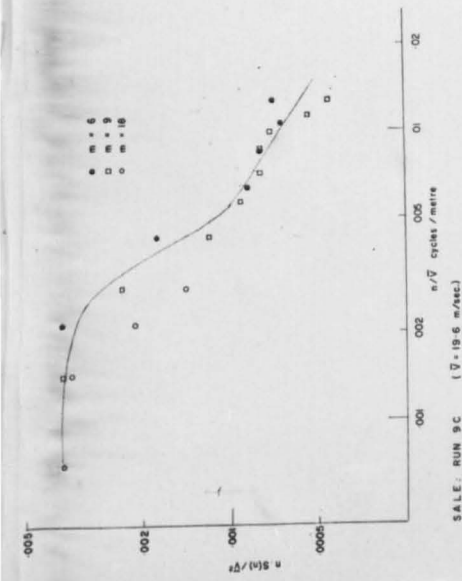
APPENDIX II

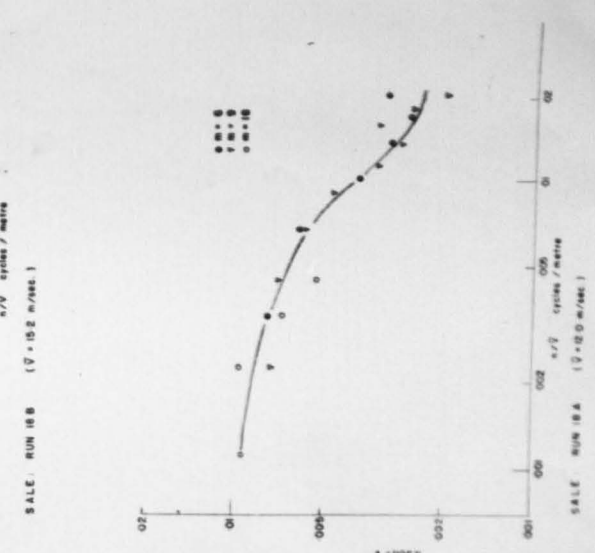
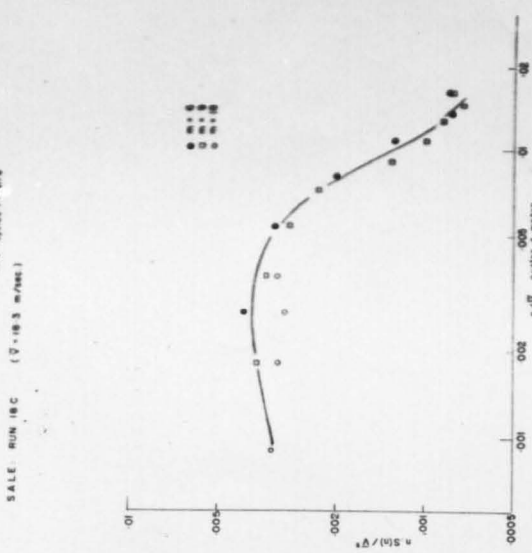
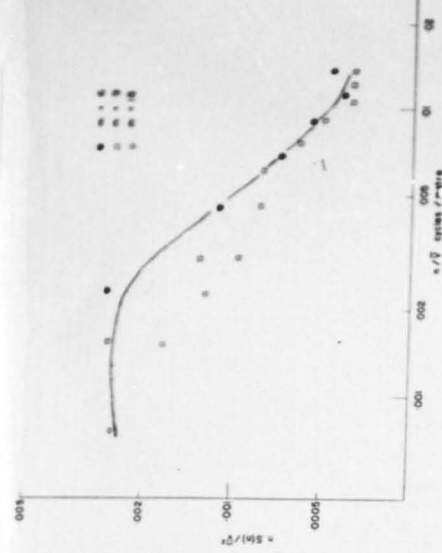
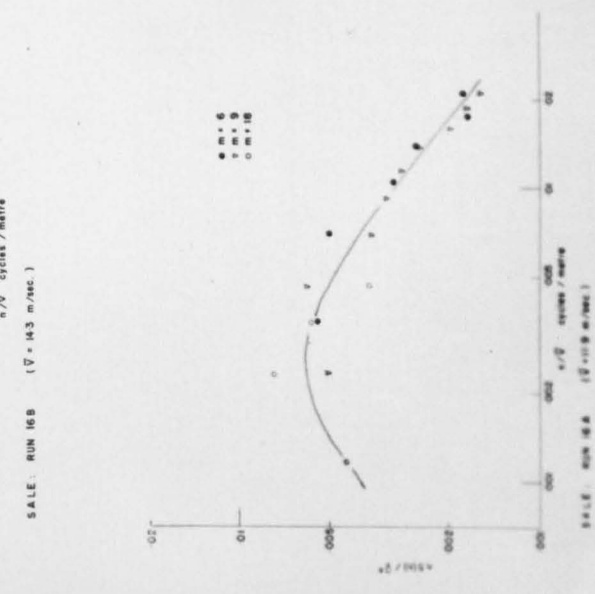
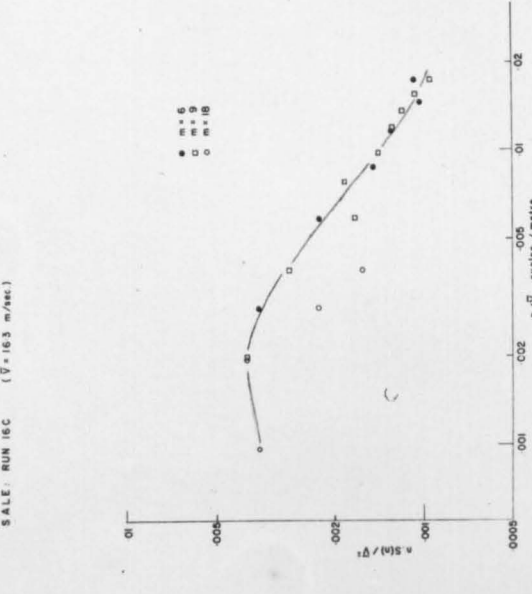
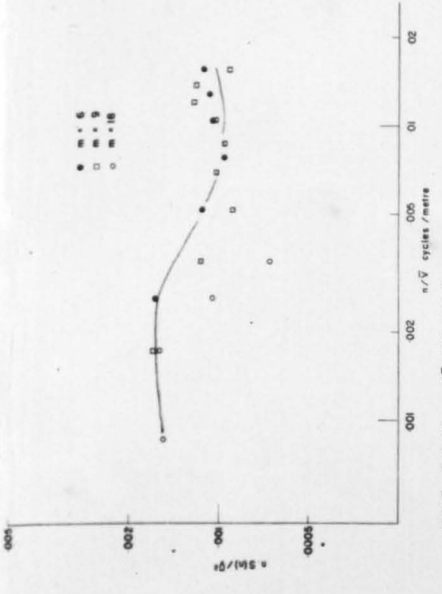
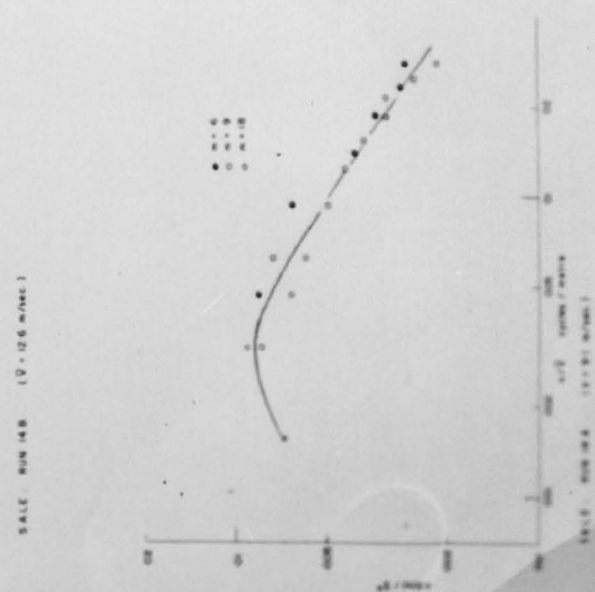
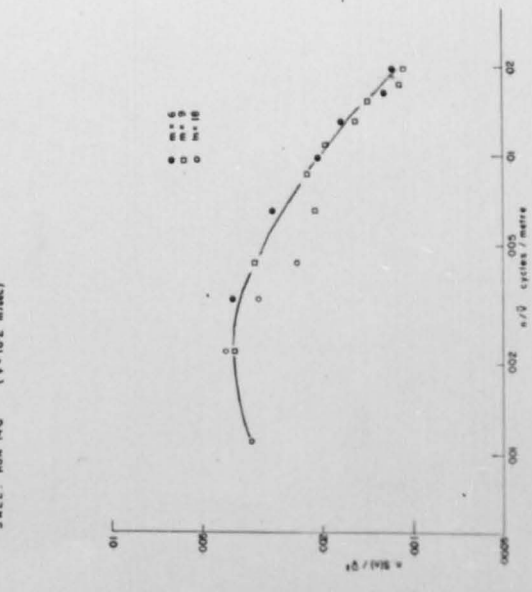
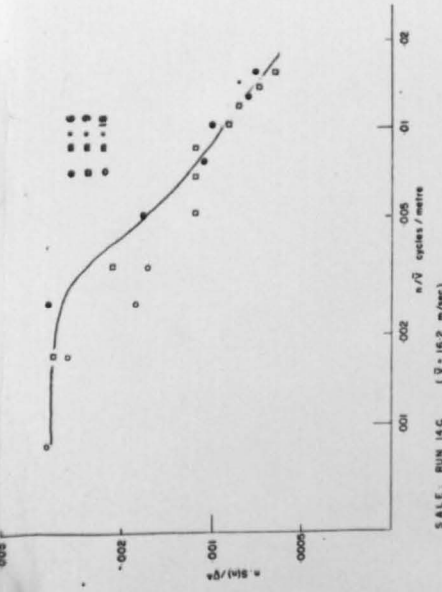
HORIZONTAL VELOCITY SPECTRA AT THREE HEIGHTS ON A TALL MAST

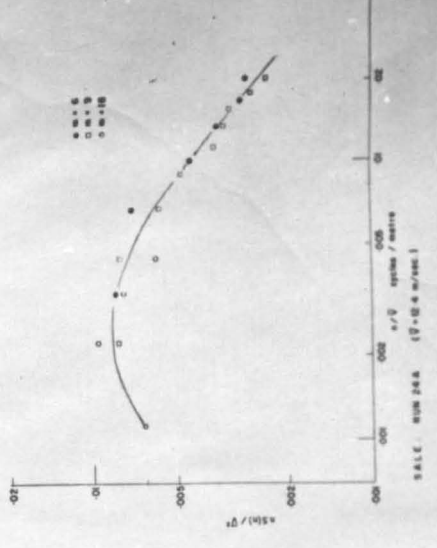
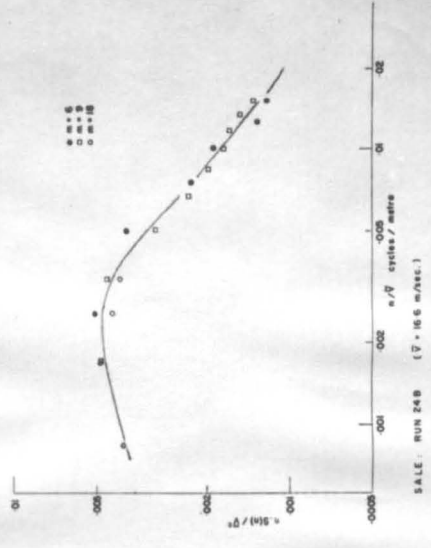
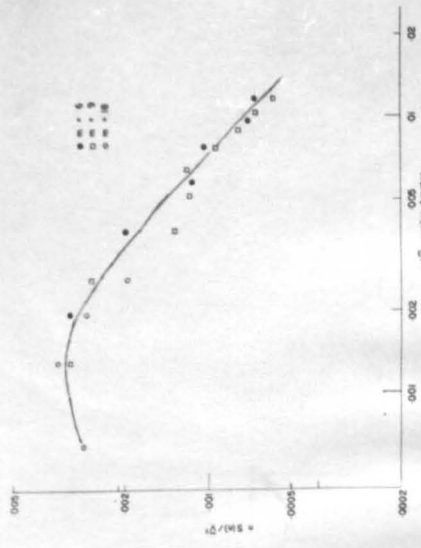
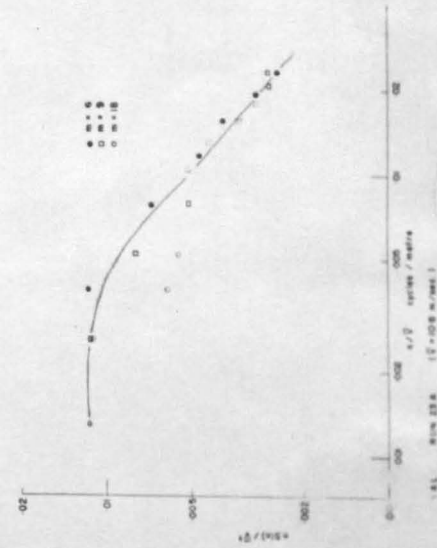
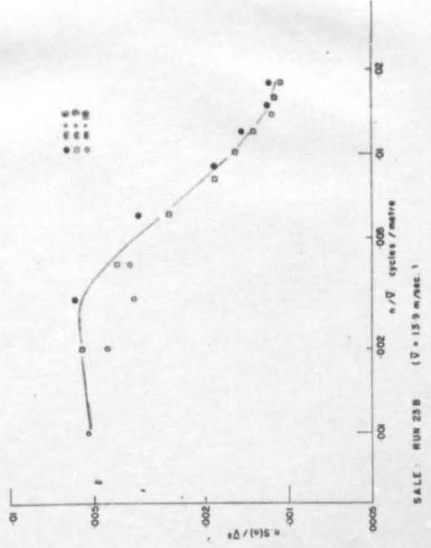
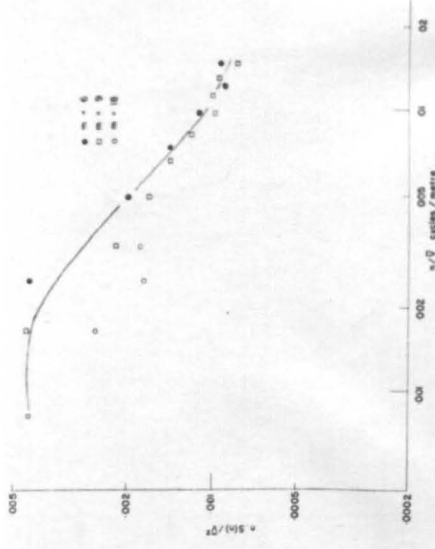
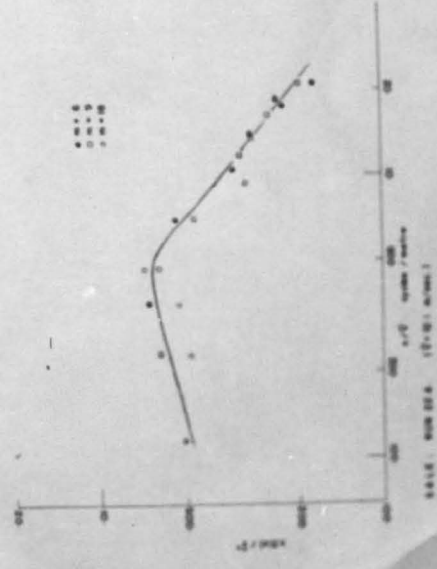
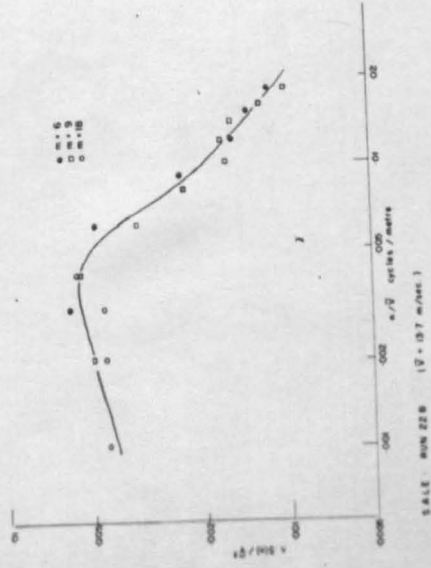
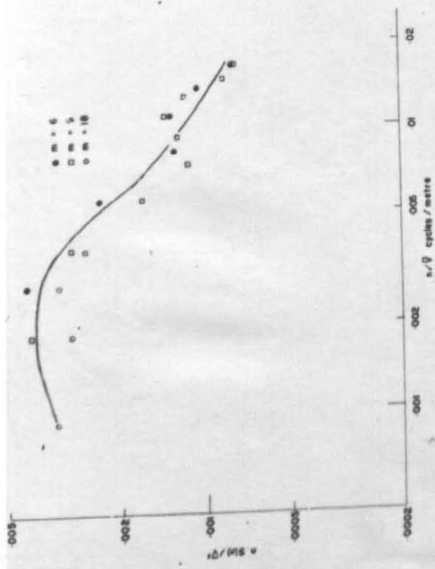
The following six figures show the spectra of the horizontal components of gustiness computed from records of 20 occasions of strong wind at heights of 40, 210 and 503 ft. on a tall mast. The experimental details have been fully described by Davenport in a paper entitled "The spectrum of horizontal gustiness near the ground in high winds" to be published in the Quarterly Journal of the Royal Meteorological Society. The spectra have been computed using 6, 9 and 18 auto-correlation coefficients. The summarised estimates of the normalised logarithmic spectrum $\frac{n \cdot S(n)}{V^2}$ at specific wave numbers appearing in the above paper were obtained from the "by eye" curves shown in the diagrams.

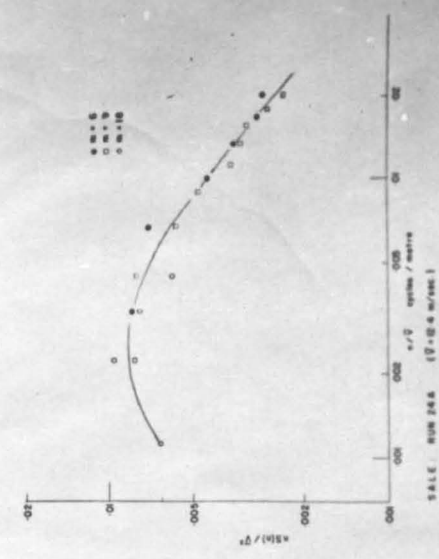
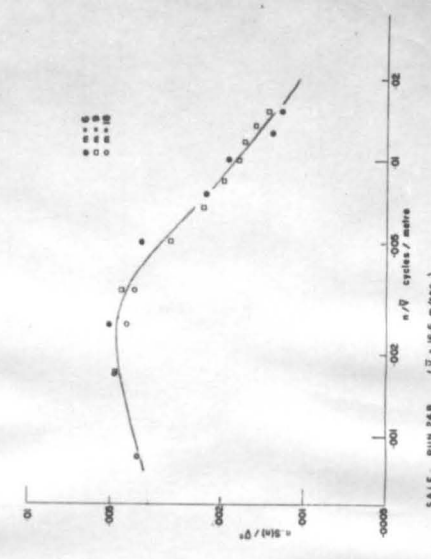
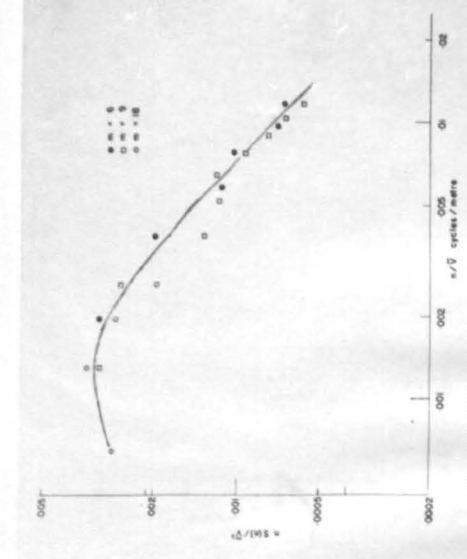
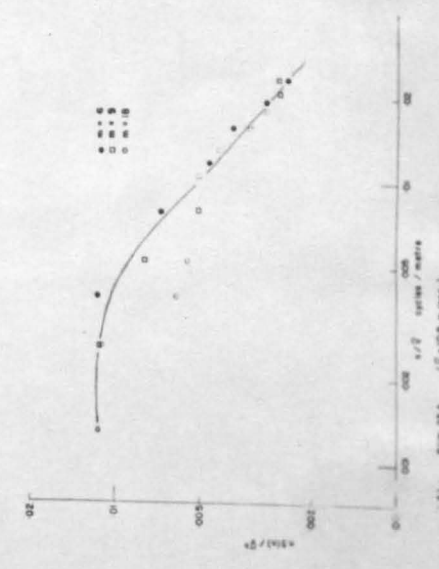
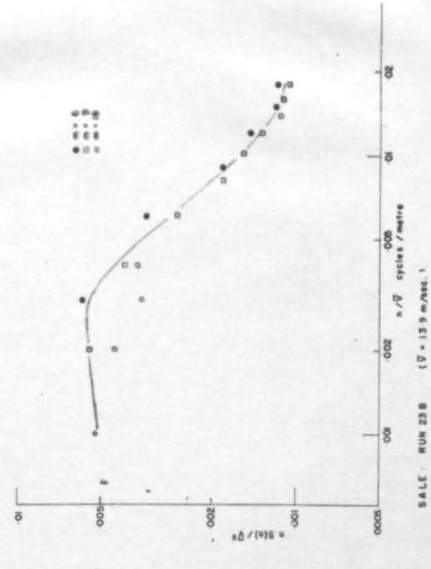
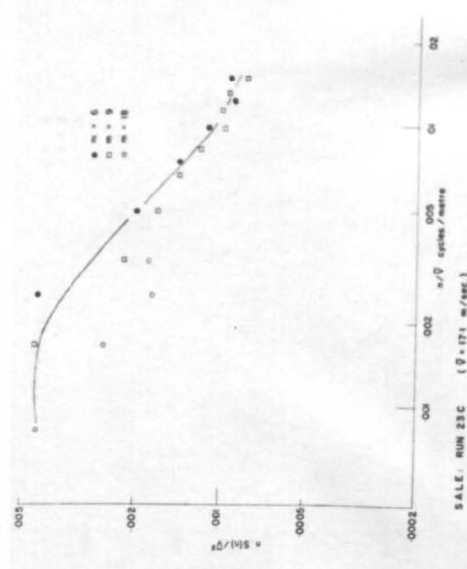
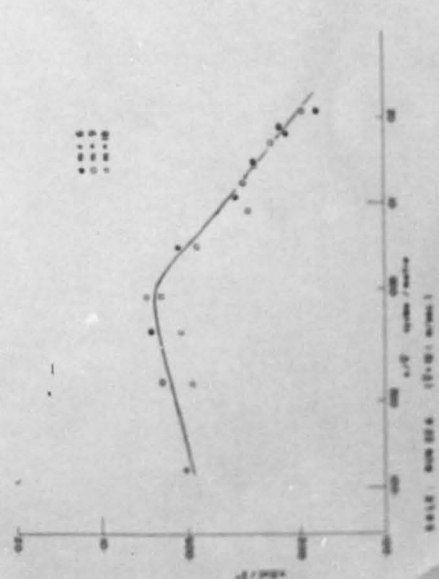
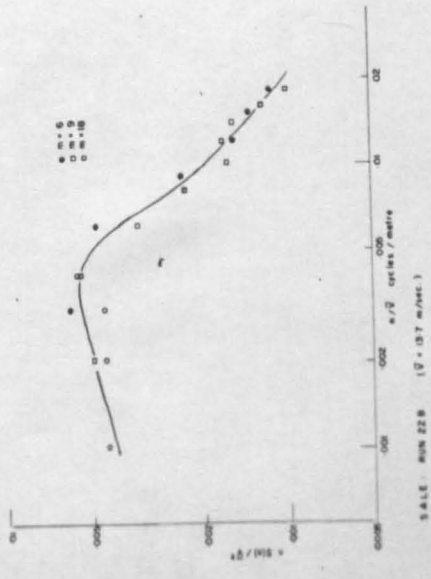
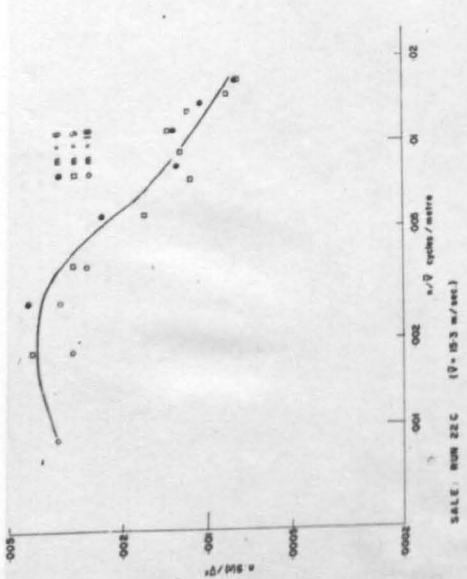


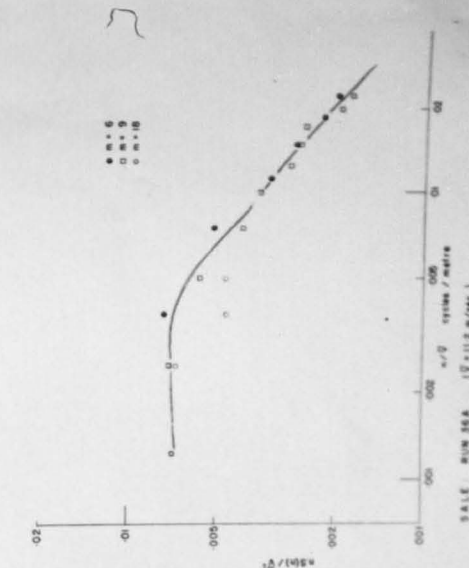
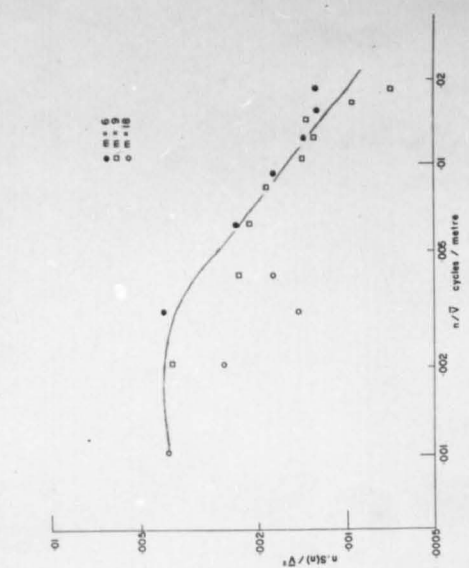
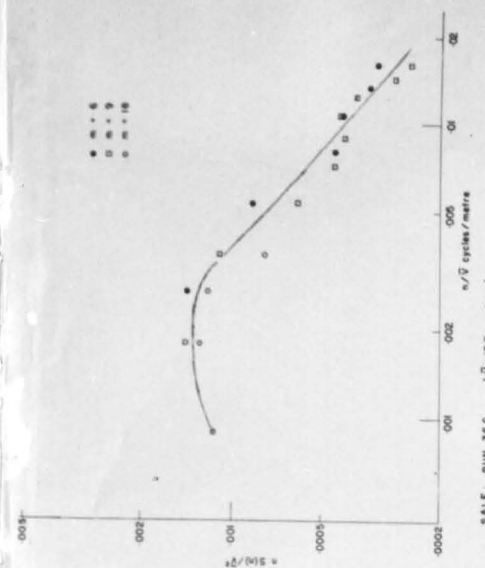
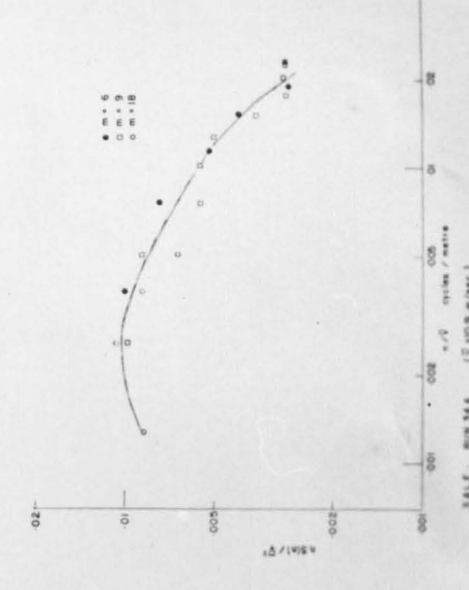
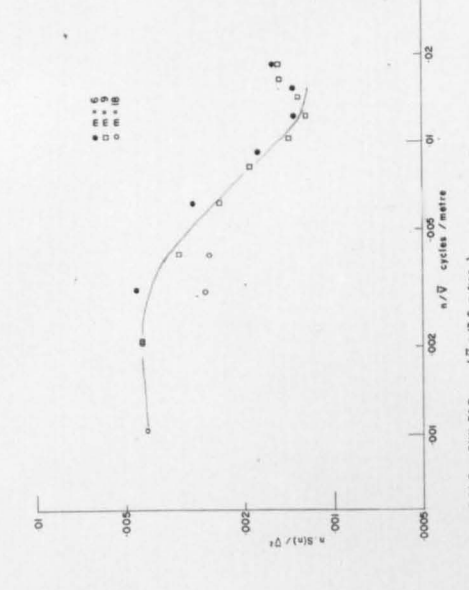
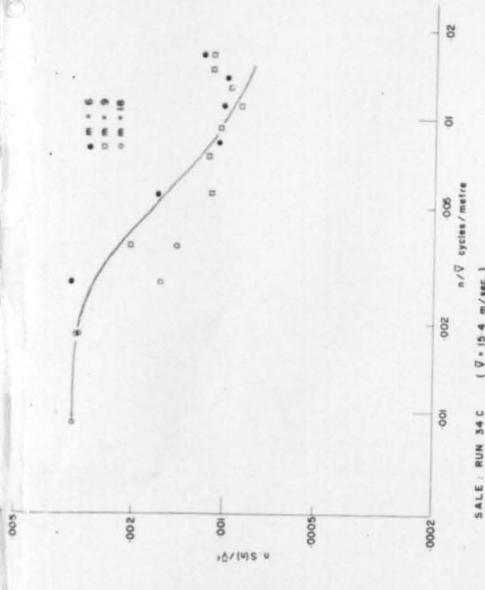
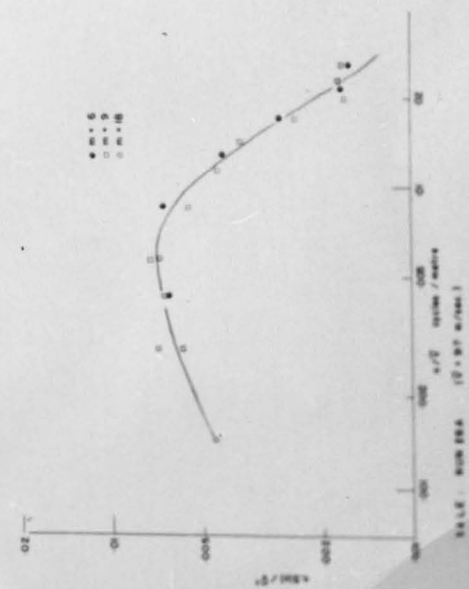
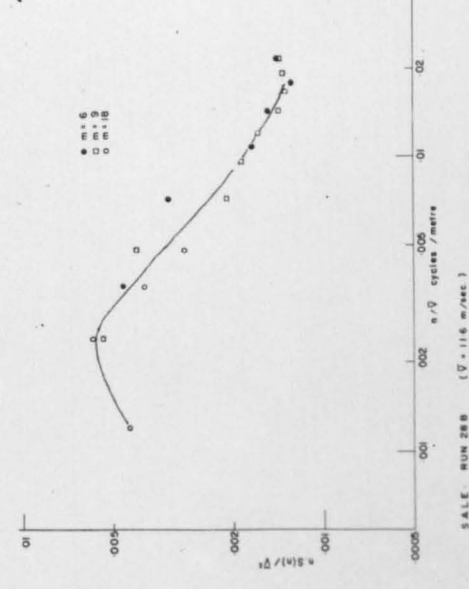
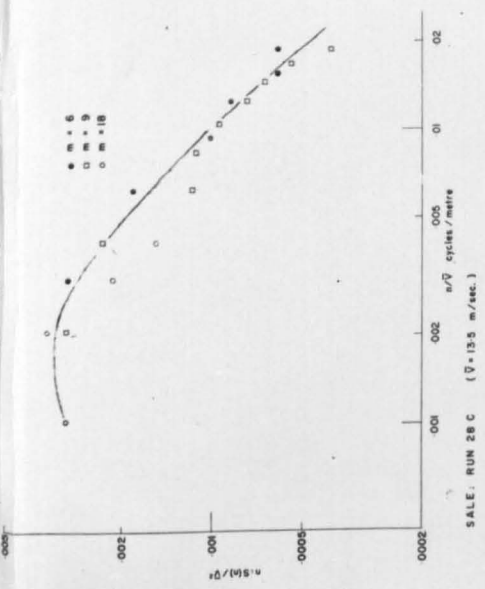


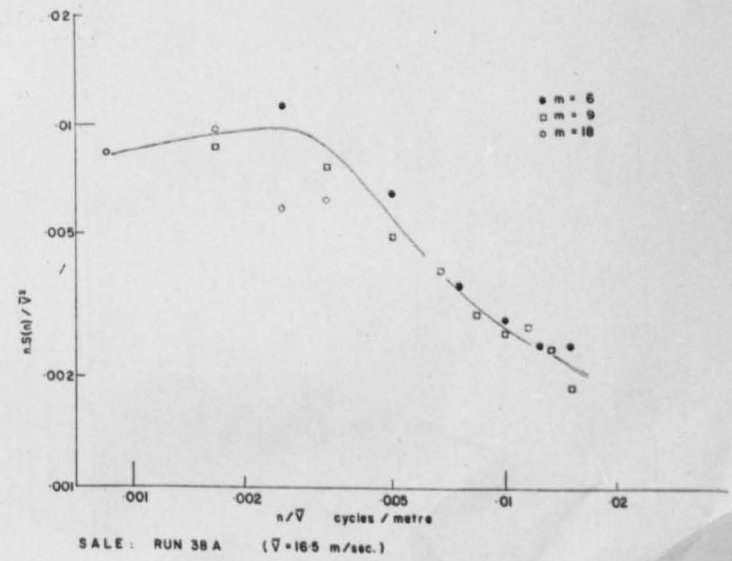
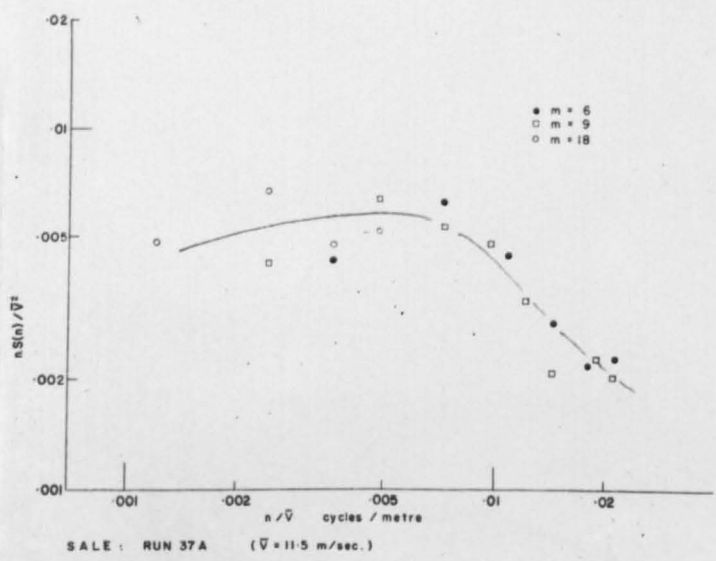
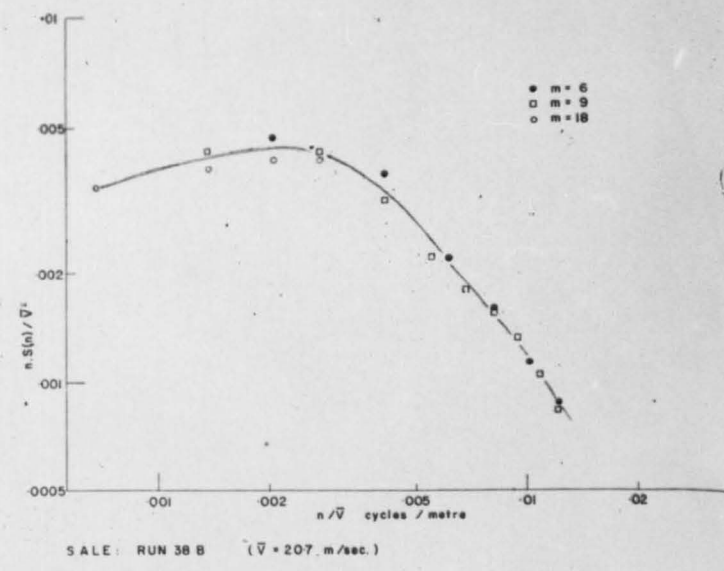
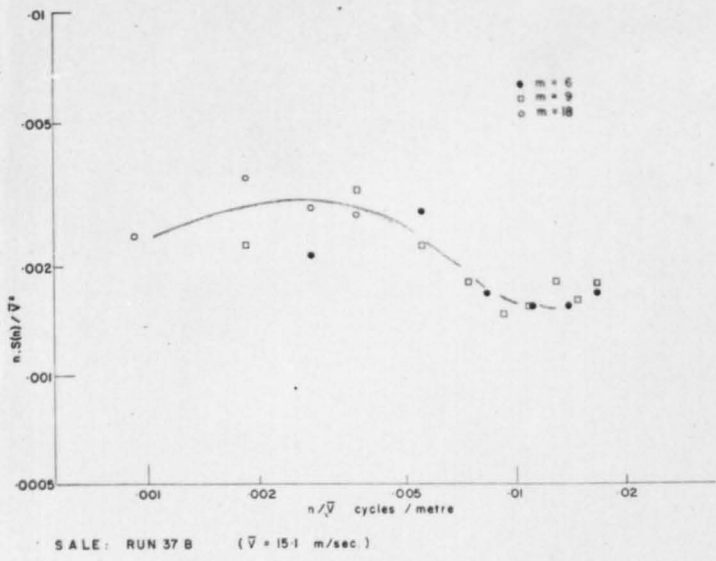
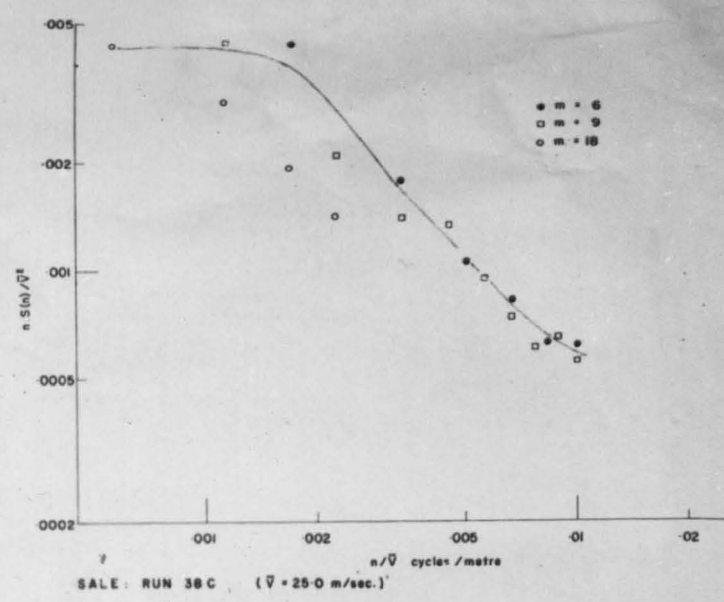
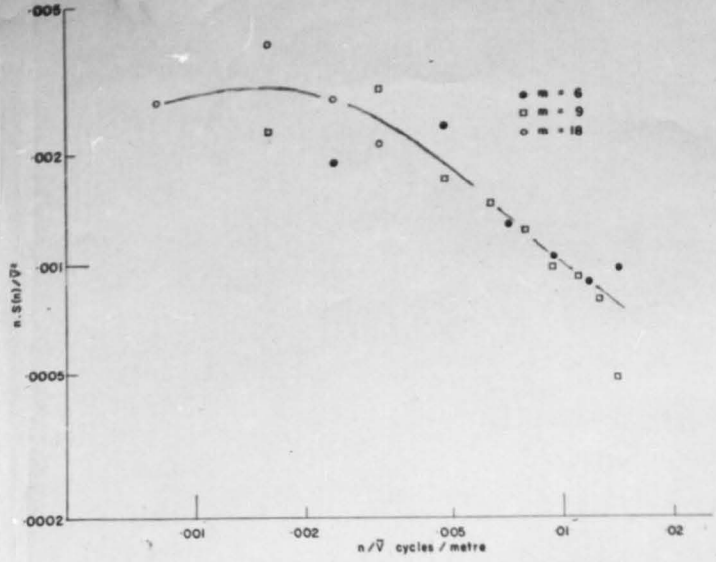












REFERENCES

1.0 INTRODUCTION

Historical

- Baker, B. (1895) "Experiments on wind pressure" - "Engineering" 60 p. 787
- Beamish, R. (1862) "Sir Marc Isambard Brunel" - 2nd Ed. Longman Green Longman Roberts, London p. 179 also p.282
- Bishop, J.G. (1897) "The Brighton Chain Pier - In Memoriam" - "Brighton Herald", Brighton
- Brunel, I.K. (1841) "Observation on the effect of wind on the suspension bridge over the Menai Straits" - Min. of Proc, Inst. Civ. Engrs. 1 pp. 74 - 80
- Eiffel, G. (1885) "Projet d'une tour en fer de 300 metres de hauteur" - Memoires de la Societe des ingenieurs civils I pp. 345 - 370
- Eiffel, G. (1913) "The resistance of air and aviation experiments" - 2nd Ed. (Transl. Jerome C. Hunsaker) Houghton Mifflin Co. Boston
- Leonhardt, F. (1956) "Der Stuttgarter fernsehturm" - Beton und Stahlbetonbau 4/5
- Smeaton, J. (1755-63) "An experimental enquiry concerning the natural powers of the wind to turn mills and other machines depending on circular motion" - Proc. Roy. Soc. II p. 366
- Stanton, T.E. (1903-4) "On the resistance of plane surfaces in a uniform current of air" - Min. Proc. Inst. Civ. Engrs. 156 Pt. II p. 78
- (1907-8) "Experiments on wind pressure" - Min Proc. Inst. Civ. Eng. 171 Pt. I p. 175
- Sturgis, S.D. (1954) "World's third tallest structure erected in Greenland" - Civ. Eng. (NY) 24 pp. 59-63

Valuable general background information was obtained from the following sources.

- Pugsley, A.G. (1957) "The theory of suspension bridges" - Edward Arnold
- Steinman, D.B. (1945) "Design of bridges against wind" - A series of articles published in Civil Engineering 15 pp. 469 - 472; pp. 501 - 504

Aeroelastic Problems

- Baird, R.C. (1955) "Wind induced vibrations of a pipeline suspension bridge and its cure" - Am. Soc. Mech. Eng. Paper No. 54 PET - 12
- Bleich, McCullough, (1950) "The mathematical theory of the vibration in suspension bridges" - Bur. Public Roads
Rosencrans, Vincent
- Davenport, A.G. (1959) "The wind induced vibration of guyed and self supporting cylindrical columns" - Transactions Eng. Inst. Canada 3 pp. 119 - 141
- den Hartog, J.P. (1954) "Recent technical manifestations of von Karman's wake" - Proc. Nat. Acad. of Sc. of U.S.A. 40, No. 3
- Farquahson, F. B. (1952) "Model verification of the classical flutter theory as adapted to the suspension bridge" - Int. Ass. Br. & Struct. Eng. 12 pp. 147-66
- Frazer, R.A. (1952) "A summarised account of the Severn Bridge aerodynamic investigation" - HMSO
Scruton, C.S.
- Husband, H.C. (1958) "Jodrell Bank radio telescope" - Proc. Inst. Civ. Eng. 9
- Scruton, C.S. (1955) "Wind excited oscillation of tall stacks" - The Engineer
- (1959) discussion of paper by Farquahson, F.B. "Structures subject to oscillation" - J. Struct. Div. Proc. Am. Soc. Civ. Eng. 85 p. 187

The Gust Loading Problem

- Anonymous (1937) "Report on towers built in Far East" - The Engineer

- Bailey, A. (1939) "Wind pressure experiments at the Severn Bridge" - J. Inst. Civ. Eng. 11, p. 363
Vincent, N.D.G.
- Davenport, A.G. (1960) "A rationale for the determination of basic design wind velocities" - Jnl. Str. Div. Proc. Americal Society of Civil Engineers
(1961) "The application of statistical concepts to the wind loading of structures" - Proc. Jnl. Inst. Civil Engineers. (to be published)
- Deacon, E.L. (1955) "Gust variation with height up to 150m." - Quart. Journal Royal Met. Soc. 81 pp. 562 - 573
- Irminger, (1936) "Wind pressures on buildings" 2nd series, Nokkentved Ingeniorvidenskabelige skrifter No. 24, Copenhagen.
- Sherlock, R.H. (1947) "Gust factors for design of buildings" International Association Bridge & Structural Engineering 8
(1953) "Variation of wind velocity and gusts with height" - Trans. Am. Soc. Civ. Eng. 118
- Stanton, T.E. (1925) "Report on the measurement of the pressure of the wind on structures" - Proc. Inst. of Civ. Eng. 219, pp. 125-158.

The Stationary Random Process

- von Karman, T. (1937) "On the statistical theory of turbulence" - Proc. Nat. Acad. 23 p. 38
- Liepmann, H.W. (1952) "On the application of statistical concepts to the buffetting problem" - Jnl. Aero. Sc. 19 pp. 793-800.
- Lin, C.C. (1943) "On the motion of a pendulum in a turbulent fluid" - Qu. App. Maths. 1 p. 43
- Taylor, G.I. (1922) Proc. London Maths. Soc. 20 p. 196
(1935) "The statistical theories of turbulence" Proc. Roy. Soc. London Series A. Vol. 151 pp. 421-444 also pp. 455-464

Climate of Extreme Winds

- Shellard, H.C. (1958) "Extreme wind speeds over Great Britain and Northern Ireland" - Met. Magazine 87 pp. 257-265
- Thom, H.C.S. (1960) "Distributions of extreme winds in the United States" - Jnl. of Str. Div. Proc. Am. Soc. Civ. Engrs.

2.0 WIND STRUCTURE NEAR THE GROUND

- Davenport, A.G. (1960) "A rationale for the determination of design wind velocities" - J. Str. Div. Proc. Am. Soc. Civ. Eng. 86 pp. 39-68
- Shellard, H.C. (1958) "Extreme wind speeds over Great Britain and Northern Ireland" - Met. Magazine 87 pp. 257-265
- Sutton, O.G. (1953) "Micrometeorology" - 1st Ed. McGraw-Hill Book Co. Inc.
- Thom, H.C.S. (1960) "Distributions of extreme winds in the United States" - J. Str. Div. Proc. Am. Soc. Civ. Engrs. 86
- Wax, M.P. (1956) "An experimental study of wind structure" - Electrical Research Assn. Tech. Rep. C/T 114

3.0 THE RESPONSE OF BEAMS TO STATIC AND STOCHASTIC LOADING

- Davenport, A.G. (1961) "The application of statistical concepts to the wind loading of structures" - To be published in Proc. Inst. Civil Engineers
- Davenport, A.G. (1959) "The wind induced vibration of guyed and self supporting cylindrical columns." - Trans, Eng. Inst. Canada 3 pp. 119-141
- Eringen, A.C. (1953) "Response of beams and plates to random loads" - Journal of Applied Mechanics 20 p. 461
- Selberg, A. (1944) "Calculation of the lateral truss in suspension bridges" - Pub. Int. Ass. Br. & Str. Engrg. Zurich

4.0 PROPERTIES OF ATMOSPHERIC TURBULENCE

- Bailey, A. (1939) "Wind pressure experiments at the Severn bridge" - J. Inst. Civil Engineers 11 p. 363
Vincent, N.D.G.
- Best, A.C. (1935) "Transfer of heat and momentum in the lower layers of the atmosphere" - Geophys. Memoirs No. 65 pp. 40-66
- Cramer, H.E. (1958) "Use of power spectra and scales of turbulence in estimating wind loads" - Unpublished paper presented at the 2nd National Conference on Applied Meteorology, Ann Arbor, Michigan.
- Davenport, A.G. (1961) "The spectrum of horizontal gustiness near the ground in high winds" - To be published in Qu. Jnl. Roy. Met. Soc.
- Giblett, M.A. (1939) "Structure of wind over level country" - Geophys. Mem. No. 54 Met. Office London
- Graham, A. (1936) "Note on the structure of turbulence in a natural wind containing also a description of a sensitive pressure gauge" - Tech. rep. Aero. Res. Comrs. II R. & M. No. 1704 p. 927
- Hesselberg, Th. (1929) "Über das verteilungsgesetz der wind ruhe" - Beit. Phys. Frei. Atmos. Band 15 p. 121
Bjorkdal, E.
- Huss, P.O. (1949) "Study of natural wind and computation of Austausch turbulence constant" - Daniel Guggenheim Airship. Inst. Rep. Rep. No. 156 Akron Univ. Also Rept. 1 (Same title) Jan. 1948
Portman, D.J.
- Panofsky, H.A. (1954) "Properties of spectra at atmospheric turbulence at 100 metres" - Qu. Journal of Royal Met. Soc. 80 p. 156
McCormick, R.A.
- Panofsky, H.A. (1958) "The relation between Eulerian time and space spectra" - Qu. Jnl. Roy. Met. Soc. 84 p. 270-273
Cramer, H.E.
Rao, V.R.K.
- Panofsky, H.A. (1959) "The Spectrum of vertical velocity near the surface" - College of Mineral Industries, Penn. State University (unpublished paper)
McCormick, R.A.
- Taylor, G.I. (1922) Proc. London Maths. Soc. 20 196
- (1935) "The statistical theories of turbulence" - Proc. Roy. Soc. London Series A. 151 pp. 421-444, 455-464

- Townsend, A.A. (1958) Proc. I.U.T.A.M. symposium on boundary layer research - 1957 Springer
- (1956) "The structure of turbulent shear flow" - Cambridge Univ. Press monograph series
- Von Karman, Th. (1937) "On the statistical theory of turbulence" - Proc. Nat. Acad. Sc. 23 p. 98
- Webb, E.K. (1955) "Autocorrelations and energy spectra of atmosphere turbulence" - C.S.I.R.O. Aust. Div. Met. Phys. Tech. paper No. 5

5.0 AERODYNAMIC RESPONSE TO FLUCTUATING FLOW

- Biggs, J.M. (1954) "Wind loads on truss bridges" - Trans. Am. Soc. Civ. Eng. 119 p. 879
- Bingham, H.H. (1952) "The cylinder and semi-cylinder in sub-sonic flow" - Princeton Univ. Dept. of Physics
Weimar, D.K. Tech. Rep. II - 13, 1952
Griffiths, W.
- Cohen, E. (1957) "Design of multi-level guyed towers"-
Perrin, H. Jnl. of Str. Div. Proc. Am. Soc. Civ. Eng. Papers 1355, 1356, 83
- Davenport, A.G. (1959) "The wind induced vibration of guyed and self supporting cylindrical columns" - Transactions Eng. Inst. Canada. 3 pp. 119-141
- Fedyayevsky, K.R. (1954) "The aerodynamic forces acting on buildings
Belotserkovsky, S.M. in squalls" - Izv. Akad. Navk. U.S.S.R. Otd. Tekhn. pp. 13-24
- Flachsbart, O. (1932) "Wind pressure on solid-walled and framed structures" - International Assn. for Bridge and Structural Engineering. 1 pp. 153-72
- Frazer, R.A. (1919) "The dependence of the resistance of bodies
Simmons, V.A. upon acceleration" - Aero. Res. Comm. R. and M. No. 590
- Frazer, R.A. (1952) "A summarised Account of the Severn bridge
Scruton, C.S. aerodynamic investigation" - H.M.S.O.
- Keulegan, G.H. (1958) "Forces on cylinders and plates in oscillating
Carpenter, L.H. fluid" - Jnl. Bur. Stds. 60 No. 5
- McNown, J.S. (1957) "Drag in unsteady flow" - Proc. IX Int. Cong. Appl. Mech. Brussels

- O'Brien, M.P. (1952) "The forces exerted by waves on objects" -
Morison, J.R. Trans. Am. Geophys. Union 33 pp. 32-38
- Redwood, R.G. (1960) "Wind loads on antenna towers" - M.A. Sc.
Thesis, University of Toronto
- Schott, G. (1954) "Analysis of structural behaviour of guyed
Thurston, P. antenna masts" - Nat. Res. Council of
Pocock, P. Canada Div. Mech. Eng. Report MM-238
- Schwarz, W.H. (1957) "Some effects of isotropic turbulence on a
Corssin, S. pendulum at moderate Reynold's number" -
Heat Trans. and Fluid Mech. Inst. Calif.
Inst. Techno. Pasadena Calif. pp. 421-439
- Stelson, J.M. (1955) "Virtual mass and acceleration in fluids" -
Mavis, F.T Proc. Am. Soc. Civ. Eng. 81 p. 670

6.0 DYNAMIC AND STATIC BEHAVIOUR OF THE SUSPENSION
BRIDGE AND TALL MAST

- Bleich (1950) "The Mathematical theory of vibration in
McCullough suspension bridges" - Bur. Public Roads
Rosencrans
Vincent
- Davenport, A.G. (1959) "The wind induced vibration of guyed
and self-supporting cylindrical columns" -
Trans. Eng. Inst. of Canada 3 pp. 119-141
- Kolousek, V. (1947) "Solution statique et dynamique des
pylones d'antenne haubanes" - Pub. Int.
Assn. of Bridge & Structural Engineers 8
- Steinman, D.B. (1959) "Modes and natural frequencées of suspension
bridges" - Trans. Eng. Inst. of Canada 3
pp. 74-83

7.0 MECHANICAL AND AERODYNAMIC DAMPING

- Davenport, A.G. (1959) "The wind induced vibration of guyed and
self-supporting cylindrical columns" -
Transactions Eng. Inst. Can. 3 pp. 119-141
- Farquahson, F.B. (1949 - "Aerodynamic stability of suspension bridges" -
Smith, F.C. 1954) U. of Washington Bull No. 16 Pt. 1 (1949):
Vincent, G.S. Pt. 2 (1950): Pt. 3 (1952): Pt. 4 (1954):
Pt. 5 (1954)
- Frazer, R.A. (1952) "A summarised account of the Severn bridge
Scruton, C.S. aerodynamic investigation" - H.M.S.O.

8.0 TIME-HISTORY RELATIONSHIPS

- Davenport, A.G. (1961) "The application of statistical concepts to the wind loading of structures" - To be published in J. of Inst. Civ. Engrs.
- Longuet Higgins, M.S. (1952) "On the statistical distribution of the heights of sea waves" - Jnl. of Marine Res. 11 pp. 245-266
- Rice, S.O. (1945) "Mathematical analysis of random noise" Part III - Bell System Tech. Jnl. 24 pp. 46-155

9.0 APPLICATIONS

- Deacon, E.L. (1955) "Gust variation with height up to 150 m." - Quart. Journal Royal Met. Soc. 81 pp. 562-573
- Freudenthal, A.M. (1956) "Safety and probability of structural failure" - Trans. Am. Soc. Civ. Eng. 121 p. 1337
- Pugsley, A.G. (1951) "Concepts of safety in structural engineering" - Proc. of Inst. Civ. Engrs.
- Sherlock, R.H. (1947) "Gust factors for design of buildings" - Pub. Intern'l Assn. Bridge and Struct. Eng. 8
- Vincent, G.S. (1958) "Golden Gate bridge vibration studies" - Jnl. of struct. Div. #1817 Proc. Am. Soc. Civ. Eng. 84

APPENDIX 1

- Davenport, A.G. (1960) "Rationale for the determination of design wind velocities" - J. Str. Div. Proc. Am. Soc. Civ. Eng. 86 pp. 39-68